# EROSION OF A FLUID MUD LAYER DUE TO ENTRAINMENT

## Numerical modelling

By: Yvonne van Haaren
Delft University of Technology
Faculty of Civil Engineering
Division of Hydraulic and Geotechnical Engineering
Hydromechanics Section

Delft, May 1995

**SUPERVISORS:**

| | |
|---|---|
| Prof.dr.ir. J.A. Battjes | Hydromechanics Section, Faculty of Civil Engineering, Delft University of Technology |
| Dr.ir. C. Kranenburg | Hydromechanics Section, Faculty of Civil Engineering, Delft University of Technology |
| Ir. J.C. Winterwerp | Delft Hydraulics, Delft |
| Prof.ir. K. d'Angremond | Hydraulic and Offshore Engineering Section, Faculty of Civil Engineering, Delft University of Technology |

*'Le bon sens est la chose du monde la mieux partagée, car chacun pense en être bien pourvu'*

Descartes

*'For all building up is done with debris, and nothing in the world is new but shapes. But the shapes must be perpetually destroyed.... Break every cup from which you drink.'*

Marcel Schwob

## PREFACE

This report contains the study on the erosion of a fluid mud layer due to entrainment, which I performed as my final graduation project at the Delft University of Technology and by order of Delft Hydraulics. I have chosen this subject as my thesis project because of the combination of research on a small and large scale.
During my seven months of graduation I have experienced that simulating the desirable situation is more difficult than expected. I have also experienced that logically thinking is still the best solution to solve practical problems.

Writing this report I would like to seize the opportunity to thank the persons who have supported me through my graduation time and helped me solving problems. Special thanks I would like to give to my supervisors K. Kranenburg and H. Winterwerp and to professor J. Battjes for guiding me through the whole project. Furthermore I would like to thank some people from Delft University and Delft Hydraulics: From Delft University I would like to thank Thijs and Moniek for their company and for sharing their room with me, Carlita and Steven for their company and support during the lunch breaks and A. den Toom for his assistance with adapting Entcar. From Delft Hydraulics I would like to thank ir. Wang for helping me with his numerical knowledge, Antoon Koster for making the beautiful colour pictures, Paulien Thoolen for her company and for sharing her room with me, Kees Koree for his computer assistance and all the other people of the Department MST who accepted me as a lunch partner and office partner.

Delft, May 1995

Yvonne van Haaren

## ABSTRACT

A continuous transport cycle of mud material can be noticed in a natural water environment. Aggregation, settling, deposition, consolidation and erosion are typically interlinked. These processes are influenced by the cohesive properties of the mud and by the characteristics of its environment.
Fluid mud is a highly concentrated near-bed sediment suspension with a sediment concentration between about 10 and 300 g/l, and can be formed by hindered settling or by the fluidization of the bed. Once formed, the fluid mud can be transported due to

- horizontal pressure gradients, frictional and gravitational forces.
- turbulence and instability of the interface between the fluid mud layer and the water layer above, resulting in mass transport from a non-turbulent layer to a turbulent layer. This process is defined as entrainment.

This report concentrates on the process of entrainment by turbulent water flow.
A quantitative measure for entrainment is the dimensionless entrainment rate $E$, which is the ratio of the entrainment rate $u_e$ (i.e. the entrained volume of fluid mud per unit area and per unit time) to a characteristic flow velocity. Dimensional analysis indicated that $E$ is a function of an overall Richardson number.
From the literature it followed that the entrainment of fluid mud resembles the fresh/saline water entrainment process, though properties of the cohesive sediments may greatly influence the entrainment behaviour.

Two numerical models have been used to predict the entrainment of fluid mud: an entrainment model describing the small scale behaviour (1) and the two-layer fluid mud model which considers mud transport on a larger scale (2). The results have been compared with experimental data or observations.

(1) From the analysis of the integral entrainment model of Kranenburg (1994), it resulted that the values taken for the empirical coefficients involved and the assumptions made for the effects of viscous drag and side wall friction are satisfactory. The effect of consolidation and the related change from entrainment to floc erosion becomes apparent for large times.

(2) The two-layer fluid mud model, developed by Delft Hydraulics, showed the importance of entrainment for mud transport. When applying a settling velocity, which varies with the sediment concentration, upward transports (due to entrainment) and downward transports (caused by settling) are much larger than in the case of a constant settling velocity. Also the results agree better with observations then. The major limitation of this model originated from the fact that in the model no differences in bed material were made and only neap tide was simulated instead of a neap tide - spring tide cycle.

The incorporation of the integral entrainment model of Kranenburg into the two-layer fluid mud model will only be one step forward and further improvements are needed.

## TABLE OF CONTENTS

# 1.0 INTRODUCTION

*This chapter gives a short introduction to mud and gives a description of fluid mud. The motivation of the present work is defined in this introductory chapter and the layout of this report is presented.*

## 1.1 Introduction to mud

Mud is defined as a fluid-sediment mixture consisting of (salt)water, silt, clay and organic material. This mixture is generally observed in many estuaries and near-shore shelf environments. Especially because of its cohesive properties mud differs from sand.
There is a growing interest in the transport of mud. This interest is twofold. One motivation for this interest is that mud causes ecological and water quality problems. The fine sediment particles are important carriers for substances such as heavy metals, radio nuclides and organic pollutants, due to their adsorptive capacity. This has an adverse effect on the water quality. Another reason for the interest is that mud causes siltation problems in harbours and navigation channels, resulting in high dredging costs and high costs of disposal when the mud is polluted.
To get an impression of the sedimentation in the Rotterdam Waterway during the past 80 years see figure 1.1. It shows the amount of dredged material as a function of time. The increase in the 1960's resulted from the enlargement of the harbour area and the deepening of the estuary (Van Leussen, 1988).

## 1.2 Fluid mud characteristics

Fluid mud can be defined as a highly concentrated near-bed sediment suspension with a sediment concentration between 10 and 300 g/l, either mobile or stationary. Such suspensions are found in numerous estuaries, navigational channels, harbour basins and along some coasts. The observed thicknesses of these layers ranges from a few centimetres to several metres. Other names of fluid mud are 'sling mud' and 'crême de vase'.

The formation of a fluid mud layer can result from rapid settling, when the deposition rate is larger than the rate of consolidation. Therefore it will only occur in areas where the suspended concentration is high enough, for example in a turbidity maximum at slack water. Fluid mud layers can also be formed by the fluidization of soft mud beds by wave action or by tidal flow, because the oscillatory pressures and currents can weaken the surface layer of the bed deposit. Dredging operations can also disturb the bottom and fluidize its surface layer.

Fluid mud can be transported in two ways:
1. Transport due to turbulence and instability of the interface between the fluid mud layer and the water layer above. This causes erosion of the fluid mud layer.
2. Transport due to flow of the fluid mud layer itself. Shear stresses from the flowing water above and streamwise pressure gradients, bottom slopes, or a slope in the surface of a fluid mud layer can initiate a mud layer to flow.

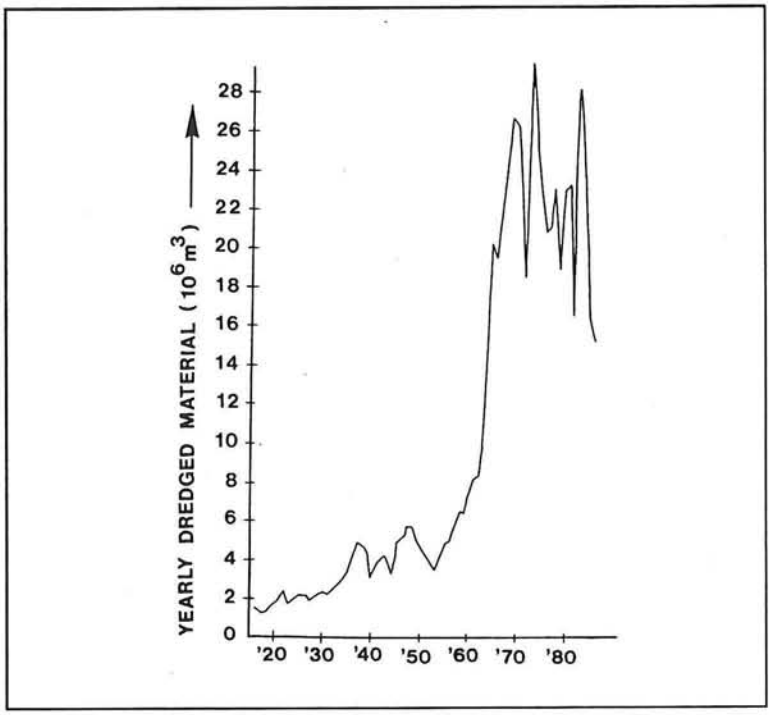


Figure 1.1: Volume of dredged material in the Rotterdam Port area (Van Leussen, 1988)

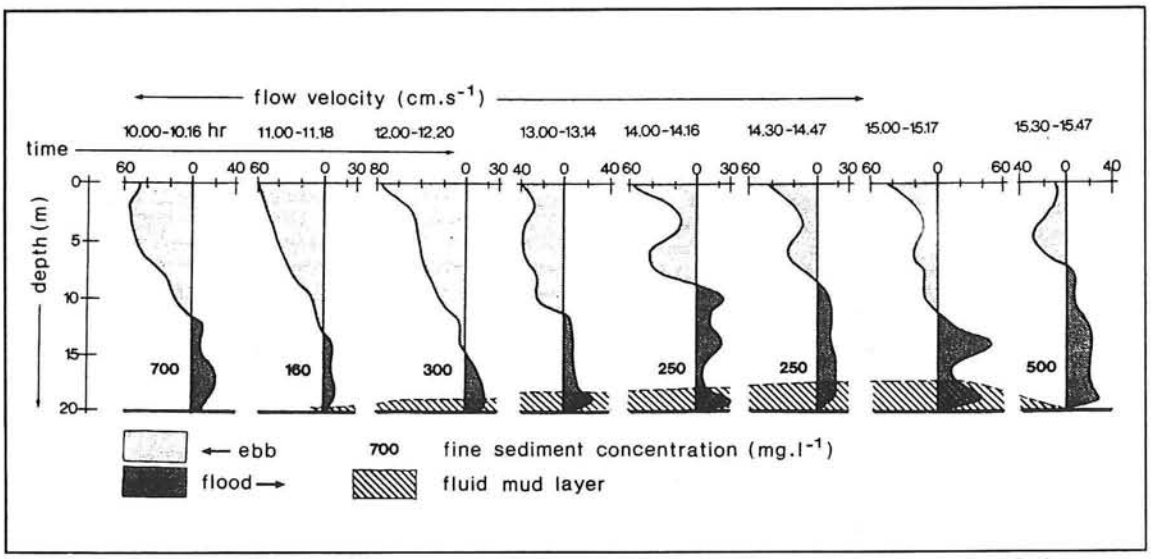


Figure 1.2: Flow velocities and sediment concentrations in the mouth of the Rotterdam Waterway (Van Leussen, 1988)

Due to the extremely high sediment concentration, the fluid mud layer can contribute highly to the sediment transport, even though the flow velocity in the fluid mud layer is relatively small. An example from the mouth of the Rotterdam Waterway is given in figure 1.2. It shows (from 11.00 to 17.00 h) a moving layer of high concentration (> 40 g/l) with a sharp interface separating the suspended sediment above, which has relatively low concentrations (about 0.25 g/l). In four hours this layer is responsible for a transport of more than 60 tonnes of sediment per m width. This shows the importance of the transport of fluid mud layers (Van Leussen, 1988).

This report concentrates on the erosion of the interface by turbulence in the water layer (1), resulting in mass transport from a non-turbulent layer to a turbulent layer. This process is also defined as entrainment.

## 1.3 Purpose of the present work

As mentioned above, fluid mud occurrences are a nuisance to many authorities, because these can result in large siltation rates and because mud may be polluted. Hence, accurate modelling of the behaviour of fluid mud layers is necessary for morphological and ecological studies and for management. Some models for analysing the relevant processes already exist, but these are lacking physically accurate and correct mathematical formulae describing the behaviour of the fluid mud, e.g. the mobility of the mud, the entrainment behaviour, the damping of turbulence, the rheological properties related to the history of the mud.
In this report an attempt is made to analyze the entrainment process of fluid mud layers using two new numerical models. The main purpose is to compare the numerical results with experimental data or observations reported in the literature in order to verify the modelling assumptions and indicate the possible lackings.

## 1.4 Layout of the report

The development of a deposited mud layer is described in Chapter 2. Hereby the distinction in the processes of aggregation, settling, deposition and consolidation is made. Also other factors influencing these processes are discussed. Winterwerp et al. (1993) showed empirically that the entrainment process of a fluid mud layer of Western Scheldt mud resembles the (well-known) entrainment process of fresh/salt water layers. Winterwerp and Kranenburg (1994) carried out entrainment experiments with kaolinite. Properties of the cohesive sediments, however, have a great influence on the entrainment behaviour and little is known about this influence.
Therefore, the erosional processes due to entrainment for both fresh/salt water layers and fluid mud layers are reported in Chapter 3. The entrainment model of Kranenburg (1994) is presented in Chapter 4, followed by numerical simulations with this model and comparison with experimental data in Chapter 5. A two-layer fluid mud model is discussed in Chapter 6 to study the behaviour of fluid mud layers on a larger scale. In Chapter 7 numerical results are presented and the results are compared with observed mud layers in nature. A final discussion of results is given in Chapter 8. The appendices present the various results of the numerical simulation.

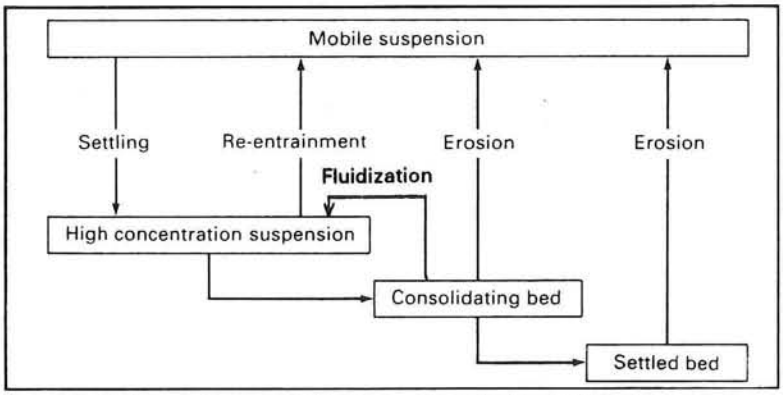


Figure 2.1: Fine sediment dynamic network (Parker, 1986)

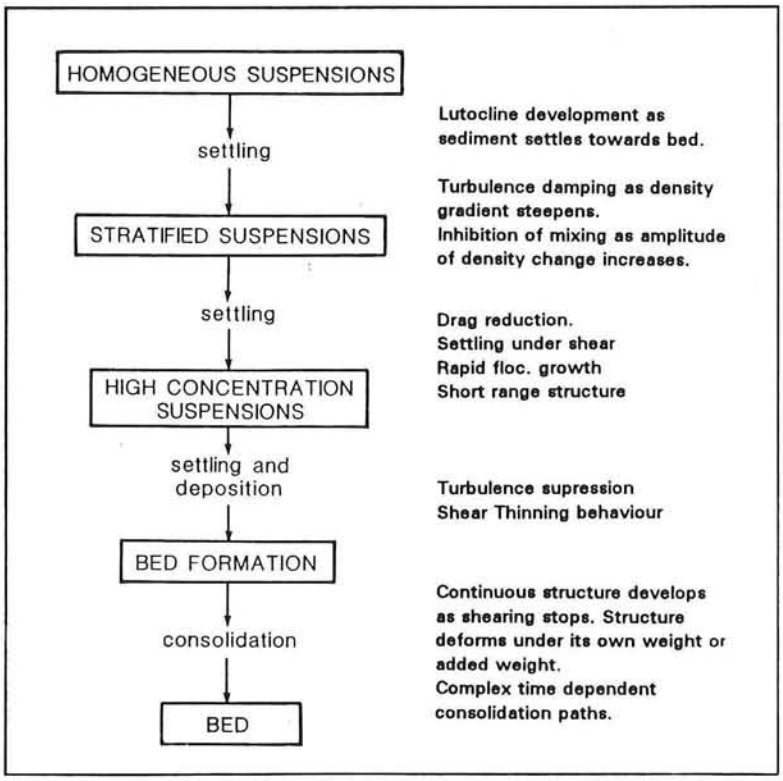


Figure 2.2: Forms of occurrence of fine sediment (Parker, 1986)

# 2.0 DEVELOPMENT OF A DEPOSITED MUD LAYER

*A continuous transport cycle of mud material can be observed in a natural environment. Aggregation, settling, deposition, consolidation and erosion are typically interlinked (figure 2.1). In this chapter the role of these processes in the development of a deposited mud layer is described (figure 2.2). Attention is also given to factors influencing these processes.*

## 2.1 Aggregation

### 2.1.1 Forces between clay particles

A sediment mixture of clay (particle size $< 2\mu$m) and silt (2 to 60 $\mu$m) possesses various degrees of cohesion. Cohesive sediments are composed of particles small enough and of specific area (area per unit mass of particles) large enough so that the surface physico-chemical forces may become much more important than their weight. Dominance of interparticle cohesion over gravitational forces increases with decreasing particle size. Thus the effect of cohesion on the behaviour of clays is much more pronounced than on silts, and in fact, cohesion in clayey muds is primarily due to the presence of clay-sized sediment, for a fraction of clay particles larger than about 10%.

Other binding forces are chemical forces (hydrogen bonds, cementation, coating of organic materials)

Essentially two kind of forces dominate the interaction between clay particles in a suspension, namely the attractive Van der Waals forces and repulsive electrostatic forces. The attractive Van der Waals forces ($V_A$) are generated by the mutual influence of the motions of electrons of the atoms and are independent of the properties of the fluid. They decay very rapidly with distance. The repulsive forces ($V_R$) are due to ion clouds of similar charge repelling each other. Positive ions in the fluid form a cloud of ions around the negatively charged clay particles (double layer, figure 2.3). The net effect of these physico-chemical interparticle forces can be repulsion or attraction depending on the relative strengths (number of positive ions) and the distance between the particles, see figure 2.4.
In case the net effect is repulsion, particles tend to stay dispersed in suspension and, since their settling velocities are very low, very high concentrations can be maintained in suspension even at small flow velocities.
In case the net force is attractive, particles are bond together forming aggregates (known as flocs) in a process called flocculation. The size and settling velocity of flocs (aggregates) are much larger than those of individual particles. In a suspension of fine cohesive sediments, the floc becomes the basic settling unit. Its average size and the size distribution depend on the physico-chemical properties of the sediment and water and on the flow conditions (De Wit, 1992).

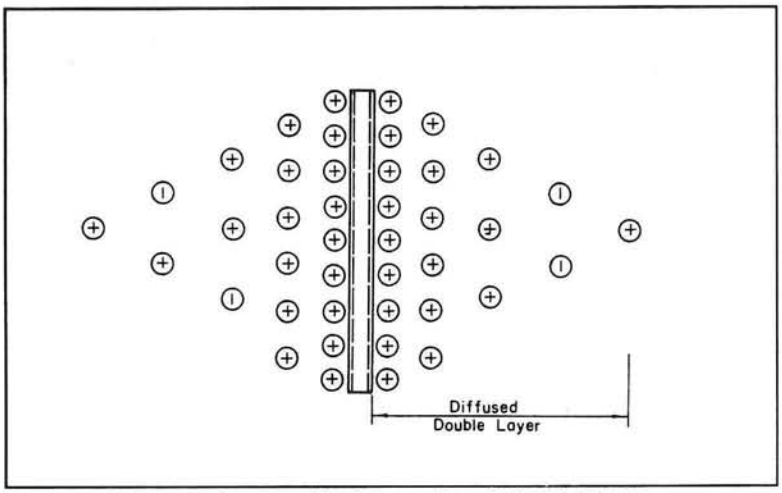


Figure 2.3: The double layer (De Wit, 1992)

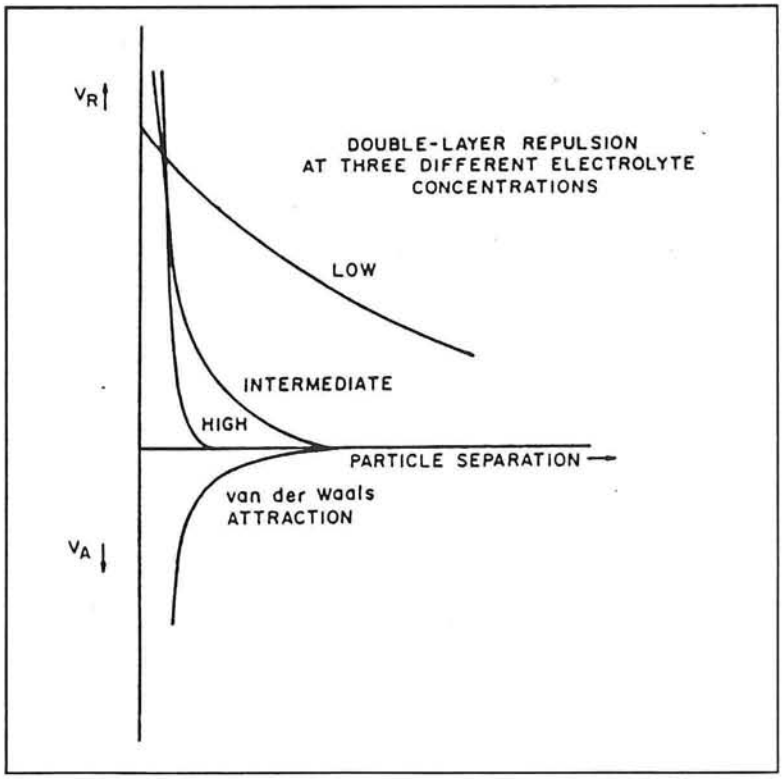


Figure 2.4: Electrical forces as a function of distance between particles at three concentrations (De Wit, 1992)

### 2.1.2 Floc forming mechanisms

Flocculation occurs when the net force between clay particles is attractive. Then the sediment particles do not behave as individual particles but tend to stick together forming flocs (aggregates).

For the binding of the particles, which form the aggregates, two conditions must be fulfilled:

a. Collisions between the particles: The particles have to be brought close enough to each other.
b. Cohesive properties of the particles: A certain percentage of the collisions must result in adhesion of the particles.

The three most important mechanisms for particle collisions are:

1. Brownian motion of the particles due to the random bombardment by the thermally agitated water molecules; the number of collisions is linearly proportional to the concentration.
2. Turbulent mixing due to the presence of velocity gradients within the suspending liquid.
3. Differential settling of the suspended particles, because the larger particles have larger settling velocities and may therefore 'fall' on the smaller particles.

Aggregates formed by Brownian motion have a ragged structure, are weak and easily dispersed by shearing or easily crushed in a deposit. The mechanism of aggregation by velocity gradients is very important in the mixing zone of an estuary. The aggregates formed by velocity gradients tend to be spherical and are stronger than those formed by other mechanisms of collisions. The mechanisms of differential settling contributes to the rapid clarification of water during near-slack periods in mixing zones where the concentration is high. There is little stress on aggregates colliding under such conditions, and the resulting aggregates are ragged, weak and have low density (Van Leussen, 1988; Metha, 1973; Parchure, 1984; Van Rijn, 1993).

Besides particle collision mechanisms other factors affecting flocculation are:

*1. Particle size*
A small particle size in combination with a large concentration greatly intensifies the flocculation process because of the relatively small distance between the particles.

*2. Temperature*
A low temperature also enhances the flocculation process because the double layer repulsive energy decreases in magnitude, thus a decreasing repulsion.

*3. Organic material*
Organic materials in and on the flocs significantly intensify the flocculation process, because of the binding properties of some organic materials. The binding forces become larger due to the presence of organic material (biogenic forces) and the flocs become larger.

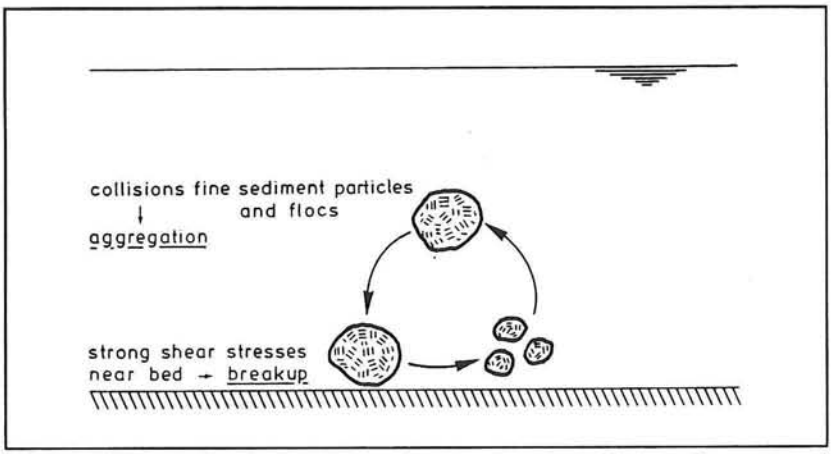


Figure 2.5: Schematic picture of disruption and aggregation of mud flocs (Van Leussen, 1988)

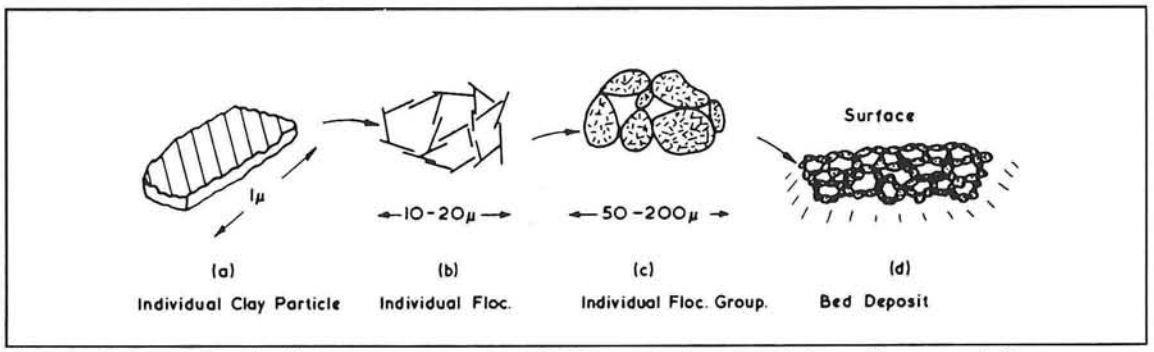


Figure 2.6: Typical arrangements and sizes of clay particles, flocs and floc groups (Van Leussen, 1988)

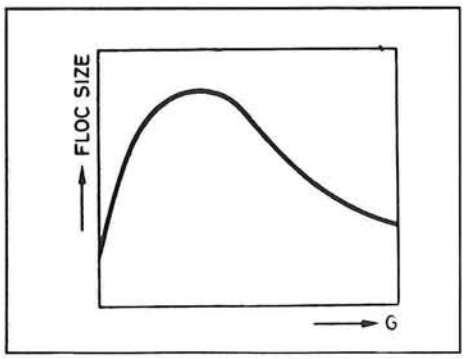


Figure 2.7: Effect of turbulence on floc size (Van Leussen, 1988)

*4. Salinity*
An increase in salinity results in a compression of the cloud of positive ions around the sediment particle, and thus in a stronger decrease of the repulsive forces with distance and ultimately in enhanced flocculation of colliding particles because the Van der Waals force then is dominating. Van Leussen (1988) reports for clay minerals kaolinite and Illite that salinity contents above 2 ppt did not produce an increase of flocculation; for clay mineral Montmorillonite there still is an increase of flocculation at higher salt concentrations.

*5. Turbulence*
Under the influence of turbulence there is a continuous process of flocculation and break-up resulting in a dynamic equilibrium of the distribution of floc size, density and strength, see figure 2.5. Break up of the flocs is caused by shearing forces in the fluid. When these forces are larger than the strength of the flocs, the flocs are broken into smaller flocs or particles. Large shearing forces exist close to the bottom (where the velocity gradients are largest) and in small-scale eddies everywhere in the fluid.

When there is no turbulence present the flocs may grow to larger sizes due to differential settling collisions. However, as the flocs get larger they fall faster until the fluid shear on the flocs becomes greater than the floc strength resulting in break up. Ongoing flocculation leads to increasing floc sizes and decreasing density of the flocs (consisting of sediment, fluid, organic materials).

In general three stages of flocculated suspensions may be considered (Parchure, 1984), figure 2.6:
1) a small cluster of primary clay particles referred to as a floc [b];
2) floc aggregates formed by flocs which may join together [c];
3) an aggregate network formed by floc aggregates [d].

### 2.1.3 Floc destroying mechanisms

The floc size is influenced by turbulence in two opposing ways:
- An increase in turbulence intensity results in an increase of the number of collisions per unit time and hence in larger flocs, as shown in section 2.1.2.
- An increase in the turbulence intensity results in an increase in turbulent shear stresses in the flow. When these are larger than the strength of the flocs, the flocs will be broken down, so that the turbulence can result in a limitation of the floc size.

This is schematically shown in figure 2.7, in which $G$ is the root mean square (rms) velocity gradient due to turbulence (Van Leussen, 1988).

Most studies on flocculation have focused on particle aggregation without considering floc breakage. Proper characterization of floc disruption is an important problem, because in estuaries the turbulent flow will limit the floc growth and the turbulent structure will determine the maximum floc size.

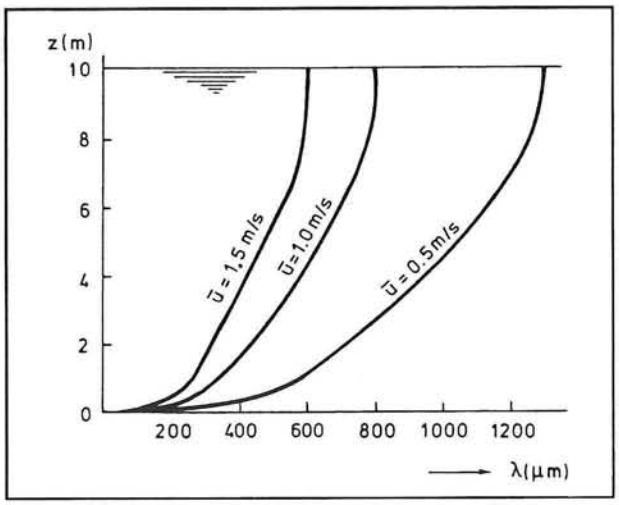


Figure 2.8: Kolmogorov-microscale (Van Leussen, 1988)

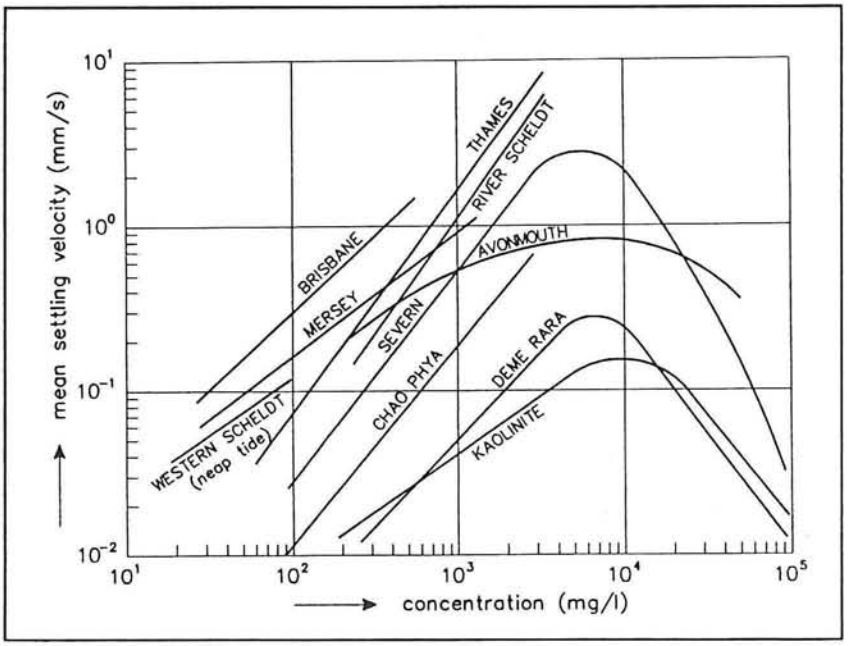


Figure 2.9: The influence of sediment concentration on the settling velocity (Van Rijn, 1993)

An important factor in floc breaking is the ratio of the diameter of the floc, $d_f$, to the size of the dissipating eddies, $\lambda$, in the turbulent flow. Kolmogorov (1941) defined the microscale of turbulence, based on dimensional reasoning, as:

$$\lambda = \left(\frac{\nu^3}{\varepsilon}\right)^{\frac{1}{4}}$$

where $\nu$ = kinematic viscosity
$\varepsilon$ = energy dissipation per unit mass and time

Kolmogorov proposed a cascade of turbulent energy from energy-containing eddies of size $L$ to energy-dissipating eddies of size $\lambda$, with a universal equilibrium range of the energy density spectrum between $L$ and $\lambda$. The requirement that $L \gg \lambda$ is satisfied if the Reynolds number $(\bar{U}L)/\nu$ is large, as will be the case in normal turbulent tidal flows.
For $\lambda \ll d_f \leq L$ inertial effects dominate. The floc with diameter $d_f$ will be ruptured by the turbulent velocity fluctuations across the floc, when the eddy scales are comparable to the floc size scales and when the forces exceed the strength of the aggregate.
For $d_f < \lambda \ll L$ inertial effects can be ignored and viscous effects dominate.
An impression of the distribution of the Kolmogorov-microscale for turbulence in an open channel flow is given in figure 2.8. (Van Leussen, 1988)

## 2.2 Settling

### 2.2.1 Settling velocity

An important parameter in modelling the mud transport in estuaries is the settling velocity $w_s$ of the mud flocs. For spherical particles and low particle Reynolds number ($Re_p < 1$) a good estimate of the settling velocity is obtained by Stokes' law:

$$w_s = \frac{g}{18\nu}\frac{\rho_d - \rho_w}{\rho_w} d^2$$

However, it is not easy to use this formula in predicting the settling velocities of mud flocs, because the floc density and drag coefficient are strongly dependent on the floc size. The exponent $n$ in $w_s :: d_f^n$ was measured and found to be in the range of 0.4-1 for mud flocs. Other experiments showed a significantly greater settling velocity than follows from Stokes' law. These deviations, especially for smaller particles, can be attributed to a non-linear viscous drag reduction. However, the physical mechanisms responsible for this reduction are not well understood.

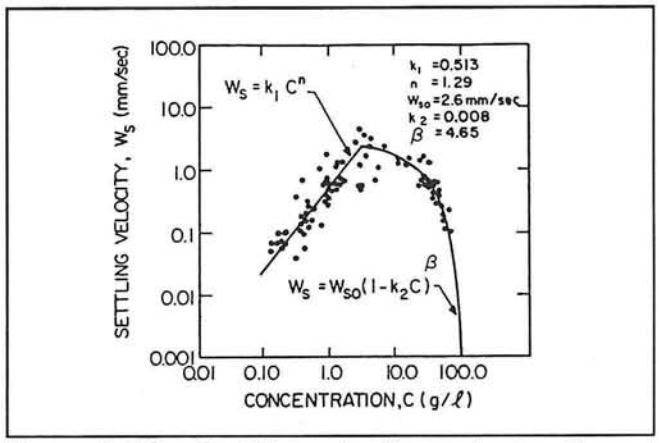


Figure 2.10: Settling velocity against sediment concentration (Thorn, 1981)

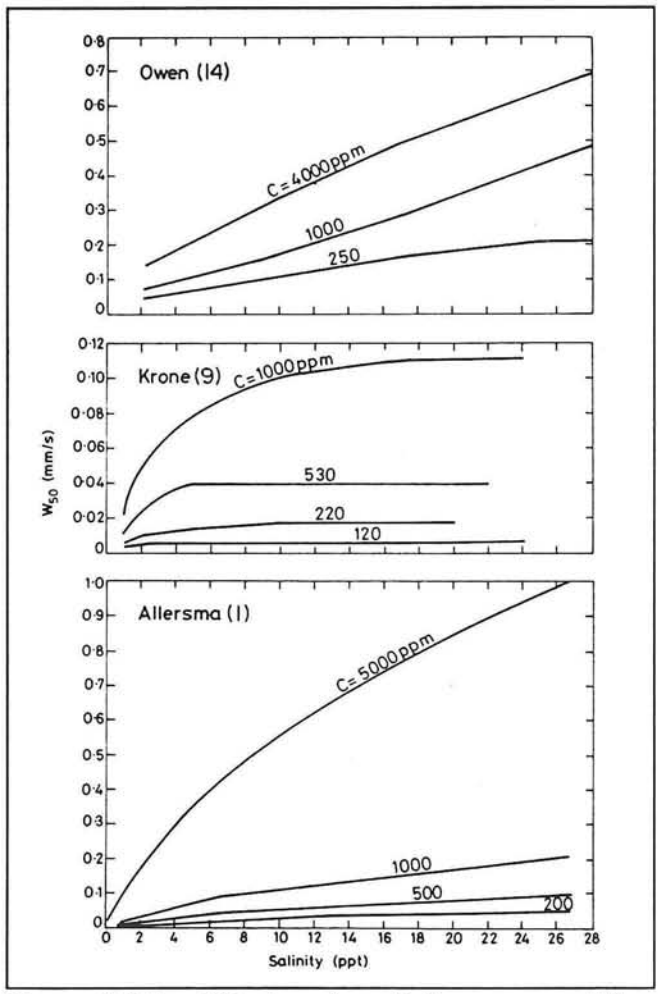


Figure 2.11: Effect of salinity on settling velocity (Burt, 1986)

### 2.2.1 Factors influencing the settling velocity

Analysis of laboratory experiments and field measurements has shown that parameters influencing the settling velocities of the aggregates are a.o. the sediment concentration, salinity, turbulence, water depth, temperature.

*Influence of concentration* (figure 2.9)
The suspended sediment concentration is the most important factor influencing the aggregation process and thus the settling velocities of the aggregates. Three concentration ranges can be discerned, see figure 2.10 (Krone, 1962):

1. At very low concentrations (0-10 mg/l), the rate of aggregation is negligible and the settling velocity, $w_s$, does not depend on the concentration.
2. At moderate concentrations (about 10-10000 mg/l), aggregation causes $w_s$ to increase with the concentration. The settling velocity can be described by the empirical formula

$$w_s = KC^m$$

   where $C$ is the suspended fine sediment concentration by mass, $K$ and $m$ are coefficients, depending among other factors upon the type of sediment, the salinity and the turbulence. $m$ has been found to vary from 1 to 2, with a mean of 1.3.
3. At high concentrations (> about 10000 mg/l), the fluid must escape upward past the flocs and through the interstitial spaces for settling to occur. Settling is thus hindered, and $w_s$ decreases with increasing concentration. The following relationship is generally used in this range

$$w_s = w_{s0}(1-k_2C)^{\beta}$$

   where $w_{s0}$ = settling velocity of individual particles
   $k_2$ ≈ 0.01, depending on sediment composition
   $\beta$ ≈ 5 (Richardson and Zaki, 1954)

At very large concentrations the vertical water velocity can be so large that the upward fluid drag forces on the flocs become nearly equal to the downward gravity forces resulting in hardly any vertical movement of the flocs. This state, which occurs close to the bed, is generally called fluid mud.
In the laboratory the hindered settling velocity can be quite accurately determined from settling tests by measuring the subsidence of the sediment-fluid interface. This is not possible for lower concentrations, because no well-defined interface can be observed.

*Influence of salinity*
Laboratory experiments showed that as a consequence of the influence of the salinity on the flocculation process, the settling velocity is greatly affected by this parameter, depending on the mineralogical properties of the sediment and the chemical properties of the water. Above a certain value of the salinity (of about 10 ppt), however, there is not much effect for sediment concentrations smaller than 1000 mg/l. For sediment concentration larger than 1000 mg/l an increase in the settling velocity with the salinity can be observed, see figure 2.11 (Burt, 1986).

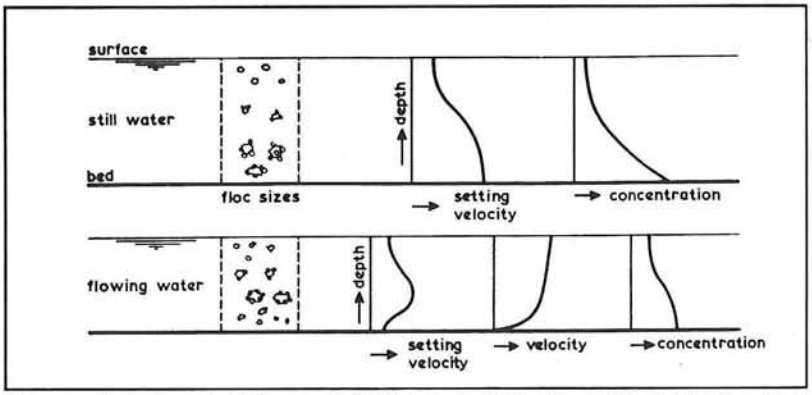


Figure 2.12: Settling and flocculation in still and flowing water (Van Leussen, 1988)

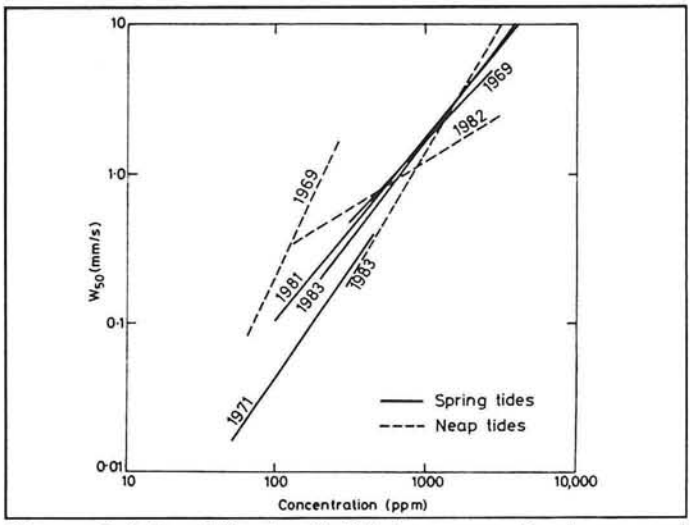


Figure 2.13: Effect of tidal range: Springs and Neaps (Burt, 1986)

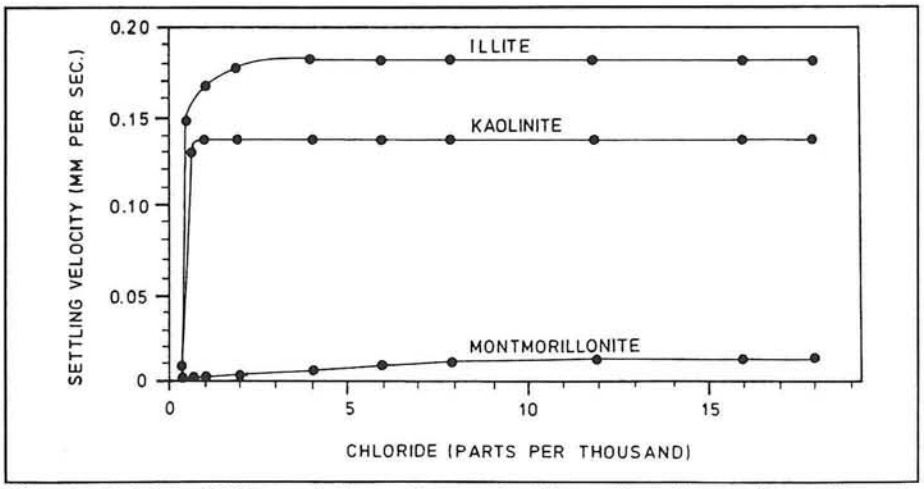


Figure 2.14: Differential settling velocities of various clay minerals (Van Leussen, 1988)

For very high salinity the cohesive behaviour can disappear by substitution of ions on particle surfaces.

*Influence of waterdepth*
Owen (1970) found that a minimum height of 2 m was required to achieve maximum flocculation and settling velocities due to differential settling. Consequently, in natural conditions the settling velocities in the lower layers will be larger than those in the upper layers, and will be maximal close to the bed for heights ≤ 2 m.

*Influence of flow*
The settling process in a laboratory column is representative of the settling process during the slack water period (low velocities) of a tidal cycle in an estuary. At higher flow velocities the settling velocities near the bed may be significantly reduced due to the presence of disruptive shear forces (velocity gradients) in the boundary layer, see figure 2.12. Larger flocs will be break up to form smaller flocs, the latter being suspended in the flow (Van Leussen, 1988).
There is no consistent effect of the tidal range on the settling velocity. Figure 2.13 gives an impression of the effect of the tidal range for the Thames. The flocs are mainly affected by eddy scales comparable to the floc size scales. These smaller eddy scales will be present during nearly all tidal conditions with exception of the slack tide periods (Burt, 1986).

*Influence of temperature*
According to Lau (1994), the settling velocity decreases with increasing temperature. An explanation is, that the repulsive forces between particles increase, while attractive forces remain the same. Therefore, the flocs are weaker, resulting in less flocculation and smaller floc sizes. This effect has a larger influence on the settling velocity than the decrease in the viscosity of the fluid.

*Influence of mineralogical properties*
The settling velocity is also influenced by the mineralogical properties of the sediment, because of their effects on the flocculation process. As each sediment has another mixture of mineral compounds, this means that for each mud the settling velocity has to be determined, see figure 2.14 (Van Leussen, 1988) .
Also properties as organic content can affect the settling velocity significantly (coating).

*Influence of turbulence*
Turbulence affects the flocculation, and therefore the settling velocity, in two opposing ways (as mentioned in section 2.1.3):
1. Turbulence increases the number of collisions between the particles, thus resulting in larger flocs and larger settling velocities.
2. Turbulence results in turbulent shear stresses, thus limiting the floc size and settling velocity.

*Influence of time*
Also the time scale acts upon the flocculation. A certain time period is necessary for flocculation to occur, depending on the situation.

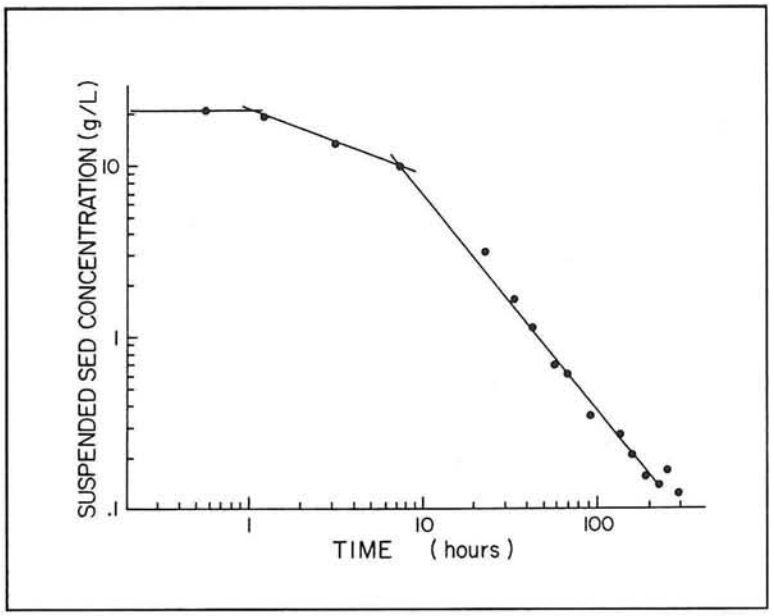


Figure 2.15: Deposition experiments of Krone (1962), $C_o$ = 20 kg/m$^3$ (Krone, 1962)

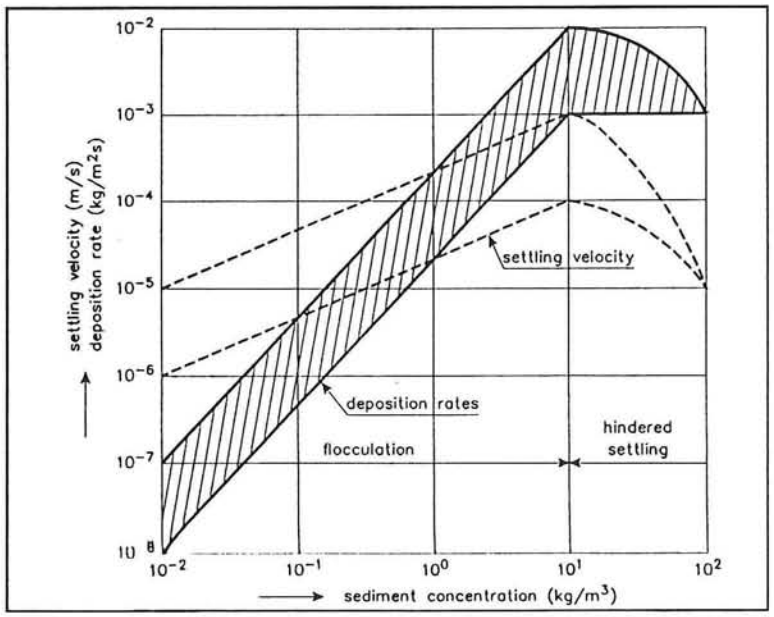


Figure 2.16: Deposition rate as a function of concentration (Van Rijn, 1993)

## 2.3 Deposition

### 2.3.1 Deposition phases

The time rate of decrease of suspended sediment mass per unit bed area, $m$, under steady turbulent flow is given by:

$$\frac{dm}{dt} = -p w_s C$$

where $p[0,1]$ is the probability of deposition, $w_s$ is the settling velocity and $C$ is the near-bed suspended sediment concentration.
The settling velocity and the probability of deposition, $p$, depend on the time-mean value of the bed shear stress, $\tau_b$, and on a critical shear stress for deposition, $\tau_{cd}$, which depends on the sediment-water composition. Krone (1962) found:

$p = 1 - (\tau_b/\tau_{cd})$ when $\tau_b < \tau_{cd}$
$p = 0$ when $\tau_b \geq \tau_{cd}$

The critical shear stress for deposition is the bed shear stress above which no deposition occurs.

Generally, the settling velocity and the probability of deposition are also dependent on the frequency of interparticle collisions, and therefore on the concentration.

Three distinct stages of the deposition processes can be noticed, depending on the mud concentration (Van Rijn, 1993):

1. C > about 10 g/l (depending upon the type of sediment-fluid mixture)
   This type of settling is characterized by the formation of a continuous aggregate network through which the interstitial water must escape upward for settling to occur. The settling velocity will be relatively small near the bed and relatively large at the upper layers resulting in the formation of a near-bed fluid mud layer with increasing sediment concentrations. The thickness of the fluid mud layer will increase as long as the deposition rate at the upper side of the layer is larger than the consolidation rate at the bottom side.
2. about 10 g/l > C > about 0.1 g/l
   The deposition process in this concentration range is dominated by flocculation effects, because the concentration is high enough for interparticle collision.
3. C < about 0.1 g/l
   In this concentration range the mutual particle interference is relatively weak and $w_s$ may be assumed to be independent of $C$. For this range the concentration can be described by a simple exponential decay law implying suspension dilution by deposition. Deposition in this stage could be increased significantly by intensifying flocculation.

Figure 2.15 shows the effect of different deposition stages in case of an initial mud concentration of 20 kg/m$^3$ and a flow velocity of about 0.1 m/s. A period of about 10 hours with relatively slow deposition (1) and a period of about 100 hours with more rapid deposition (2) can be observed. A period of long duration with a very slow deposition (3) occurs for larger times.

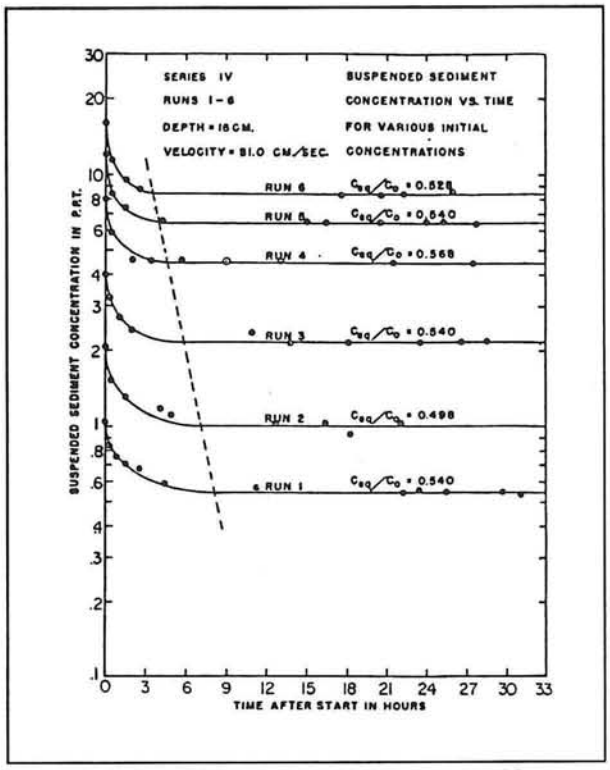


Figure 2.17: Variation of sediment concentration with time (Parteniades, 1973)

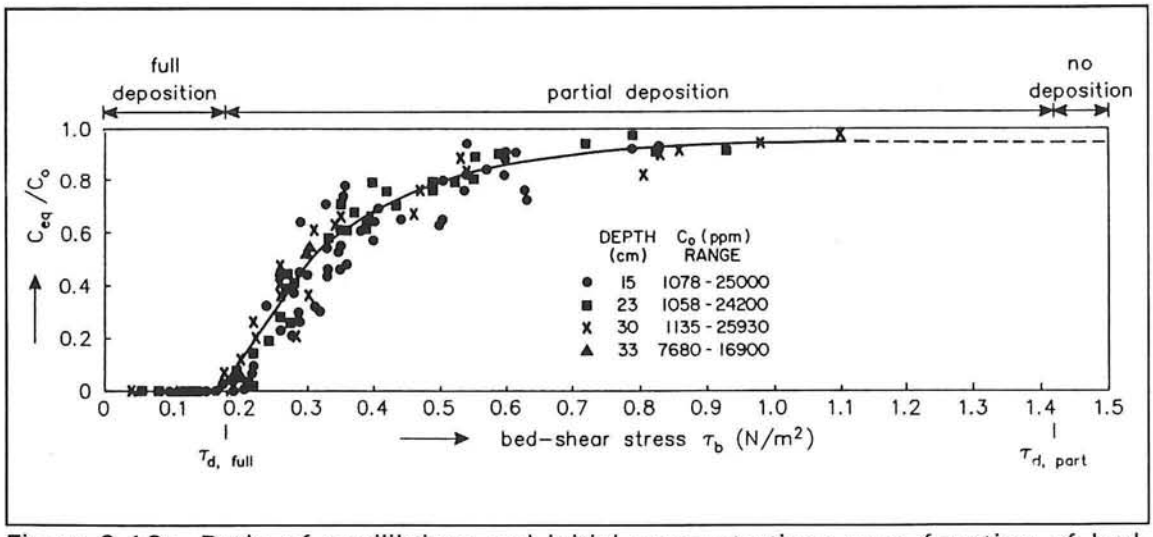


Figure 2.18: Ratio of equilibrium and initial concentrations as a function of bed-shear stress (Van Rijn, 1993)

The maximum deposition rate ($dm/dt = w_s C$) will occur at low flow conditions. Figure 2.16 shows the (maximum) deposition rate as a function of concentration, based on a settling velocity in the range of $10^{-6}$ to $10^{-3}$ m/s. The deposition rate is largest in the flocculation range and smallest in the hindered settling range, as can be observed.
At higher flow velocities the deposition rates will be reduced due to the effect of turbulence, resulting in a smaller deposition rate.

### 2.3.2 Threshold for deposition

Figure 2.17 shows an example of suspended sediment concentration - time curves for constant flow conditions but variable initial concentration, $C_0$ (Partheniades, 1973). After a short period of rapid deposition, it is observed that the ratio $C_{eq}/C_0$ remains practically constant and independent of $C_0$. This leads to the conclusion that a given flow can maintain in suspension a constant fraction of a particular sediment regardless of the absolute value of the concentration. $C_{eq}$ represents, therefore, that part of sediment which can never form flocs with sufficiently strong bonds to reach and join the bed permanently.
When the bed shear stress was varied, the equilibrium concentration was found to be dependent on the applied bed-shear stress $\tau_b$, the type of sediment material and the initial concentration $C_0$. For various initial concentrations $C_0$ there is a constant ratio $C_{eq}/C_0$ at a constant bed-shear stress $\tau_b$.

The curves can be interpreted by assuming that there are two groups of flocs: The first have sufficiently strong bonds to resist the disruptive near-bed stresses and will be able to reach the bottom and form strong bonds with deposited flocs. The second does not have sufficiently strong bonds. They will be broken down before reaching the bed resulting in resuspension or they are eroded very quickly after being deposited because of the relatively weak bond between the floc and the bed. The ratio $C_{eq}/C_0$ represents the percentage of the flocs that remains in suspension. These flocs have a floc strength smaller than the bed-shear stress. The ratio $C_{eq}/C_0$ which depends solely on the $\tau_b$-value is shown in figure 2.18.
The difference $1\text{-}C_{eq}/C_0$ represents the portion of the sediment that deposits permanently on the bed.

It follows that deposition is predominant when the bed-shear stress $\tau_b$ falls below a critical value for deposition $\tau_{cd}$. Based on the work of Mehta and Partheniades, two critical bed-shear stresses for deposition can be distinguished: $\tau_{cd,full}$ and $\tau_{cd,part}$.
The minimum bed-shear stress for full deposition ($\tau_{cd,full}$) is defined as the bed-shear stress below which full deposition of the sediment flocs will occur. The maximum bed-shear stress for deposition ($\tau_{cd,part}$) is defined as the bed-shear stress above which no deposition of the sediment flocs will occur. For a bed-shear stress in the range between $\tau_{cd,full}$ and $\tau_{cd,part}$ partial deposition may occur (see figure 2.18).

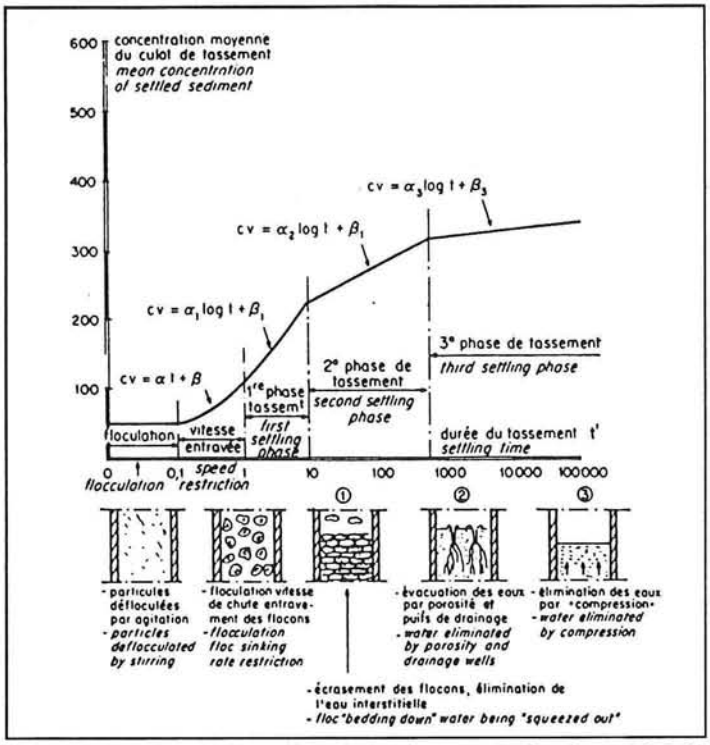


Figure 2.19: Consolidation phases (Migniot, 1989)

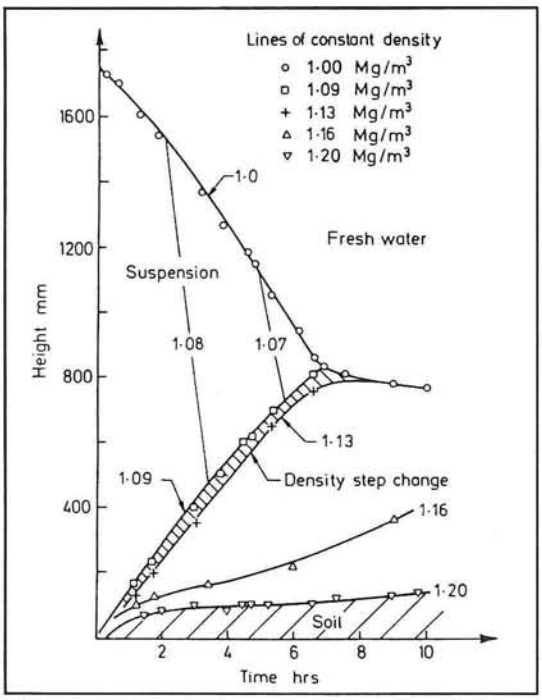


Figure 2.20: Changes of density with time (Sills, 1986)

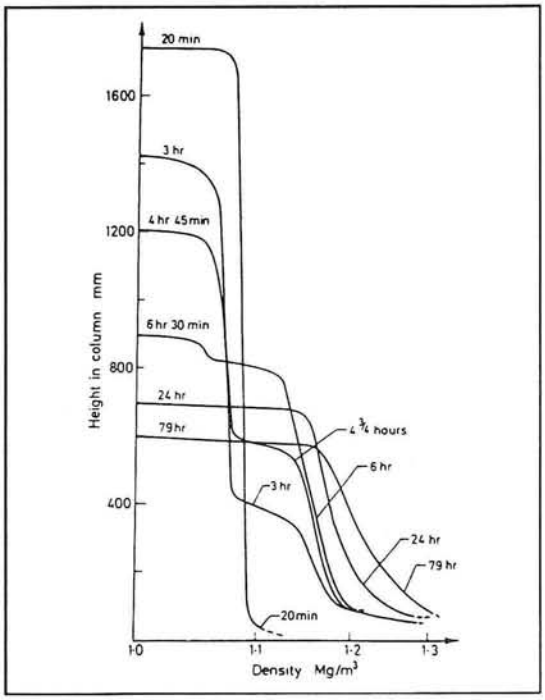


Figure 2.21: Density profiles (Sills, 1986)

## 2.4 Consolidation

Consolidation is a process of floc compaction under the influence of gravity forces with a simultaneous expulsion of pore water and a gain in strength of the bed material. The rate of deposition (from the suspension) minus the rate of consolidation of the bed is equal to the increase in the level of the fluid-bed interface.

Consideration of the consolidation of cohesive sediment beds is essential in modelling mud transport because:

a. The susceptibility to erosion of a consolidating bed decreases with time due to the continual increase in bed shear strength.
b. The accompanying density increase changes the mass of sediment eroded per unit bed thickness.

In general, three consolidation phases can be identified, see figure 2.19 (Migniot, 1989):

1. Initial phase (days)
   The process consists of hindered settling and consolidation. The flocs in a freshly deposited layer are grouped in an open structure with a large pore volume. The weakest bonds are broken down first and the network gradually collapses. The bed surface drops with time $t$. Stationary fluid mud layers develop a certain strength, as a continuous network is formed, within about half a day.
2. Secondary phase (weeks)
   The pore volume between the flocs is further reduced. Small thin vertical pipes (drains) are formed allowing the pore water to escape.
3. Final phase (years)
   The pore volume inside the flocs is further reduced and the flocs break up.

Figure 2.20 shows the development of various density values with time, after putting a mud suspension with an initial concentration of 140 g/l (initial density 1.09 $Mg/m^3$) quickly into a settling column. A transition from suspension to structured phase occurs between concentrations of 140 g/l and 200 g/l (densities 1.09 $Mg/m^3$ and 1.13 $Mg/m^3$). The matching density profiles for different moments are presented in figure 2.21 (Sills, 1986).

Factors affecting the consolidation process are (Van Rijn, 1993):

*Initial thickness of the mud layer*
A thin layer of mud consolidates faster than a thick layer with the same initial concentration, because the pore water in the thick layer must travel a longer distance to the mud surface. In a thick layer the material is however more compacted (higher density) in its lower part after the same consolidation period (for large $t$) due to the larger overburden. A thicker final bed layer resulting in a lower dry density can occur due to the presence of organic materials.

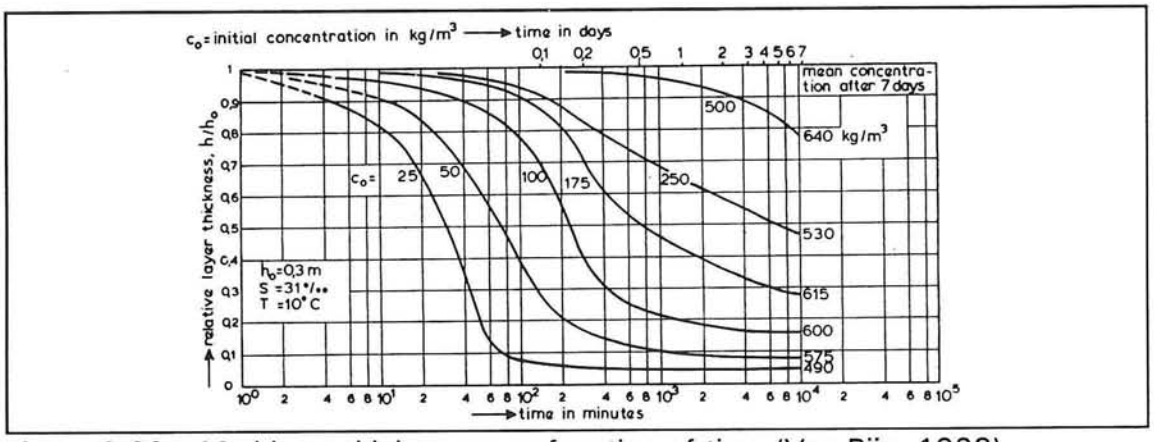


Figure 2.22: Mud layer thickness as a function of time (Van Rijn, 1993)

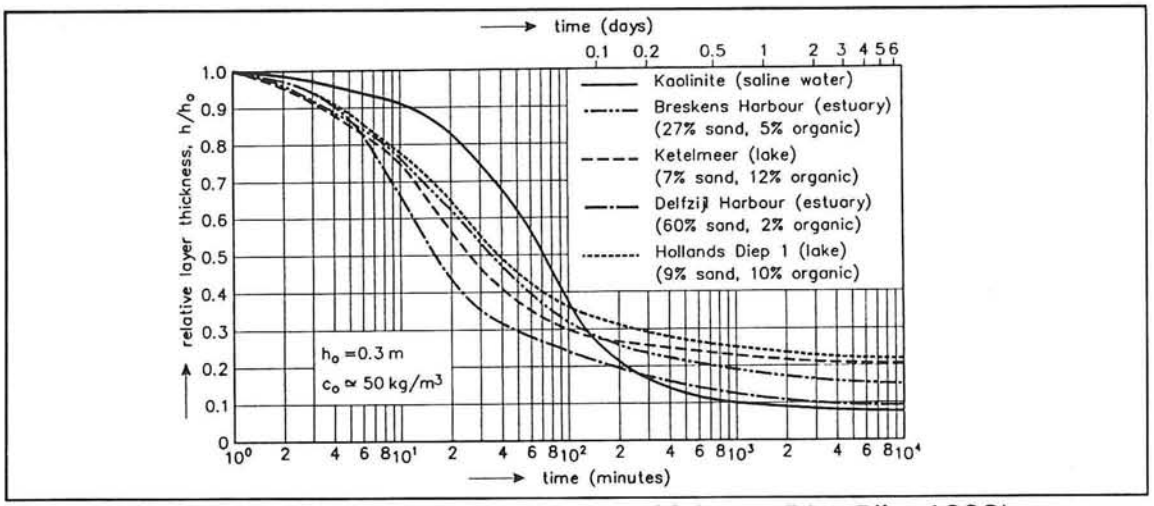


Figure 2.23: Kaolinite and natural mud layers thickness (Van Rijn, 1993)

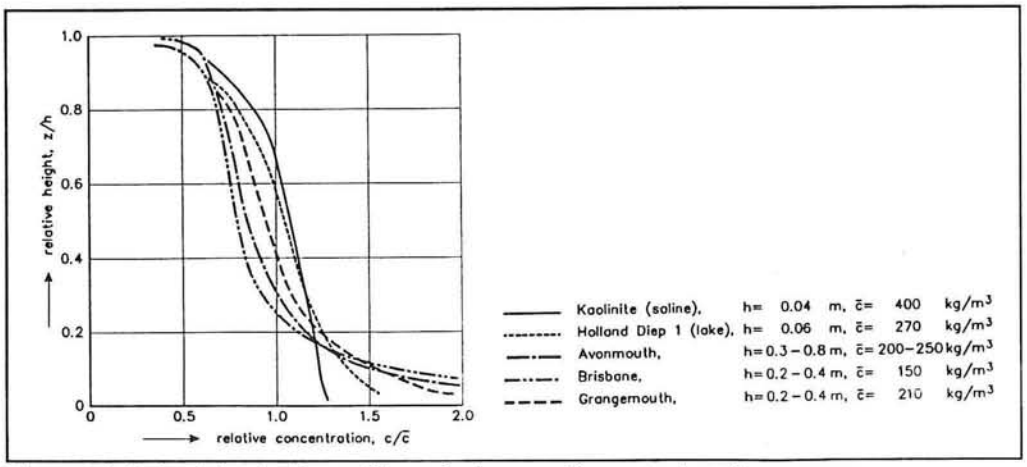


Figure 2.24: Vertical profile of dry sediment density (Winterwerp et al., 1992)

*Initial concentration of the mud layer*
A higher initial concentration will give a larger final bed thickness and thus a larger consolidation time. The final density also increases with increasing initial concentrations because more dense flocs are formed (figure 2.22).

*Permeability of the mud layer, depending on sediment composition and size, content of organic material, salinity, water temperature*
The consolidation behaviour of each natural mud differs because of the different size ranges and the content of organic material, see figure 2.23. Gas bubbles e.g. may escape during the initial consolidation phase when the material strength is low, thereby retarding the consolidation process. During later stages (or deeper layers) with increasing material strength, the gas bubbles may remain in the bed and affect the consolidation process, depending on the permeability of the bed material.

For information on the vertical distribution of the sediment concentration of consolidated mud layers see figure 2.24. Thin mud layers show higher densities in the upper layers ($z > 0.5$) than thick mud layers.
Salinity has no marked influence on the density distribution.
The concentration distribution is also influenced by the particle size distribution. Large particles settle fast and form a high-density layer near the bottom.

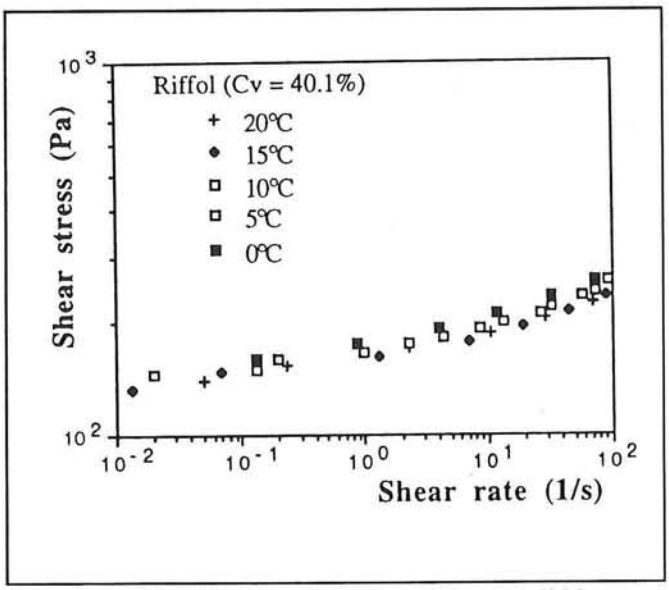


Figure 2.30: Flow curves for different temperatures (Coussot, 1994)

6. *Temperature*
Results of tests made in the temperature range of $0^0$-$20^0$ C are presented in figure 2.30. The flow curves are very close to each other and it seems to be that a small but consistent variation is possible to distinguish which would be due to a change in temperature. So in these ranges of shear rate and temperature, the temperature changes on viscosity is insignificant (Coussot, 1994).

According to Lau (1994) a higher water temperature causes the double layer to grow thicker, corresponding to a decrease in strength.

# 3.0 EROSIONAL PROCESSES DUE TO ENTRAINMENT

*The previous chapter described the development of a deposited mud layer. The nature of the settled and consolidated material mainly determines the modes of erosion. The different erosion processes are described in Section 3.1. The erosional processes occurring to a fluid mud layer are further considered, first by regarding the theoretical background of entrainment in Section 3.2. Turbulent entrainment in stratified fluids is the subject of Section 3.3, which is followed by a study on erosion of fluid mud due to entrainment in Section 3.4.*

## 3.1 Modes of erosion

The resistance to erosion depends on a number of factors, including sediment composition, composition of pore fluid and eroding fluid and the degree of consolidation of the deposit. The deposit itself may be in the form of a static, high density suspension (without an yield stress) or a bed (with a measurable yield stress). The bed may be soft, partially consolidated, with a high water content, or a more dense fully consolidated bed, as described in chapter 2. The modes of erosion vary both with the magnitude of the bed shear stress and the nature of the deposit.

Three modes of erosion have been identified:
1. *Aggregate-by-aggregate erosion of a bed (also referred to as surface erosion)*
2. *Mass erosion of a bed*
3. *Re-entrainment of a high density suspension*

The rate of erosion, $\varepsilon$ (mass of sediment eroded per unit bed area per unit time), can be expressed as, $\varepsilon = \varepsilon(\tau_b - \tau_s, \nu_1, \nu_2 .. \nu_i)$, where $\tau_b - \tau_s$ is the bed shear stress in excess of the cohesive bed strength with respect to erosion, $\tau_s$, and $\nu_1, \nu_2 .. \nu_i$ are erosion resistance specifying parameters.

Surface erosion is a one by one removal of aggregates and typically occurs at low to moderate values of the excess shear stress, $\tau_b - \tau_s$. This form of erosion is prevalent in estuaries subject to currents of low to moderate strength. Quantification of the range of $\tau_b - \tau_s$ is highly dependent on the degree of resistance provided by the bed, which is site-specific.
Mass erosion occurs when $\tau_b - \tau_s$ becomes large, or when rapidly accelerating flows occur, the bed may fail at some plane below the surface and clumps of material are torn out. Mass erosion can be dominant in areas of strong tidal currents and also under storm-generated flows and waves.
Erosion of a high density suspension is called re-entrainment. During the process of re-entrainment, the suspension density increases with the progress of erosion. Turbulence is essential for entrainment to occur. Turbulent eddies entrain sediment directly from the bed, or remove material from breaking internal waves. As the flow velocity increases the rate of entrainment can become quite high. Re-entrainment occurs for instance at times following slack water and also when wind-generated waves superimposed on tidal currents act on recently formed fluid mud.

In the present work re-entrainment of a high density suspension (3) is examined.

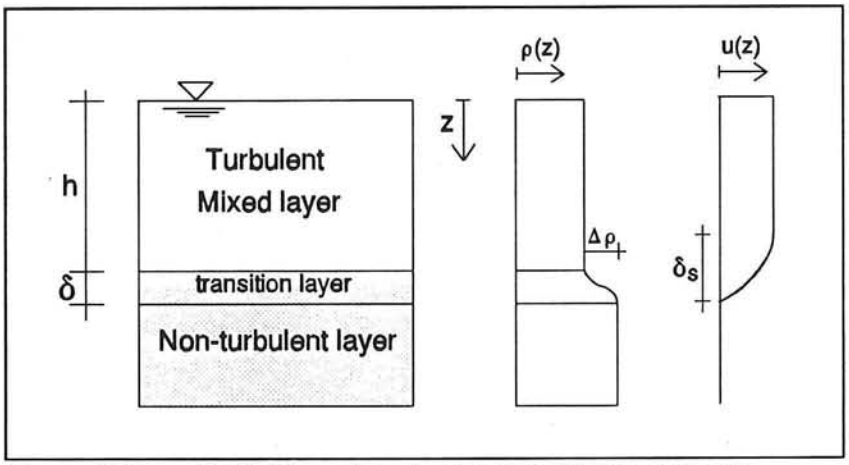


Figure 3.1: Definition sketch of a two-fluids system

## 3.2 Theoretical background

In order to understand the process of entrainment of a fluid mud layer, it is necessary to review the theoretical background upon which entrainment definitions are based.

The analysis can be set up by considering a two-fluids system with a turbulent mixed layer of thickness $h$ above a predominantly non-turbulent layer, with a higher density, as shown in figure 3.1. The two layers are separated by a density interfacial layer of thickness $\delta$, in which shear production and vorticity are concentrated. The vertical density profile, $\rho(z)$, where $z$ is the vertical coordinate measured positive downward, is characterized by a large concentration gradient (lutocline) within the transition layer. The horizontal velocity profile, $u(z)$, is characterized by a shear layer of thickness $\delta_s$.

For a stable stratification, the non-stationary, turbulent kinetic energy balance for the upper water (mixed) layer with mean flow in the longitudinal direction can be written as:

$$\frac{\partial q}{\partial t} \approx \overline{u'w'}\frac{\partial \bar{u}}{\partial z} - \frac{g}{\rho}\overline{w'\rho'} - \varepsilon \qquad (3.1)$$

(I) (II) (III) (IV)

where

$$q = \tfrac{1}{2}(\overline{u'^2} + \overline{v'^2} + \overline{w'^2}) \qquad (3.2)$$

$q$ = the turbulent kinetic energy per unit mass (TKE)
$u'$ = instantaneous turbulent fluctuation of the longitudinal velocity $u$
$v'$, $w'$ = velocity fluctuations in the lateral and vertical directions
$\rho'$ = instantaneous turbulent fluctuation of $\rho$
$\varepsilon$ = rate of energy dissipation per unit mass

Overbars represent turbulence averaging.
Viscous stress-related terms have been ignored. In addition, two terms that have not been included in eq. (3.1) are flux divergences arising from kinetic energy transport and pressure transport. Atkinson et al. (1984) have considered their role in entrainment, and have shown that they can be functionally scaled in the same way as the rate of production (source term) of TKE by shear (term (II)). For simplification they are not included in eq. (3.1).

In eq. (3.1), the rate of change of TKE, $\partial q/\partial t$, (I) is shown to arise from:
- shear production, i.e. the transfer of kinetic energy from the mean to the turbulent motion, (II)
- gravity (buoyancy) work, i.e. conversion of potential to kinetic energy, (III)
- viscous dissipation, i.e. the transfer of TKE into internal energy of the fluid (heat), (IV)

In stable stratification, term (III) is positive so TKE is reduced and the turbulence is damped while the potential energy of the system increases. In unstable stratification, turbulent energy is produced at the expense of potential energy.
Term (IV) is always relatively large.

Also for turbulence in local equilibrium the effect of the flux divergences arising from kinetic energy transport and pressure transport may be neglected in the turbulent energy balance. A further characteristic is that $\partial q/\partial t = 0$. Hence, for turbulence in local equilibrium the sum of the terms on the right-hand side of eq. (3.1) is equal to zero.

Coefficients for turbulent exchange of momentum and mass are defined by:

$$\overline{u'w'} = -\nu_t \frac{\partial \overline{u}}{\partial z} \quad ; \qquad \overline{w'\rho'} = -K_t \frac{\partial \overline{\rho}}{\partial z} \tag{3.3}$$

where $\nu_t$ : eddy viscosity
$K_t$ : eddy diffusivity

For turbulence under conditions of local equilibrium eqs. (3.1) and (3.3) imply:

$$\varepsilon = \nu_t \left(\frac{\partial \overline{u}}{\partial z}\right)^2 \left(1 - \frac{Ri}{\sigma_t}\right) \quad ; \qquad Ri = -\frac{g}{\rho} \frac{\frac{\partial \overline{\rho}}{\partial z}}{\left(\frac{\partial \overline{u}}{\partial z}\right)^2} \tag{3.4}$$

where $Ri$ : *Gradient Richardson number*, defined by eq. (3.4)
$\sigma_t$ : turbulent Prandtl number, $\sigma_t = \nu_t K_t^{-1}$
The above result indicates that the stability of a horizontal shear flow increases with the gradient Richardson number, *Ri*.

Equation (3.4) leads to upper bounds of existence criteria of turbulence:

$$Ri < Ri_{cr} = \sigma_t \quad ; \qquad R_f = \frac{g\overline{\rho'w'}}{\overline{\rho}\,\overline{u'w'}\,\frac{\partial \overline{u}}{\partial z}} = \frac{Ri}{\sigma_t} < R_{f,cr} < 1 \tag{3.5}$$

where $R_f$ : *Flux Richardson number*, defined by eq. (3.5)

For large *Ri* (*Ri* > 0.25, according to classical linear stability theory) a stable stratification will occur, i.e. small-amplitude interfacial instabilities will not grow. For small *Ri* (*Ri* < 0.25) instability occurs in free-turbulence shear layers, i.e. interfacial instabilities will grow.
For turbulence under conditions of local equilibrium the flux Richardson number, $R_f$, represents the mixing efficiency, i.e. the efficiency of the conversion from turbulent kinetic energy to potential energy (= term(III) / term(II) of eq. (3.1)).

Mixing processes in stratified flows are often related to an *overall Richardson number*, $Ri_0$, which results from dimension analysis:

$$Ri_0 = \frac{g\Delta\rho d}{\rho\chi^2} \tag{3.6}$$

where $d$ = thickness of the mixed layer
$\chi$ = typical known velocity scale
$\Delta\rho$ = density difference between the two layers

For appropriate choices of $d$ and $\chi$, $Ri_0$ can be regarded as the ratio between the work required to establish mixing (or the buoyancy effect opposing mixing) and the kinetic energy available for mixing. $\chi = U_0$ when a velocity is imposed, $\chi = u_*$ when the friction velocity is known, with $u_*$ defined as:

$$u_* = \sqrt{\frac{\tau_b}{\rho}} = \left(\sqrt{\overline{u'w'}}\right)_b \tag{3.7}$$

with $b$ = boundary

## 3.3 Process of turbulent entrainment in stratified fluids

Entrainment is defined as the mass transport from a non-turbulent layer to a turbulent layer. In case the lower layer is stagnant and the upper layer is flowing, as in figure 3.1, the turbulent motions in the upper layer erode the lower layer and mix the lower layer fluid into the upper layer. The lower layer becomes thinner. When the two layers are also of different density, buoyancy effects become important as these will oppose the mixing processes.

The mixing processes are quantified by the dimensionless entrainment rate $E$, which is the ratio of the entrainment rate $u_e$ (in case of figure 3.1 the thinning of the lower layer) and the characteristic flow velocity $\chi$. Often used definitions for this characteristic velocity are the friction velocity $u_*$ or the mean velocity of the mixed layer $u$, depending on which condition is imposed. The entrainment rate $u_e$ itself is the change in height of the density interface with time, $u_e = dH/dt$, where $H$ is the thickness of the mixed layer.
The results of experiments can be arranged by means of dimensional analysis, from which it follows that the entrainment rate $u_e$ is primarily correlated with an overall Richardson number, $Ri$.
From studies where one of the layers is flowing the entrainment of fresh/clear water into saline/turbid water is given by:

$$E_0 \propto Ri_0^{-n} \tag{3.8}$$

Where $0.5 < n < 1.2$, depending on the experiment.
The scatter of the experimental data is very large. This affects the accuracy of relation (3.8).

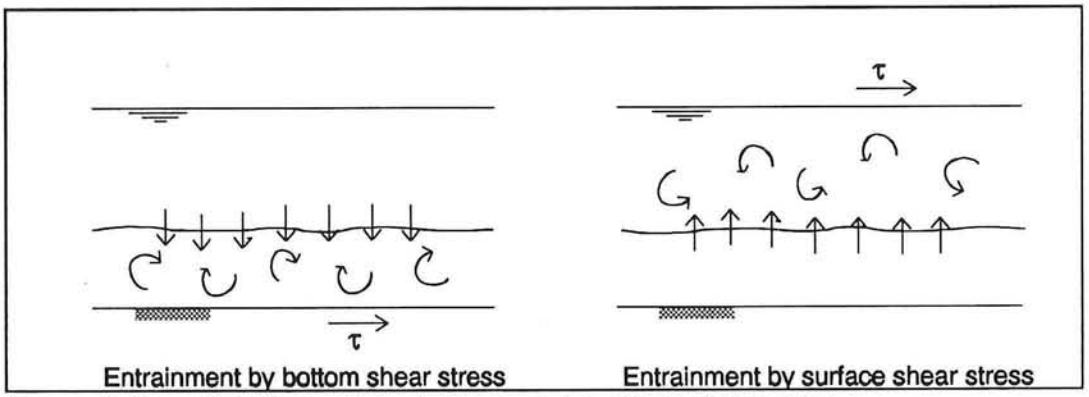


Figure 3.2: Entrainment by bottom and surface shear stress

| Reference | Type of experiment | Proposed law | Range of *Ri* |
|---|---|---|---|
| Ellison&Turner, 1959 | buoyant overflow | $u_e/u \sim Ri_o^{-1}$ | $0.05 < Ri_o < 0.75$ |
| Kato & Phillips, 1969 | surface stress linearly stratified fluid | $u_e/u_* = 2.5\ Ri_*^{-1}$ | $15 < Ri_* < 350$ |
| Kantha et al., 1977 | surface stress two homogeneous layers with a density difference | $u_e/u_* = f(Ri_*)$ | $30 < Ri_* < 1100$ |
| Lofquist, 1960 | density current | $u_e/u \sim Ri_o^{-1}$ | $8 < Ri_o < 100$ |
| Kit et al., 1980 | surface stress influence of 'end' walls | $u_e/u_* = 1.5\ Ri_*^{-3/2}$ | $30 < Ri_* < 500$ |

Table 3.1: Summary of experimental results

*Types of experiments*
Two different types of fresh/saline water experiments were carried out in the past to study the process of entrainment :

In the first kind, the turbulence is produced by one or two oscillating grids in a tank filled with stratified fluid. The result is the appearance of a stable density interface separating an essentially homogeneous turbulent layer of fluid from almost quiescent fluid. There is no significant mean flow or mean shear in these experiments, so it is difficult to apply the results of these experiments directly to field situations. Experiments of this kind where done a.o. by Turner (1968, 1973).

The second type of experiments involves shear-flow turbulence produced either by a bottom shear stress or a surface stress (figure 3.2) in an annular tank (Kato & Phillips, 1969, Kantha et al., 1977)) or a flume (Lofquist, 1960). This kind of experiments is of a greater interest for the studies on erosion of fluid mud.
A characteristic property of this type of experiments is that if a constant shear stress is applied (or a constant velocity) to a two-layer fluid, conservation of mass requires that the overall Richardson number remains constant throughout an experiment.

*Short discussion of experiments on fresh/saline water described in the literature*
Table 3.1 summarizes a number of experimental results.
Observations in various flows indicate a substantial differentiation in the mechanism of interfacial mixing, depending on the overall Richardson number. For example, Kantha et al., in their study of entrainment due to surface stress, identified three regions of $Ri_*$, defined in terms of the shear velocity $u_*$. For small values, $Ri_* < 100$, they observed massive convolutions of the interface. For large values, $Ri_* > 300$, the interface was essentially flat with slight ripples and cusps which were being detached from time to time. In the intermediate range of $Ri_*$ the convolutions of the interface were of a smaller scale and accompanied by groups of eddies arising from localized instabilities.
The results of the experiments of Kantha et al. (KPA) are shown in figure 3.3, together with the results of Kato and Phillips (KP). $R_\tau = B/u_*^2$ is a bulk Richardson number, cf. eq.(3.6), and $B = bh$ is the total mixed layer buoyancy, with $b = g\delta\rho/\rho$. In the KPA experiments, the flume initially contained two homogeneous layers of different density and $h/L = 0.25$, where $h$ is the mixed layer depth and $L$ is the width of the flume. In the KP experiments, a linear density variation in the entire lower layer was obtained and $h/L$ varied from 0.2 to 0.6. Kato & Phillips found an entrainment rate of about half of that found by Kantha et al. The factor two arises because half the available momentum supply (screen stress minus side-wall drag) must be used to accelerate the mixed layer in the linear stratified case in order to maintain $u_*$ constant as $Ri_\tau$ increases with $h$. Also energy could be lost from the turbulent layer by radiation or internal waves. When the ratio $h/L \rightarrow 0$, all of the available momentum supply is used to accelerate entrained fluid in the two-layer case, where $B$ is constant.
A further observation is that for the KPA experiments the entrainment rate shows no simple power-law dependence on $Ri_*$ over the whole range studied. For $Ri_* < 400$ the slope is about $Ri_*^{-1}$, but beyond that the rate of decrease in $E_*$ is much stronger.

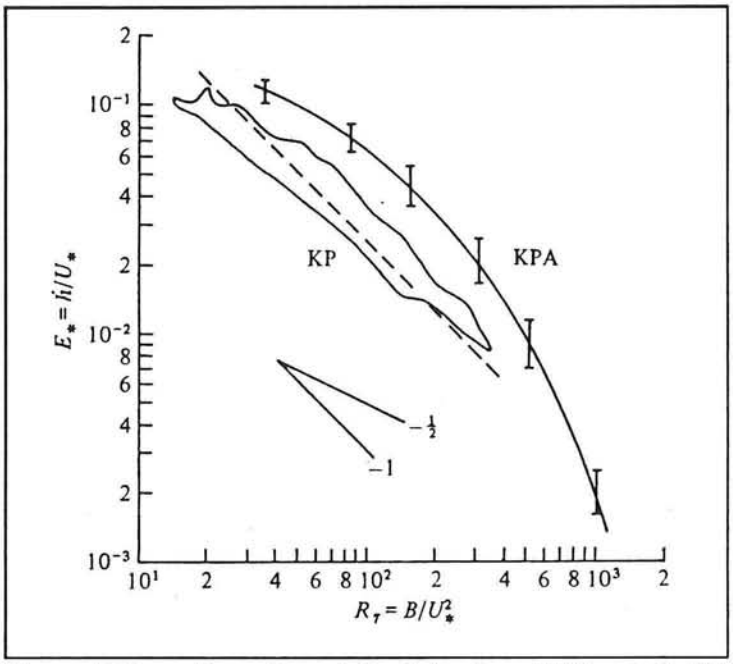


Figure 3.3: Experimental data by KPA and KP (Price, 1979)

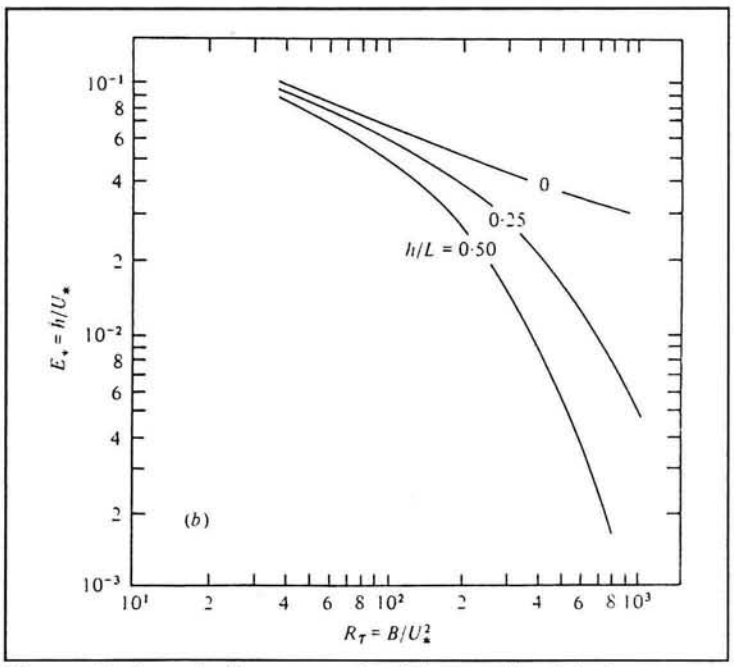


Figure 3.4: Influence of side walls friction (Price, 1979)

*Effect of side wall drag*
Price (1979) re-analysed the data by Kato & Phillips and Kantha et al.. He corrected the original data for the effects of the drag of the side-walls of the flume and obtained the relation

$$E_* \propto Ri_*^{-1/2} \qquad (3.9)$$

The influence of side-wall friction is shown in figure 3.4. It can be seen that the influence increases with increasing $Ri_*$ and that the entrainment rate grows with decreasing ratio $h/L$, where $h$ is the mixed layer depth and $L$ is the width of the flume.

Kranenburg (1983) found that sidewall friction reduces both the entrainment rates and the mean velocities in the mixed layer, especially in the case of high Richardson numbers (very stable flow).

*Effect of viscosity*
Towards the end of an experiment at high $Ri_*$ an accelerating flow in the fluid below the interface layer could be noticed, which was a result of the viscous shear stresses. From these observations it followed that a lower velocity difference between the mixed layer and upper part of the denser layer reduces the entrainment rate.

*Effect of diffusivity*
Turner (1968) found in experiments using an oscillating grid, that $E_* = u_e/u_* \propto Ri_*^{-1}$ at low Richardson numbers. For higher values of $Ri_*$, $E_* \propto Ri_*^{-1}$ when the stratification was produced by temperature differences and $E_* \propto Ri_*^{-3/2}$ when it was the result of salinity differences. Turner attributes this difference in behaviour to the differences in molecular diffusivity. At low Péclet numbers $Pe = uh/k$, with $k$ the molecular diffusivity, it is the molecular diffusivity that mixes packages of fluid, ejected from one layer into the other, with its environment. At higher Péclet numbers, the mixing will be dominated by small scale turbulent motions. This would imply that the actual entrainment rate occurring in nature is expected to be significantly larger than those observed during small scale laboratory experiments.
The viscosity was varied only slightly in laboratory experiments and therefore cannot play a significant role, according to Turner.

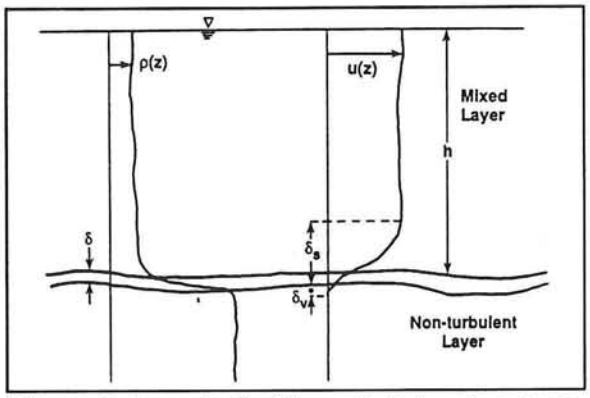


Figure 3.5: Definition sketch of a two-layered flow (Metha and Srinivas, 1993)

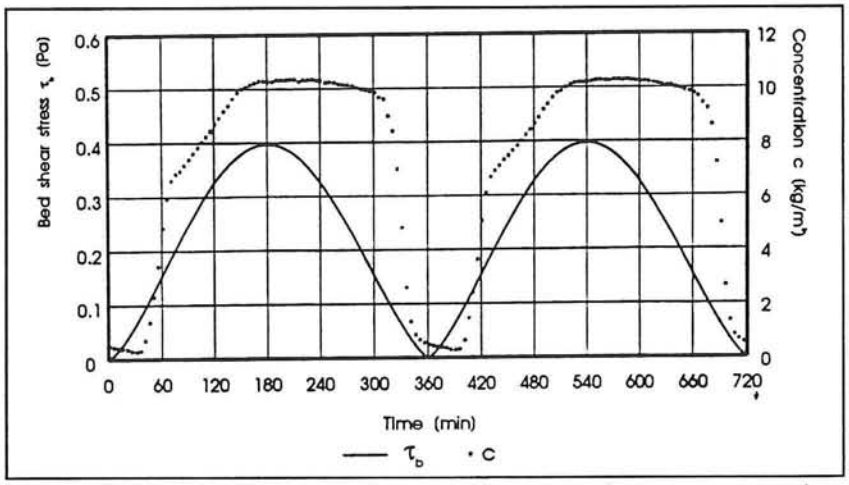


Figure 3.6: Bed shear stress and suspension concentration versus time (Winterwerp et al., 1992)

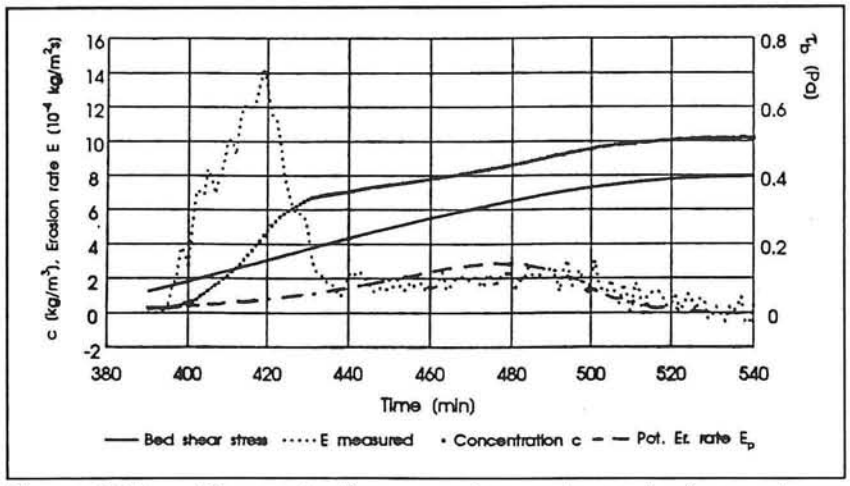


Figure 3.7: Concentration, erosion rate and shear stress (Winterwerp et al., 1992)

## 3.4 Process of erosion of fluid mud due to entrainment

A fluid mud layer can be (partly) eroded by an entrainment process that closely resembles the entrainment process of a stratified layer of salt water underneath flowing fresh water. This physical analogy makes it convenient to examine fluid mud entrainment in essentially the same way as the (well known) entrainment of salt-stratified layers.
Unlike the case of salt entrainment however, entrainment of fluid mud is influenced by the cohesive properties and response of mud subjected to shear.
Replacing salt by cohesive sediment affects the entrainment mechanism in several ways. Particulate settling is one. Since the rate of entrainment is measured from the increase of the dry mass of sediment (or salt) in the mixed layer per unit time per unit bottom area, i.e. *dm/dt*, it is evident that the rate of entrainment of sediment will in general be lower than that of salt. A higher viscosity (lower) fluid is likely to cause a considerably lower degree of mixing at the interface with the upper fluid, because the viscous lower layer is dragged along with the upper layer. Another effect is that cohesion would appear to retard entrainment. There is a (unknown) relation between a higher viscosity and cohesion.
Very little is known in a quantitative sense about the effects of settling, cohesion and viscosity difference on mud entrainment, but it is recognized that the rate at which mud is entrained decreases relative to the rate of salt entrainment with increasing *Ri*.

For analysing the erosion of fluid mud due to entrainment, consider the situation of a two-layered flow with a turbulent mixed layer above a highly viscous, predominantly non-turbulent layer as shown in figure 3.5. When the upper layer starts to flow, interfacial shear leads, with increasing flow, to internal wave generation, destabilization of the interface and its breakup, and entrainment of lower layer fluid due to turbulence. The mode of instability is influenced by the position and relative thickness $\delta$ of the layer with a density gradient and by the thickness $\delta_s$ of the layer with a velocity gradient. If $\delta \approx \delta_s$, the prime mode of instability is of the Kelvin-Helmholtz type, characterized by a roll-up and pairing of the interfacial vortices. When $\delta$ is much smaller than $\delta_s$, with increasing stratification Holmboe type of instability results, characterized by sharp-crested interfacial cusps which protrude alternatively into both fluids. The appearance of turbulence is essential for this process to occur.

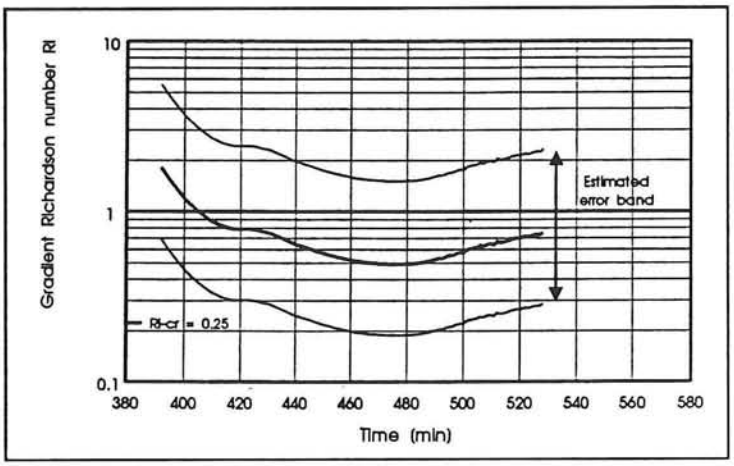


Figure 3.8: Gradient Richardson number versus time (Winterwerp et al., 1992)

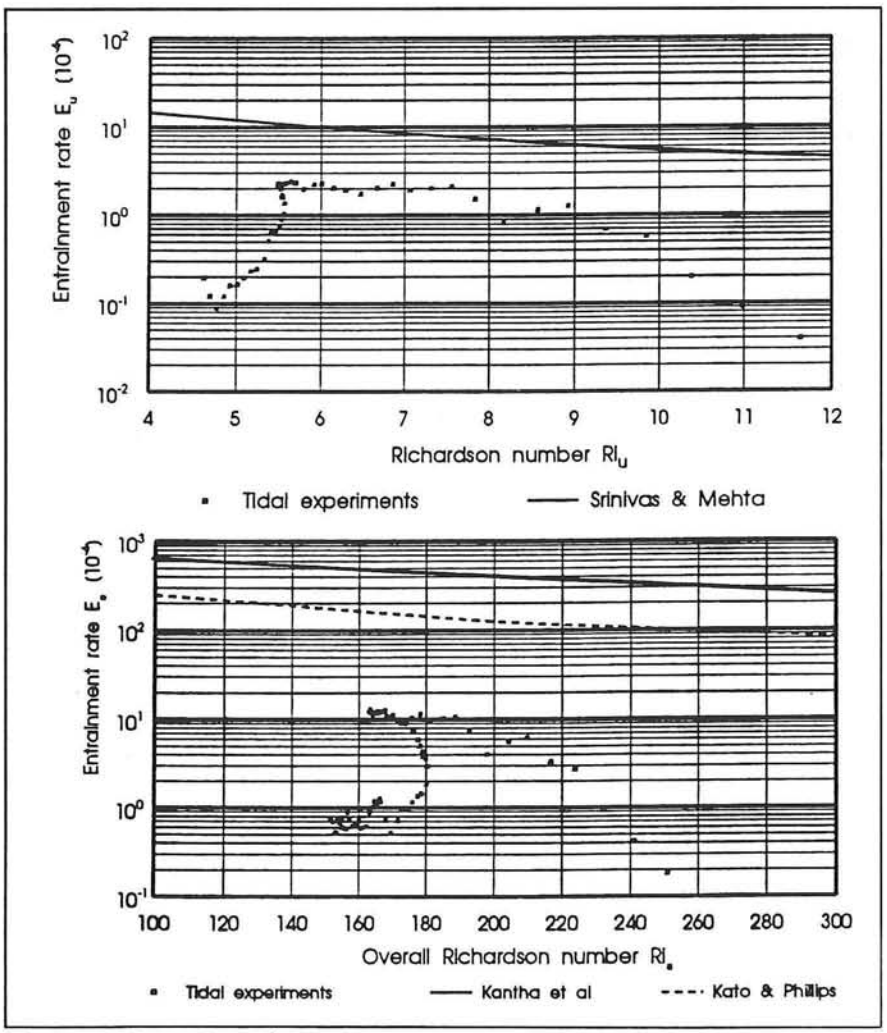


Figure 3.9: Entrainment rate versus overall Richardson number (Winterwerp et al., 1992)

*Discussion of experiments on soft mud layers described in the literature*

Winterwerp et al. (1992) carried out tidal experiments with natural mud from the Western Scheldt in an annular flume, by varying the flow velocity sinusoidally. During decelerating flow and slack tide, a fluid mud layer formed on the bed, with sediment concentrations ranging between 30 and 180 kg/m$^3$ down within the layer. This layer was eroded during accelerating flow, first rapidly due to the entrainment process. After some time, the intensity of these instabilities decreased and the soft bed became exposed to smooth surface erosion. This difference in mode must be related to some discontinuity in the bed structure, possibly generated by the interfacial instabilities. Also consolidation may play a role.
The time variation of bed shear stress and concentration of the suspension during two tidal cycles can be seen in figure 3.6. Figure 3.7 presents a detailed view of the erosion/re-entrainment phase.
Time variation of the estimated gradient Richardson number, $Ri$, is shown in figure 3.8. $Ri$ first decreases in time because of an increasing flow velocity, $u$, in the mixed layer (the bed concentration, $c_b$, remains more or less constant). At the end of the erosion period, $Ri$ increases due to a rapid increase of $c_b$ ($u$ increases only slowly). Around $t=420$ minutes a kink is observed in the curve because of the transition of entrainment erosion to surface erosion.

To analyze the experimental data, and to compare these with data of other entrainment experiments, an overall Richardson number $Ri_u$ is used. Figure 3.9. shows a comparison with the results by Kantha et al, Kato & Phillips and Srinivas and Mehta (1990). The latter results were measured with kaolinite in a race track flume.
In figure 3.9 $Ri_* = (g\Delta\rho h)/(\rho u_{*,s}^2)$ and $E_* = u_e/u_{*,s}$, with $u_{*,s}$ is the shear velocity at the water surface (rotating lid) and $h$ is the water depth. $Ri_u = (g\Delta\rho h)/(\rho U^2)$ and $E_u = u_e/U$, with $U$ is the mean mixed layer velocity.
Three important observations are:

1. An inverse trend in the data of Winterwerp et al. around $Ri_* \approx 170$ (and to a lesser extent around $Ri_u \approx 5.5$), due to a deviation of $c_b$ used from the actual $c_b$ profile, resulting in an inverse trend in $Ri_*$ itself.
2. The slope of the data agrees well with the results by Srinivas and Mehta, but only partly with the results by Kantha et al. However, the values $E_*$ and $E_u$ of the 'tidal' experiments are much smaller.
   Cohesion may only play a small role in this because of the low viscosity and yield strength at the concentrations of interest, and the experiments of Srinivas and Mehta were also carried out with cohesive material. The difference lies more in the fact that the experiments by Winterwerp are tidal, i.e. dynamic, while the other experiments are based on equilibrium conditions (steady, uniform flow). Also the ratio $h/W$, with $h$ the height and $W$ the width of flume, may attribute to the difference in results. $h/W$ is about 6.1 for the equipment of Srinivas and Mehta and $h/W \approx 1.5$ for the experimental arrangement of Winterwerp et al..
   Neither $\tau_b$ nor $u_*$ are known properly for the various studies.
3. For decreasing $Ri$, the data show a rapid drop when $Ri_* < 170$, or $Ri_u < 5.5$, due to the character of the interfacial instabilities described above. As the internal waves grow to a greater height, they may overtop and inject large quantities of sediment into the flow, so that in this case the gradient Richardson number can not be the only parameter describing the stability of the interface.

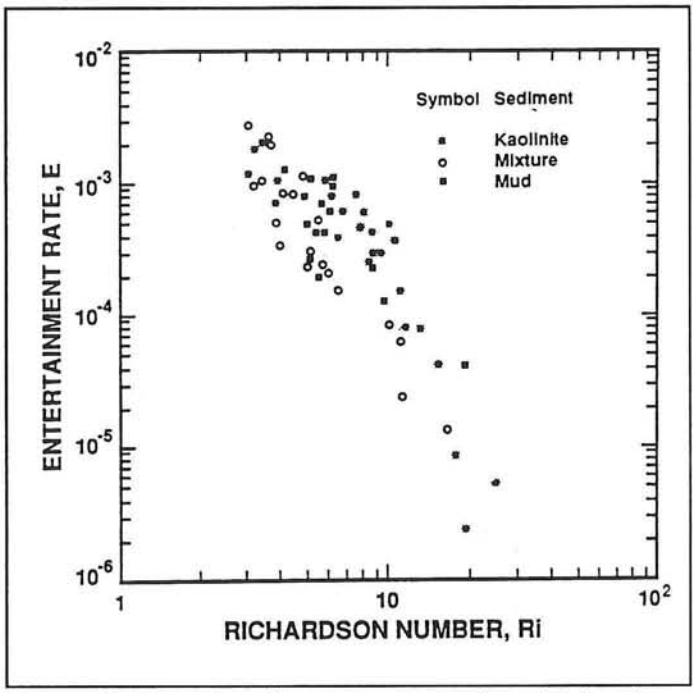


Figure 3.10: Entrainment rate against Richardson number (Metha and Srinivas, 1993)

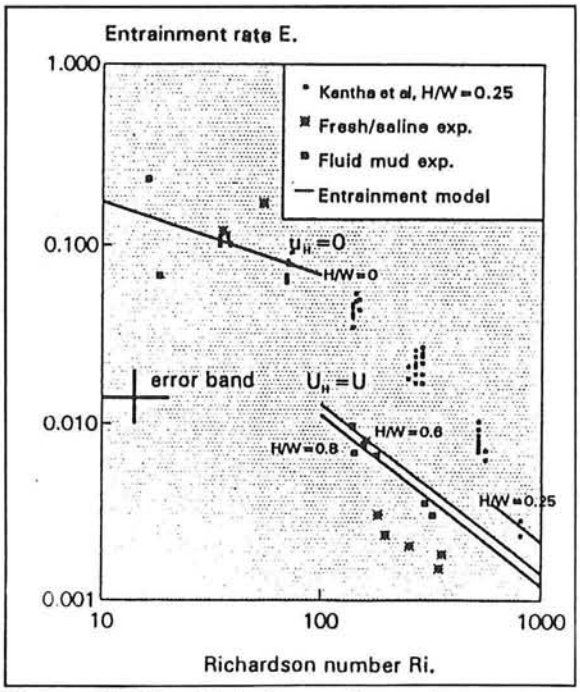


Figure 3.11: Entrainment rate versus Richardson number (Winterwerp and Kranenburg, 1994)

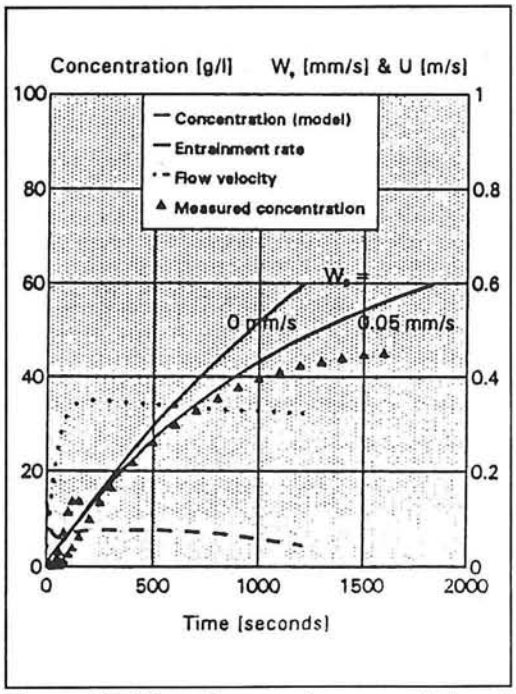


Figure 3.12: Comparison model and measurements (Winterwerp and Kranenburg, 1994)

Experiments with kaolinite, a mixture (bentonite) and a natural lake mud, carried out by Srinivas and Mehta (1993), were done in a race track flume (≈ an annular flume but of oval shape). The initial mud density ranged between 1020 and 1050 kg/m$^3$; the velocity was about 10 cm/s. An overall Richardson number, $Ri_u$, is defined as:

$$Ri_u = \frac{g\Delta\rho h}{\rho U^2} \tag{3.10}$$

where $h$ is the entire flow depth and $U$ is the mean mixed layer velocity. $Ri_u$ was varied between 3 and 29.
At low $Ri_u$ ($\leq$ 5), entrainment appeared to be turbulence dominated, resulting in a diffuse and highly irregular interface. As $Ri_u$ increased above 5, the interface became better defined. As a result interfacial waves break, injecting wisps of fluid into the upper layer. With increasing $Ri_u$, the disturbances decreased and the interface became more regular. For $Ri_u$ larger than 20, the intensity of entrainment decreased rapidly with increasing $Ri_u$. Both Kelvin-Helmholtz and Holmboe waves were observed over the range of tests.
The entrainment rate $E$, defined as $E = u_e/U$, is plotted against $Ri_u$ ($= Ri$ in the figure) for all three fluid muds in figure 3.10. Entrainment decreases rapidly for $Ri_u > 10$ and above a value of $Ri_u = 15$ there is little entrainment. The scattering in data points is due to unquantifiable effects of dewatering of the fluid mud layer during the experiments and also due to experimental errors, e.g. inaccuracy in the measured density of the interface and the small width-to-depth ratio of the mixed layer flow. Note that kaolinite did not entrain as efficiently as the other two sediments. Kaolinite was less cohesive than the mixture, though it had a higher settling velocity. The relative importance of settling and consolidation under dynamic conditions as in these experiments is unknown.

Winterwerp and Kranenburg (1994) studied also the erosion of a soft mud layer by entrainment. Experiments with fresh/saline water and with a kaolinite suspension were carried out in an annular flume. $Ri_*$ and $E_*$ are defined by: $Ri_* = (g\Delta\rho h/\rho u_*^2)$ and $E_* = u_e/u_*$. These experiments show that, at identical overall Richardson number $Ri_*$, the initial entrainment rate $E_*$ of fluid mud corresponds with that of saline water.
Figure 3.11 shows that the initial entrainment rates of fluid mud at large $Ri_*$ are somewhat, but consistently larger than those for the fresh/saline water experiments. An explanation may be that the drag of the mean flow was of more importance during the fresh/saline water experiments.
Because observed vertical turbulence scales were comparable or less than the calculated viscous-layer thickness for the fresh/salt-water experiments, it can be concluded that the experiments were affected by viscous effects, i.e. part of the lower layer was dragged along by the surface layer. Fluid mud has a higher viscosity than salt water which makes the argument concerning viscous effects on the entrainment process transferable. As a result part of the fluid mud layer was dragged along by the mixed layer.
Figure 3.12 shows a deviation in concentration between the measurements and the model results (with the settling velocity, $w_s$, of 0 and 0.05 mm/s) for $t$ larger than about 800 s. The difference is due to the gradual change in the erosion process from entrainment to surface erosion. Then mechanical work has to be done within the mud layer to erode the bed. This process is not accounted for in figure 3.12 and it is subject of further study.

From the experimental results described in this section, it follows that in general the entrainment process occurring to a fluid mud layer resembles the classical fresh/saline water entrainment process.
Unlike the case of fresh/salt water entrainment, entrainment of fluid mud is influenced by the cohesive properties of mud. Various measurements with cohesive sediments seem to be comparable with each other, though little is known about the effect of cohesion and settling on the entrainment. Furthermore, an important next step in the study on erosion of fluid mud is the application of the experimental results to full scale. However, in laboratory studies the influence of screen and/or side walls are dominant, whereas in nature turbulence is mainly produced at the interface, or at the fixed bed when there is a flow in the fluid mud layer also.
Additional research has to be carried out to improve the understanding of factors influencing the entrainment of fluid mud. The next Chapter presents an integral approach to model the entrainment of a fluid mud layer more suitably.

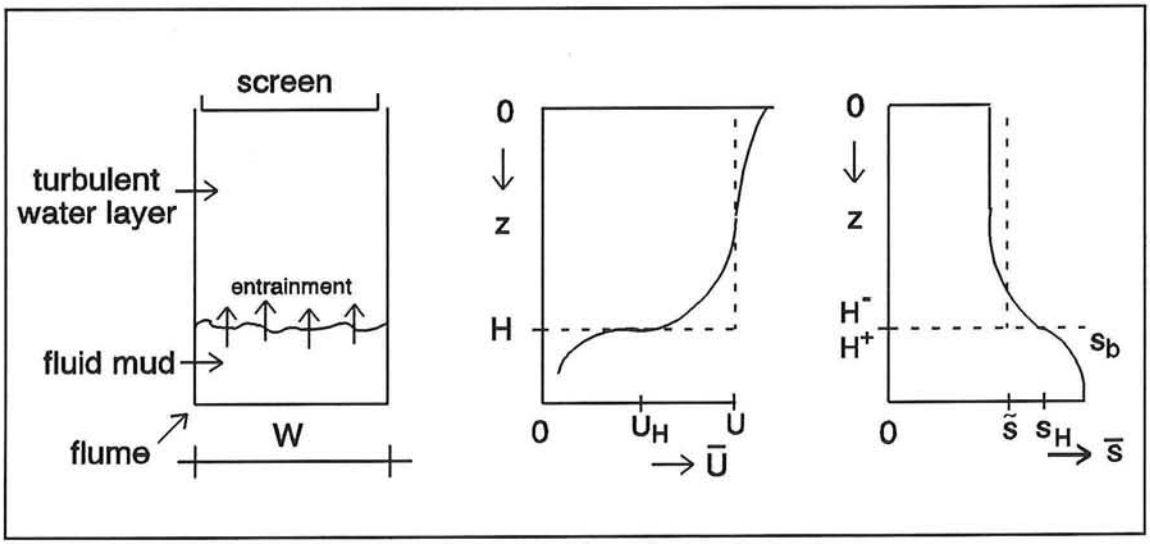


Figure 4.1: Definition sketch for flow driven by surface shear stress

# 4.0 THE ENTRAINMENT MODEL OF KRANENBURG (1994)

*Kranenburg (1994) developed an integral entrainment model for fluid mud in order to simulate the entrainment processes occurring at the interface between a two layer stratified fluid. In Section 4.1 a short introduction of this model with its modelling assumptions is presented, followed by a more detailed description of the used equations and assumptions in Section 4.2.*

## 4.1 Introduction to the entrainment model of Kranenburg

Various authors have developed entrainment models in the last years, e.g. Ross & Mehta (1989) developed a one-dimensional vertical model, le Hir (1994) used a two-dimensional vertical model to analyze field observations of fluid mud in the Loire Estuary in France, Odd & Cooper (1993) used a two layer model to simulate fluid mud behaviour in the Severn in Great Britain (see Chapter 6 and 7).
These models have the disadvantage that they are lacking mathematical formulae describing the physical processes of interest with sufficient accuracy, such as the rheological behaviour of fluid mud and the re-entrainment behaviour.

In order to determine the entrainment rate of a fluid mud layer more properly, Kranenburg (1994) used an integral approach to model the entrainment of a fluid-mud layer by turbulent flow. An entrainment model was derived by integration of the equation for turbulent kinetic energy (TKE) across the mixed layer. The resulting integral entrainment model is applied in conjunction with the momentum and mass balance equations. The model incorporates the effects of side wall friction and viscous drag. Only uniform flow is considered and molecular diffusion of sediment particles is assumed to be negligible. Consolidation of the fluid mud layer during the entrainment process is not taken into account. The empirical model constants involved are determined from experiments reported in the literature. A short description of this model is given in Section 4.2. For a more detailed analysis reference is made to Kranenburg (1994).

## 4.2 The equations for the entrainment model of Kranenburg

Consider the situation of a flow driven by a surface shear stress above a quiescent fluid mud layer. The water layer is the turbulent mixed-layer and fluid mud is entrained into this layer. This results in an increase in depth of the water layer with time, whereas the depth of the fluid-mud layer decreases. A definition sketch is given in figure 4.1.

Assuming uniform flow and adopting the Boussinesq approximation, the width-averaged form of the TKE equation of the mixed layer is written as

$$\underset{\text{(I)}}{\frac{\partial \overline{q}}{\partial t}} + \underset{\text{(II)}}{\overline{u'w'}\frac{\partial \overline{u}}{\partial z}} - \underset{\text{(III)}}{\frac{2}{W}\frac{\tau_w}{\rho_r}\overline{u}} - \underset{\text{(IV)}}{\alpha\frac{g}{\rho_r}\overline{w's'}} + \underset{\text{(V)}}{\frac{\partial D}{\partial z}} + \underset{\text{(VI)}}{\varepsilon} = 0 \qquad (4.1)$$

In which
term (I) : storage of TKE
term (II) : shear production by the vertical velocity gradient
term (III) : shear production by sidewall shear stress
term (IV) : buoyancy destruction
term (V) : redistribution term
term (VI) : dissipation rate.

In the notations: $\overline{q}$ is the mean TKE, $W$ the width of the flume, $\rho_r$ a reference density, $\tau_w$ the sidewall shear stress, $\alpha = (\rho_s-\rho_r)/\rho_s$ is a fractional density difference, $g$ the acceleration of gravity, $s$ the sediment concentration by weight, $t$ the time, $z$ the vertical coordinate ($z = 0$ at the free surface or screen), and $u$ and $w$ are streamwise and vertical velocity components. $D$ is a redistribution term for flux divergences arising from kinetic energy transport and pressure transport.

The width-averaged conservation equations of momentum and mass read

$$\frac{\partial}{\partial z}\overline{u'w'} = -\frac{\partial \overline{u}}{\partial t} - \frac{1}{\rho_r}\frac{\partial \overline{p}}{\partial x} - \frac{2}{W}\frac{\tau_w}{\rho_r} \qquad (4.2)$$

$$\frac{\partial}{\partial z}\overline{w's'} = -\frac{\partial \overline{s}}{\partial t} - \frac{\partial}{\partial z}(w_s\overline{s}) \qquad (4.3)$$

In the notations: $p$ is the pressure and $w_s$ a settling velocity.
Using boundary conditions at $z = 0$ and at $z = H^+$, the following integral forms of (4.2) and (4.3) can be derived

$$\frac{d}{dt}(UH) \approx u_*^2 - u_H^2 + U_H\frac{dH}{dt} - \frac{H}{\rho_r}\frac{\partial \overline{p}}{\partial x} - 2\frac{\lambda}{W}U^2H \qquad \left[\frac{dH}{dt} \geq 0\right] \qquad (4.4)$$

$$\int_0^H \overline{s}dz = Hs = H_0s_0 + \int_{H_0}^H s_b(z)dz \qquad (4.5)$$

In the notations: $u_*$ and $u_H$ are friction velocities at $z = 0$ and $z = H^+$, $U_H$ is a possible velocity in the mud layer, $s_b(z)$ the dry density in the bed, the subscript 0 refers to the initial situation. $\lambda$ is a sidewall friction factor in a quadratic friction law.

The integral form of the TKE equation (4.1) can be written as

$$\underset{(I)}{\frac{d}{dt}\int_0^H \overline{q}dz} + \underset{(II)}{\int_0^H \overline{u'w'}\frac{\partial \overline{u}}{\partial z}dz} \underset{(III)}{- 2\frac{\lambda}{W}U^3H} \underset{(IV)}{- \alpha\frac{g}{\rho_r}\int_0^H \overline{w's'}dz} + \underset{(VI)}{\int_0^H \varepsilon dz} = 0 \qquad (4.6)$$

To obtain a closed set of equations the following approximations and substitutions are introduced:

$$\text{term I} \sim \frac{d}{dt}(u_+^2 H) \qquad \text{with } u_+ = \max[u_*, u_H] \qquad (4.7)$$

$$\text{term II} \approx -[u_H^2(U - U_H) + u_*^2(U_* - U) + \tfrac{1}{2}(U - U_H)^2\frac{dH}{dt}] \qquad (4.8)$$

In equation (4.8) the first two terms on the right side represent turbulence production due to shear stresses, the third term describes production caused by entrainment. $U_*$ is the velocity at the top of the mixed layer.

$$\text{term IV} \approx -\alpha\frac{g}{\rho_r}[\tfrac{1}{2}H(s_H - s)\frac{dH}{dt} + Hw_s s] \qquad (4.9)$$

Term V is zero in the integral form.
Term VI is accounted for in various ways:

1. It is assumed that the production terms II and III are reduced by empirical factors.
2. The velocity difference $U - U_*$ in term II has to be replaced by the velocity difference $U - U_H$ across the lutocline to model the net production of TKE by surface stress properly, because most of the energy is instantly dissipated near the surface.
3. The mechanical work done to erode material from a bed that has gained a certain strength is included, by introducing terms proportional to $(U - U_H)u_b$ (representing failure of the bed) and $u_b^2 dH/dt$ (representing entrainment of bed material). $u_b^2$ is the work per unit mass of the bed needed to destroy the bed structure ($u_b^2 = 0$ in case for mud in a fully fluidized state).

Not modelled separately is the dissipation of TKE resulting from fluctuating motions in the bed.

A modelled form of (4.6) can now be written as

$$c_q \frac{d}{dt}(u_*^2 H) - 2c_H u_H^2 (U - U_H) - c_* u_*^2 (U - U_H) - c_H (U - U_H)^2 \frac{dH}{dt} - 2c_w \lambda \frac{H}{W} U^3 + B\frac{dH}{dt} + (U - U_H)u_b^2 + c_b u_b^2 \frac{dH}{dt} + 2\frac{\alpha s}{\rho_r} g w_s H = 0 \qquad \text{for } \frac{dH}{dt} > 0 \tag{4.10}$$

where $B = \alpha g H(s_H - s)/\rho_r$ is the total buoyancy, and $c_q$, $c_H$, $c_*$, $c_w$ and $c_b$ are empirical constants. Empirical evidence suggests $c_q = 6.4$, $c_H = 0.28$, $c_* = 0.22$, $c_w = 0.082$ and $\lambda$ is calculated using Blasius' law ($\lambda \approx 0.0037$ for the experiments of Kantha et al., $\lambda \approx 0.0018$ for the annular flume of Delft University).
For strongly stratified flows the precise value of $c_q$ is irrelevant, as is the value of $c_w$ for small aspect rations $H/W$. A stirring term proportional to $u_*^3$ has been neglected in (4.10). The value of $u_b$ is unknown, but it is likely that $u_b$ increases with $s_H$.

Time histories of mixed layer depth $H$, concentration $s$ and velocity $U$ are obtained by integrating (4.4) and (4.10) simultaneously using (4.5).

*Drag of the viscous fluid-mud layer*

The friction velocity $u_H$ at the interface is given by $u_H^2 = -\nu(\partial u/\partial y)_{y=0} = \nu u_H/\delta$ with $\delta$ the boundary-layer thickness. This gives $u_H^2 \approx U_H w_e$ for large $t$ so that the boundary layer has developed.
If the thickness of the viscous boundary layer in the fluid-mud layer becomes significant, the effective velocity difference $U - U_H$ across the interface may be reduced. In order to parameterise the influence of laminar flow in the quiescent layer on the effective velocity difference, the following relation is assumed

$$\frac{U - U_H}{U} = f_2(K), \qquad \text{with } K = \frac{\alpha g |s_H - s| \nu}{\rho_r (U - U_0)^2 w_e} = \frac{Ri_*}{E_* Re}\frac{u_*}{U} \tag{4.11}$$

where $Ri_* = B/u_*^2$ is an overall Richardson number, $E_* = w_e/u_*$ is the dimensionless entrainment rate, and $Re = UH/\nu$ the mixed layer Reynolds number. $f_2(0) = 1$ (no viscous effect) and $f_2(\infty) = 0$ (dominating effect of viscosity). The following function satisfies these conditions

$$f_2(K) = \exp(-c_\nu K^n) \tag{4.12}$$

where $c_\nu$ and $n$ are positive empirical coefficients. Recommended empirical values are: $c_\nu = 8$ and $n = 2$.

*Special solutions of the entrainment model*

When the variables $u_b$ , $\partial\overline{p}/dx$ , $w_s$ are zero, $u_*$ and $\rho_b$ are constant, no sidewall friction ($W \rightarrow \infty$) and no viscous effects ($u_H = U_H = 0$), for low values of $Ri_*$ and large times, the solution of (4.4) and (4.10) becomes

$$E_* = \frac{1}{u_*}\frac{dH}{dt} = \left[\frac{c_* + c_H}{c_q + Ri_*}\right]^{\frac{1}{2}}, \qquad U = \frac{u_*^2}{dH/dt} \tag{4.13}$$

For large values of $Ri_*$ viscous effects become important. As a consequence a considerable upper part of the lower layer is dragged along with the mixed layer, so that $U_H \approx U$. The variation in the momentum becomes negligible and turbulence production is mainly due to side-wall friction, so the entrainment rate becomes

$$E_* \approx \frac{c_w}{\left[2\lambda\frac{H}{W}\right]^{\frac{1}{2}}(c_q + Ri_*)} \tag{4.14}$$

This models explains the relation $E_* \sim Ri_*^{-\frac{1}{2}}$ for low values of $Ri_*$ and the relation $E_* \sim Ri_*^{-1}$ for high values of $Ri_*$.

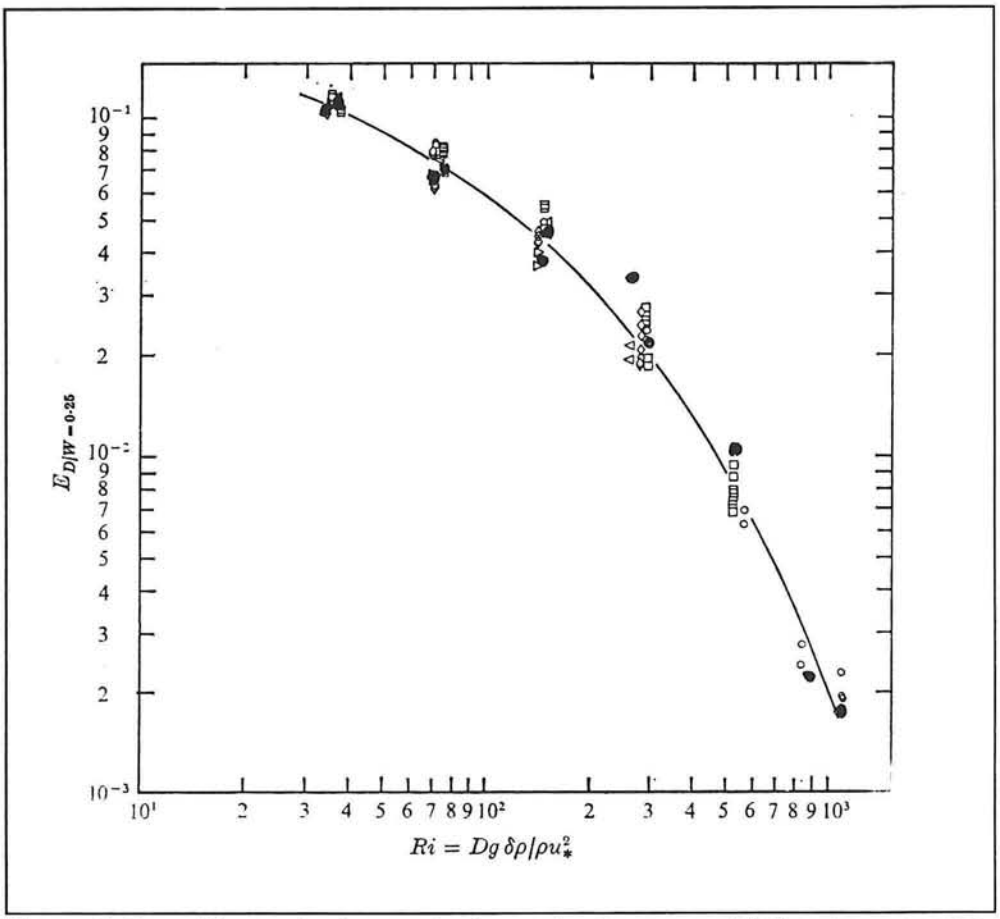


Figure 5.1: Dimensionless entrainment rate versus Richardson number for the experiments of Kantha et al. (*H/W* = 0.25) (Kantha et al., 1977) and the model, • = model results

# 5.0 SIMULATION OF ENTRAINMENT AND COMPARISON WITH EXPERIMENTS

*In this chapter numerical simulation of the entrainment of fluid mud is described, followed by a comparison of the simulation with experimental results. The simulation was carried out by using the integral entrainment model of Kranenburg (1994) as presented in the previous chapter. First the entrainment model is calibrated with the results of the experiments of Kantha et al. (1977) in Section 5.1. Simulation and comparison of transient unidirectional flow experiments with kaolinite are described in Section 5.2. Section 5.3 discusses the simulation of a tidal flow experiment with mud from the Western Scheldt and compares the simulation with the experiment.*

## 5.1 Simulation and comparison of the experiments of Kantha et al. (1977)

Equations (4.4), (4.10) and (4.5) are integrated numerically with a predictor-corrector scheme, so time histories of mixed layer depth $H$, (or concentration $s$), velocity $U$ and entrainment rate $E$ can be obtained with this model. A surface shear stress (this Section) or a velocity of the upper lid (Sections 5.2 and 5.3) can be imposed in the numerical model in order to simulate the annular flume experiments properly.

Values of most of the empirical constants in (4.10) and (4.13) are derived from the experiments of Kantha et al. (1977). In order to verify the entrainment model, simulation of the experiments of Kantha et al. (1977) is carried out. For this purpose, $c_q = 6.4$, $c_H = 0.28$, $c_* = 0.22$, $c_w = 0.082$, $\lambda = 0.0037$, $c_v = 8$ and $n = 2$, see Section 4.1. Next, the simulation is compared with the experimental results obtained by Kantha et al..

The experiments of Kantha et al. involve shear-flow turbulence produced by a surface shear stress in an annular flume. The flume initially contains two homogeneous layers with a density difference caused by a NaCl or a $CaCl_2$ solution. Conservation of mass implies that the overall Richardson number, $Ri_* = Hg\delta\rho/\rho u_*^2$, remains constant in each experiment (see also Section 3.3). $Ri_*$ is varied from about 30 to 1100. The (constant) friction velocity $u_*$ is 1.41 cm/s in the experiments considered herein, the ratio between water depth and flume width, H/W, is 0.12 for an initial water depth $H_i$ of 2.7 cm and this ratio is 0.24 for an initial water depth $H_i$ of 5.4 cm. The width of the flume is 0.228 m. The viscosity is taken from Kantha et al. (Kantha et al. (1977), figure 2).

Figure 5.1 shows the experimental entrainment data versus Richardson number $Ri_*$, from Kantha et al. corrected for a constant aspect ratio H/W = 0.25. The figure also shows the results of the entrainment model. The maximum entrainment values are plotted. The agreement between the values obtained from the entrainment model and the values obtained by Kantha et al. is good. This agreement can still be observed when also for the numerical simulation the entrainment rate is corrected for a constant aspect ratio $H/W = 0.25$, e.g. by taking the instant when $H/H_0 \approx 2$ in figure 5.3 and deriving the entrainment rate for this moment in figure A6 in appendix A.

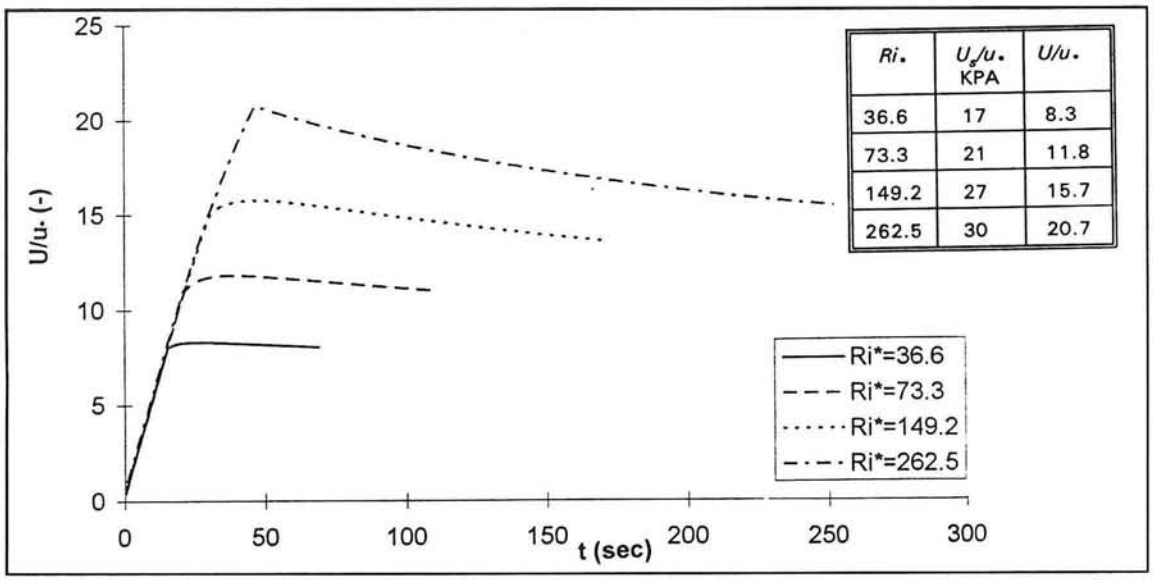


| Ri. | $U_*/u.$ KPA | U/u. |
|---|---|---|
| 36.6 | 17 | 8.3 |
| 73.3 | 21 | 11.8 |
| 149.2 | 27 | 15.7 |
| 262.5 | 30 | 20.7 |

Figure 5.2: Dimensionless velocity of the mixed layer versus time at various Richardson numbers; NaCl solution, $H_i$ = 2,7 cm

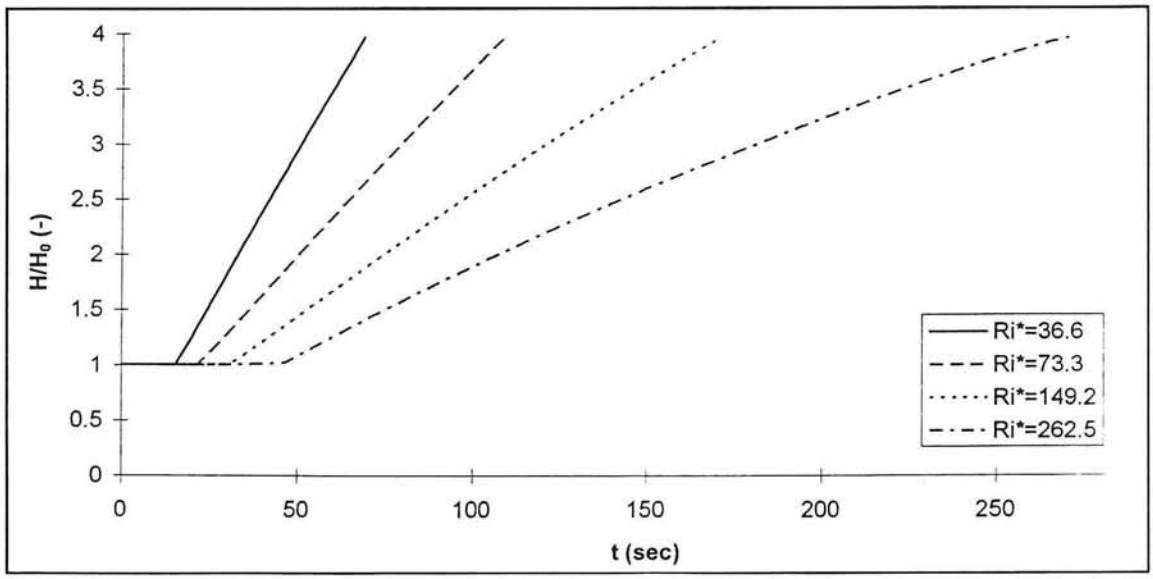


Figure 5.3: Dimensionless depth of the mixed layer versus time at various Richardson numbers; NaCl solution, $H_i$ = 2,7 cm

The deviation for $Ri_* = 262$ is due to the fact that in the entrainment model hardly any drag is accounted for at $Ri_* = 262$, as explained by Kranenburg (1994). The assumptions for the effects of viscous drag and for the effects of sidewall friction for large values of $Ri_*$ (see Section 4.2) are satisfied.

The dimensionless velocity of the turbulent layer $U/u_*$ as a function of time for various values of $Ri_*$ is shown in figure 5.2 and in figures A1 and A2 of appendix A. The values of $U_s/u_*$, with $U_s$ the velocity of the screen, taken from Kantha et al. at the instant where $dU/dt = 0$ are listed in the added table.
The ratio $U/u_*$ is within the range observed by Kantha et al. ($U/u_* \approx 0.5$ à $0.7\ U_s/u_*$).

The depth of the mixed layer $H$ as a function of time at various Richardson numbers $Ri_*$ is presented in figure 5.3 and in figures A3 and A4. It can be noticed that the mixed-layer depth starts to increase after an 'initialization' phase. The time of initiation increases with increasing Richardson number. The increase in waterdepth $H$ is also slower for increasing Richardson number.
An explanation is that at low Richardson numbers, more turbulence and random fluctuations can be expected, the entrainment proceeds faster and the mixed-layer depth increases faster than at higher Richardson numbers. When $Ri_*$ is lower dan about 150 there is little curvature in $H(t)$, which means hardly any influence of side-wall drag or viscous drag. At higher Richardson numbers (> about 300) turbulence appears to be suppressed and the influence of side-wall friction and viscous drag is more pronounced: the slopes decrease with increasing Richardson number.
The kink after the 'initialization' phase in the figures is due to plot inaccuracies. A more gradually transition should be expected.

These results correspond with the observations of Kantha et al. (see Figure A5).
For high values of $Ri_*$ the increase in the upper layer depth proceeds substantially faster in the numerical model than observed by Kantha et al.. A preliminary explanation is that in the numerical model the influence of the curvature of the annular flume is not incorporated. The curvature not only influences the mean flow, but in the long run also the 3-D turbulence structure.

Figures A6, A7 and A8 show the dimensionless entrainment rate $E_* = (dH/dt)/u_*$ as a function of time. The entrainment rate increases rapidly after an initialisation phase, reaches its maximum value and then decreases slowly with time. The time of initiation increases with increasing Richardson number, in agreement with the explanation given for figure 5.3. Because the stability increases with increasing Richardson number, logically, the maximum entrainment rate decreases with increasing Richardson number. Kantha et al. did not report on the entrainment rate versus time.

Generally, it can be concluded that the numerical results match well with the experimental results of Kantha et al.. The values taken for the empirical coefficients and the assumptions made for the effects of viscous drag and side wall friction are satisfying.

## 5.2 Entrainment in transient unidirectional flow experiments

### 5.2.1 Simulation of the entrainment in transient unidirectional flow experiments

In this Section numerical simulations of the entrainment of kaolinite are presented. The simulation is carried out in agreement with the programme of the fluid mud experiments with kaolinite in the annular flume carried out by Winterwerp and Kranenburg (1994), see Section 3.4. During these experiments a constant velocity of the upper lid was imposed.
The experimental programme used for the kaolinite simulation is shown in table 5.1. Experiments K1 and K2 were not simulated because of the inaccurate measurements.

| Run no. | $U_s$ (m/s) | $S_1$ (g/l) | $S_2$ (g/l) | $b$ (m) | $H_0$ (m) | $\nu$ ($m^2/s$) |
|---|---|---|---|---|---|---|
| K3 | 1.39 | 175 | 275 | 0.093 | 0.18 | 1.3E-04 |
| K4 | 1.28 | 175 | 275 | 0.103 | 0.17 | 1.3E-04 |
| K5 | 0.91 | 175 | 275 | 0.093 | 0.18 | 1.3E-04 |
| K6 | 1.39 | 180 | 280 | 0.073 | 0.20 | 1.5E-04 |
| K7 | 1.28 | 180 | 280 | 0.083 | 0.19 | 1.5E-04 |
| K8 | 0.91 | 180 | 280 | 0.083 | 0.19 | 1.5E-04 |

Table 5.1: Programme for kaolinite simulations

In table 5.1: $U_s$ = velocity of upper lid
$S_1$ = concentration at top of fluid mud layer
$S_2$ = concentration at bottom of fluid mud layer
$d_{m,0}$ = initial height of lower layer
$H_0$ = initial height of upper layer
$\nu$ = kinematic viscosity of fluid mud layer

In order to describe the sediment concentration in the fluid mud layer, an empirical relation is used

$$s_b(z) = S_1 + \left[\frac{z - H_0}{d_{m,0}}\right]^5 (S_2 - S_1)$$

The differences in concentration profiles are a result of different consolidation times.

Viscous effects play an important role in the behaviour of fluid mud. Measurements of the viscosity of fluid mud at low shear rates, however, may be inaccurate. De Wit (1994) measured the dynamic viscosity versus shear rate for high concentrations (300 - 600 g/l) of kaolinite. As an approximation for the dynamic viscosity at the concentration of interest (about 180 g/l), the dynamic viscosity versus concentration at a shear rate of 1 $s^{-1}$, taken from De Wit (1994), is plotted on double logarithmic paper.

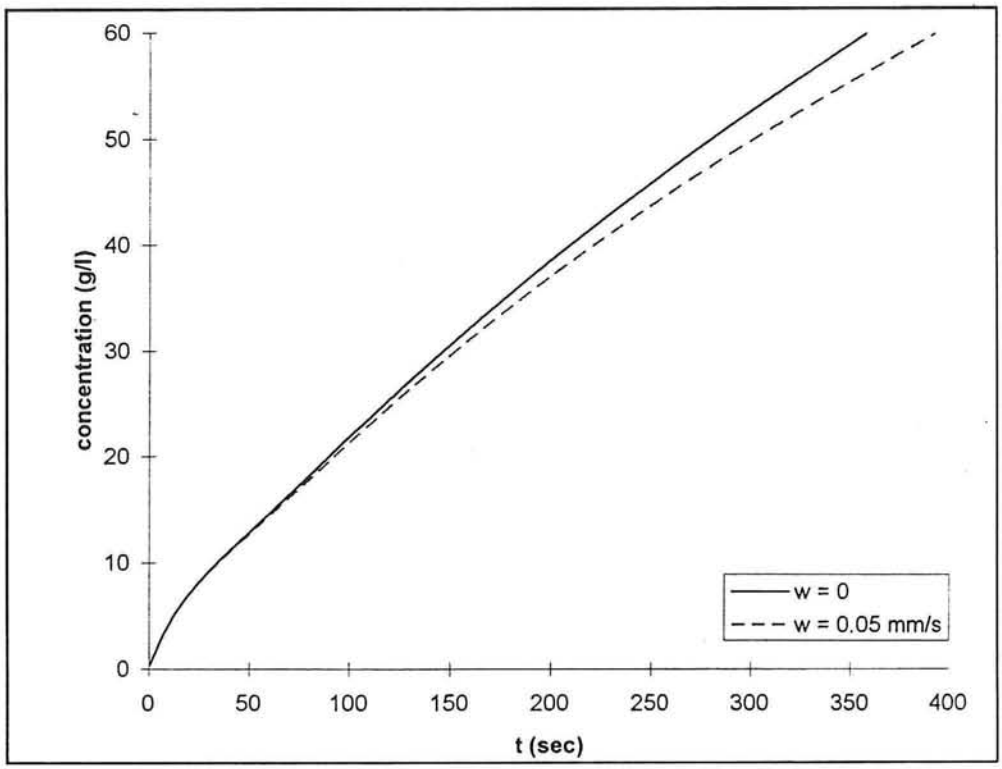


Figure 5.4: Concentration versus time for simulation K3 of kaolinite

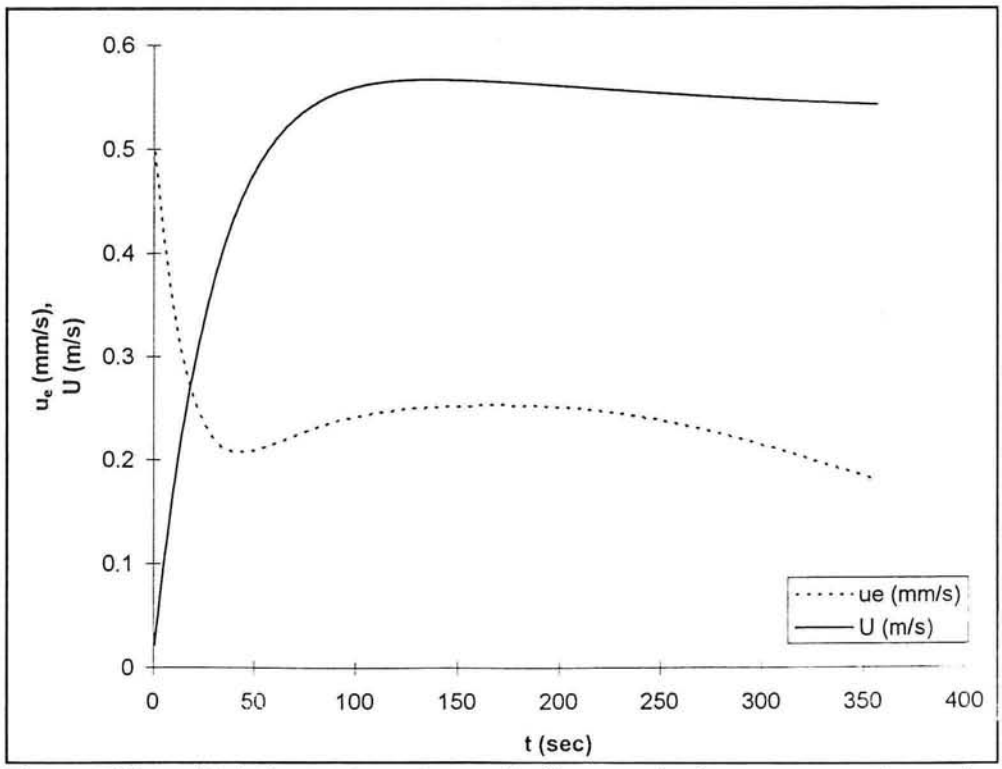


Figure 5.5: Entrainment rate and flow velocity versus time for simulation K3 of kaolinite

The dynamic viscosity at a concentration of about 180 g/l is obtained by linear extrapolation, see figure B1 of appendix B. The kinematic viscosity is derived by dividing the dynamic viscosity by the bulk density.

The width of the flume is 0.3 m. The empirical coefficients are set as mentioned in Section 4.2. From the sedimentation rate a settling velocity $w_s$ = 0.05 mm/s was derived, so $w_s$ is given this value of 0.05 mm/s. Also the situation $w_s$ = 0 (no settling) is simulated.
At $t$ = 0 the simulation started with the mean velocity of the upper layer $U$ = 0 and the mean concentration of the upper layer $C$ = 0 and the velocity of the upper lid $U_s$ according to table 5.1.

Figure 5.4 shows for $w_s$ = 0 and $w_s$ = 0.05 mm/s the computed suspended sediment concentration $C$ versus time for simulation K3 and figure 5.5 shows for $w_s$ = 0 the entrainment rate $u_e$ and the mean flow velocity $U$ in the upper layer versus time for simulation K3. For the results of the simulations K4 to K8 reference is made to figures B2 t/m B11.
Only simulation K3 will be discussed here in detail.

It can be observed that the simulated flow velocity $U$ first increases with time up to 0.56 m/s and starts to decrease for $t$ > 125 s. The initial increase is due to the acceleration of the fluid in the upper layer, the slow decrease is caused by side wall friction, entrainment and an increasing thickness of the upper layer.
The entrainment rate $u_e$ has an initial value of 0.5 mm/s. After the start of the simulation the entrainment rate $u_e$ first decreases to 0.2 mm/s and begins to increase after 40 seconds. After 150 seconds the entrainment rate decreases again. The initial decrease is due to acceleration of the flow in the upper layer, because at $t$ = 0, $u$ = 0 and $(U_s - u) \sim u_*$, hence $u_*$ is maximal. The subsequent increase in $u_e$ is caused by the production of TKE by side wall friction and entrainment. The following decrease is a result of a continuing increase in bed density, hence an increase in $Ri_*$.
The settling velocity $w_s$ has little effect on the flow velocity and entrainment rate in this experiment.
The effect of the settling velocity, $w_s$ = 0.05 mm/s, on the concentration is a slower increase in concentration of the upper layer for $t$ > 60 s.

In a qualitative sense, the results of simulations K4 to K8 are similar to the results of K3. For simulations K5 and K8 the entrainment process is much slower because of the smaller $U_s$, hence a smaller $u_*$. As a result of a smaller $u_*$, the influence of $w_s$ is larger because for each experiment it will take the same amount of turbulent energy to keep the particles in suspension, but in K5 and K8 relatively less energy is available.

When comparing simulations K4 and K7 or K5 and K8, it is seen that the influence of settling/consolidation time, which resulted in different concentration profiles at the start of the experiments, is not remarkable. Apparently, the (small) differences in bed concentration profile are not very important for these experiments.
As a consequence of the decrease in $U_s$, hence a smaller $u_*$, from K3 to K5 (or from K6 to K8) the entrainment rate and mean flow velocity are lower and the duration of the entrainment process is longer.

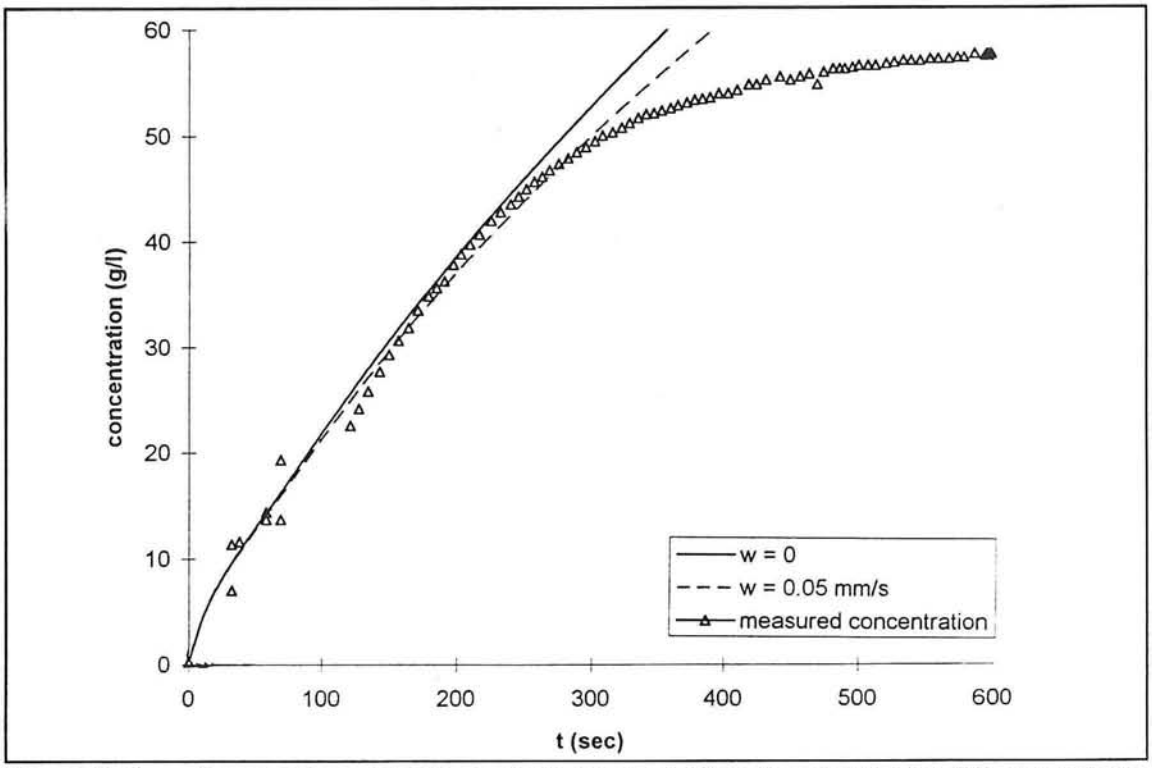


Figure 5.6: Comparison of concentration versus time for simulation K3 of kaolinite

### 5.2.2 Comparison of transient unidirectional flow simulations with experiments

In figure 5.6 the concentration of simulation K3 is compared with the measured concentration of experiment K3. A good agreement can be observed from $t = 0$ to 300 s. For $t > 300$ s, the model overestimates the measured concentration $C$. Apparently the bottom layer, which was deposited first, had gained a certain strength. The explanation that in the entrainment model the empirical coefficients are tuned to experiments with small aspect ratio ($H/W = 0.25$), while in these experiments the aspect ratio is much larger ($H/W$ = about 0.7) is of less importance. In the numerical model the influence of flow curvature is not incorporated, which also may contribute to the difference between the numerical and experimental data.
For a comparison of the numerical and measured concentrations for K4 to K8 reference is made to appendix C, figures C1 to C5.

When the same comparison of concentration as for K3 is made for K5 and K8, it can be observed that for $t > 800$ s, the model starts to overestimate the measured concentration considerably. This is due to the gradual change in the erosion process from entrainment to surface erosion. Then the mechanical work which has to be done within the bed to erode the bed becomes more pronounced. This process has not yet been modelled in the numerical entrainment model.

Figures C7 to C12 show the measured height of the upper layer as a function of time for K3 to K8. Again only K3 will be explained in detail.

An overall agreement between the simulated and experimental data can also be seen for the entrainment rate $u_e$: An entrainment rate of about 0.3 mm/s at $t = 120$ s was measured during experiment K3, as presented in figure C7 (the slope of the curve is the entrainment rate, $dH/dt = u_e$) as compared to a simulated entrainment rate of 0.25 mm/s (see figure C6). The decrease of $u_e$ during K3, however, starts after about 200 s, whereas in the numerical model the decrease occurs after 125 s. At the end of the entrainment process the entrainment rate is about 0.1 mm/s lower than the simulated one. This may be due to the mechanical work which has to be done in the bed and due to the influence of flow curvature during the experiment, which also leads to a lower entrainment rate at the end of the experiment.

Figure C13 shows the measured mean flow velocity for experiment K4. The flow velocity is increasing rapidly up to 150 s to a value of about 0.3 m/s and then slowly increases to about 0.32 m/s after 650 s. When looking at the simulation of the flow velocity of K4 (see figure C14), the flow velocity increases to 0.52 m/s after 110 s and then decreases slowly till the end of the simulation to a value of 0.50 m/s. This is due to an increasing influence of side wall friction.
The measured and the simulated flow velocities cannot be compared with each other, because the measurement is taken at a height of 10 cm above the flume bottom, while in the numerical model the mean velocity of the mixed layer is simulated.

It may be concluded that the simulation of the concentration of the upper layer agrees well for the most part with the measured values of the experiments in the flume. The deviations are attributed to the fact that the numerical model does not incorporate the processes of surface erosion and flow curvature.

## 5.3 Entrainment in tidal flow experiment

### 5.3.1 Simulation of the entrainment in tidal flow experiment

The entrainment behaviour of natural mud from the Western Scheldt under tidal flow conditions was investigated by Winterwerp et al. (1992). They carried out tidal flow experiments in the annular flume of Delft Hydraulics by imposing a sinusoidal variation with time of the velocity of the upper lid, in such a way that a shear stress at the bed was produced estimated at ranging between -0.4 and +0.4 Pa (see Section 3.3).
This tidal experiment was simulated with the numerical model for the first 1/4 of the tidal period $T$, i.e. the accelerating period. The velocity $U_s$ of the upper lid now increases sinusoidally with time till it reaches its maximum value at 1/4 $T$.

For the annular flume the following relation between bed shear stress and velocity is used: $\tau_b = 0.275\ V^{1.37}$, where $\tau_b$ is the bed shear stress (Pa), $V$ is the velocity difference between annular lid and channel (= $U_s$ in the numerical model, m/s). Substituting $\tau_b$ = 0.4 Pa yields $U_s$ = 1.31 m/s.

For the simulation of the tidal flow experiment the other input values are

| | | |
|---|---|---|
| $S_1$ | = 30 g/l | concentration at top of fluid mud layer |
| $S_2$ | = 180 g/l | concentration at bottom of fluid mud layer |
| $d_{m,o}$ | = 0.049 m | initial height of lower layer |
| $H_o$ | = 0.22 m | initial height of upper layer |
| $\nu$ | = 4E-06 m$^2$/s | kinematic viscosity |
| $\lambda$ | = 0.001 | sidewall friction coefficient (tuned) |
| $T$ | = 12 hours | tidal period |
| $W$ | = 0.2 m | width of the flume |

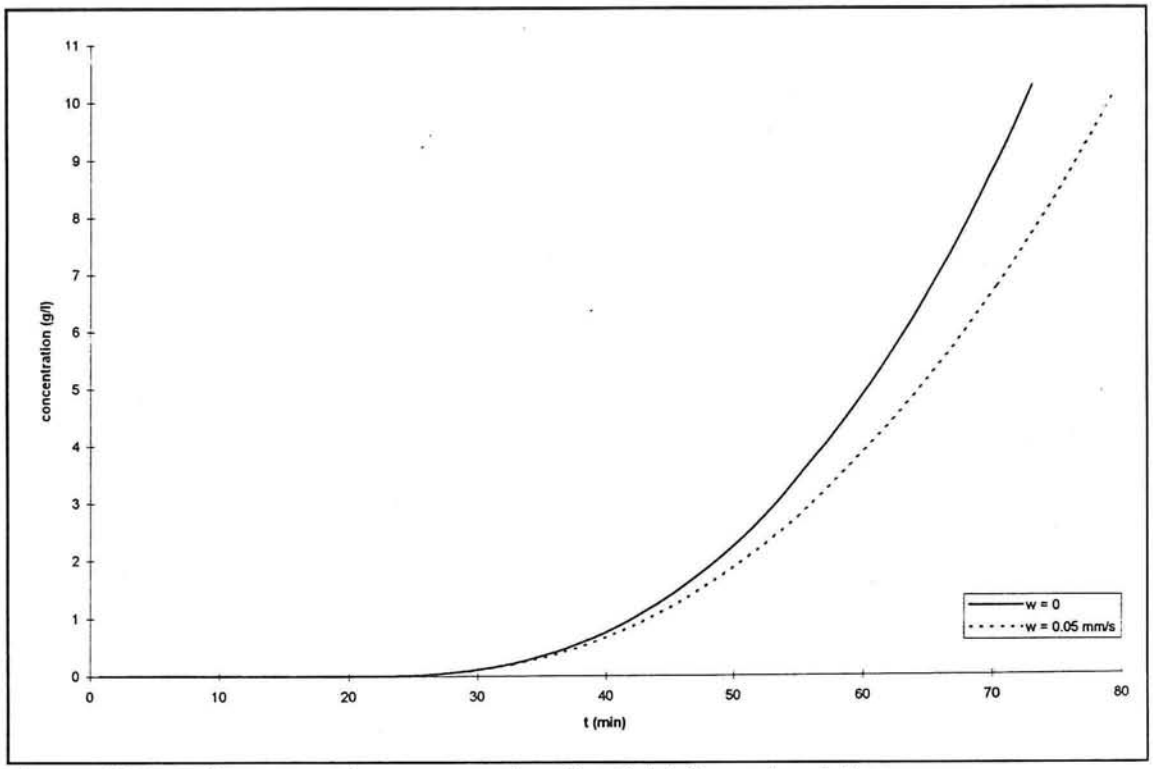


Figure 5.7: Concentration versus time for tidal flow simulation

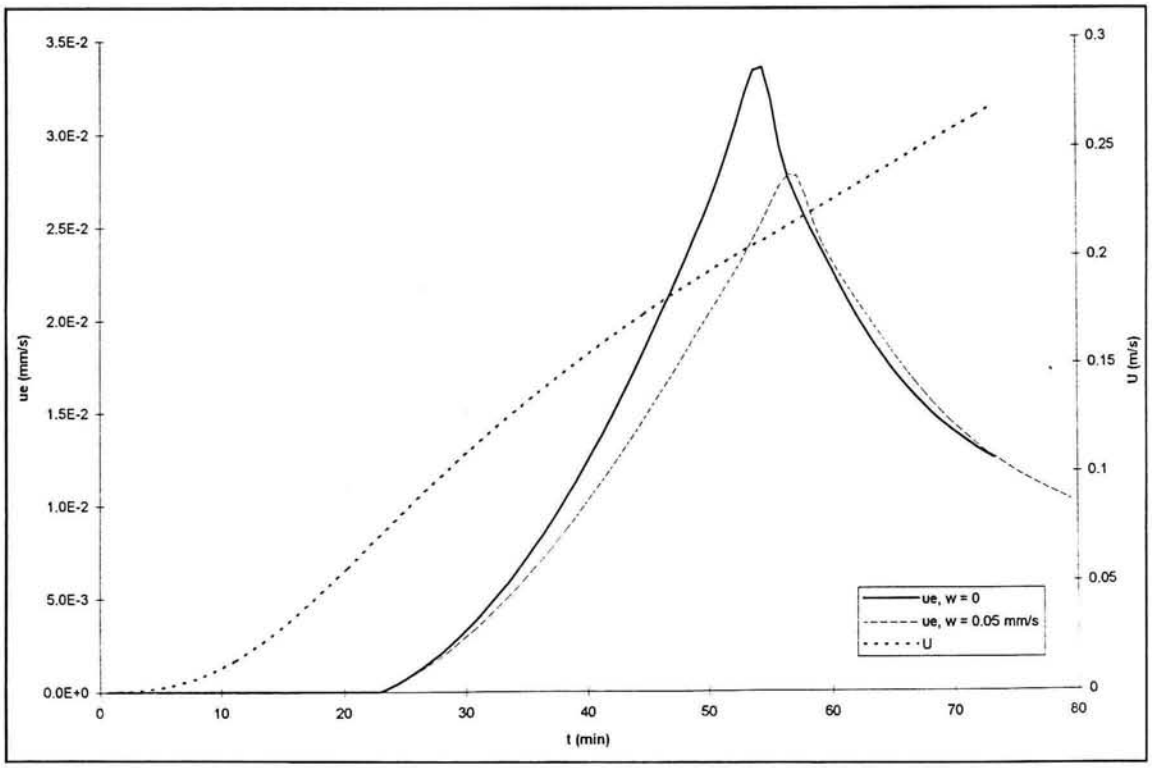


Figure 5.8: Entrainment rate $u_e$ and flow velocity $U$ for tidal flow simulation

$S_1$, $S_2$ and $b$ are derived from figure D2, appendix D. For the concentration profile in the fluid mud layer the empirical relation mentioned in Section 5.2 is used.
The dynamic viscosity is derived from figure D1 when $C \approx 30$ g/l and corrected for the high shear rate. The dynamic viscosity is divided by the bulk density to obtain the kinematic viscosity. $\lambda$ is taken as an approximation for the used annular flume.
The values of the empirical coefficients are set as mentioned in Section 4.2 and $w_s = 0$ or $w_s = 0.05$ mm/s (measured during the entrainment phase).
At $t = 0$ the simulation started with the mean flow velocity $U = 0$ and the mean concentration of the upper layer $C = 0$. The results are shown in figure 5.7 and 5.8.
From figure 5.7 it can be observed that for $t < 25$ min. the velocity $U_s$, hence $u_*$ is too small to produce sufficient TKE to transport any sediment from the lower to the upper layer. The concentration starts to increase for $t > 25$ min.
After 35 min. the settling velocity starts to influence the increase of concentration in the upper layer. The increase in concentration is slower then.

Figure 5.8 shows the entrainment rate $u_e$ and the mean flow velocity $U$ as a function of time. It can be seen that the flow velocity starts to increase after 4 min. and reaches a value of 0.27 m/s after 70 min. For $t < 24$ min. no entrainment takes place, due to the low velocity $U_s$, which results in almost zero values of $u_*$. The entrainment rate starts to increase at $t = 24$ min. due to production of TKE by friction and entrainment, and reaches its maximum value of 0.033 mm/s at $t = 54$ min.. The subsequent decrease of entrainment rate is caused by a continuing increase in bed density.

The settling velocity $w_s$ has no effect on the flow velocity, but it does influence the entrainment rate. For a settling velocity of $w_s = 0.05$ mm/s the increase in entrainment proceeds slower and the entrainment rate reaches a lower maximum value. The subsequent decrease in entrainment rate is more or less independent of $w_s$.

### 5.3.2 Comparison of tidal flow simulation with experiment

The results of the tidal flow experiments are given in figures D3 and D4 of appendix D. Before a comparison is made with the numerical simulation it has to be noticed that in addition to entrainment the tidal experiment also included the processes of deposition, consolidation and floc erosion. Entrainment took place from $t \approx 390$ min. until $t \approx 420$ min.. In the figures the time axis of the numerical simulation is modified to the time axis of the measured concentration to facilitate comparison. (As a consequence the simulation started at $t = 360$ min., i.e. slack water, instead of $t = 0$.)

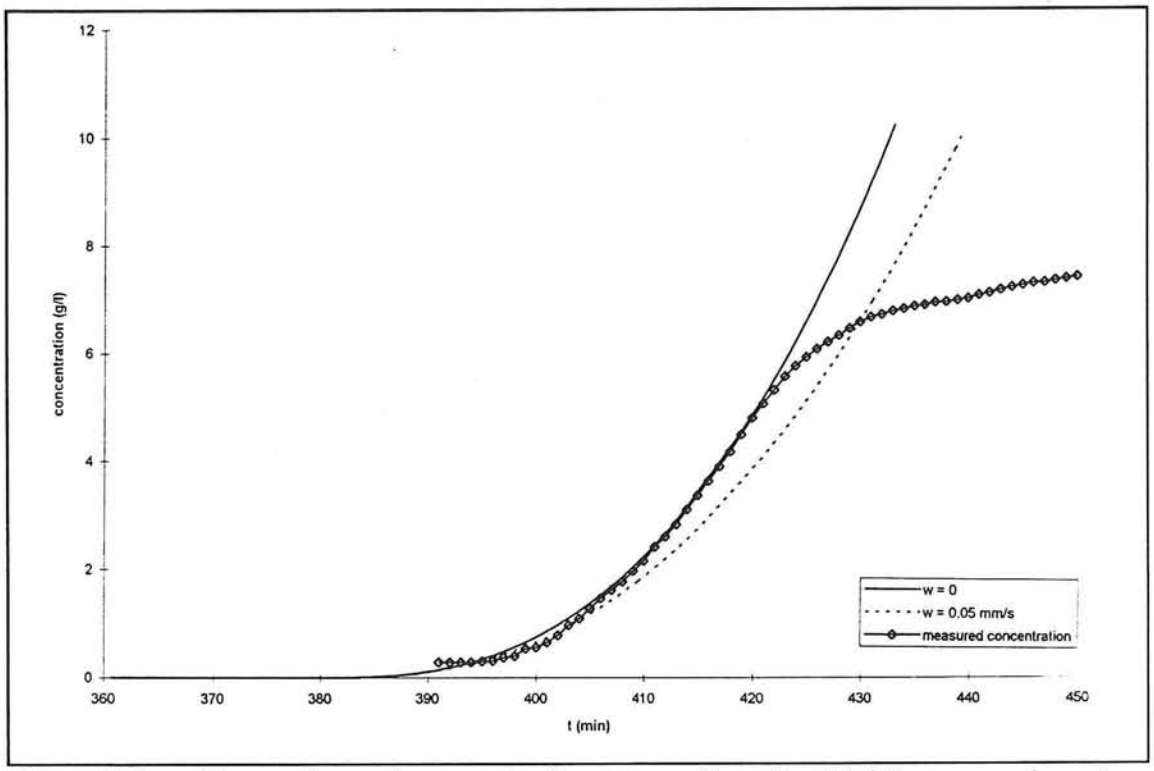


Figure 5.9: Comparison of concentration versus time for tidal flow experiment

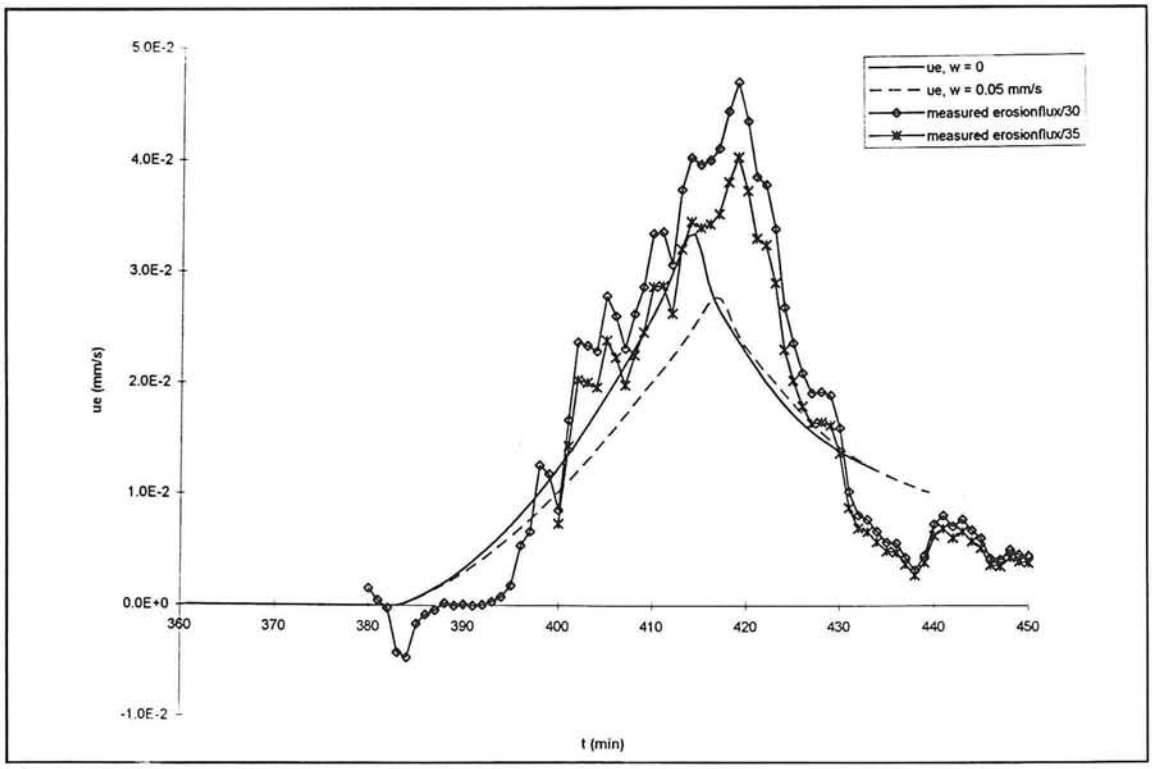


Figure 5.10: Comparison of entrainment rate $u_e$ for tidal flow experiment

When comparing the simulated concentration with the measured concentration a fair agreement can be observed for 390 min. $< t <$ 422 min. (figure 5.9). For smaller $t$ the measured sediment concentration showed an initial value (see figure D3 and D4), because not all the suspended sediment had been deposited during the preceding deposition/consolidation period, whereas the numerical simulation starts with $C$ = 0. The measured values for $t <$ 390 min. are not drawn in figure 5.9. For $t >$ 422 min. the model overestimates the measured concentration considerably. As mentioned in Section 5.2.2, this is caused by a change in erosion process from entrainment to surface erosion, because more work has to be done within the bed to erode bed material. Also the effect of consolidation and flow curvature in the annular flume which are not incorporated in the numerical model will attribute to the difference between the numerical simulation and the experimental results. The relation for the concentration profile in the fluid mud layer may deviate from the actual profile in the mud layer.

A comparison between the computed entrainment rate $u_e$ and the measured entrainment is more difficult to make. For the experiments the measured erosion rate $E$ is obtained from the mass balance: $E = (h\text{-}d_m)(dc_s/dt)$, with $h$ = depth of annular flume, $d_m$ = thickness of sediment bed, $c_s$ = sediment concentration of the suspension. Hence the dimension of $E$ reads $[ML^{-2}T^{-1}]$. In the numerical entrainment model the entrainment rate is obtained by integration of the TKE of the upper layer (see Section 4.2) and the dimension for $u_e$ is $[LT^{-1}]$.

In order to compare the measured erosion rate with the computed entrainment rate, the erosion rate $E$ is divided by the bed concentration of the upper part of the lower layer (= 30 g/l). This result is drawn in figure 5.10 together with $E$ divided by a concentration of 35 g/l, because after some time the bed with a concentration of 30 g/l is eroded and a bed concentration of about 35 g/l will now be exposed to erosion (see figure D2).
From figure 5.10 the following conclusions can be drawn. A fair agreement can be noticed from about 395 min. till about 415 min.. For $t <$ 395 min. no agreement can be observed between the computed and measured values. The measured erosion rate is derived from the mass balance, so when settling occurs during the experiment, the measured erosion rate decreases and for $t <$ 395 min. the erosion rate is even negative. This trend can be seen during the whole entrainment period as a local decrease in the erosion rate. Notice that a small inaccuracy in measuring $C_s$ lead to a considerable inaccuracy of $E$. During the experiment internal waves were observed at the fluid-bed interface from about 400 min. till about 430 min.. At $t \approx$ 415 min. the entrainment rate in the numerical model starts to decrease when $w_s$ = 0, whereas the measured entrainment rate reaches its higher maximum value about 5 min. later. An explanation is that floc erosion starts to play a role for the measured values and also the settling velocity may attribute to the difference, which can be seen when considering $u_e$ for $w_s$ = 0.05 mm/s. During the erosional process the settling velocity will decrease and becomes almost zero.

In figure 5.9 deviations between the numerical and experimental results start at $t \approx$ 422 min., whereas in figure 5.10 the computed entrainment rate becomes larger than resulted from the experiments for $t >$ 430 min.. The deviations are due to a high increase in bed concentration, which is now exposed to erosion.

The subsequent decrease in entrainment rate proceeds faster for the measured entrainment because of the increase in bed density due to consolidation. For $t >$ 430 min. less agreement can be noticed, but now floc erosion will dominate the erosion process.

Generally, it can be concluded that in the entrainment phase an overall agreement can be observed between the computed and experimental results of the tidal experiment. The deviations are due to the way the erosion flux was measured, the effect of consolidation and the change in erosion process. So a next step in the modelling of entrainment will be the incorporation of consolidation and the change from entrainment to floc erosion into the model. Also careful attention has to be paid to the way of measuring the entrainment rate.

# 6.0 A TWO LAYER FLUID MUD MODEL

*In order to describe the transport and behaviour of fluid mud, a two layer fluid mud model has been developed. In this model the processes of formation, growth, decay and movement of a fluid mud layer are included. A short introduction of this model with its specifications and restrictions is given in Section 6.1. The equations of the model are discussed in Section 6.2.*

## 6.1 Introduction to the model

Fluid mud often occurs in estuaries and sometimes in the coastal zone where waves are obviously present. Due to high concentrations fluid mud layers have a large influence on the sediment transport, even though the flow velocity in fluid mud layers may be relatively small. This explains the importance of correct modelling of fluid mud, its formation, growth, decay and its movement.

The transport and behaviour of fluid mud layers can be described by a two-layer approach, see figure 6.1. The upper layer consists of a dilute suspension of mud and behaves as a Newtonian fluid in turbulent flow. The lower layer is the fluid mud layer.

When modelling fluid mud, some difficulties and problems arise:
- the viscous shear stress and yield stress cannot be neglected. Fluid mud should be considered as a general plastic fluid.
- the density of the water-sediment mixture, the fall velocity, the eddy viscosity and diffusivity are dependent on the sediment concentration.
- there is no clear definition of the bed.

Thus schematizations are necessary to apply the equations of mass and motion to a fluid mud layer in a numerical model.

A two-dimensional (horizontal) model of the movement of fluid mud has been developed at Delft Hydraulics by adapting the two layer fluid mud model of Odd and Cooper (1989). In the model obtained, the processes of generation, motion and disappearance of a fluid mud layer are included. A distinction is made between the upper suspension layer and the fluid mud layer, the latter having a constant density. The interaction between the two layers is not taken into account for modelling the movement of the suspension layer. First a 2DH flow field is computed, after which this flow field is one of the driving forces for the fluid mud model. Thus the model is a 2DH decoupled two-layer model. There is, of course, an exchange of sediment between the layers. Leaving out of the feed back from the fluid mud movement to the flow computation of the suspension layer gives no problems when the thickness of the fluid mud layer is small with respect to the water depth. It is assumed that the flow velocity in the suspension layer is much larger than the velocity in the fluid mud layer. Another simplification is the schematisation of the bottom into two layers: a fluid mud layer and a consolidated layer. The fluid mud is considered to be a Bingham fluid.

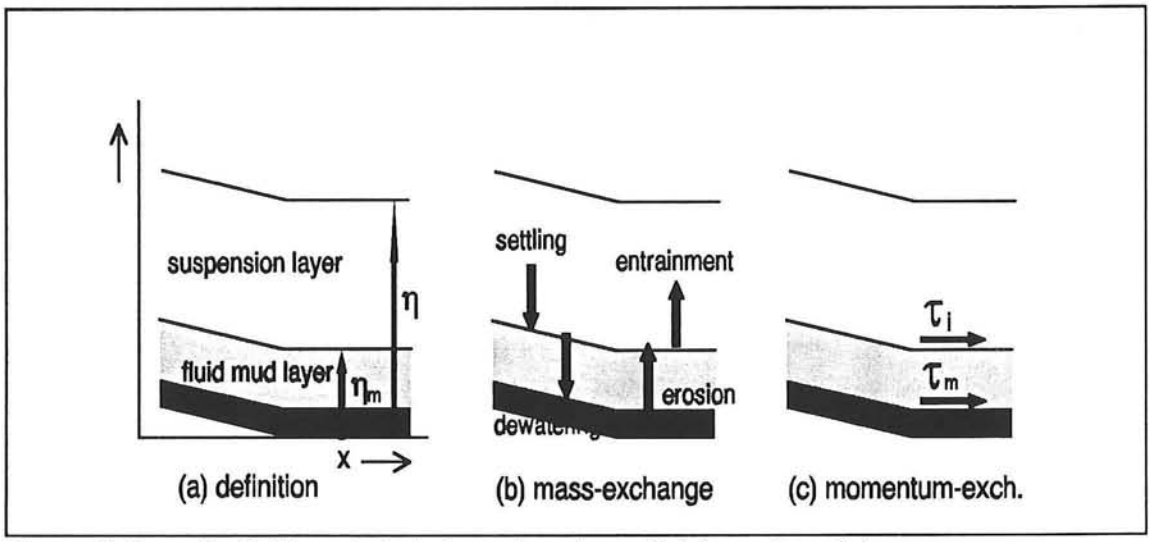


Figure 6.1: Definition sketch for a two-layer fluid mud model

The influence of wave driven flow in the suspension layer is not taken into account. Only the stirring up effect of waves can be incorporated via a correction for the shear stress on the bottom.

Horizontal movement of the fluid mud layer can occur due to:
1. Gravity effects on a sloping bed
2. Longitudinal pressure gradients due to elevation of the water surface
3. Longitudinal pressure gradients due to gradients in fluid mud thickness
4. Drag by the suspension layer

Furthermore the following mechanisms are included in the model:
1. Settling and deposition from the suspension layer to the fluid mud layer
2. Entrainment from the fluid mud layer to the suspension layer
3. Dewatering of the fluid mud layer (consolidation)
4. Erosion from the bed layer

## 6.2 The equations for the model

In order to describe the movement of fluid mud the following equations are used in the model; see figure 6.1 for a definition sketch.
The mass balance equation for the fluid mud layer can be written as

$$\frac{\partial d_m}{\partial t} + \frac{\partial u_m d_m}{\partial x} + \frac{\partial v_m d_m}{\partial y} = \frac{1}{C_m}\frac{dm}{dt} \tag{6.1}$$

The momentum equations of the fluid mud layer in the two horizontal directions read

$$\frac{\partial u_m}{\partial t} + g\frac{\partial \eta}{\partial x} + \frac{g\Delta\rho}{(\rho_0+\Delta\rho)}\left(\frac{\partial \eta_m}{\partial x} - \frac{\partial \eta}{\partial x}\right) - \Omega v_m + \frac{1}{d_m(\rho_0+\Delta\rho)}\left[\frac{u_m}{(u_m^2+v_m^2)^{0.5}}\tau_m - \frac{\Delta u}{(\Delta u^2+\Delta v^2)^{0.5}}\tau_i\right] = 0 \tag{6.2}$$

$$\frac{\partial v_m}{\partial t} + g\frac{\partial \eta}{\partial y} + \frac{g\Delta\rho}{(\rho_0+\Delta\rho)}\left(\frac{\partial \eta_m}{\partial y} - \frac{\partial \eta}{\partial y}\right) + \Omega u_m + \frac{1}{d_m(\rho_0+\Delta\rho)}\left[\frac{v_m}{(u_m^2+v_m^2)^{0.5}}\tau_m - \frac{\Delta v}{(\Delta u^2+\Delta v^2)^{0.5}}\tau_i\right] = 0 \tag{6.3}$$

For a definition of the symbols, see pages 85 and 87.

In equations (6.2) and (6.3) the non-linear convective terms are neglected. The internal Froude number, $Fr_i$, is related to these terms. When the flow is internal super-critical $Fr_i > 1$. This condition gives numerical complications. Fortunately the convective terms are small compared to the other terms.

In equation (6.1) the source term on the right hand side is a crucial term. The processes of settling, entrainment, consolidation ( = dewatering) and erosion are taken into account in this term. The expression adopted is

$$\frac{dm}{dt} = \underset{(I)}{w_s C H[\tau_{dm}-\tau](1-\frac{\tau}{\tau_{dm}})} - \underset{(II)}{V_e C_m H[10-Ri_B]} + \tag{6.4}$$

$$- \underset{(III)}{V_0 C_m H[400-Re_e]} + \underset{(IV)}{H[\tau_m-\tau_e]H[Re_e-600]M_e(\tau_m-\tau_e)}$$

In which
term (I) : settling from the suspension layer to the fluid mud layer
term (II) : entrainment from the fluid mud layer to the suspension layer
term (III) : dewatering of the fluid mud layer (consolidation)
term (IV) : erosion from the bed layer

The water layer will only entrain mud from the fluid mud layer when the bulk Richardson number for the lower layer, $Ri_B$, is less than 10. (See page 85 for the definition of $H[x]$.)

Odd and Cooper used a simple expression for the definition of the entrainment term (term II). Only entrainment from the fluid mud layer to the suspension layer is considered. It is not correct to base the bulk Richardson number on the lower layer herein. The entrainment term only incorporates the velocity difference between the overlying water and the fluid mud layer, the reduced gravity and the thickness of the mud layer, through a Richardson number for the lower layer. The concentration of the mud layer is taken constant and the effect of viscosity of the mud is not modelled.
The integral approach of Kranenburg (see Chapter 4) is more suited to model the entrainment behaviour of a fluid mud layer by turbulent flow. Viscous effects and a varying concentration profile for the fluid mud layer are incorporated.
Using the integral entrainment model of Kranenburg for the definition of the entrainment term in the two-layer fluid mud model will improve the modelling of entrainment, because the entrainment rate will be approached more accurately: The model uses an integral form of the equation for turbulent kinetic energy of the upper layer depth, it considers the Richardson number of the upper layer depth, viscous effects, a varying concentration profile for the mud layer and an effective velocity difference between the two layers. Yet, some complications remain: First the fluid mud layer in the two layer fluid mud model has a constant density, hence the entrainment rate cannot vary with the concentration as in the integral model. Secondly, little is known about how to correct the entrainment rate obtained from experiments to full scale, in other words, there is insufficient evidence that the entrainment rate resulting from the integral model will predict the entrainment rate occurring in reality. Also, when the integral entrainment model is applied, it is more difficult to recognize what the influence of the entrainment term is (e.g. in comparison with the settling term) on the behaviour of the fluid mud layers.

It can be concluded that the entrainment term of eq. (6.4) needs some improvements, e.g. by basing the Richardson number on the upper layer depth. The incorporation of the integral entrainment model of Kranenburg will only be a step forward when this is done in combination with other improvements, i.e. incorporation of a fluid mud layer with a varying density and when there is more evidence for the application of the results to full scale.

The processes of consolidation and erosion are dependent on the flow condition. For laminar flow, consolidation can take place, bed material is eroded when the flow is turbulent. The flow condition is related to the effective Reynolds number for Bingham fluids, $Re_e$, which is defined by

$$\frac{1}{Re_e} = \frac{1}{Re} + \frac{1}{Re_y} \quad , \text{ with } \quad Re = \frac{u_m d_m}{\nu_m} \quad , \quad Re_y = \frac{2\rho_m u_m^2}{\tau_y} \tag{6.5}$$

The critical Reynolds number for transition from laminar to turbulent flow is established at 500-750.
In the fluid mud model the bed erodes when $Re_e > 600$, the fluid mud layer consolidates when $Re_e < 400$.

The shear stresses $\tau_m$ and $\tau_i$ in equations (6.2) and (6.3) are related to the flow velocities

$$\tau_m = \tau_B + \frac{f\rho_m}{8}(u_m^2 + v_m^2) \tag{6.6}$$

$$\tau_i = \frac{f\rho_o}{8}(\Delta u^2 + \Delta v^2) \tag{6.7}$$

The friction coefficient $f$ in these equations is not known a priori and should be established through calibration.

In the previous equations the following notations are used:

$C$ = (volume) sediment concentration in the suspension layer
$C_m$ = constant volume concentration of the fluid mud layer
$d_m$ = thickness of the fluid mud layer
$dm/dt$ = net rate of mass exchange of mud
$Fr_i$ = internal Froude number = $\frac{u^2}{\frac{\Delta\rho}{\rho}gh}$
$f$ = friction coefficient
$g$ = gravitational acceleration
$H$ = Heaviside step function: $H[x] = 1$ when $x$ is positive or zero, $H[x] = 0$ when $x$ is negative
$M_e$ = erosion constant

$Re$ = Reynolds number
$Re_e$ = effective Reynolds number
$Re_y$ = cohesive Reynolds number
$Ri_B$ = bulk Richardson number for the lower layer = $(\Delta\rho g d_m)/(\rho_0 \Delta U^2)$
$t$ = time
$u,v$ = velocity components in the suspension layer from the 2DH flow computation
$u_m$ = flow velocity of the fluid mud layer in $x$-direction
$v_m$ = flow velocity of the fluid mud layer in $y$-direction
$\Delta u$ = $u - u_m$
$\Delta v$ = $v - v_m$
$\Delta U$ = velocity difference between the overlying water and the fluid mud = $(\Delta u^2 + \Delta v^2)^{0.5}$
$V_e$ = entrainment velocity: $V_e = \Delta U \dfrac{0.1}{(1+63Ri_B^2)^{\frac{3}{4}}}$
$V_0$ = dewatering velocity
$w_s$ = fall velocity
$x,y$ = horizontal spatial coordinates
$\eta$ = water surface elevation
$\eta_m$ = elevation of the upper surface of the mud layer
$\nu_m$ = kinematic viscosity of the fluid mud layer
$\rho_0$ = density of the water in the suspension layer
$\rho_m$ = $\rho_0 + \Delta\rho$
$\Delta\rho$ = density excess of the fluid mud with respect to water
$\tau$ = bed shear stress (from the 2DH flow computation) =

$$\tau = \rho_0 g \frac{u^2 + v^2}{C^2} \qquad (6.8)$$

$C$ = Chézy coefficient
$\tau_B$ = Bingham yield stress strength
$\tau_{dm}$ = critical shear stress for settling from suspension to the mud layer
$\tau_e$ = critical shear stress for erosion
$\tau_i$ = shear stress between the suspension layer and the fluid mud layer
$\tau_m$ = shear stress between the fluid mud layer and the underlying bed
$\tau_y$ = yield strength
$\Omega$ = Coriolis parameter

In the model it is assumed that no fluid mud layer is present when the thickness of the fluid mud layer is smaller than a critical, user provided depth (= VAR parameter), because then 'drying' occurs. In that case the shear stress $\tau$, from the 2DH flow computation, appears as the shear stress between the bed layer and flow layer.

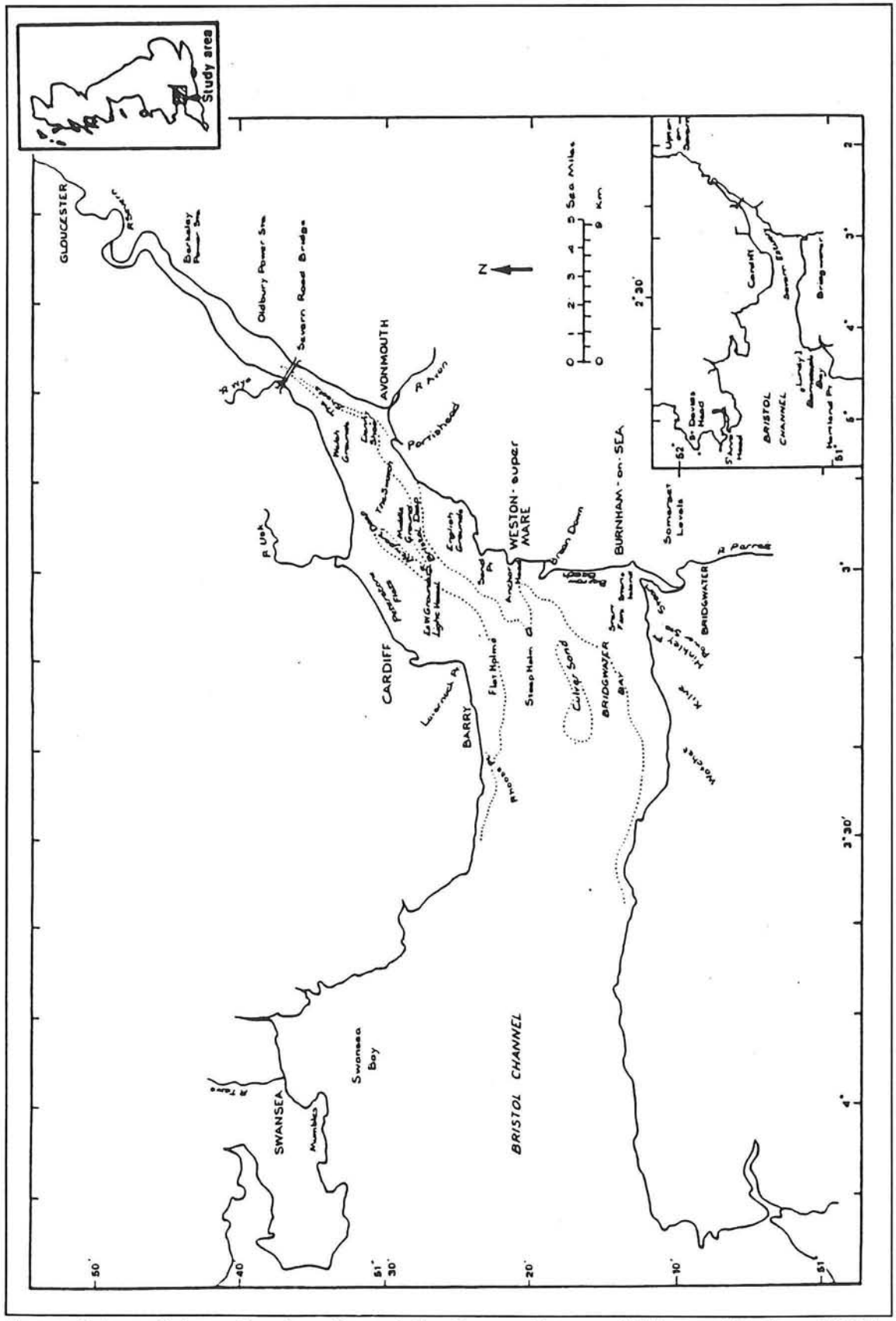


Figure 7.1: Schematic plan view of the Severn Estuary (Kirby and Parker, 1980)

# 7.0 SIMULATION OF FLUID MUD TRANSPORT IN THE SEVERN ESTUARY

*Chapter 6 introduced a two layer fluid mud model to describe the transport and behaviour of fluid mud layers. In this Chapter numerical simulations with the model are described for the Severn Estuary. First a description of the characteristics of the Severn Estuary is given in Section 7.1. The computational results of the development and movement of fluid mud in the Severn are the subject of Section 7.2 (phase I) and 7.3 (phase II). Some modelling restrictions of phase I were improved in phase II. For both phases the computational results are discussed and compared with observations of fluid mud layers in the Severn.*

## 7.1 Description of the characteristics of the Severn Estuary

*Location and dimensions*

The Severn Estuary is located along the west coast of the United Kingdom, at the border between England and Wales. It is of funnel shape with a main east-west orientation. A schematic plan view of the eastern part of the Severn is shown in figure 7.1.

In the mouth of the estuary, i.e. downstream of Swansea, the bed is fairly flat with a depth of 30 to 50 m CD. Bristol Channel has a depth of about 25 m CD, its channel reaches a depth around 35 m CD. Shoals and some mud banks are encountered along the banks. Around Bristol and further upstream, the bathymetry is more complicated owing to the presence of a number of intertidal shoals, extensive mud banks well above mean sea level and channels. More upstream, the Severn becomes very shallow, of the order of a few metres.

The Severn river is the largest river that discharges into the estuary, with a mean flow of (only) 50 $m^3/s$.

*Tidal elevations and currents*

The Severn Estuary is a macro-tidal basin, with a mean tidal range of about 8 m, dominated by the semi-diurnal component. Spring tide has a range of about 12 m, the range for neap tide is about 4 m. The tidal range increases from the mouth to the Severn Road Bridge. Further upstream the tidal wave is damped.

Because of the large elevations, large tidal currents are present in the Severn. On an average spring tide velocities exceed 1.5 m/s near Avonmouth. The mean and extreme tidal current velocities near Swansea are about 1.5 m/s and 2.0 m/s respectively.

A considerable asymmetry in the tide develops due to the large tidal range. This asymmetry, induced by the bathymetry, results in a net inflow along the southern shore and a net outflow along the northern shore, thus a net counterclockwise circulation is induced.

Due to the high tidal energy the estuary can be considered well mixed.

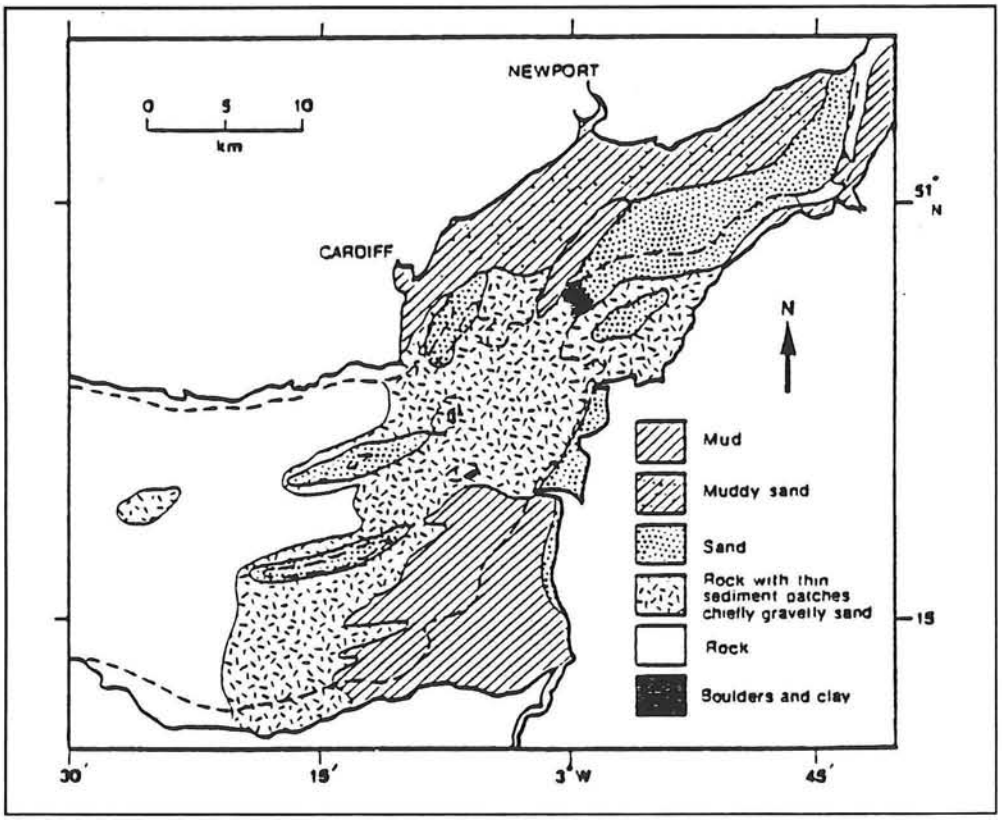


Figure 7.2: Distribution of bed surface sediment in the Severn (Kirby and Parker, 1980)

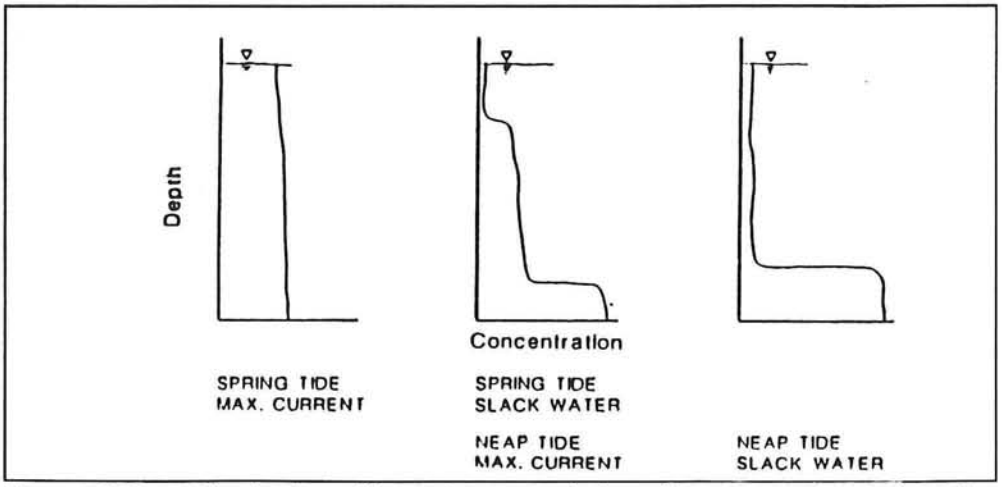


Figure 7.3: Vertical profiles of suspended sediment concentration during spring and neap tides (Dyer, 1984)

*Morphology and suspended sediment*
The Severn Estuary is a very dynamic estuary with high rates of sediment transport (about 16,000,000 kg a year). All sediment movement can be considered as a redistribution of the sediments within the Severn. Figure 7.2 gives an impression of the distribution of bed sediments in the estuary. Bristol Channel bed mainly consists of rock. More sediment is present along the shore, especially in and around Swansea Bay. The east part of the estuary has a pattern of gravel, sand and mud. Further upstream it becomes more muddy. The bed of Bridgwater Bay, Cardiff and Newport consists of large mud banks, well above mean sea level.
The large variations in the tidal velocities result in a large range of concentration of suspended sediment. During spring tide concentrations exceed 5 g/l, during neap tide the concentration is of the order 100 mg/l. A vertical stratification can develop. Figure 7.3 schematically shows the vertical profiles of suspended sediment concentration during spring and neap tides. Most of the time a lutocline exists. The resulting density gradient affects the intensity of turbulence, hence the effective vertical mixing.
In the southern part of the estuary the concentrations are very large due to the presence of large quantity of fluid mud in the channels here.

*Fluid mud*
Because of the large tidal range, the tidal flow is the dominating driving force for the fluid mud motion in the Severn. Fluid mud is generated during slack tide from deposition of the sediment suspension. It can flow in deeper channels through gravity and tidal flow. During neap tide some layers gain a thickness of about 1.5 m.
From penetrating echo sounders and data of local stations, Kirby and Parker (1983) observed layers of fluid mud in Swansea Bay, Cardiff Channel and in the approaches to Bridgwater Bay. Large pools of fluid mud were found in Newport Deep, where a mud thickness of 0.5-1.5 m was reported to be stable during tides with a 6 m range. The largest and most persistent fluid mud layers were encountered in the main channel between Clevedon and Avonmouth and in the Shoots Channel (up to 5 m thick). In Avonmouth area ephemeral layers of 3 m thick were found at high water. Sediment concentrations in the mud pools between 4 and 440 g/l were found. Odd and Cooper (1989) reported fluid mud occurrences on slopes at angles between $0.25^{o}$ and $7.5^{o}$.
See figure 7.4 for an impression of fluid mud occurrences in the Severn.
Only a rough comparison between the observed and computed results is possible.

## 7.2 Simulation phase I

### 7.2.1 Computational results

Odd and Cooper (1989) used their fluid mud model to set up a pilot model of mud transport in the Severn Estuary during spring and neap tides. They aimed to simulate the growth and decay of fluid mud layers as observed by Kirby and Parker (1983). Initial and boundary conditions for the suspended mud concentrations were based on observations from Kirby and Parker (1983, 1982) and Hydraulics Research (1981). The results of Odd and Cooper for a neap tidal range of 6.8 m at Avonmouth can be found in figure E28 of appendix E.

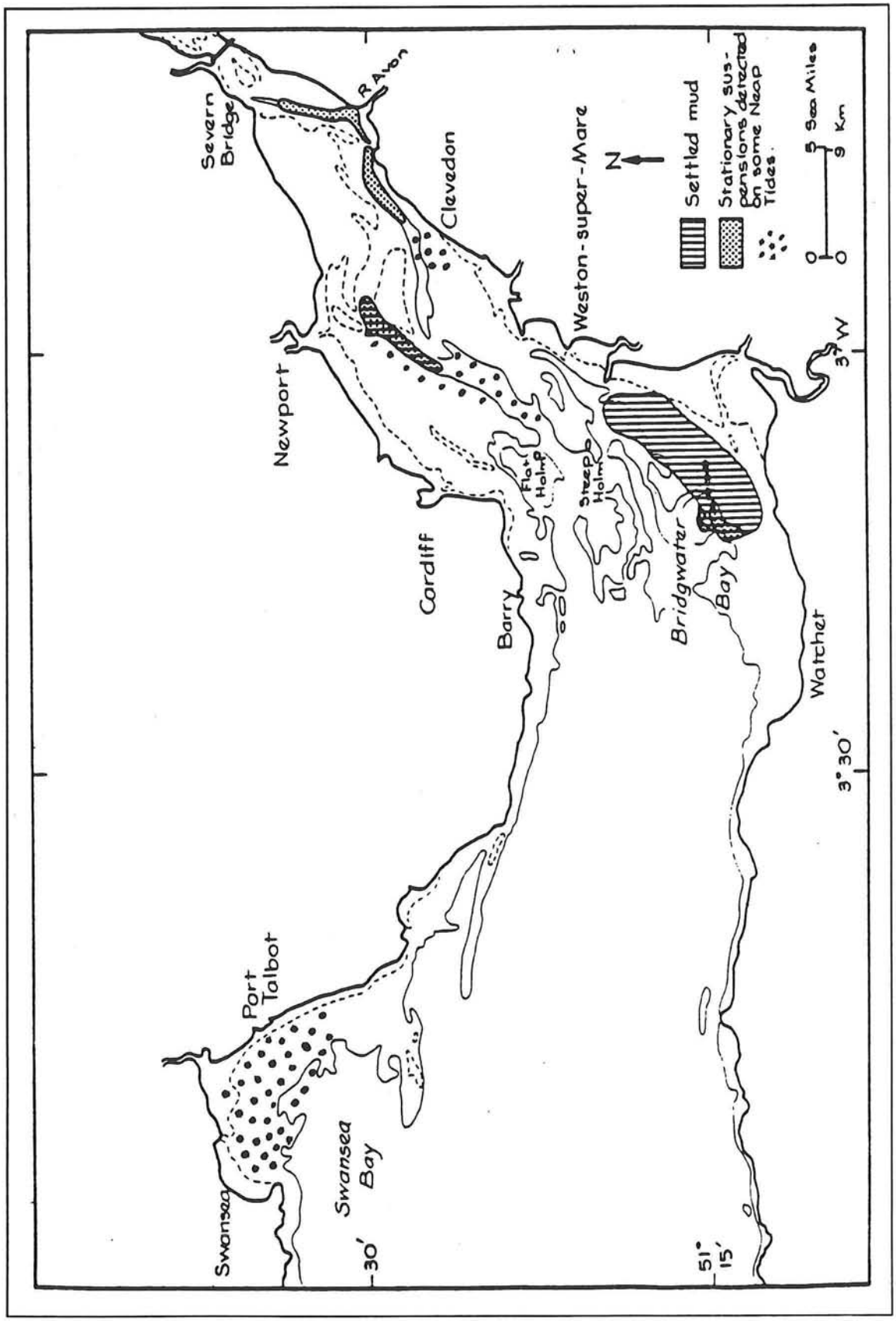


Figure 7.4: Fluid mud occurrences in the Severn Estuary (Kirby and Parker, 1980)

As mentioned in Chapter 6, the two layer fluid mud model of Delft Hydraulics was derived by adapting the model of Odd and Cooper (1989). It is calibrated to simulate conditions in the Severn during neap tide. Because of the dominating semi-diurnal component, only the $M_2$ and $S_2$ components are used to simulate the tide. The tidal period is 12.5 hours. The simulation starts at $t$ = 1500 minutes and eight tidal cycles are run.

Figure E3 of appendix E gives an impression of the grid dimensions of the study area. The water and mud level points and the concentration points are defined in the centre of a cell, whereas the velocity components are defined on the faces of the cell, see figure 7.6. The grid of the model is drawn through the depth values.
The coarse resolution, which causes inaccuracies, is a weakness of the present Severn model.

In figure E1 of appendix E the bathymetry for the Severn Estuary used in the model is given. This figure also shows the locations of the two stations where time histories of the suspension layer and fluid mud layer are given, i.e. time histories of water and mud level, suspended sediment concentration, directions and velocities of the two layers. Station 7 is called after Odd & Cooper, because their model results are presented for this location. Their computational results will be discussed later.
The simulated neap tidal water level elevations and flow velocities are given for the two stations in figure E2. Station 1 has a water depth of 20.5 m with respect to MSL, station 7 has a depth of 14.8 m with respect to MSL. The initial transients due to the adaptation time can be noticed in the figures. Consequently, this results in an adaptation time for the fluid mud behaviour.
The flow velocity of the study area at time $t$ = 6000 min. (i.e. 3.1 hours after low water in the mouth of the estuary) is illustrated in figure E3. For Station 1 this is just before turning of the tide, with a flow velocity of about 0.5 m/s. For Station 7 the this is about one hour after low water, the flow velocity is about 0.7 m/s. In the following, all reference times are with respect to high and low water in the mouth of the estuary.

Once formed, the fluid mud layer is assumed to flow under the influence of gravity, horizontal pressure gradients and frictional forces (see also Chapter 6):
1. drag by the suspension layer ($\tau_i$)
2. bottom slope ($g$)
3. water surface slope
4. slope of the lutocline of the fluid mud layer

This already indicates the complexity of the processes inducing the transport and behaviour of a fluid mud layer.
For simplification of the analysis, the set up of the simulation programme in phase I is as follows:

I. The vertical transport of fluid mud only due to settling and entrainment is regarded first.
II. Next, only horizontal transport of fluid mud is considered.
III. Finally the simulation is extended to include both the processes of horizontal and vertical transport of fluid mud.

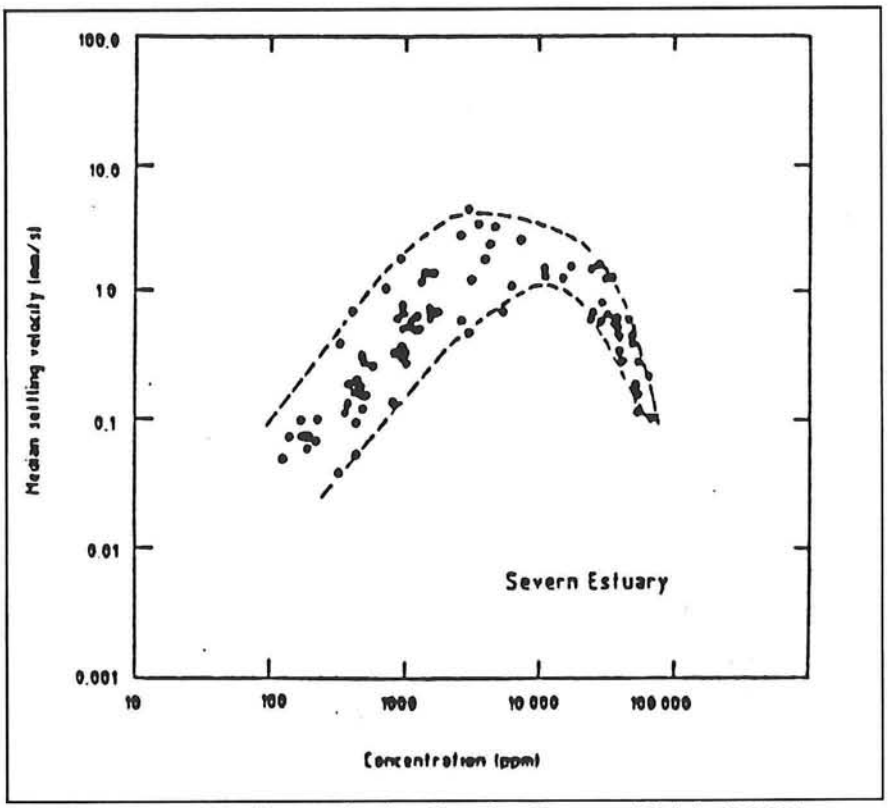


Figure 7.5: Settling velocity for the Severn (Odd, 1988)

| Simulation | I | | | II | III | | |
|---|---|---|---|---|---|---|---|
| Run no. | 1 | 2a | 2b | 3 | 4a | 4b | 5 |
| Settling | + | + | + | - | + | + | + |
| Entrainment | - | + + | + | - | + + | + | + |
| Dewatering | - | - | - | - | - | - | + |
| Erosion | - | - | - | - | - | - | + |
| Gravity (sliding) | - | - | - | + | + | + | + |
| Drag by water | + | - | - | + | + | + | + |
| Init. mud layer (m) | 0.01 | 0.4 | 0.5 | 0.5 | 0.1 | 0.1 | 0.1 |
| VAR (m) | 0.5 | 0.5 | 0.5 | 0.05 | 0.05 | 0.05 | 0.05 |

\+ = influence of the parameter
\- = no influence of the parameter

Table 7.1: Simulation programme of phase I

Values of the coefficients, the initial and boundary conditions are adopted from the simulation of Odd and Cooper (1989):

| | | | |
|---|---|---|---|
| $\rho_o$ | = | 1020 kgm$^{-3}$ | density of suspension layer |
| $\rho_m$ | = | 1066 kgm$^{-3}$ | density of fluid mud layer ($C_{fluid\ mud}$ = 75 gl$^{-1}$) |
| $f_i$ | = | 0.008 | friction coefficient between suspension layer and mud layer |
| $f_m$ | = | 0.006 | friction coefficient between mud layer and bed |
| $\tau_B$ | = | 0.1 Pa | Bingham yield stress strength |
| $\tau_e$ | = | 0.3 Pa | critical shear stress for erosion |
| $\tau_{dm}$ | = | 0.4 Pa | critical shear stress for settling |
| $C_m$ | = | 0.0283 | (volume) concentration in mud layer (= 75 gl$^{-1}$) |
| $C_b$ | = | 0.15 | (volume) concentration in bed (= 400 gl$^{-1}$) |
| $C_o$ | = | 0.0011 | initial (volume) concentration in the suspension layer (= 3 gl$^{-1}$) |
| $d_{m,0}$ | = | 0.01-0.5 m | initial depth of fluid mud layer |
| $C_{sea}$ | = | 0.00075 | boundary condition for the sediment (volume) concentration at the sea side (= 2 gl$^{-1}$) |
| $C_{riv}$ | = | 0 | boundary condition for the sediment (volume) concentration at the river side |
| $\Delta t$ | = | 5 min. | simulation time step |
| $C$ | = | 55 m$^{½}$s$^{-1}$ | Chézy coefficient for the 2DH flow computation |

The boundary conditions for fluid mud are that the mud layer cannot flow out of the model.

Values of the other parameters are

| | | | |
|---|---|---|---|
| $w_s$ | = | $10^{-3}$ ms$^{-1}$ | settling velocity taken for the Severn, see figure 7.5 |
| $M_{ers}$ | = | 2E-08 ms$^{-1}$ | parameter for erosion |
| $V_o$ | = | 5E-07 ms$^{-1}$ | consolidation velocity |

In order to influence the magnitude of the entrainment term, an entrainment coefficient $E$ is invoked. The entrainment term becomes:

$$\textit{Entrainment:}\quad \frac{dm}{dt} = EV_eC_mH[10-Ri_B] \qquad (7.1)$$

$$\text{with}\quad V_e = \Delta U\frac{0.1}{(1+63Ri_B^2)^{0.75}}\ ,\qquad Ri_B = \frac{\Delta\rho g d_m}{\rho_o \Delta U^2}$$

The simulations are carried out in the form of a sensitivity analysis; the various parameters are varied with respect to the parameters mentioned above. Table 7.1 gives a summary of the physical parameters which characterize a simulation.
Sliding along slopes due to gravity can be prevented by choosing $\tau_B$ > about 1000 Pa.

During the simulation patches of mud developed at the boundaries of the model due to boundary effects. These anomalies will not be discussed in the analysis.

Values of the parameters which are characteristic for a simulation are repeated in the text.

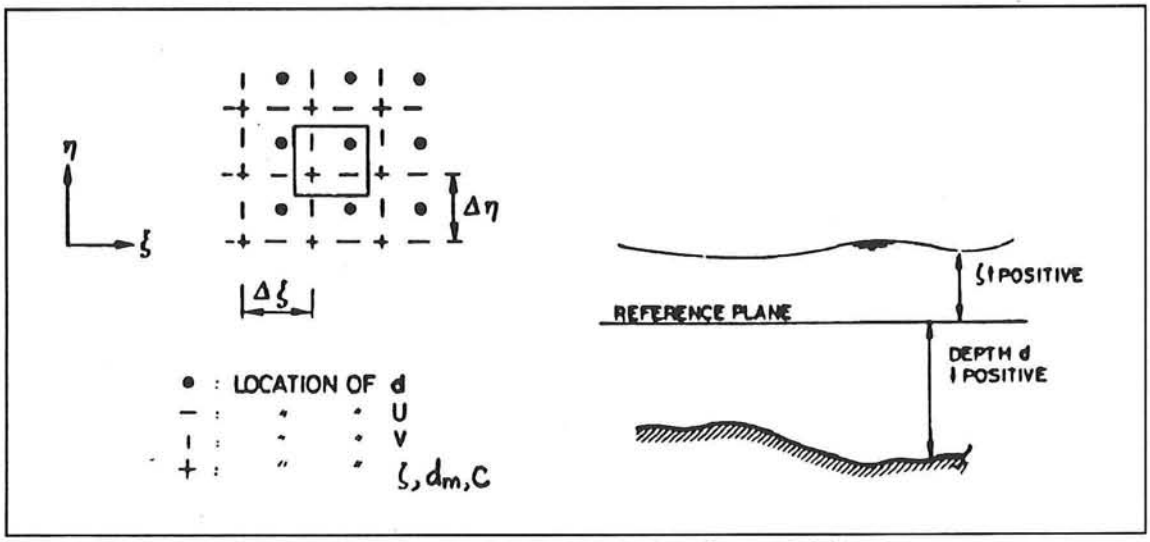


Figure 7.6: The computational grid (Delft Hydraulics, 1988)

I. *Vertical transport of fluid mud*

**RUN 1**. *Vertical transport because of settling*
$w_s = 10^{-3}$ ms$^{-1}$, $\tau_B$ = 10,000 Pa, $E = M_{ers} = V_o = 0$, $d_{m,0}$ = 0.01 m, VAR = 0.5 m
The thickness of the fluid mud layer increases because of settlement from the suspension layer.
All the sediment will settle to the bottom according to

$$\frac{d(hC)}{dt} = w_s C(1-\frac{\tau}{\tau_{dm}})H[\tau_{dm}-\tau] \ , \quad \text{thus} \quad C(t) \approx C_0 e^{-(\frac{Bw_s}{h})t} \qquad (7.2)$$

with $B$ a function of $\tau$.

The results are given in appendix E. The growth of the fluid mud layer and decrease of the suspended sediment concentration with time for Stations 1 and 7 are given in figure E4. For Station 1 -20.5 m is the (consolidated mud) bottom with respect to MSL, the bottom of Station 7 lies 14.8 m below MSL. A picture of the thickness of the mud layer for the Severn at $t$ = 6000 minutes (3.1 hours after low water) is given in figure E5. After 6000 minutes the mud layer of Station 1 has gained a thickness of 0.98 m and at Station 7 0.49 m.
For this simulation the VAR parameter was set at 0.5 m. This means $\tau$, from the 2DH flow computation, appears as shear stress between the fluid mud layer and the flow layer when the mud thickness is smaller than 0.5 m, as explained in Chapter 6. When the mud thickness exceeds 0.5 m, $\tau_i$ is the acting shear stress.
From the figures it can be noticed that settling only occurs for low flow velocities, when $\tau < \tau_{dm}$ (or $\tau_i < \tau_{dm}$ in case the mud thickness is larger than 0.5 m), resulting in an increase in the mud thickness. When $\tau \geq \tau_{dm}$ the flow velocities are too high to cause the sediment to settle. For areas where the flow velocities are low, the growth of the fluid mud layer increases faster with time in comparison with areas subjected to higher flow velocities. The sediment concentration in the suspension layer decreases in agreement with the increase in the fluid mud layer thickness.
As mentioned in Chapter 6, it is assumed that no mud is present when the mud layer thickness is smaller than the value of the VAR parameter. Physically, this can be interpreted as 'no flow of the mud layer'. A mud layer with a thickness larger than the value of VAR can be transported. During the simulation, the mud layer started to flow when its thickness exceeded the critical value of 0.5 m. This explains the areas in figure E5 with relatively large differences in mud thicknesses.
Because $\tau_B$ was set at 10,000 Pa the mud cannot slide from the bed slopes due to its own weight.
Thick mud layers up to 2 m can be found in the middle of Bristol Channel.
Mud velocities, resulting from horizontal pressure gradients and frictional forces, as explained above, are in the range of $10^{-7}$-$10^{-6}$ ms$^{-1}$.

**RUN 2.** *Vertical exchange by settling and entrainment*
$w_s = 10^{-3}$ ms$^{-1}$, $\tau_B$ = 10,000 Pa, $M_{ers} = V_o = 0$, $d_{m,0}$ = 0.4 m, $f_i = 0$, $E$ = ..., VAR = 0.5 m
The purpose of the simulation is to obtain a dynamic balance by the processes of settling and entrainment.
The condition $f_i = 0$ implies that no driving force is present for the fluid mud layer due to tidal flow. A consequence is that settling is not reduced by the shear stress $\tau_i$. However, this only counts for mud thicknesses larger than 0.5 m (value of VAR parameter). For mud thicknesses smaller than 0.5 m, $\tau$ from the 2DH flow computation appears as bed shear stress.
Sliding of mud from slopes is suppressed due to the high Bingham shear strength.

The source term becomes

$$\frac{dm}{dt} = w_s C(1-\frac{\tau}{\tau_{dm}})H[\tau_{dm}-\tau] - EV_e C_m H[10-Ri_B] \qquad (7.3)$$

$$\text{with} \quad V_e = \Delta U \frac{0.1}{(1+63Ri_B^2)^{0.75}}, \quad Ri_B = \frac{\Delta\rho g d_m}{\rho_0 \Delta U^2}$$

When the mud thickness is smaller than the value of the VAR parameter for 'drying', i.e. if $d_m$ < VAR = 0.5 m in this case, the following relation is applied
If Entrainment term > Settling term
then : Entrainment = Settling and $dm/dt = 0$
(This process is referred to as 'hindered entrainment' in the following)
else : $dm/dt$ = *(Settling - Entrainment)*

Two simulations with a different entrainment coefficient are regarded:
**Run 2a.** $E$ = 5E-02
**Run 2b.** $E$ = 5E-03

**RUN 2a.** $E$ = 5E-02
The results for Stations 1 and 7 are presented in figure E6. Station 1 is characterized by growth and subsequent quick decay of the fluid mud layer. For Station 7 the high entrainment rate prevents settling and growth of a fluid mud layer, apart from some initial effects.
A short analysis is given for Station 1:
Mud thickness and sediment concentration are derived from figure E6. The flow velocities $u$, $v$ and $\Delta U$ ($u_m \approx v_m \approx 0$) come from the 2DH flow computation, the magnitude of the flow velocity, $\Delta U$, can also be seen in figure E2. $\tau$ results from equation (6.8) and the other parameters are obtained with equation (7.3).

$t$ = 3000 min.: $d_m = 0.23$m, $u = 0.50$ms$^{-1}$, $v = 0.03$ms$^{-1}$, $\Delta U = 0.50$ms$^{-1}$, $C = 0.0012$
Settling: $\tau = 0.8$ Pa > $\tau_{dm}$ : no settling, $dm/dt = 0$
Entrainment: $Ri_B = 0.42$, $Ve$ = 7.6E-03 : $dm/dt$ = 1.1E-05 ms$^{-1}$
Conclusion: entrainment > settling, thus $dm/dt = 0$

$t$ = 3250 min.: $d_m$=0.33m, $u$=0.01ms$^{-1}$, $v$=0.005ms$^{-1}$, $\Delta U$=0.01ms$^{-1}$, $C$=0.0011
Settling: $\tau$=3.5E-04 Pa < $\tau_{dm}$ : $dm/dt$ = 1.1E-06 ms$^{-1}$
Entrainment: $Ri_B$ = 1153 : $dm/dt$ = 0
Conclusion: growth of fluid mud layer by settling,
$(dm/dt)/C_{mud}$ = 3.8E-05 ms$^{-1}$ ≈ 0.23 cm/min

$t$ = 4000 min.: $d_m$=0m, $u$=0.01ms$^{-1}$, $v$=0.005ms$^{-1}$, $\Delta U$=0.01ms$^{-1}$, $C$=0.0011
Settling: $\tau$=3.2E-04 Pa < $\tau_{dm}$ : $dm/dt$ = 1.05E-06 ms$^{-1}$
Entrainment: $Ri_B$ = 0, $Ve$ = 1.0E-03 : $dm/dt$ = 1.4E-06 ms$^{-1}$
Conclusion: entrainment > settling, thus $dm/dt$ = 0

$t$ = 6500 min.: $d_m$=0.18m, $u$=0.37ms$^{-1}$, $v$=0.12ms$^{-1}$, $\Delta U$=0.39ms$^{-1}$, $C$=0.0006
Settling: $\tau$=0.82 Pa > $\tau_{dm}$ : no settling, $dm/dt$ = 0
Entrainment: $Ri_B$ = 0.51, $Ve$ = 0.12 : $dm/dt$ = 6.1E-07 ms$^{-1}$
Conclusion: entrainment > settling, thus $dm/dt$ = 0

$t$ = 7000 min.: $d_m$=0.36m, $u$=0.01ms$^{1}$, $v$=0.005ms$^{-1}$, $\Delta U$=0.01ms$^{-1}$, $C$=0.0009
Settling: $\tau$=3.1E-04Pa < $\tau_{dm}$ : $dm/dt$ = 9.3E-07 ms$^{-1}$
Entrainment: $Ri_B$ = 1367 : $dm/dt$ = 0
Conclusion: growth of fluid mud layer by settling,
$(dm/dt)/C_{mud}$ = 3.3E-05 ms$^{-1}$ ≈ 0.20 cm/min

Growth around $t$ = 7000 min.:
In 80 minutes the mud layer grows about 0.20 cm/min • 80 min. ≈ 16 cm.. This growth agrees with the increase in mud thickness observed for Station 1 in figure E6.

The decay of the mud layer around $t$ = 3750 min. cannot result from entrainment only, because $dm/dt$ = 0.65m/15min ≈ 7.2E-04 ms$^{-1}$ which is much larger than the entrainment rate.
Besides the processes of settling and (hindered) entrainment, a slope of the lutocline of the fluid mud layer or a gradient in the water layer depth largely attributes to the pattern of mud layers. In order to understand the mud occurrences at one location, the physical processes of its environment have to be considered too. This is briefly elucidated by considering 6 locations around Station 1 in Swansea Bay. The positions and time histories of mud level for these locations are given in figure E27. For 3 Stations a continuous increase in mud level can be observed, though the other Stations are characterized by a sudden decay of the mud level. The sudden decay of mud level is caused by horizontal transport of fluid mud. Probably this is not realistic because of the coarse grid and large simulation time step.

Figure E7 shows the mud thickness of the study area at $t$ = 6000 min. (3.1 hours after low water). The mud thickness of Station 1 is 6 cm. Except for Swansea Bay and a southern part in the mouth of the Severn no significant fluid mud layers can be observed. During the tidal cycle no layers of importance were formed, besides some shallow spots up to 0.5 m thick in and around Bristol Channel and Bridgwater Bay. From these results it may be concluded that the entrainment rate is too large to cause growth of fluid mud layers.

**RUN 2b.** $E$ = 5E-03
See figure E8 for the results of Stations 1 and 7. For Station 1 the entrainment rate is too low and the mud layer grows continuously because of settling. Again a short analysis is given for Station 1:

$t$ = 3250 min.: $d_m = 1.29$m, $u = 0.01$ms$^{-1}$, $v = 0.005$ms$^{-1}$, $\Delta U = 0.01$ms$^{-1}$, $C = 0.0008$
Settling: $d_m$ > VAR: $\tau_i = 0$ : $dm/dt$ = 8.3E-07 ms$^{-1}$
Entrainment: $Ri_B$ = 5766 : $dm/dt$ = 0
Conclusion: growth of fluid mud layer by settling,
$(dm/dt)/C_{mud}$ = 2.9E-05 ms$^{-1}$ ≈ 0.18 cm/min

$t$ = 4000 min.: $d_m = 1.79$m, $u = 0.01$ms$^{-1}$, $v = 0.005$ms$^{-1}$, $\Delta U = 0.01$ms$^{-1}$, $C = 0.0004$
Settling: $d_m$ > VAR: $\tau_i = 0$ : $dm/dt$ = 4.5E-07 ms$^{-1}$
Entrainment: $Ri_B$ = 8000 , $dm/dt$ = 0
Conclusion: growth of fluid mud layer by settling,
$(dm/dt)/C_{mud}$ = 5.9E-05 ms$^{-1}$ ≈ 0.10 cm/min

$t$ = 6500 min.: $d_m = 2.93$m, $u = 0.37$ms$^{-1}$, $v = 0.12$ms$^{-1}$, $\Delta U = 0.39$ms$^{-1}$, $C = 0.0002$
Settling: $d_m$ > VAR: $\tau_i = 0$ : $dm/dt$ = 2.0E-07 ms$^{-1}$
Entrainment: $Ri_B$ = 8.61, $Ve$ = 6.9E-05 : $dm/dt$ = 9.8E-09 ms$^{-1}$
Conclusion: growth of fluid mud layer by settling,
$(dm/dt)/C_{mud}$ = 6.7E-06 ms$^{-1}$ ≈ 0.04 cm/min

Settling dominates at Station 1 during the whole simulation.
Also the locations around Station 1 show a continuing increase in mud level. Both the processes of hindered entrainment and settling are taking place for Station 7. Also sudden disappearances of mud layers generated by the hydrostatic forces can be noticed. An impression of the mud thickness at $t$ = 6000 min. (3.1 hours after low water) is given in figure E9. For Station 1 the mud thickness is 1.7 m, for Station 7 the thickness is about 0.1 m. The 'white spots' are due to the large gradients in the mud thicknesses, resulting in a dense pattern of white isolines drawn by the plotter. Generally it can be noticed that the mud layers present in simulation 2a are enlarged, especially in the mouth of the estuary and in Bristol Channel mud pools up to 4 m have developed. Some little spots up to 3.5 m thick are encountered in Bristol Deep, Cardiff Bay and in Bridgwater Bay.
When considering figures E6 to E9, it can be concluded that no dynamic equilibrium between the settling and entrainment processes can be obtained for the whole area. For simulation 2a and simulation 2b the velocities in the mud layer are in the range of $10^{-7}$-$10^{-6}$ ms$^{-1}$.

II. *Horizontal transport of fluid mud*

**RUN 3.** *Horizontal transport of fluid mud*
$w_s = E = M_{ers} = V_0 = 0$, $\tau_B$ = 0.1 Pa, $d_{m,0}$ = 0.5 m, VAR = 0.05 m
When there is no vertical exchange of fluid mud, the mud layer will only grow or be transported because of hydrostatic, frictional and gravitational forces. On account of these various processes it is difficult to tell beforehand where and how mud layer develop. The results of the mud levels and magnitude of the mud velocities for

Stations 1 and 7 can be found in figure E10. The mud velocities are $\approx 10^{-4}$-$10^{-3}$ ms$^{-1}$. Figure E11 gives an impression of the mud thickness at $t$ = 6000 min., i.e. 3.1 hours after low water. Station 1 has a mud thickness of 0.05 m, the thickness of Station 7 is 0.4 m. Especially in areas where steep bed slopes are encountered the mud has flown to deeper parts, e.g. in Newport Deep and in the Shoots Channel. Again persistent mud layers can be observed in the northern and southern part of the estuary mouth and in Swansea Bay.
When comparing the direction of the flow and mud velocities (figure E12) it can be noticed that for Station 1 the direction of the mud velocity is independent of the direction of the flow velocity. Probably the slope of the bed is the main reason for the transport of mud. Some dependency on the flow direction for the direction of the mud movement can be seen at Station 7, where the direction of the mud velocity reverses around slack water. The fluid mud is flowing backwards and forwards along the channel. From this it follows that the hydrostatic force due to the water surface slope, and not the slope of the bed, is probably the main mechanism for moving the fluid mud along the channels.
When comparing figures E13 and E14, where respectively the flow and mud direction are presented for $t$ = 4125 min. (3.1 hours after high water), the complexity of the different processes inducing the flow of fluid mud is obvious.

III. *Vertical and horizontal transport of fluid mud*

**RUN 4.** *Vertical exchange by settling and entrainment, horizontal transport of mud*
$w_s = 10^{-3}$ ms$^{-1}$, $M_{ers} = V_0 = 0$, $\tau_B$ = 0.1 Pa, $d_{m,0}$ = 0.1 m, VAR = 0.05 m
Two simulations with a different entrainment coefficient are considered:

**RUN 4a.** $E$ = 5E-03
**RUN 4b.** $E$ = 1E-03

**RUN 4a.** $E$ = 5E-03
The results for Stations 1 and 7 are presented in figures E15 and E16 respectively. At Station 1 a small mud layer of about 16 cm appears once during the tidal cycle (when the flow velocities are lowest, i.e. at high water), but it disappears when the flow velocity becomes larger. This change in mud level is accompanied by a small mud velocity of about 0.2 cm/s and a local decrease and increase in sediment concentration. A short analysis is given for this location

$t$ = 4000 min.: $d_m = 0.034$m, $u = 0.01$ms$^{-1}$, $v = 0.005$ms$^{-1}$, $u_m = v_m = 0$,
$\Delta U = 0.01$ms$^{-1}$, $C = 0.0013$
Settling: $d_m <$ VAR, $\tau = 3.2$E-04 Pa : $dm/dt$ = 1.3E-06 ms$^{-1}$
Entrainment: $Ri_B$ = 125.5 : $dm/dt$ = 0
Conclusion: growth of fluid mud layer by settling,
$(dm/dt)/C_{mud} \approx 0.27$ cm/min

$t$ = 4050 min.: $d_m = 0.14$m, $u = 0.26$ms$^{-1}$, $v = 0.06$ms$^{-1}$, $u_m = 0.2$cms$^{-1}$,
$v_m = 0.07$cms$^{-1}$, $\Delta U = 0.26$ms$^{-1}$, $C = 0.0011$
Settling: $d_m >$ VAR, $\tau_i = 0.07$ Pa : $dm/dt$ = 9.3E-07 ms$^{-1}$
Entrainment: $Ri_B$ = 0.91, $Ve$ = 3.5E-04 : $dm/dt$ = 5.0E-08 ms$^{-1}$
Conclusion: settling dominates, $(dm/dt)/C_{mud} \approx 0.19$ cm/min

Growth around $t$ = 4050 min.:
In 80 minutes the mud layer grows about 0.23 cm/min • 80 min. ≈ 16 cm.. This growth agrees with the increase in mud layer thickness observed for Station 1 in figure E15.

$t$ = 4500 min.: $d_m$=0m, $u$=0.49ms$^1$, $v$=0.03ms$^{-1}$, $u_m$=$v_m$=0, $\Delta U$=0.49ms$^{-1}$, $C$=0.0011
Settling: $d_m$ < VAR, $\tau$=0.8 Pa : no settling, $dm/dt$ = 0
Entrainment: $Ri_B$ = 0, $Ve$ = 0.05 : $dm/dt$ = 6.9E-06 ms$^{-1}$
Conclusion: entrainment > settling, thus $dm/dt$ = 0

The same tendency can be noticed for Station 7, though an increase in mud level appears two times during a tidal cycle. After the increase during low water, the mud level stays constant ($d_m$ < VAR, hence entrainment is suppressed), until it becomes high water. Then the mud thickness grows again and reaches a thickness of about 17 cm, whereafter the mud layer disappears. Only the increase at high water results in a small mud velocity of about 1.0 cm/s. An impression of the mud thickness at $t$ = 6300 min. (2 hours after high water) and $t$ = 6600 min. (low water) is given in figures E17 and E18. At $t$ = 6300 min. the mud thickness of Station 1 is about 10 cm, of Station 7 the thickness is about 12 cm. For both stations the entire mud layer has disappeared at $t$ = 6600 min. due to entrainment and horizontal transport of fluid mud. Most of the shallow mud pools present at $t$ = 6300 have disappeared at $t$ = 6600 min. due to the processes of entrainment and horizontal transport. Persistent mud layers up to 4 m thick are encountered in the northern and southern part of the mouth of Severn, in Swansea Bay and in a part of Bridgwater Bay.

**RUN 4b.** $E$ = 1E-03
Station 1 in figure E19 is characterized by a process of net increase in the mud thickness during a tidal period when $t$ < 3750 min.. This is due to the low entrainment rate. After $t$ > 3750 min. the mud layer starts to slide along the slope and the local mud thickness decreases. Again the direction of the mud velocity is independent of the flow direction. For Station 7 in figure E20 a dynamic cycle of development and decay of the mud layer can be noticed. The mud thickness becomes larger with a maximum thickness of 0.17 m in comparison with simulation 4a. The direction of the mud velocity differs from simulation 3, from which follows that the processes of entrainment and settling influence the direction of mud transport. Generally, only during slack water the mud velocity follows the direction of the flow velocity.
Figures E21 and E22 present a map of the mud thickness for $t$ = 6300 min. (2 hours after high water) and $t$ = 6600 min. (low water) respectively. The mud thickness at Station 1 is 0.53 m and 0.47 m respectively. At Station 7 the mud layer of 10 cm thick present at $t$ = 6300 min. has vanished at $t$ = 6600 min. due to entrainment and horizontal transport. In comparison with simulation 4a, more extended and persistent mud pools are encountered in Swansea Bay, Bridgwater Bay and in the mouth of the estuary. Also a persistent mud layer has appeared near Avonmouth.
Generally, in the east part of the estuary shallow mud layers develop only during slack water. Due to the lower entrainment rate, these mud layers can extend to a larger area and they reach a little larger thickness in comparison with simulation 4a.

**RUN 5.** *Vertical and horizontal transport of fluid mud*
$w_s$ = 10$^{-3}$ ms$^{-1}$, $E$ = 1E-03, $M_{ers}$ = 2E-08 kgm$^{-2}$s$^{-1}$, $V_0$ = 5E-07 ms$^{-1}$, $\tau_B$ = 0.1 Pa, $d_{m,0}$ = 0.1 m, VAR = 0.05 m
For the computational results see figures E23 to E26. In figure E25 ($t$ = 6300 min., i.e. 2 hours after high water) the mud thicknesses of Stations 1 and 7 are respectively 0.5 m and 0.14 m. In figure E26 ($t$ = 6600 min., i.e. low water) Station 1 has a thickness of 0.43 m, while the processes of entrainment and horizontal transport of fluid mud cause the mud layer of Station 7 to have disappeared. The 'white spots' are due to the large gradients in mud thicknesses.
During a tidal cycle the velocities in the fluid mud layer are too low to cause any erosion of the consolidated bed. The effective Reynolds number $Re_e$, resulting from eq. (6.5), is about 0.03 for Station 1 and about 0.4 for Station 7. Because of the laminar flow condition a continuous process of consolidation of fluid mud is taking place at a constant dewatering velocity of $V_0$ = 5E-07 ms$^{-1}$. This results in a 3 cm increase in bed level after 8 tidal periods, which can be seen in a 3 cm increase in bottom level for Station 7 in figure E24. Time histories of the suspended sediment concentration and mud level differ a little from the results of simulation 4b. The effect of consolidation is hardly noticeable in figures E25 and E26.

Eventually the process of consolidation will lead to the situation where all the sediment concentration and mud have consolidated, resulting in an increase in the thickness of the consolidated mud bed. In the model this corresponds with an increase in the bottom level.

### 7.2.2 Discussion of results

*Comparison with the results of Odd and Cooper*
When comparing the computational results of simulation 5 in figures E25 and E26 with the results of Odd and Cooper for Station 7 in figure E28a, a general agreement between the flow velocity and flow direction can be observed. However, the differences between the results for the fluid mud layer are obvious. Odd and Cooper obtained a maximum thickness of almost one metre for the fluid mud layer, while the maximum thickness according to the present model is only 0.15 metres. Also the mud velocity is about 20 times smaller than results from Odd and Cooper. No agreement can be noticed for the direction in which the mud layer transports. Figure E28b shows the simulated distribution and depth of fluid mud at HW slack obtained by Odd and Cooper. Their model predicted much thicker layers of fluid mud in the Shoots Channel, Bristol Deep, Newport Deep and even further downstream in comparison with simulation 5. No mud was formed on the bed slopes, in contradiction with the results of simulation 5, where also boundary effects are obviously present.

The differences in mud thickness and mud velocity are difficult to explain. The entrainment rate in the model was 5E-03 times the term modelled by Odd and Cooper, though Odd and Cooper reached a much higher mud thickness. Their obtained mud thickness of almost one metre is not realistic when this results from settling and density currents during one tidal period only. Odd and Cooper didn't

report on simulation of mud layers in the mouth of the Severn or in Bristol Channel.

*Comparison with observations of mud by Kirby and Parker, see figure 7.4*
The pattern of fluid mud pools resulting from simulation 5 in figures E25 and E26 showed some global similarity with the observations of mud deposits by Kirby and Parker, see Section 7.1 and figure 7.4. These similarities concern Swansea Bay, Bridgwater Bay, Bristol Deep and Newport Deep. The observed mud thicknesses for the Shoots Channel and Avonmouth area were considerably larger than calculated with the present model. Mud pools in the mouth of the Severn, which resulted from the simulation, were not observed in reality.
The present model only considered neap tide, while in reality spring and neap tide alternate, which may be of importance for preventing mud accumulations by horizontal transport. In reality, more turbulence is generated in the mouth of the Severn, by waves and the neap tide - spring tide cycle, which prevents mud occurrences here. Also the flow in the mud layer can be turbulent with mud velocities of the order 0.1 m/s, which results in erosion of the mud layer. Because of the laminar flow condition during the simulation, erosion of bed material was hindered and a continuous process of consolidation of the mud layer took place in the present model.

The main discrepancies between the observed and computational results may be explained by

1. The fact that in the numerical model no differences in bed material are made. The model assumes that the whole study area consists of a consolidated mud layer, upon which a fluid mud layer can grow or entrain. The suspension layer starts with a uniform depth averaged sediment concentration. In reality some parts of the Severn consist of (non-erodible) rock beds, the sediment concentration varies over the area and near the bed the concentration is normally significantly higher than the averaged value. A limitation of the model is that variables in the water layer and fluid mud layer are depth-averaged values and therefore cannot represent vertical variations in the suspended mud concentration.
2. In the Severn a pattern of growth and decay of fluid mud appears to repeat each tidal cycle, varying with the changing tidal range. This pattern of mud is very difficult to simulate in the numerical model. The model only considers neap tide variation and there is little experimental evidence for the formulation of the entrainment term, the dewater velocity and shear stresses.
3. The model uses a constant settling velocity. In reality the settling velocity depends on the concentration, hence it varies over the study area.
4. Inaccuracies due to the large grid dimensions and the large simulation time step.
5. The model only considers neap tide variation, while in reality spring and neap tide alternate.
6. In reality the fluid mud movement interacts with the flow field in the suspension layer.
7. The lack of field observations of fluid mud which can distinguish between mobile fluid mud with density of about 1066 $kgm^{-3}$ and a stationary low density soil with a density of about 1200 $kgm^{-3}$. Also, the echosounder used couldn't detect fluid mud layers less than about 0.25 m thick.
8. In reality more turbulence is generated at the seaside, which prevents the occurrences of mud layers in the mouth of the estuary.

An improvement of the model can be achieved by varying the settling velocity with the concentration. A concentration dependent settling velocity enhances the process of settling in areas where large concentrations are present and reduces the formation of fluid mud in areas with low concentrations.
This aspect has been incorporated in the model (phase II) and is highlighted in the next Section.

## 7.3 Simulation phase II

### 7.3.1 Computational results

The previous Section showed that it is possible to simulate the processes of formation, growth, decay and movement of fluid mud layers in the Severn. However, the model showed some imperfections.
One of the limitations of the model originated from the fact that variables in the suspension layer and the fluid mud layer are both depth-averaged values and so cannot represent vertical variations in the suspended mud concentration. During the simulation the settling velocity $w_s$ was taken constant for the whole area:

$$\text{Settling:} \quad \frac{dm}{dt} = w_s C H[\tau_{dm} - \tau](1 - \frac{\tau}{\tau_{dm}})$$

with $w_s = 10^{-3}$ ms$^{-1}$ and the other parameters as explained in Section 6.2.
However, as already shown in figure 7.5, the settling velocity depends on the suspended sediment concentration. In order to improve the model it is assumed that the settling velocity varies with the sediment concentration as follows:

$$w_s \text{ (ms}^{-1}) = 13.25\ C \qquad \text{for } C \leq 0.0038 \ (= 10 \text{ gl}^{-1})$$
$$w_s \text{ (ms}^{-1}) = 0.05 \qquad \text{for } C > 0.0038 \ (= 10 \text{ gl}^{-1})$$

with $C$ is the depth-averaged suspended volume concentration.
Only flocculation effects are modelled in the settling process.

The high value of the coefficient compensates for the fact that the concentration of the suspended mud near the bed is usually significantly higher than the depth averaged values in the Severn.

This improvement will have the following effects:
→ A mud layer develops relatively more quickly in areas with high sediment concentrations than resulted in phase I, so in these areas the mud layer can reach a larger thickness in the same period.
→ Entrainment can have a much more pronounced effect when thicker mud layers have developed in the preceding period. When the thicker mud layer is entrained, this will result in a high sediment concentration in the water column above, resulting in again a thick mud layer in the next period when settling can occur. A continuous process takes place in which settling and entrainment alternate more intensely than in phase I.

| Simulation no. | 6 | 7 | 8 | 9 |
|---|---|---|---|---|
| Settling | + + | + + | + + | + + |
| Entrainment<br>Ve<br>Constant | + + | + | + | <br><br>+ |
| Dewatering | + | + | + | + |
| Erosion | - | - | - | - |
| Gravity (sliding) | + | + | + | + |
| Drag by water | + | + | + | + |
| Init. mud layer (m) | 0.1 | 0.1 | 0.1 | 0.01 |
| VAR (m) | 0.05 | 0.05 | 0.05 | 0.05 |

\+ = influence of the parameter
\- = no influence of the parameter

Table 7.2: Simulation programme of phase II

At high entrainment rate settling can still occur in comparison with simulation phase I, though a higher entrainment rate reduces the period in which settling can occur.

The simulation programme of phase II is an extension of the programme of phase I: Both vertical and horizontal transport of fluid mud is considered.

From phase I it resulted that the erosion rate was of no importance for the results because of the laminar flow condition. In phase II this term is left aside.

The source term becomes

When $C < 0.0038$ ($= 10$ gl$^{-1}$) :

$$\frac{dm}{dt} = 13.25C^2H[\tau_{dm}-\tau](1-\frac{\tau}{\tau_{dm}}) - EV_eC_mH[10-Ri_B] - V_0C_mH[400-Re_e]$$

When $C \geq 0.0038$ ($= 10$ gl$^{-1}$) :

$$\frac{dm}{dt} = 0.05CH[\tau_{dm}-\tau](1-\frac{\tau}{\tau_{dm}}) - EV_eC_mH[10-Ri_B] - V_0C_mH[400-Re_e]$$

$$\text{with} \quad V_e = \Delta U \frac{0.1}{(1+63Ri_B^2)^{0.75}} \quad , \quad Ri_B = \frac{\Delta\rho g d_m}{\rho_0 \Delta u^2}$$

Table 7.2 presents the simulation programme. The point meriting attention is the entrainment term:
Sim. 6: First the simulation is carried out with a large entrainment term.
Sim. 7, 8: Next, the entrainment term is reduced in two different ways
Sim. 9: Finally, a simulation with a constant entrainment rate is considered.

Again, values of the parameters which are characteristic for a simulation are repeated. The other parameters are set as in Section 7.2.

**RUN 6.** *Vertical and horizontal transport of fluid mud: A high entrainment rate*
$E = 1$, $V_0 =$ 5E-07 ms$^{-1}$, $\tau_B = 0.1$ Pa, $d_{m,0} = 0.1$ m, VAR $= 0.05$ m
The results for Stations 1 and 7 are illustrated in figure F1. The occurrences of fluid mud at the selected stations coincided with periods when mud was settling rapidly from the overlying water, only once during the tidal period.
For Station 1 the fluid mud existed for 85 minutes at high water slack reaching a thickness of about 0.78 m. The fluid mud was nearly 0.36 m thick at Station 7, where it occurred for only 25 minutes just after low water slack.

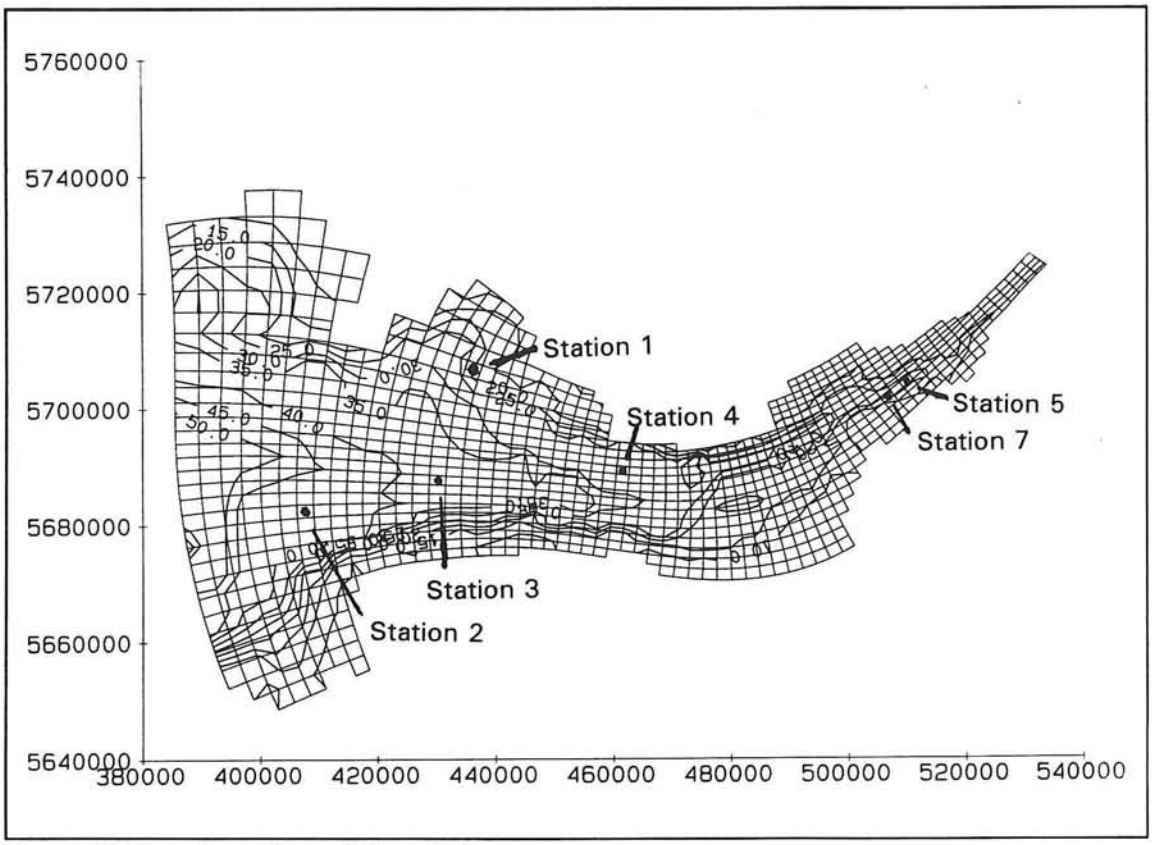


Figure 7.7: Location of the stations

A short analysis is given for Station 1:

$t$ = 6280 min.: $d_m = 0.73$m, $u = 0.15 ms^{-1}$, $v = 0.03 ms^{-1}$, $\Delta U = 0.15 ms^{-1}$, $u_m = 0.2 cms^{-1}$, $v_m = 0.07 cms^{-1}$, $C = 0.00047$
Settling: $\tau_i = 0.02$ Pa $< \tau_{dm}$ : $dm/dt$ = 2.9E-06 $ms^{-1}$
Entrainment: $Ri_B$ = 15: $dm/dt$ = 0
Conclusion: increase of fluid mud layer by settling,
$(dm/dt)/C_{mud}$ = 1.0E-04 $ms^{-1} \approx 0.6$ cm/min

t = 6300 min.: $d_m = 0.77$m, $u = 0.26 ms^{-1}$, $v = 0.06 ms^{-1}$, $\Delta U = 0.26 ms^{-1}$, $u_m = 0.2 cms^{-1}$, $v_m = 0.07 cms^{-1}$, $C = 0.00041$
Settling: $\tau_i = 0.07$ Pa $< \tau_{dm}$ : $dm/dt$ = 1.8E-06 $ms^{-1}$
Entrainment: $Ri_B$ = 0.67, $Ve$ = 2E-03 : $dm/dt$ = 5.8E-05 $ms^{-1}$
Conclusion: decrease of fluid mud layer by entrainment,
$(dm/dt)/C_{mud}$ = 2.0E-03 $ms^{-1} \approx 12$ cm/min

$t$ = 6600 min.: $d_m = 0$m, $u = 0.05 ms^{-1}$, $v = 0.09 ms^{-1}$, $\Delta U = 0.1 ms^{-1}$, $C = 0.0012$
Settling: $\tau = 0.03$ Pa $< \tau_{dm}$ : $dm/dt$ = 1.78E-05 $ms^{-1}$
Entrainment: $Ri_B$ = 0, $Ve$ = 1.0E-03 : $dm/dt$ = 2.8E-05 $ms^{-1}$
Conclusion: entrainment > settling, thus $dm/dt = 0$

Time histories of the mud layer at four other stations are given in figure F2. The locations of these stations are shown in figure 7.7, together with the bathymetry of the Severn Estuary. The neap tidal water level elevation and flow velocities are given for these stations in figures F17 and F18. From the figures it can be concluded that when the flow velocities are lowest, a mud layer can develop, and that when the flow velocity increases, the whole mud layer is entrained.

Figures F3 and F4 represent an impression of the mud thickness at respectively $t$ = 6300 min. (2 hours after high water) and $t$ = 6600 min. (low water).
The most important observation is that during the simulation no mud layers were formed in the mouth of the estuary, in agreement with observations. Mud layers up to 2.5 metres thick in Bristol Channel, Swansea Bay, Bridgwater Bay and in the channels more upstream present at $t$ = 6300 min. have disappeared at $t$ = 6600 minutes due to entrainment and horizontal transport. Only some persistent spots in the south of the mouth of the estuary, in Swansea Bay, Bridgwater Bay and some spots at the boundaries due to boundary effects are present then.
An illustration of respectively the flow and mud velocities can be found in figures F19 and F20 for $t$ = 6300 min. and $t$ = 6600 min..
The mud velocities are in the range of $10^{-4}$-$10^{-3}$ $ms^{-1}$.

The high entrainment rate prevents settling during almost the entire period. Only for a short period, when $Ri_B$ exceeds 10, entrainment is hindered and settling can occur.

It is difficult to achieve mud occurrences during longer periods. An enlargement of the critical shear stress for settling, $\tau_{dm}$, does not make any difference. The entrainment term is by far too large: When no mud is present $Ri_B = 0$, hence $V_e$ is not reduced by the Richardson number. Settling can only take place when the flow velocities are lowest, i.e. the Richardson number exceeds 10.

**RUN 7.** *Vertical and horizontal transport of fluid mud: Reduction entrainment by $V_e$*
In order to reduce the entrainment rate $V_e$ when $Ri_B$ is zero or low ($\leq 0.57$), the following condition is applied:

$$V_e = \frac{0.1}{(1+63Ri_B^2)^{0.75}}\Delta U$$

$$\text{If} \quad V_e > 0.01\Delta U\,, \quad \text{than} \quad V_e = 0.01\Delta U$$

$E = 1$, $V_0 = 5E\text{-}07\ ms^{-1}$, $\tau_B = 0.1$ Pa, $d_{m,0} = 0.1$ m, VAR = 0.05 m
The results can be found in figures F5 to F8.
When comparing figures F1 and F7 it can be noticed that the mud layers at both Stations 1 and 7 reach a larger thickness, the thicknesses are respectively about 1.4 m and 0.75 m., after which for both stations the mud layer disappears. Also the period in which the mud layer occurs is slightly longer. At Station 1 the mud layer occurred for almost 130 minutes. For Station 7 the mud layer appears two times during a tidal period, where the mud layer at high water slack was present for 75 minutes, reaching a little smaller height than at low water slack, where it occurred for 60 minutes.
The same tendency can be noticed for the Stations 3, 4 and 5 in figure F6. For Station 2 the flow velocities are too high to cause settlement of the suspended sediment concentration.

Figure F7 shows the thickness of the mud layer at $t = 6300$ minutes (2 hours after high water). When compared with simulation 6 thicker mud layers up to 2.8 metres thick have developed. This applies especially to areas in Swansea Bay, Bristol Deep, Newport Deep and the Shoots Channel. The persistent spots of mud encountered in simulation 6 are somewhat extended. The processes of entrainment and horizontal transport cause the mud layers present at $t = 6300$ min. to have disappeared at $t = 6600$ minutes (low water), except for the persistent spots of fluid mud, see figure F8.
During the simulation no mud was formed in the mouth of the Severn.
Mud velocities are in the range $10^{-3}\ ms^{-1}$.

A reduction of the entrainment rate for low Richardson numbers results in thicker mud layers. Also the period in which a mud layer occurs is longer.

In the following, instead of reducing the entrainment rate $V_e$, the entrainment coefficient $E$ is adapted in order to achieve mud occurrences during longer periods.

**RUN 8.** *Vertical and horizontal transport of fluid mud: Reduction entrainment by E*
$E$ = 0.075, $V_0$ = 5E-07 ms$^{-1}$, $\tau_B$ = 0.1 Pa, $d_{m,0}$ = 0.1 m, VAR = 0.05 m
The model predicted results for Stations 1 and 7 are presented in figure F9. The time history of the mud layer at Station 1 is characterized by growth and subsequent decay of the mud layer. At $t$ > about 4500 minutes the fluid mud layer has almost disappeared. For Station 7 a mud layer of about 0.35 m thick is observed for 50 minutes once during the tidal period for $t$ > 3000 minutes, like simulation 6. The results for the four other Stations are given in figure F10. Roughly speaking the same tendency as in simulation 6 can be noted, with the exception of Station 3. For this station the mud layer increases enormously for $t$ > 5500 minutes.

When considering figures F11 and F12, which show pictures of the mud thickness at respectively $t$ = 6300 min. (2 hours after high water) and $t$ = 6600 min. (low water), much thicker and persistent mud layers have developed than resulted from the preceding simulations. Only mud layers in Bristol channel, Newport Deep, the Shoots Channel, Newport Deep are of temporary nature.
The other areas are subjected to thick mud occurrences reaching thicknesses of nearly 10 metres. Mud layers were also present in the mouth of the Severn.
The mud velocities are in the range $10^{-3}$ ms$^{-1}$.

When the entrainment coefficient $E$ was given a value of 5E-02 or lower, settling dominated for the whole study area and caused thick mud layers to develop, especially in the mouth of the estuary.
A reduction of the entrainment term by reducing the entrainment coefficient $E$ of the order 5E-02 or lower results in the dominating process of settling.
Also from simulation 8, with an entrainment coefficient $E$ of 0.075, it can be concluded that the entrainment rate is too small.

**RUN 9.** *Vertical and horizontal transport of fluid mud: A constant entrainment rate*
In order to make an estimate of the influence of the size of the entrainment rate, the entrainment rate $V_e$ is taken constant for the whole study area in the following simulation.
The entrainment term becomes

$$\frac{dm}{dt} = V_e C_m \quad , \qquad \text{with} \quad V_e = \text{constant}$$

$V_e$ = $10^{-4}$ ms$^{-1}$, $V_0$ = 5E-07 ms$^{-1}$, $\tau_B$ = 0.1 Pa, $d_{m,0}$ = 0.01 m, VAR = 0.05 m
The computational results of the mud thickness for the selected stations are given in figures F13 and F14. Station 1 in figure F13 is characterized by a process of net increase in the mud thickness during a tidal period when $t$ < 3400 min., followed by a process of net decrease till $t \approx$ 5400 minutes, after which a small mud layer develops only once during the tidal period. For Station 7 a mud layer appears twice during the tidal period. A mud layer of about 0.75 m thick occurs for nearly 160 minutes during low water slack, at high water slack the mud layer reaches a thickness of nearly 0.20 m, where it disappeared after 120 minutes.

The same tendency as for Station 7 can be noticed for Stations 3, 4 and 5. For Station 2 settling causes a net increase in mud thickness.

Figures F15 and F16 present a map of the mud thickness at respectively $t$ = 6300 min. (2 hours after high water) and $t$ = 6600 min. (low water). Except for the persistent mud layers in the mouth of the Severn and persistent patches in Bristol Channel, Bridgwater Bay, Newport Deep and Bristol Deep some little variation in mud thickness with time can be noted. However, generally it can be concluded that an entrainment rate of $10^{-4}$ ms$^{-1}$ is a little too small.
The mud velocities are in the range $10^{-3}$ ms$^{-1}$.

When the entrainment rate was given a value of $10^{-3}$ ms$^{-1}$, entrainment dominated during the whole simulation and prevented settling to occur.

### 7.3.2 Discussion of results

The main finding from the neap tide simulation of phase II, where a concentration dependent settling velocity is applied, appears to be that:

- At a high entrainment rate settling can occur. As expected settling and entrainment alternate more intensely than in phase I, where the settling velocity was constant.
- Mud layers can reach a larger thickness in the same tidal period than resulted from phase I.
- For high entrainment rates (simulation 6 and 7), no mud layers develop in the mouth of the estuary. When the entrainment rate was reduced by an entrainment coefficient $E$ (simulation 8) or given a constant value of $10^{-4}$ ms$^{-1}$ (simulation 9) thick mud layers occurred in the mouth of the Severn.
- An (constant) entrainment rate of $10^{-4}$ ms$^{-1}$ is too small and settling dominates.

The computational results of the mud thickness of simulation 7 (entrainment rate reduced by $V_e$) show the best resemblance with the mud occurrences simulated by Odd and Cooper (see figure E28) and mud occurrences observed in reality.
In the following this is further elaborated.

*Comparison with the results of Odd and Cooper, see figure E28*
The model of Odd and Cooper predicted mud occurrences of about 0.6 m thick in Newport Deep. In Bristol Deep the mud was nearly 1 m thick, where it existed for 2.5 hours at low water and 2 hours at high water. No mud was formed on the Welse Grounds at high water, see figure E28 and Section 7.2.1.
For simulation 7 mud existed for 1.25 hours at high water and 1 hour at low water in Bristol Deep (i.e. Station 7), reaching thicknesses of about 0.75 m. The mud duration is two times as small as obtained by Odd and Cooper and the mud thickness is a little lower than their mud thickness of nearly 1 m. For Newport Deep and the Shoots Channel the mud was nearly 2.5 m thick.

No mud was encountered on the Welse Grounds during the simulation, which is in agreement with Odd and Cooper's results. Odd and Cooper also mentioned mud occurrences more downstream of Newport Deep, which also resulted from the model, but they didn't report on simulated mud occurrences in other parts of the study area. The model simulated mud velocities are about 10 times smaller than obtained by Odd and Cooper.

*Comparison with observations of mud by Kirby and Parker, see figure 7.4*
Kirby and Parker, see figure 7.4 and section 7.1, report ephemeral mud thicknesses of about 3 m near Avonmouth and mud occurrences up to 5 m thick in the Shoots Channel. The model predicted for both areas mud layers up to 2.8 m. thick. In reality mud layers are also observed in Cardiff Channel, Swansea Bay and in the approaches to Bridgwater Bay, which is in agreement with simulation 7 where ephemeral mud layers up to 2.3 m thick are encountered, except for the persistent spot of mud in Swansea Bay.
In Newport Deep the mud thickness of 0.5-1.5 m was found to be stable during neap tide, whereas in the model the mud layer is of temporary nature. No mud is encountered in the mouth of the Severn and in Bristol Channel, though for the latter the model predicted also mud occurrences, while the persistent spots in the mouth are due to the coarse resolution.

*Remarks on the results*
From simulation 8 and 9 persistent mud layers up to 10 metres thick resulted in the mouth of the esturay and in Bristol Deep. In reality thick mud layers will influence the flow in the suspension layer. The flow pattern alters (velocities increase) and it can smooth or erode the thick mud layer.
In reality more turbulence is generated at the seaside due to the influence of waves, hence all the suspended sediment is kept in suspension and the development of a fluid mud layer is prevented. Also in reality the neap tide - spring tide cycle will influence the pattern of fluid mud layers and may prevent the accumulation of mud layers caused by horizontal transport.
The persistent spots formed during the simulations are ascribed to the coarse resolution of the model.
See also Section 7.2.2 where discrepancies between observed and computational results are discussed.

Generally, the fluid mud model showed that it is possible to simulate the processes causing the growth, motion and entrainment of ephemeral fluid mud layers in the Severn Estuary. From the parameters used in the model it resulted that the vertical exchange by settling and entrainment is of more importance for the behaviour of mud than the factors causing transport of mud in horizontal directions, though horizontal transport in suspension after entrainment occurred is also of significance. The prevalence of the processes of entrainment and settling especially counts when a settling velocity is applied which varies with the suspended sediment concentration (phase II).
Flow of fluid mud in horizontal directions results from gravitational, hydrostatic pressure and frictional forces.

Erosion and consolidation are of less importance for the vertical exchange of fluid mud in comparison with settling and entrainment.

However, the model has some imperfections by which no reliable predictions of the encountered processes can be made.
Calibration of the model is very difficult. Many parameters are variable in the model, because of the lack of evidence and justification for some of the basic assumptions and the values of some coefficients describing the behaviour of fluid mud.
The mean weaknesses of the fluid mud model are:

1. Lack of evidence for defining the entrainment term for fluid mud.
   A very simple expression is used for the definition of the entrainment term. It is not correct to base the bulk Richardson number on the lower layer herein. The entrainment rate of simulation 7 is 1 to 100 times the entrainment rate of the experiments described in Chapter 3 and simulations reported in Chapter 5.
   In case of a two-fluids system consisting of saline/fresh water, the entrainment rate obtained from experimental results can be applied directly to full scale. For mud, however, this is a problem. Little is known about how to correct the entrainment rate obtained from experiments to full scale. In reality the entrainment rate may be lower than results from experiments, when the same velocity appears, because in experiments additional turbulence is generated due to side wall friction. In the model of Kranenburg, however, these effects were explicit incorporated.
   The entrainment rate of $10^{-4}$ $ms^{-1}$ (simulation 9) is a little larger then, though settling dominated.
2. The incorporation of only neap tide instead of a neap tide - spring tide cycle.
3. The grid sizes being too large, which results in numerical inaccuracies.
4. Lack of justification that the fluid mud has a Bingham yield strength of 0.1 Pa.
5. The assumption that fluid mud dewaters at a velocity of 5E-07 $ms^{-1}$.

It is recommended to investigate these processes. Especially research into the process of entrainment is important for the advancement of modelling the behaviour of fluid mud layers.

# 8.0 DISCUSSION AND CONCLUSIONS

*This Chapter presents the final discussion of this study on the erosion of a fluid mud layer due to entrainment. As described in the introduction, the purpose of the investigation is to compare the results from the numerical models with experimental data or observations reported in the literature. First the integral entrainment model of Kranenburg is reviewed. Next the two layer fluid mud model of Delft Hydraulics is evaluated. For both models conclusions are presented.*

## THE ENTRAINMENT MODEL OF KRANENBURG

An integral approach is used to model the entrainment of a fluid mud layer by turbulent flow. The effects of side wall friction and viscous drag are incorporated and the empirical model constants involved are determined from experiments reported in the literature.

The model was calibrated with the results of the experiments of Kantha et al. (1977). Both steady and tidal flow experiments were simulated.
When comparing the computational results with the experimental data reported in the literature, it can be concluded that:

- Values taken for the empirical coefficients involved and the assumptions made for the effects of viscous drag and side wall friction are satisfying.
- A good agreement can be noticed for the concentration in the mixed layer when no surface erosion took place. For large times the model overestimates the concentration because the mechanical work which has to be done in the bed to erode the fluid mud layer has to be taken into account. In the numerical model the influence of flow curvature is not incorporated, which also may attribute to the difference between the numerical and experimental data.
- The settling velocity of the particles is of greater influence for low velocities in the mixed layer, because it takes the same amount of energy to keep the particles in suspension for every experiment, but at low velocities less energy is available.
- An overall agreement can be seen for the entrainment rate $u_e$. However, for large times the mechanical work which has to be done in the bed and the influence of flow curvature explain the lower measured entrainment rate at the end of an experiment.
- The difference for the entrainment rate in the tidal experiment may be explained partly by the way of measuring the erosion rate and the bed concentration.

Generally, it can be concluded that an overall agreement can be noticed between the computational results and experimental data, as long as surface erosion is not significant. The incorporation of the effect of consolidation and the change from entrainment to floc erosion into the numerical entrainment model will be a next step forward in the modelling of entrainment.

The two-layer fluid mud model uses a simple expression for the definition of the entrainment term. The entrainment term only incorporates the velocity difference between the overlying water and the fluid mud layer, the reduced gravity and the thickness of the mud layer, through a Richardson number for the lower layer. The concentration of the mud layer is taken constant and the effect of viscosity of the mud is not modelled.
The integral approach of Kranenburg is more suited to model the entrainment behaviour of a fluid mud layer by turbulent flow. Viscous effects and a varying concentration profile for the fluid mud layer are incorporated.
Using the integral entrainment model of Kranenburg for the definition of the entrainment term in the two-layer fluid mud model will improve the modelling of entrainment, because the entrainment rate will be approached more accurately. The model considers

- An integral form of the equation for turbulent kinetic energy of the upper layer depth
- The Richardson number of the upper layer depth
- Viscous effects
- A varying concentration profile for the mud layer
- An effective velocity difference between the two layers

Yet, some complications remain:

- The fluid mud layer in the two layer fluid mud model has a constant density, hence the entrainment rate cannot vary with the concentration as in the integral model.
- Little is known about how to correct the entrainment rate obtained from experiments to full scale, in other words, there is insufficient evidence that the entrainment rate resulting from the integral model will predict the entrainment rate occurring in reality.
- When the integral entrainment model is applied, it is more difficult to recognize what the influence of the entrainment term is (e.g. in comparison with the settling term) on the behaviour of the fluid mud layers.

It can be concluded that the entrainment term used in the two layer fluid mud model needs some improvements, e.g. by basing the Richardson number on the upper layer depth. The incorporation of the integral entrainment model of Kranenburg will only be a step forward when this is done in combination with other improvements, i.e. incorporation of a fluid mud layer with a varying density and when there is more evidence for the application of the experimental results to full scale.

## LIST OF FIGURES

## LIST OF SYMBOLS

| | | |
|---|---|---|
| $B$ | $m^2\ s^{-2}$ | Total buoyancy of the mixed layer |
| $b$ | $m\ s^{-2}$ | Buoyancy |
| $C$ | $g\ l^{-1}$ | Suspended sediment concentration |
| $C$ | $m^{½}\ s^{-1}$ | Chézy coefficient |
| $C_{eq}$ | $g\ l^{-1}$ | Equilibrium concentration |
| $C_o$ | - | Initial volume concentration of the suspension layer |
| $C_b$ | - | Volume concentration of the bed |
| $C_m$ | - | Volume concentration of the fluid mud layer |
| $C$ | $g\ l^{-1}$ | Suspended sediment concentration |
| $c_b$ | $g\ l^{-1}$ | Concentration of the mud layer |
| $c_q$ | - | Empirical coefficient |
| $c_H$ | - | Empirical coefficient |
| $c_*$ | - | Empirical coefficient |
| $c_v$ | - | Empirical coefficient |
| $c_w$ | - | Empirical coefficient |
| $D$ | $kg\ m^{-2}\ s^{-1}$ | Deposition rate |
| $D$ | $m^3\ s^{-3}$ | Redistribution of TKE |
| $dm/dt$ | $kg\ m^{-2}\ s^{-1}$ | Net rate of mass exchange of mud |
| $d$ | m | Total depth of the flow |
| $d_f$ | m | Floc size |
| $d_m$ | m | Thickness of the fluid mud layer |
| $d_{m,o}$ | m | Initial thickness of the fluid mud layer |
| $E$ | - | Entrainment coefficient |
| $E$ | - | Dimensionless entrainment rate |
| $E_*$ | - | Dimensionless entrainment rate |
| $E_u$ | - | Dimensionless entrainment rate |
| $Fr_i$ | - | Internal Froude number |
| $f$ | - | Friction coefficient |
| $g$ | $m\ s^{-2}$ | Gravitational acceleration |
| $H$ | - | Heaviside step function |
| $H$ | m | Total mixed layer |
| $H_0$ | m | Initial depth mixed layer |
| $h$ | m | Total depth of the flow |
| $K$ | - | Ratio of viscous boundary layer thickness to thickness of interface |
| $k$ | $m\ s^{-1}$ | Permeability |
| $k_2$ | - | Coefficient |
| $L$ | m | Size of energy-containing eddies |
| $L$ | m | Width of the flume |
| $M_e$ | $kg\ m^{-2}\ s^{-1}$ | Erosion constant |
| $m$ | - | Empirical coefficient |
| $n$ | - | Empirical coefficient |
| $p$ | $kN\ m^{-2}$ | Pressure |
| $p$ | - | Probability of deposition |
| $Pe$ | - | Péclet number |
| $q$ | $m^2\ s^{-2}$ | Turbulent kinetic energy |
| $Re$ | - | Reynolds number of the mixed layer |

| | | |
|---|---|---|
| $Re_e$ | - | Effective Reynolds number |
| $Re_p$ | - | Particle Reynolds number |
| $Re_y$ | - | Cohesive Reynolds number |
| $R_f$ | - | Flux Richardson number |
| $Ri$ | - | Gradient Richardson number |
| $Ri_b$ | - | Bulk Richardson number |
| $Ri_\tau$ | - | Bulk Richardson number |
| $Ri_*$ | - | Overall Richardson number |
| $Ri_u$ | - | Overall Richardson number |
| $S_1$ | g $l^{-1}$ | Concentration top of fluid mud layer |
| $s_2$ | g $l^{-1}$ | Concentration bottom of fluid mud layer |
| $s$ | g $l^{-1}$ | Sediment concentration by weight |
| $s_b$ | g $l^{-1}$ | Bed sediment concentration |
| $s_H$ | g $l^{-1}$ | Bed sediment concentration at interface |
| $s_h$ | g $l^{-1}$ | Concentration at the bottom of the upper layer |
| $t$ | s | Time |
| $T$ | s | Tidal period |
| $U$ | m $s^{-1}$ | Mean velocity of the mixed layer |
| $U_H$ | m $s^{-1}$ | Horizontal velocity at the interface |
| $U_s$ | m $s^{-1}$ | Velocity top lid |
| $U_*$ | m $s^{-1}$ | Horizontal velocity at free surface or screen |
| $U_0$ | m $s^{-1}$ | Horizontal velocity of undisturbed quiescent layer |
| $u$ | m $s^{-1}$ | Horizontal velocity component |
| $u_b^2$ | $m^2$ $s^{-2}$ | Work per unit mass needed to cause failure of the bed |
| $u_H$ | m $s^{-1}$ | Frictional velocity at the interface |
| $u_e$ | m $s^{-1}$ | Entrainment rate |
| $u_m$ | m $s^{-1}$ | Horizontal flow velocity of the fluid mud layer |
| $u_*$ | m $s^{-1}$ | Frictional velocity at free surface or screen |
| $u_+$ | m $s^{-1}$ | Max [$u_H$ , $u_*$] |
| $u_0$ | m $s^{-1}$ | Velocity difference between mixed and quiescent layers |
| $V_e$ | m $s^{-1}$ | Entrainment velocity |
| $V_0$ | m $s^{-1}$ | Dewatering velocity |
| $v$ | m $s^{-1}$ | Vertical flow velocity of the suspension layer |
| $v_m$ | m $s^{-1}$ | Vertical flow velocity of the fluid mud layer |
| $W$ | m | Width of channel or flume |
| $w$ | m $s^{-1}$ | Vertical velocity component |
| $w_s$ | m $s^{-1}$ | Settling velocity |
| $w_{s,0}$ | m $s^{-1}$ | Settling velocity of individual particles |
| $x$ | m | Horizontal coordinate |
| $y$ | m | Horizontal coordinate |
| $z$ | m | Vertical coordinate |
| | | |
| $\alpha$ | - | Empirical coefficient |
| $\alpha$ | - | Fractional density difference |
| $\beta$ | - | Empirical coefficient |
| $\delta$ | m | Viscous boundary layer thickness |
| $\delta_s$ | m | Thickness of the layer with velocity gradient |
| $\varepsilon$ | $m^2$ $s^{-3}$ | Dissipation rate |
| $\eta$ | kg m $s^{-1}$ | Dynamic viscosity |
| $\eta$ | m | Water surface elevation |

| | | |
|---|---|---|
| $\eta_m$ | m | Elevation of the upper surface of the mud layer |
| $\lambda$ | m | Size of energy-dissipating eddies |
| $\lambda$ | - | Sidewall friction coefficient |
| $\nu$ | $m^2\ s^{-1}$ | Kinematic viscosity |
| $\nu_m$ | $m^2\ s^{-1}$ | Kinematic viscosity of the fluid mud layer |
| $\rho$ | $kg\ m^{-3}$ | Density |
| $\rho_0$ | $kg\ m^{-3}$ | Density of the water in the suspension layer |
| $\rho_m$ | $kg\ m^{-3}$ | Density of fluid mud layer |
| $\Delta\rho$ | $kg\ m^{-3}$ | Density excess of the fluid mud with respect to water |
| $\rho_r$ | $kg\ m^{-3}$ | Reference density |
| $\tau$ | $kg\ m\ s^{-2}$ | Bed shear stress |
| $\tau_B$ | $kg\ m\ s^{-2}$ | Bingham yield stress strength |
| $\tau_b$ | $kg\ m\ s^{-2}$ | Bed shear stress |
| $\tau_b$ | $kg\ m\ s^{-2}$ | Critical shear stress for deposition |
| $\tau_{cd}$ | $kg\ m\ s^{-2}$ | Critical shear stress for deposition |
| $\tau_{dm}$ | $kg\ m\ s^{-2}$ | Critical shear stress for deposition |
| $\tau_e$ | $kg\ m\ s^{-2}$ | Critical shear stress for erosion |
| $\tau_i$ | $kg\ m\ s^{-2}$ | Shear stress between the suspension layer and fluid mud layer |
| $\tau_m$ | $kg\ m\ s^{-2}$ | Shear stress between the fluid mud layer and the underlying bed |
| $\tau_w$ | $kg\ m\ s^{-2}$ | Sidewall shear stress |
| $\tau_y$ | $kg\ m\ s^{-2}$ | Yield strength |
| $\Omega$ | $m\ s^{-1}$ | Coriolis parameter |
| | | |
| - | | Ensemble average |
| ~ | | Depth average |
| ' | | Turbulent fluctuation |

## REFERENCES

**Abraham, G., 1988**
*'Turbulence and Mixing in Stratified Tidal Flows'*, in Physical estuaries, eds. J. Dronkers, W. van Leussen, Springer-Verlag 1988, pp. 149-180

**Atkinson, J.F., Adams, E.E., Melville, W.K., Harleman, D.R.F., 1984**
*'Entrainment in diffusive thermohaline systems: application to salt gradient solar ponds'*, Tech. Rep. No. 100, Ralph M. Parsons Lab., M.I.T., Cambridge, MA, pp. 326

**Berlamont, J. Ockenden, M., Toorman, E., Winterwerp, J.C., 1992**
*'The Characterisation of Cohesive Sediment Properties'*, Coastal Engineering, Special Issue-Draft

**Booij, R., 1986**
*'Turbulentie in de Waterloopkunde'*, Lecture notes b82, Delft University of Technology

**Burt, T.N, 1986**
*'Field settling velocities of estuary muds'*, Lecture notes on coastal and esutarine studies, 14, eds. Ashish J. Mehta, Springer-Verlag 1986, pp 126-150

**Christodoulou, G.C., 1986**
*'Interfacial mixing in stratified flows'*, Journal of Hydraulic Research, no. 24, pp. 77-92

**Coussot, P., Piau, J.M., 1994**
*'On the behavior of fine mud suspensions'*, Rheologica Acta 33:175-184

**Delft Hydraulics, 1988**
*'Trisula Manual, users' guide'*, version 0, Delft Hydraulics

**Delft Hydraulics, 1994**
*'Fluid mud system, User Manual'*, Delft Hydraulics

**Ellison, T.H., Turner, J.S., 1959**
*'Turbulent entrainment in stratified flows'*, Journal of Fluid Mechanics, vol. 6, pp. 423-448

**Hydraulic Research, 1981**
*'The Severn Estuary, observations of tidal currents, salinities, solids'*, Report EX 966, Wallingford, United Kingdom

**Kantha, L.H., Phillips, O.M., Azad, R.S., 1977**
*'On turbulent entrainment at a stable density interface'*, Journal of Fluid Mechanics, vol. 79, no. 4, pp. 753-768

**Katho, H., Phillips, O.M., 1969**
*'On the penetration of a turbulent layer into stratified fluid'*, Journal of Fluid Mechanics, vol. 37, no. 4, pp. 643-655

**Kirby, R., Parker, W.R., 1980**
*'Settled mud deposits in Bridgwater Bay, Bristol Channel'*, Institute of Oceanographic Sciences. Taunton, IOS Report No. 107

**Kirby, R., 1988**
*'High concentration suspension (fluid mud) layers in estuaries'*, Physical Processes in Estuaries, ed. by Dronkers, J. and Van Leussen, W., 463-485

**Kirby R., Parker, W.R., 1982**
*'A suspended sediment front in the Severn Estuary'*, Nature, 295, 396-399

**Kirby R., Parker, W.R., 1983**
*'Distribution and behaviour of fine sediment in the Severn Estuary and Inner Bristol Channel'*, Canadian Journal Fisheries Aquatic Science, 50, 83-95

**Kit, E., Berent, E., Vajda, M., 1980**
*'Vertical mixing induced by wind and a rotating screen in a stratified fluid in a channel'*, J. Hydraulic Research, Vol. 18, No. 1

**Kranenburg, C.**
*'Dichtheidsstromen'*, Lecture notes b81, Delft University of Technology

**Kranenburg, C., 1983**
*'The Influence of Side-Wall Friction on Shear-Stress Driven Entrainment Experiments'*, Journal of Hydraulic Research, vol. 21, no. 2

**Kranenburg, C., 1984**
*'Wind-induced entrainment in a stably stratified fluid'*, Journal of Fluid Mechanics, vol. 45, no. 9, pp. 253-273

**Kranenburg, C., 1994**
*'An entrainment model for fluid mud'*, Report 93-10, Delft University of Technology

**Krone, R.B., 1962**
*'Flume studies of the transport of sediment in estuarial shoaling processes'*, Hydraulic Engineering Laboratory and Sanitary Engineering Research Laboratory, University of California, Berkeley

**Lau, Y.L., 1994**
*'Temperature effect on settling velocity and deposition of cohesive sediments'*, Journal of Hydraulic Research, vol. 32, no. 1

**Le Hir, P., 1994**
*'Fluid and sediment integrated modelling: basis of 2DV code and application to fluid mud flows in a macrotidal estuary'*, submitted to the Proceedings of INTERCOH'94, Oxford, July 1994

**Leussen, W. van, Dronkers, J., 1988**
*'Physical Processes in Estuaries: An Introduction'*, in Physical estuaries, eds. J. Dronken, W. van Leussen, Springer-Verlag 1988, pp. 1-18

**Leussen, W. van., 1988**
*'Aggregation of Particles, Settling Velocity of Mud Flocs, A Review'*, in Physical processes in estuaries, eds. J. Dronken, W. van Leussen, Springer-Verlag 1988, pp. 347-403

**Lofquist, K., 1960**
*'Flow and stress near an interface between stratified liquids'*, The Physics of Fluids, Vol. 70, Part 2

**Metha, A.J., 1973**
*'Depositional Behaviour of Cohesive Sediments'*, Dissertation presented to the Graduate Council of the University of Florida

**Metha, A.J., 1988**
*'Laboratory Studies on Cohesive Sediment Deposition and Erosion'*, in Physical processes in estuaries, eds. J. Dronken, W. van Leussen, Springer-Verlag 1988, pp. 427-445

**Metha, A.J., McAnally, W.H., Hayter, E.J., Teeter, A.M., Schoelhamer, D., Heltzel, S.B., Carey, W.P., 1989**
*'Cohesive Sediment Transport. I: Process Description'*, Journal of Hydraulic Engineering, vol. 115, no. 8

**Metha, A.J., Srinivas, R., 1993**
*'Observations on the Entrainment of Fluid Mud by Shear Flow'*, in Coastal and Estuarine Studies, vol. 42, ed. A.J. Mehta, American Geophysical Union, Washington D.C., pp. 224-246

**Migniot, C., 1989**
*'Bedding-down and Rheology of Muds, Part 1'*, La Houille Blanche, no. 1

**Nieuwstadt, F.T.M., 1992**
*'Turbulentie, inleiding in de theorie en toepassingen van turbulente stromingen'*, Epsilon Uitgaven, Utrecht

**Odd, N.V.M, 1988**
*'Mathematical modelling of mud transport in estuaries'*, in Physical processes in estuaries, eds. J. Dronken, W. van Leussen, Springer-Verlag 1988, pp. 503-530

**Odd, N.V.M, Cooper, A.J., 1989**
*'A two-dimensional model of the movement of fluid mud in a high energy turbid estuary'*, Journal of Coastal Research, Special issue no. 5

**Owen, M.W., 1970**
*'A Detailed Study of the Settling Velocities of an Estuary Mud'*, HR Report no. INT 78, Hydraulics Research Ltd., Wallingford, England

**Parchure, T.M, 1984**
*'Erosional Behaviour of deposited cohesive Sediments'*, Dissertation presented to the Graduate Council of the University of Florida

**Parker, W.R., 1986**
*'On the observation of cohesive sediment behavior for engineering purpose'*, in Lecture notes on Coastal and Estuarine studies, 14, Springer-verlag, pp. 270-289

**Parteniades, E., 1973**
*'Engineering properties of Estuarine Sediments'*, Lecture No. 16, North Atlantic Treaty Organization, Advanced Study Institute of Estuary Dynamics, Portugal

**Price, J.F., 1979**
*'On the scaling of stress-driven entrainment experiments'*, Journal of Fluid Mechanics, vol. 90, no. 3, pp. 509-529

**Reuber, J., 1994**
*'Physical and numerical modelling of the erosion of a fluid mud layer due to entrainment'*, Report no. 8-94, Delft University of Technology

**Richardson, J.F., Zaki, W.N., 1954**
*'The sedimentation of a suspension of uniform spheres under conditions of viscous flow'*, Chem. Eng. Sci. 3:65-73

**Rijn, L.V., 1993**
*'Transport of Cohesive Materials'*, Department of Civil Engineering, Hydromechanics Section, Delft University of Technology

**Roberts, W., 1993**
*'Development of a mathematical model of fluid mud in the coastal zone'*, Maritime Board, Paper 10103

**Ross, M.A., Mehta, A.J., 1989**
*'On the mechanics of lutoclines and fluid mud'*, Journal of Coastal Research, Special Issue No 5, Summer 1989, pp. 51-62

**Shen, H.W., 1971**
*'Erosion and Deposition of Cohesive Materials'*, River Mechanics volume II, chapter 25

**Sills, G.C., Elder, D.M., 1984**
*'The transition from sediment suspension to settling bed'*, in Lecture notes on Coastal and Estuarine Studies, 14, Springer-Verlag, pp. 192-205

**Thorn, M.F.C., 1981**
*'Physical Processes of Siltation in Tidal Channels'*, Proceedings Hydraulic Modelling Applied to Maritime Engineering Problems, ICE, London, pp. 47-55

**Turner, J.S., 1968**
*'The influence of molecular viscosity on turbulent entrainment across a density interface'*, Journal of Fluid Mechanics, vol. 33, no. 4, pp. 639-656

**Turner, J.S., 1973**
*'Buoyancy effects in fluids'*, Cambridge Monographs in Mechanics & applied Mathematics, Cambridge University Press

**Visser, P.J., Booij, R., Melis, H., 1992**
*'Flow Field Observations in a rotating Annular Flume'*, Paper for 'Conference on the Remediation of Sediment', November 17-18, 1992, USA

**Williams, D.J.A., Williams, K.P., 1982**
*'Colloid Stability and Rheology of Kaolinite Suspensions'*, Trans. J. Br. Ceram. Soc., 81, 78-83, 1982

**Winterwerp, J.C., Cornelisse, J.M., Kuijper, C., 1992**
*'Cohesive sediments, report no. 38'*, Rijkswaterstaat, Delft Hydraulics

**Winterwerp, J.C., Kranenburg, C., 1994**
*'On the erosion of fluid mud layers by entrainment'*, Paper for the 4th Nearshore and Estuarine Cohesive Sediment Transport Conference INTERCOH'94

**Winterwerp, J.C., Wang, Z.B., Zhang, J.C., 1993**
*'Fluid mud in the Severn Estuary, Simulations with a two-layer fluid mud model'*, Z163-30, Delft Hydraulics

**Wit, P.J. de, 1992**
*'Clay Properties'*, Report no. 7-92, Delft University of Technology

**Wit, P.J. de, 1992**
*'Instrument used in the research on Cohesive Sediments'*, Report no. 8-92, Delft University of Technology

**Wit, P.J. de, 1992**
*'Rheological measurements on artificial muds'*, Report no. 9-92, Delft University of Technology

**Wolanski, E., Chappell, J., Ridd, P., Vetessy, R., 1988**
*'Fluidization of mud in estuaries'*, Journal of Geophysical research, volume 93, number C3, pp. 2351-2361

# EROSION OF A FLUID MUD LAYER DUE TO ENTRAINMENT

## Numerical modelling

### APPENDICES

By: Yvonne van Haaren
Delft University of Technology
Faculty of Civil Engineering
Division of Hydraulic and Geotechnical Engineering
Hydromechanics Section

Delft, May 1995

**SUPERVISORS:**

| | |
|---|---|
| Prof.dr.ir. J.A. Battjes | Hydromechanics Section, Faculty of Civil Engineering, Delft University of Technology |
| Dr.ir. C. Kranenburg | Hydromechanics Section, Faculty of Civil Engineering, Delft University of Technology |
| Ir. J.C. Winterwerp | Delft Hydraulics, Delft |
| Prof.ir. K. d'Angremond | Hydraulic and Offshore Engineering Section, Faculty of Civil Engineering, Delft University of Technology |

## TABLE OF CONTENTS



LIST OF FIGURES

## APPENDIX A: Simulation of the experiments of Kantha et al. (1977)

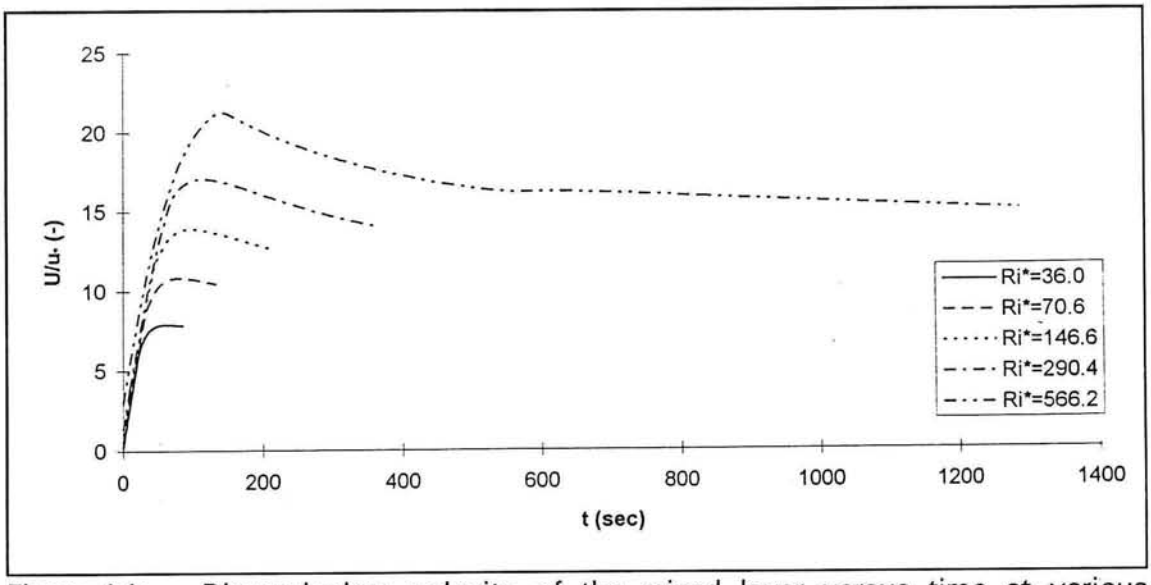


Figure A1: Dimensionless velocity of the mixed layer versus time at various Richardson numbers; $CaCl_2$ solution, $H_i$ = 5,4 cm

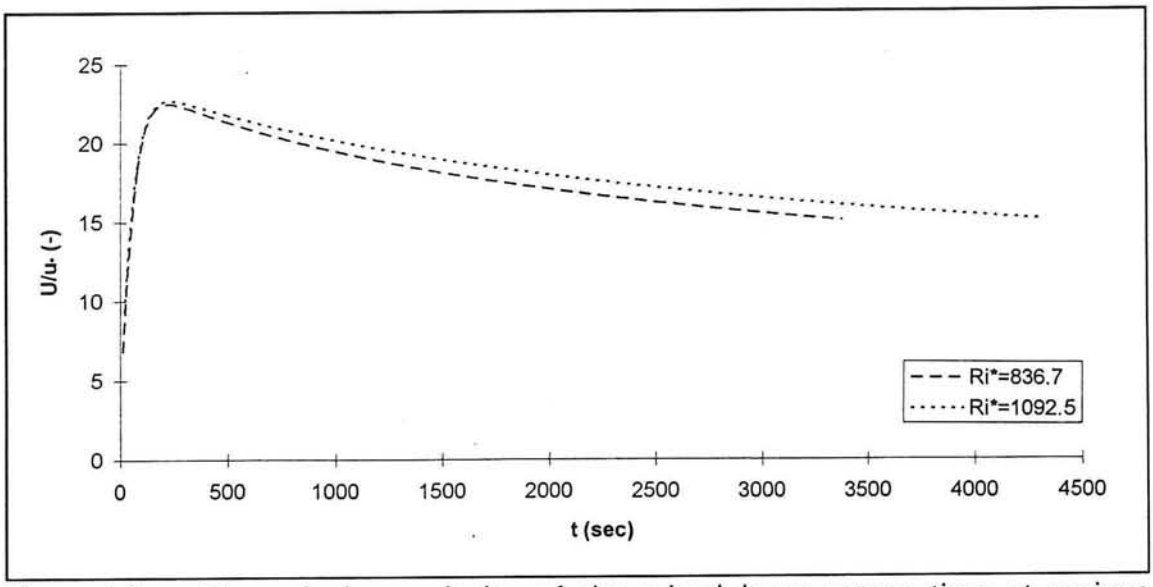


Figure A2: Dimensionless velocity of the mixed layer versus time at various Richardson numbers; $CaCl_2$ solution, $H_i$ = 5,4 cm

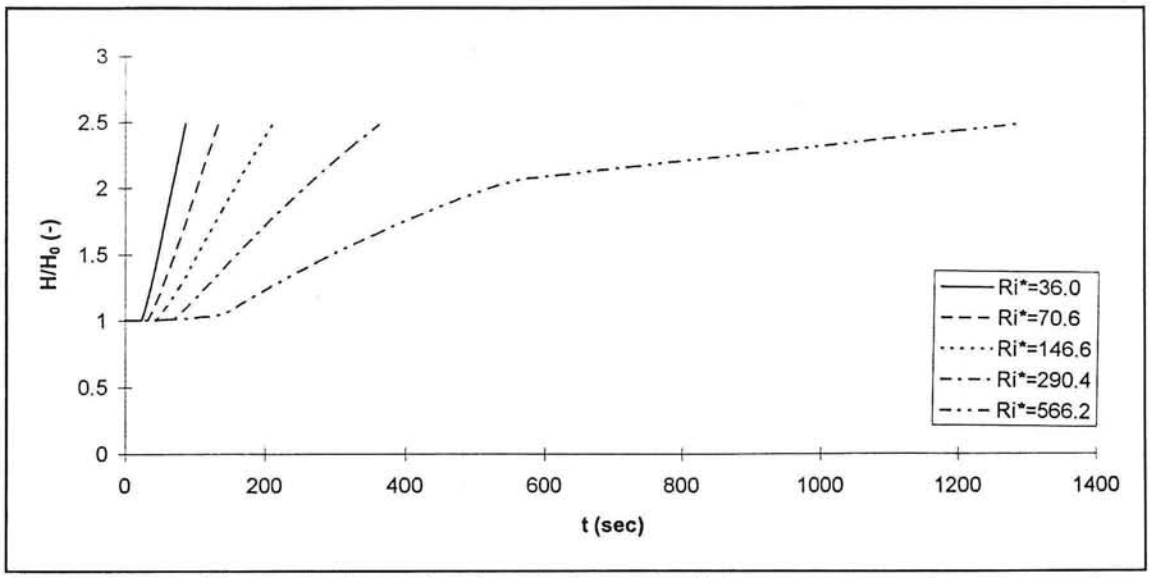


Figure A3: Dimensionless depth of the mixed layer versus time at various Richardson numbers; $CaCl_2$ solution, $H_i$ = 5,4 cm

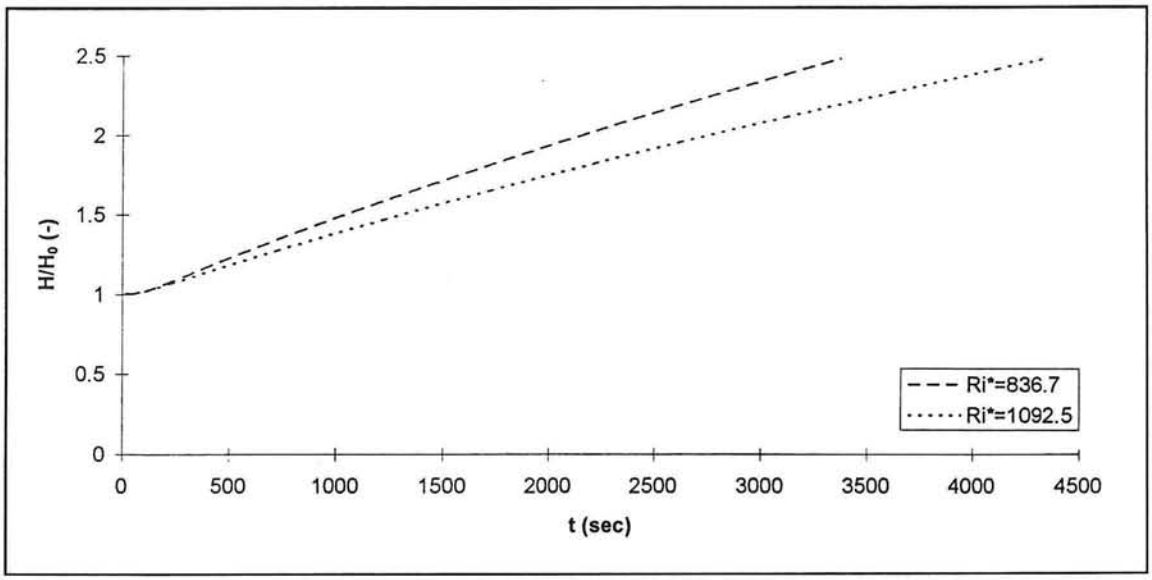


Figure A4: Dimensionless depth of the mixed layer versus time at various Richardson numbers; $CaCl_2$ solution, $H_i$ = 5,4 cm

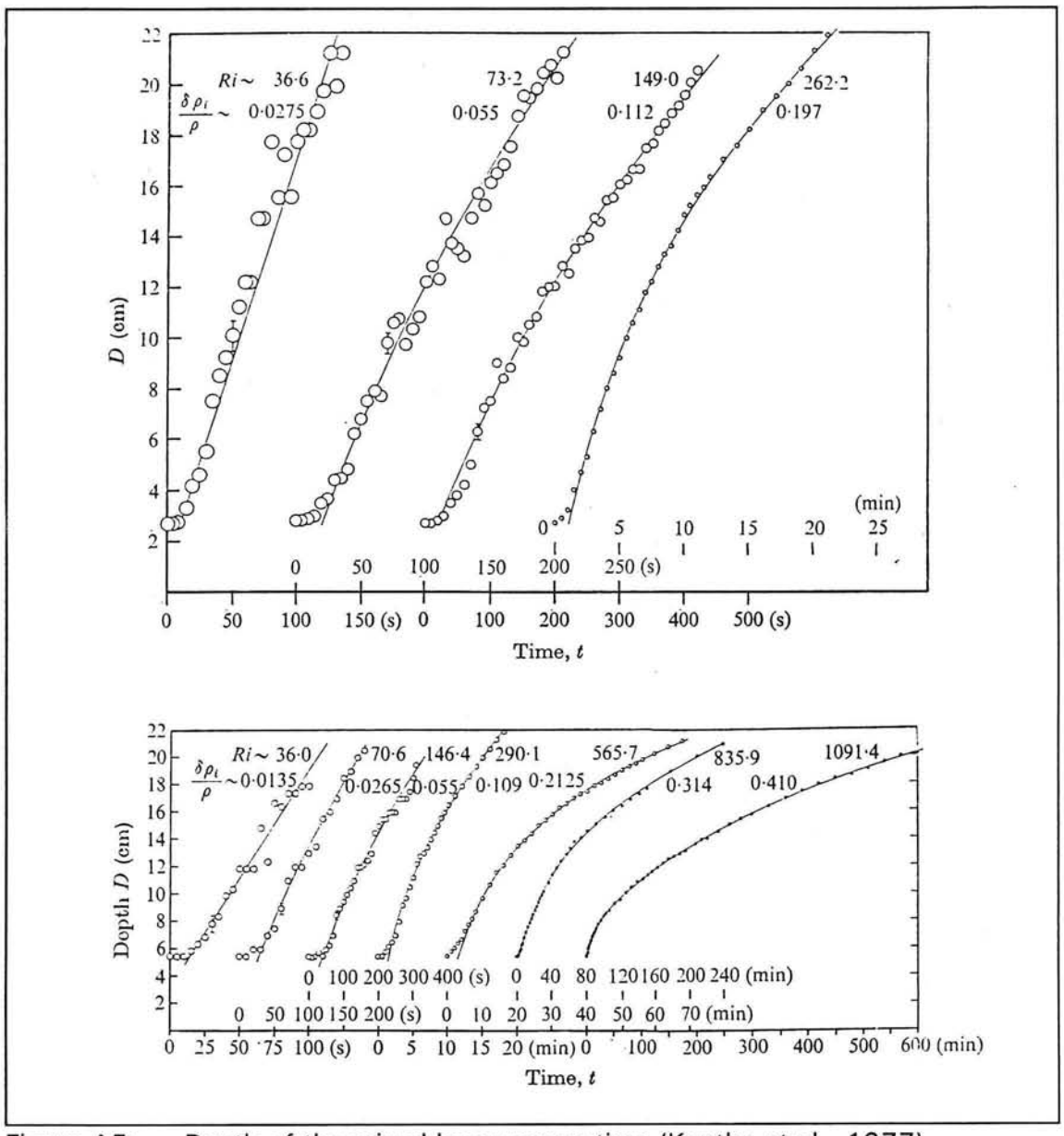


Figure A5: Depth of the mixed layer versus time (Kantha et al., 1977)

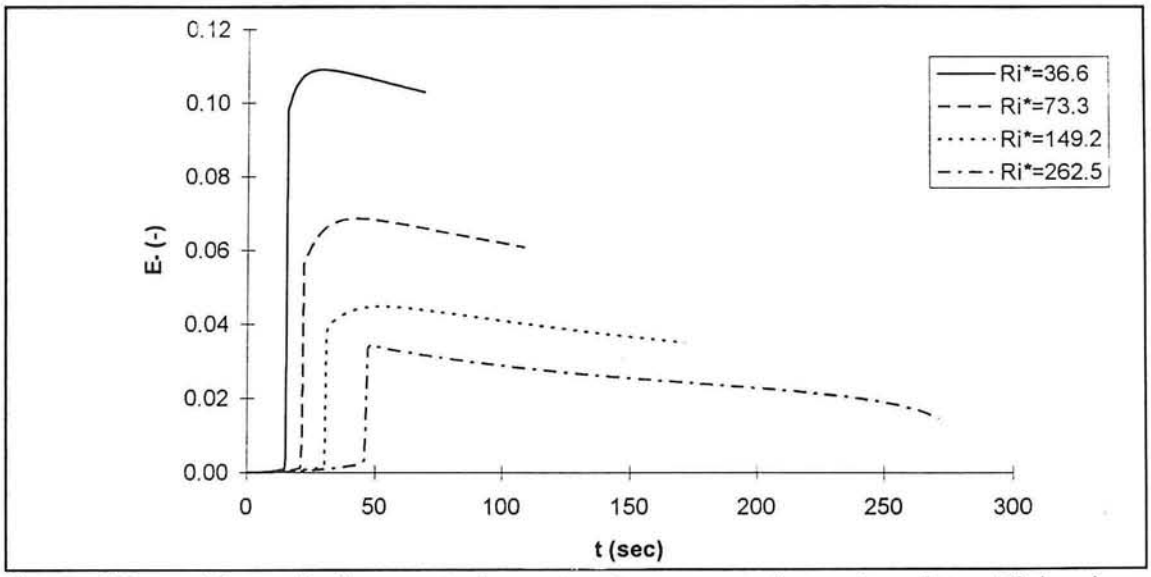


Figure A6: Dimensionless entrainment rate versus time at various Richardson numbers; NaCl solution, $H_i$ = 2,7 cm

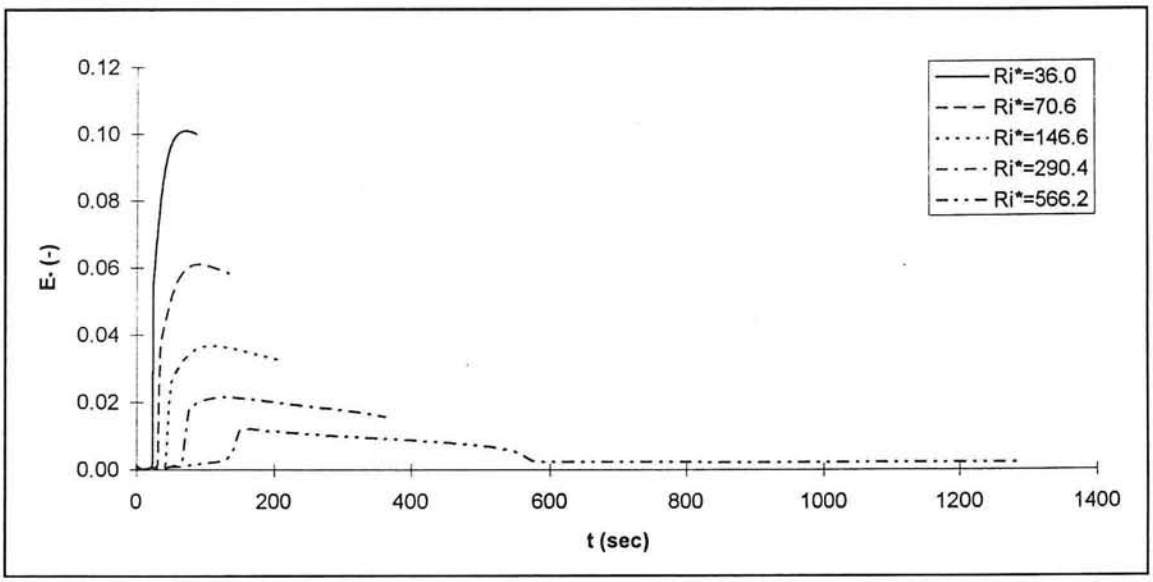


Figure A7: Dimensionless entrainment rate versus time at various Richardson numbers; $CaCl_2$ solution, $H_i$ = 5,4 cm

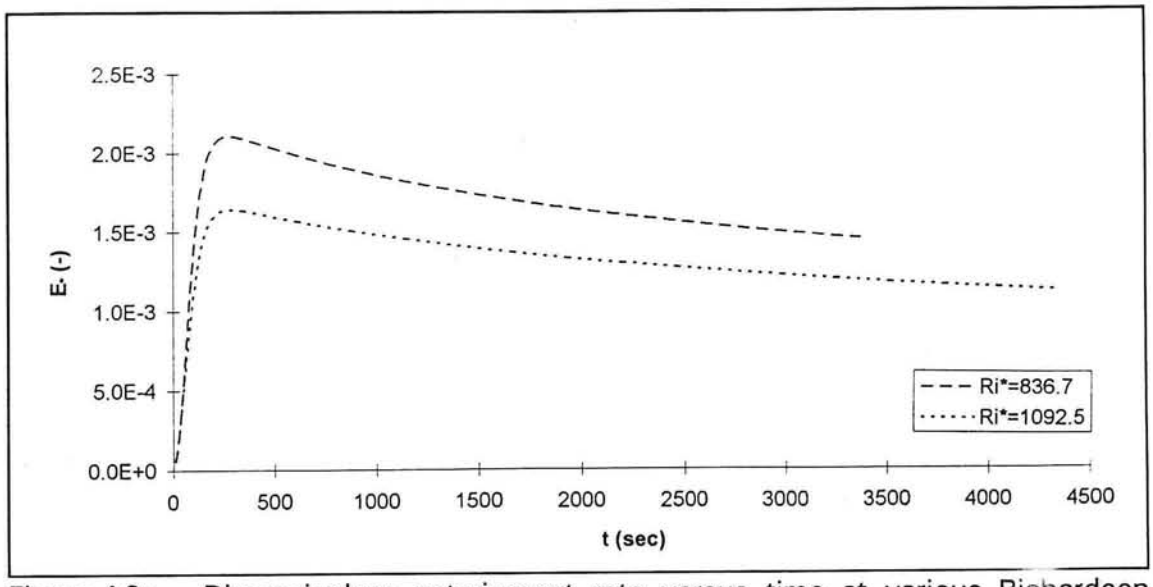


Figure A8: Dimensionless entrainment rate versus time at various Richardson numbers; $CaCl_2$ solution, $H_i$ = 5,4 cm

## APPENDIX B: Simulation of the entrainment in transient unidirectional flow experiments

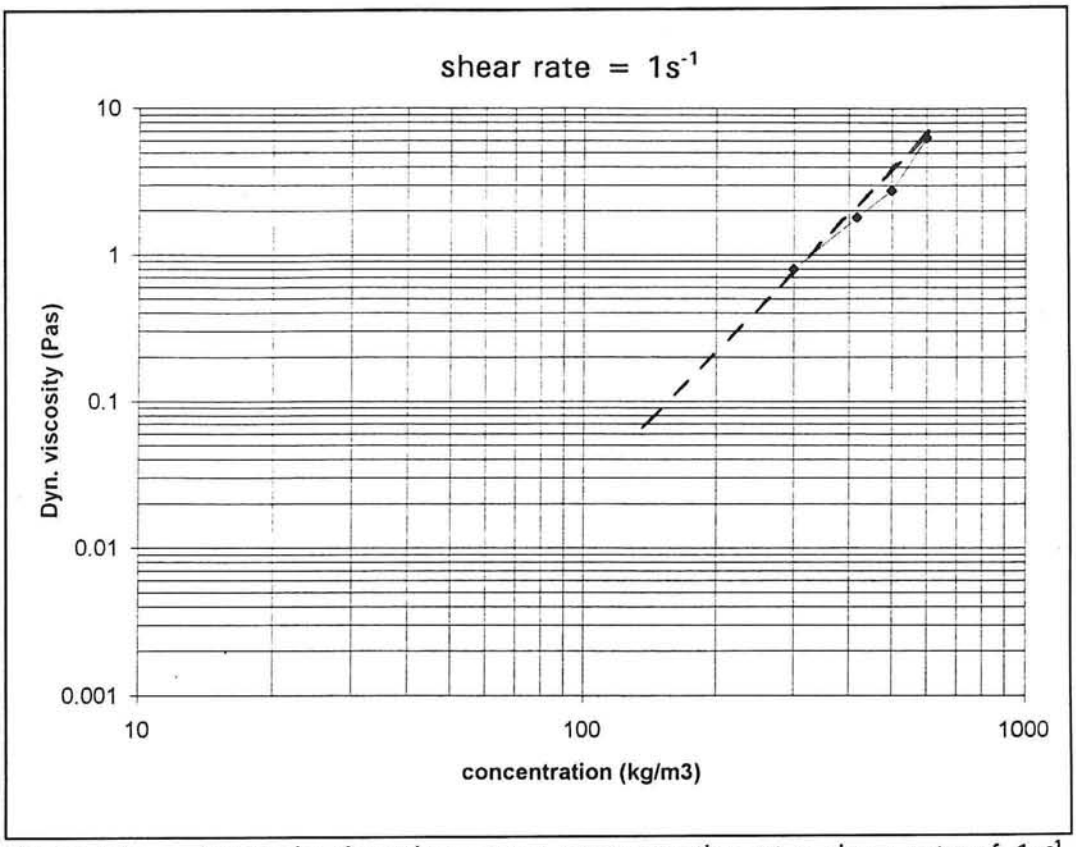


Figure B1: Dynamic viscosity versus concentration at a shear rate of $1s^{-1}$, kaolinite

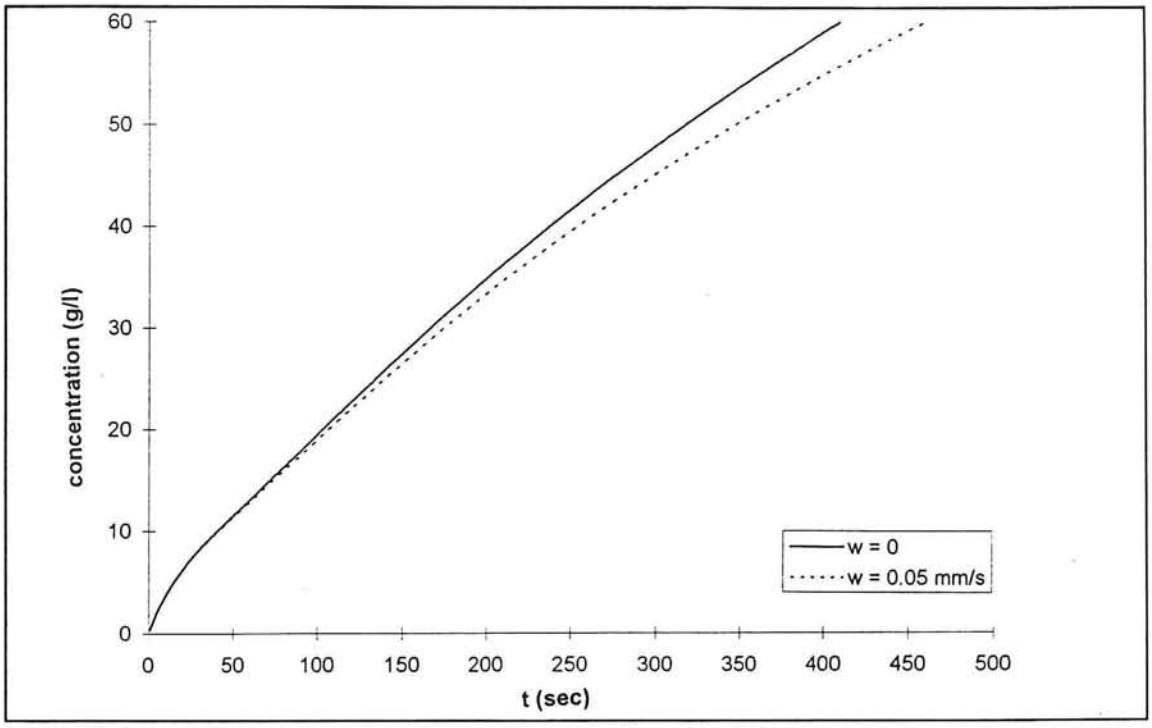


Figure B2: Concentration versus time for simulation K4 of kaolinite

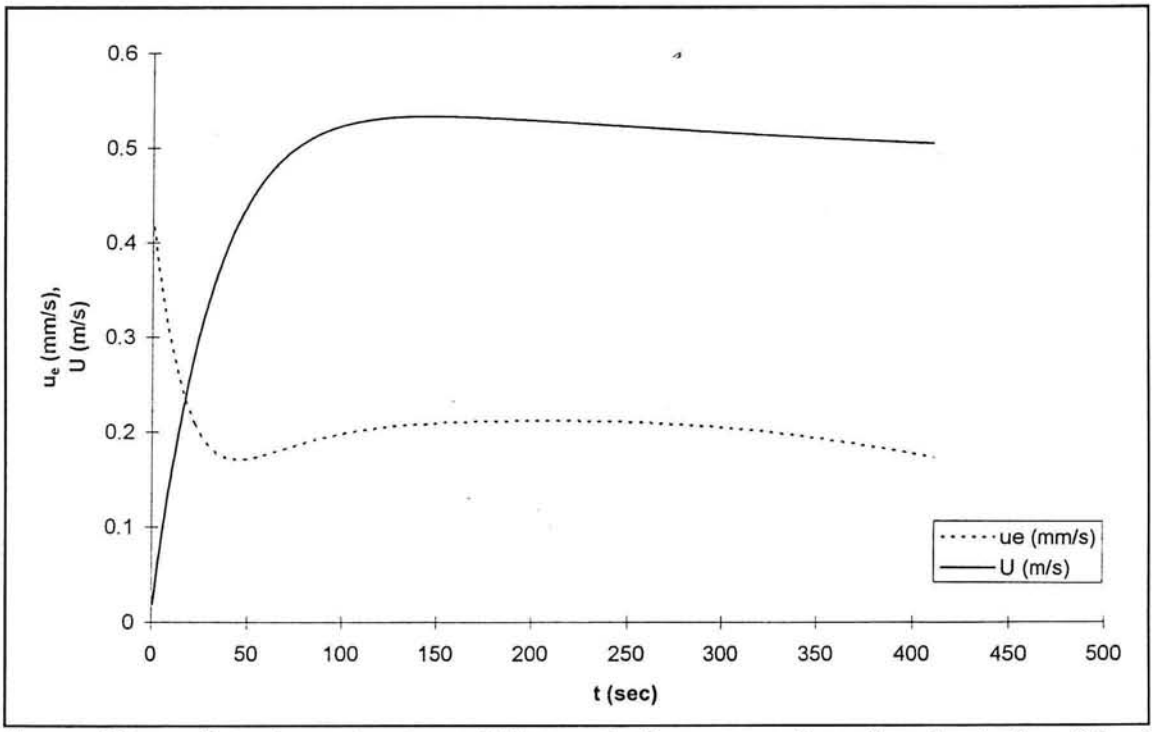


Figure B3: Entrainment rate and flow velocity versus time for simulation K4 of kaolinite

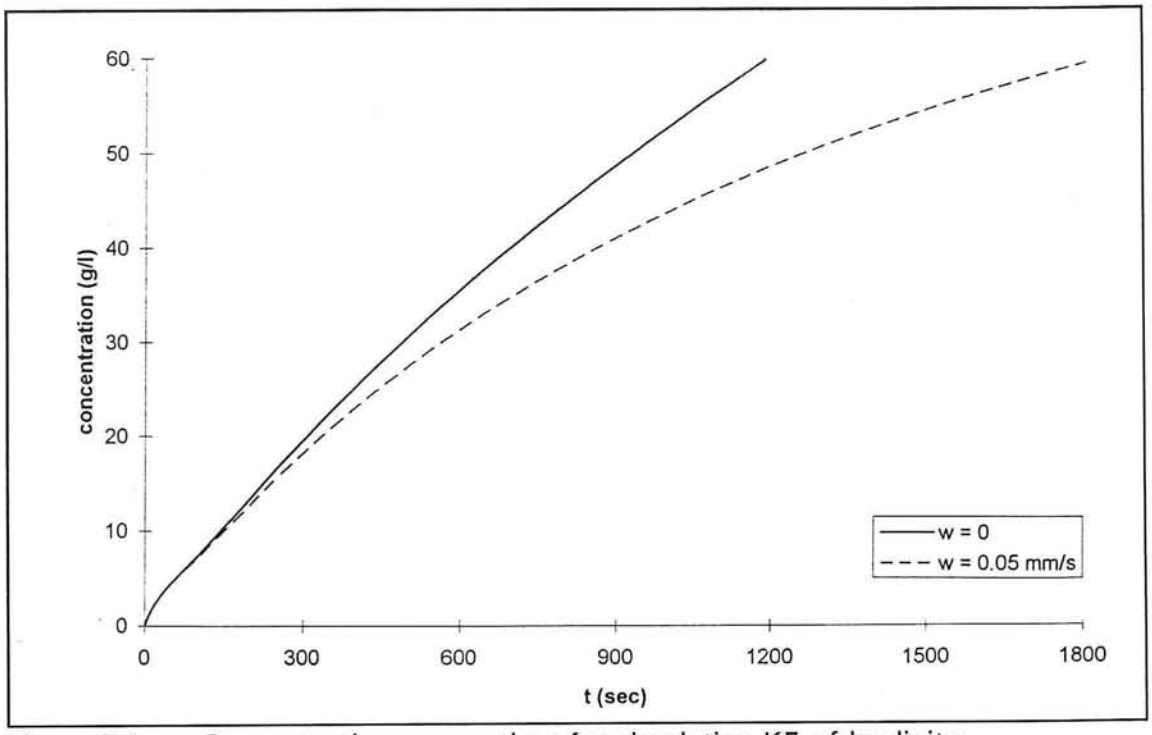


Figure B4: Concentration versus time for simulation K5 of kaolinite

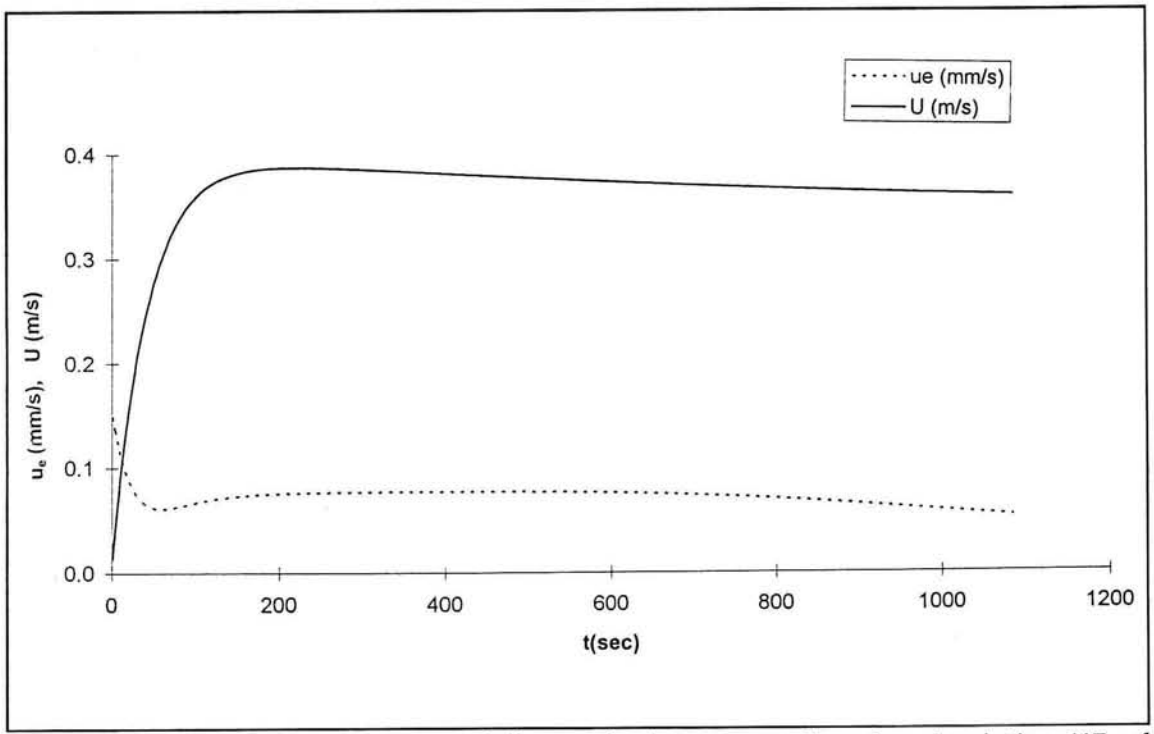


Figure B5: Entrainment rate and flow velocity versus time for simulation K5 of kaolinite

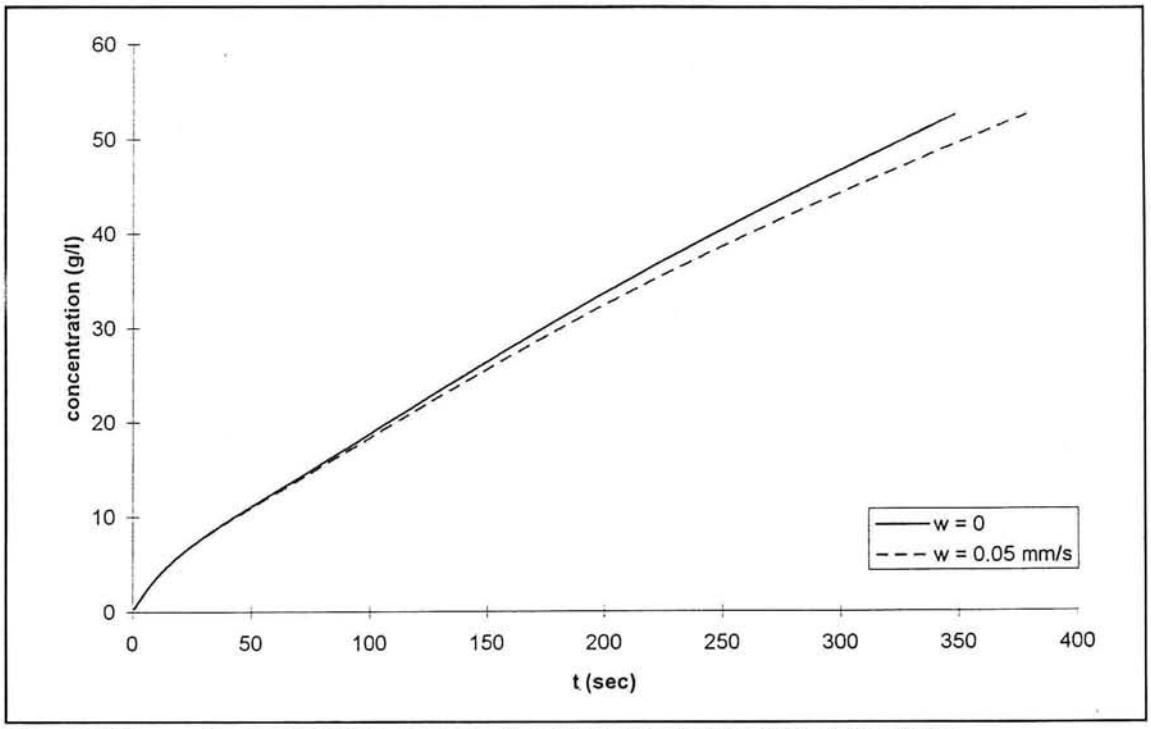


Figure B6: Concentration versus time for simulation K6 of kaolinite

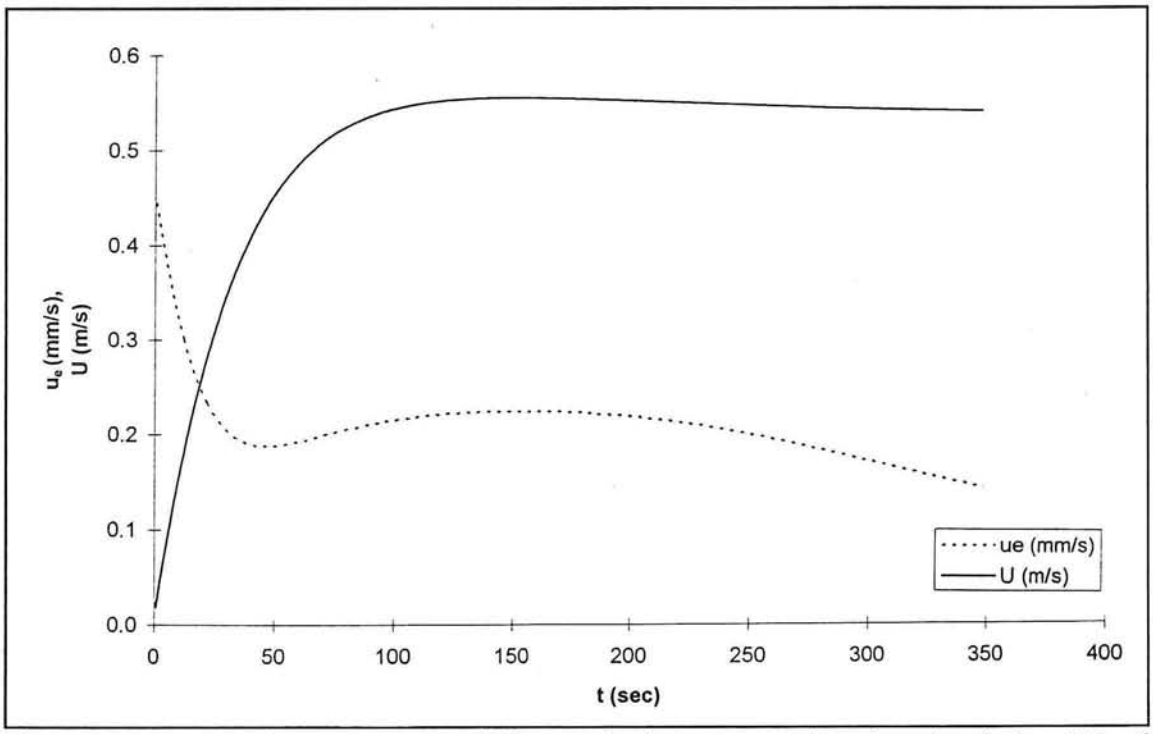


Figure B7: Entrainment rate and flow velocity versus time for simulation K6 of kaolinite

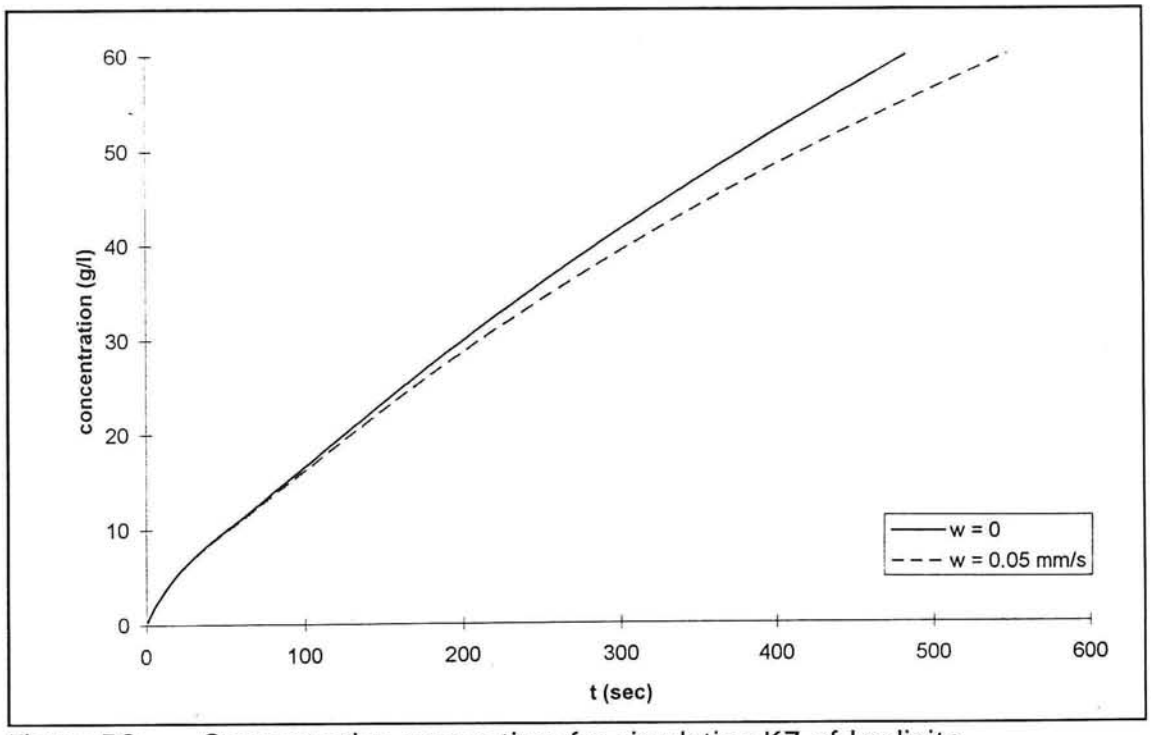


Figure B8: Concentration versus time for simulation K7 of kaolinite

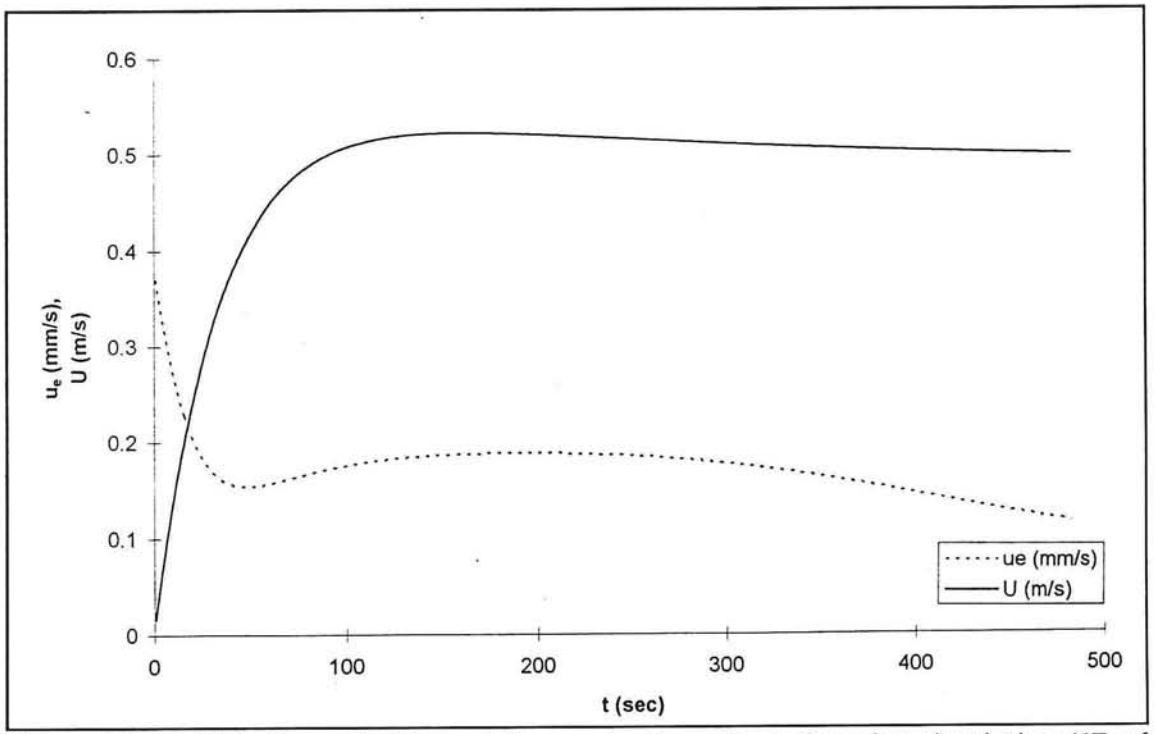


Figure B9: Entrainment rate and flow velocity versus time for simulation K7 of kaolinite

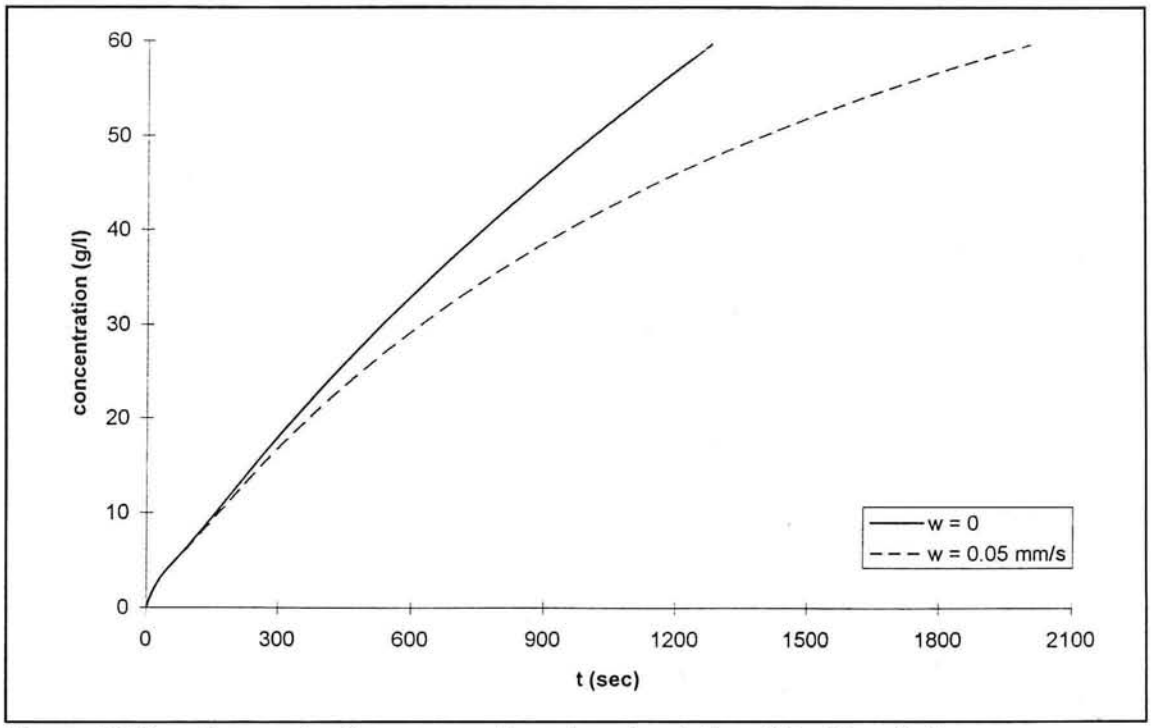


Figure B10: Concentration versus time for simulation K8 of kaolinite

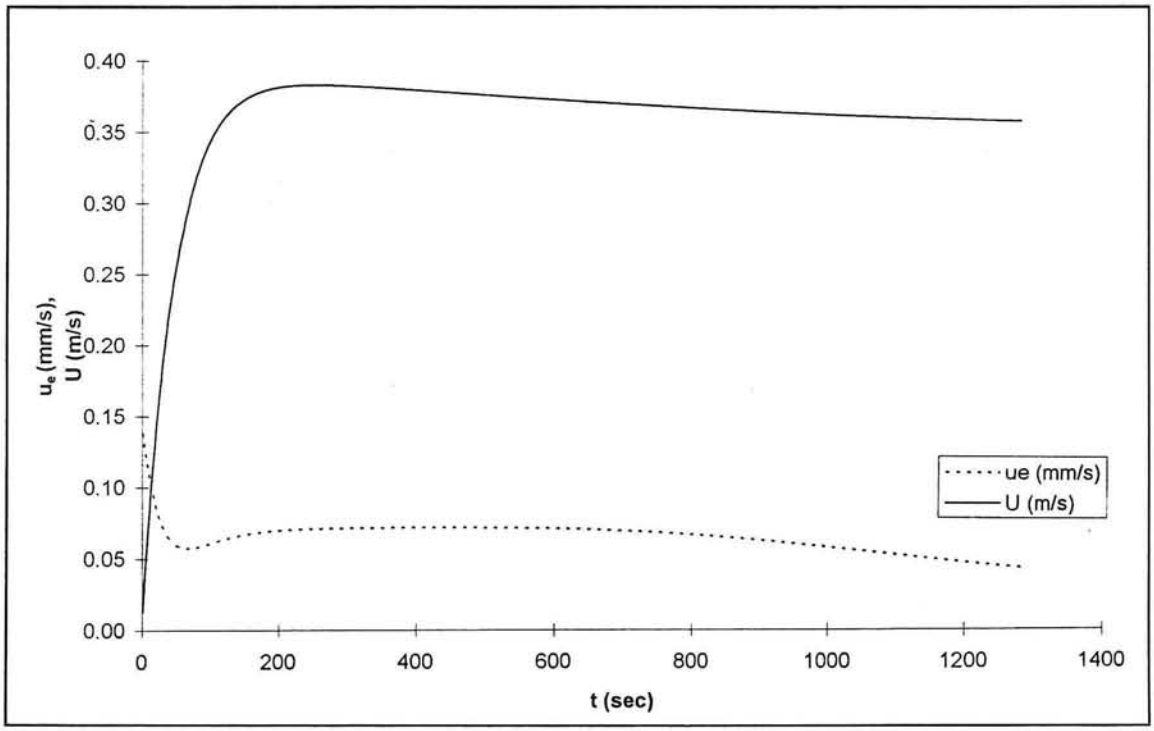


Figure B11: Entrainment rate and flow velocity versus time for simulation K8 of kaolinite

## APPENDIX C: Comparison of transient unidirectional flow simulations with experiments

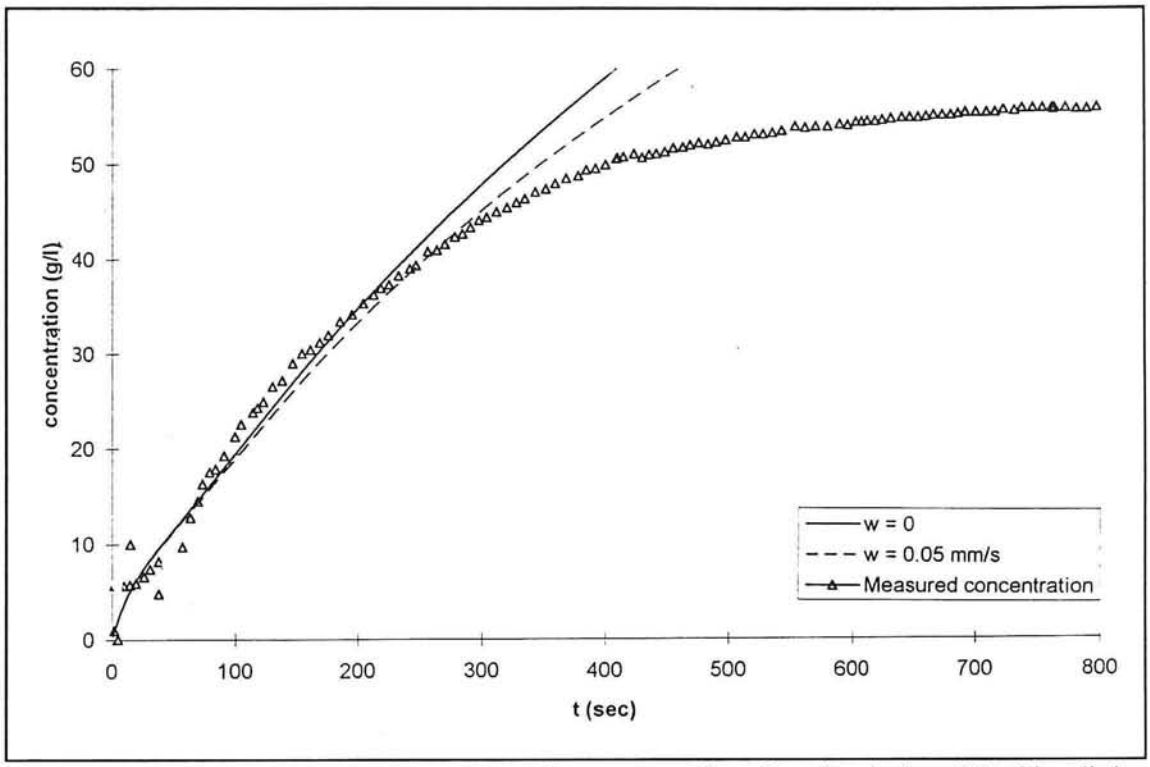


Figure C1: Comparison of concentration versus time for simulation K4 of kaolinite

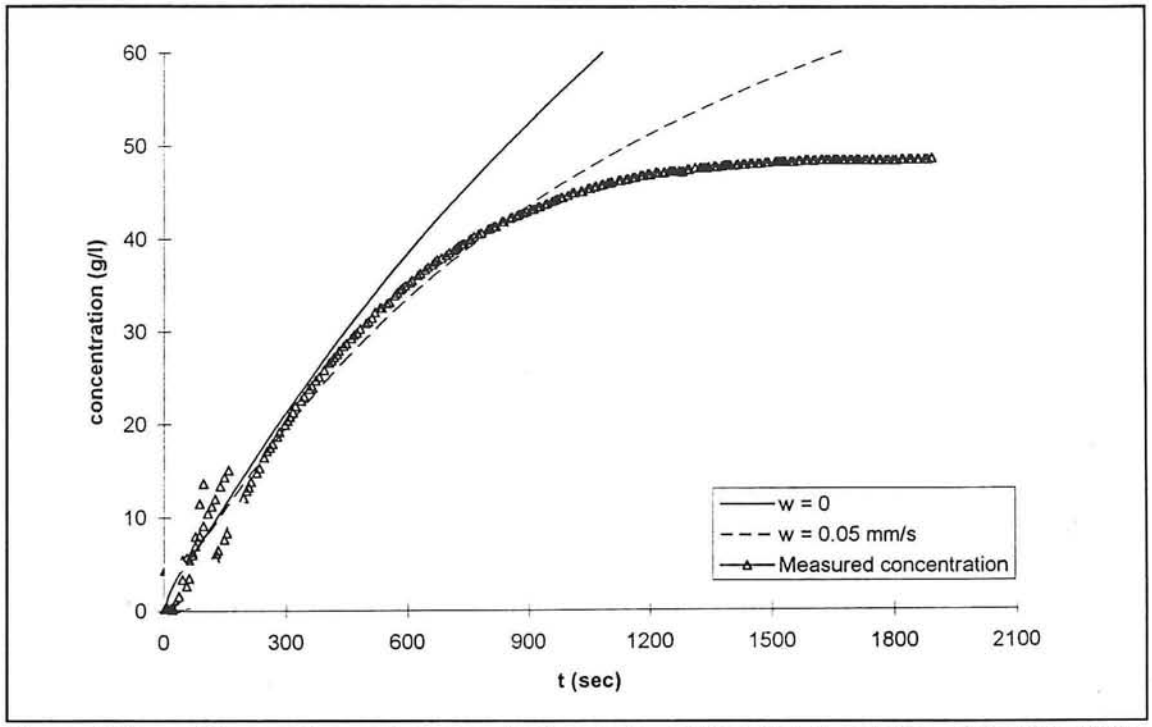


Figure C2: Comparison of concentration versus time for simulation K5 of kaolinite

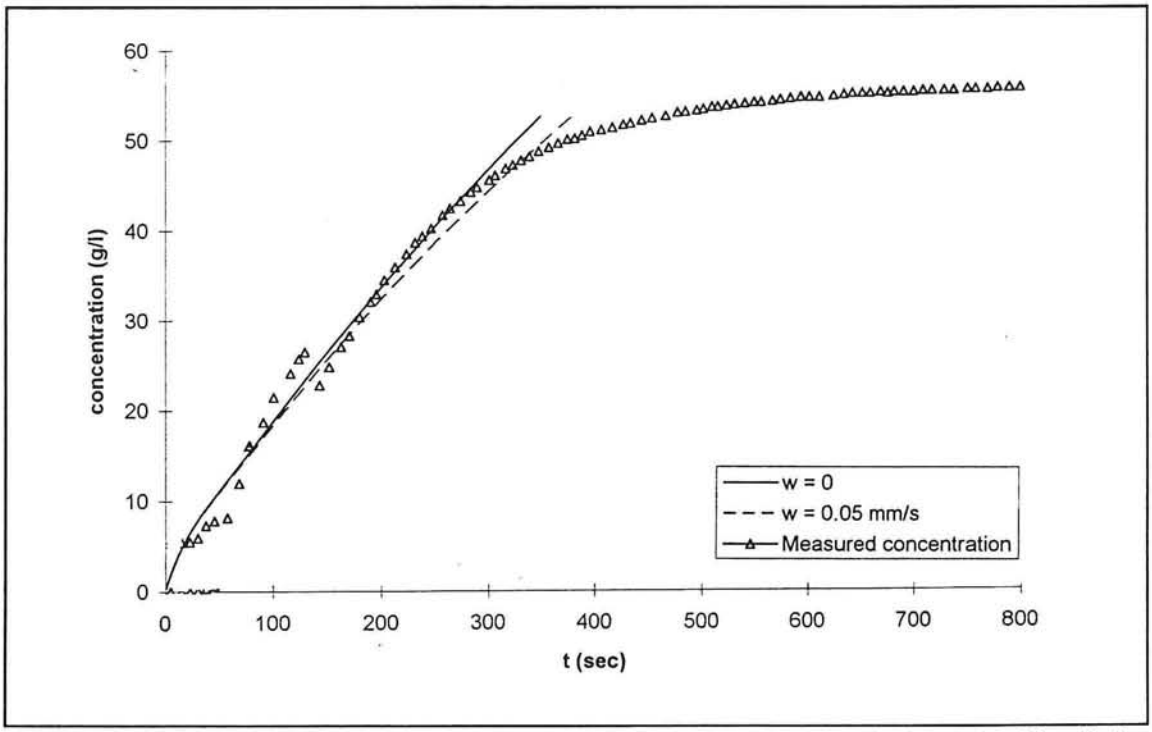


Figure C3: Comparison of concentration versus time for simulation K6 of kaolinite

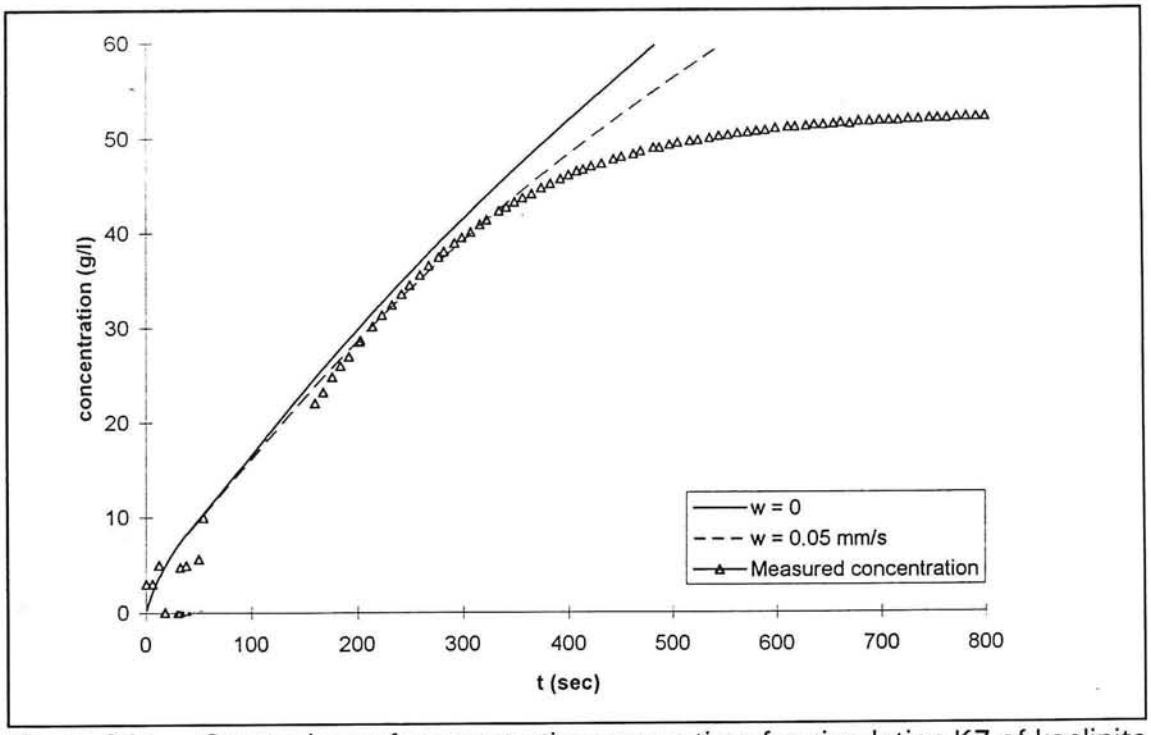


Figure C4: Comparison of concentration versus time for simulation K7 of kaolinite

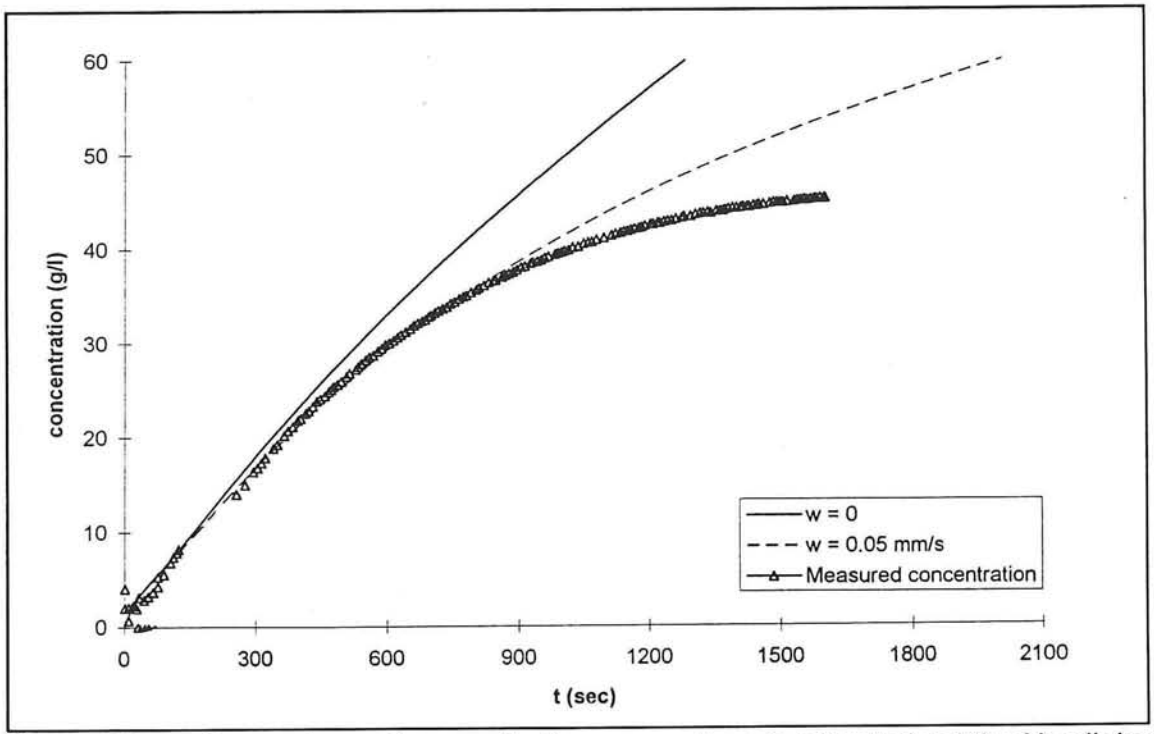


Figure C5: Comparison of concentration versus time for simulation K8 of kaolinite

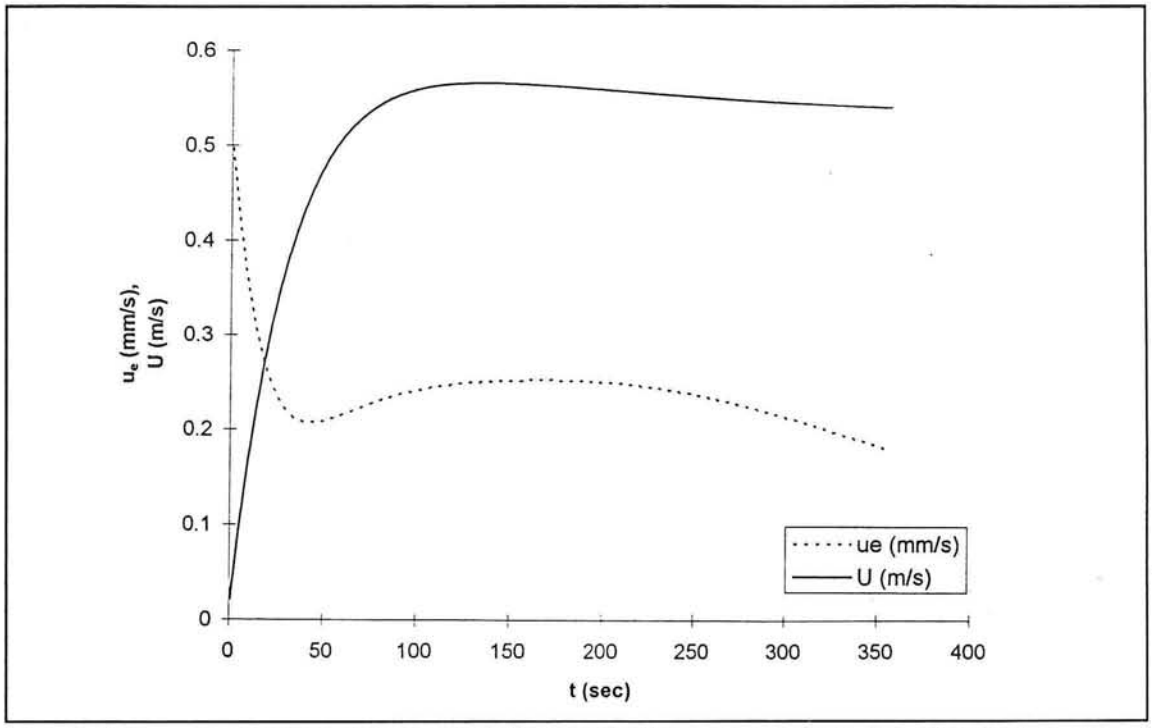


Figure C6: Entrainment rate and flow velocity versus time for simulation K3 of kaolinite

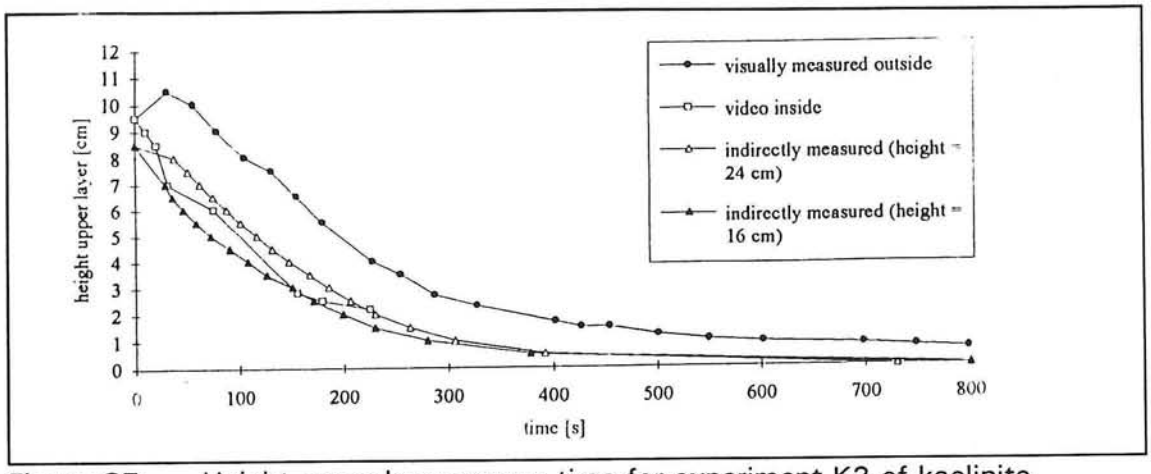


Figure C7: Height upper layer versus time for experiment K3 of kaolinite

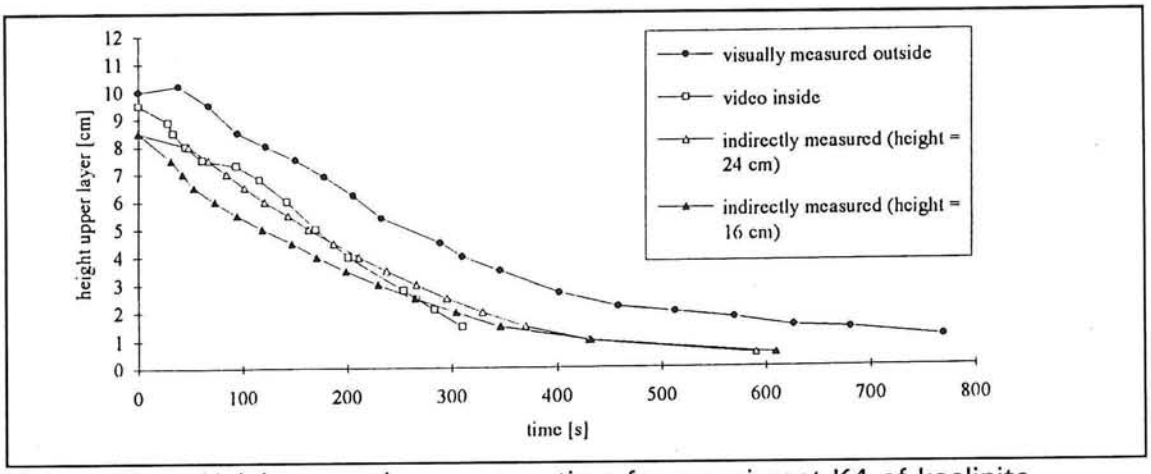


Figure C8: Height upper layer versus time for experiment K4 of kaolinite

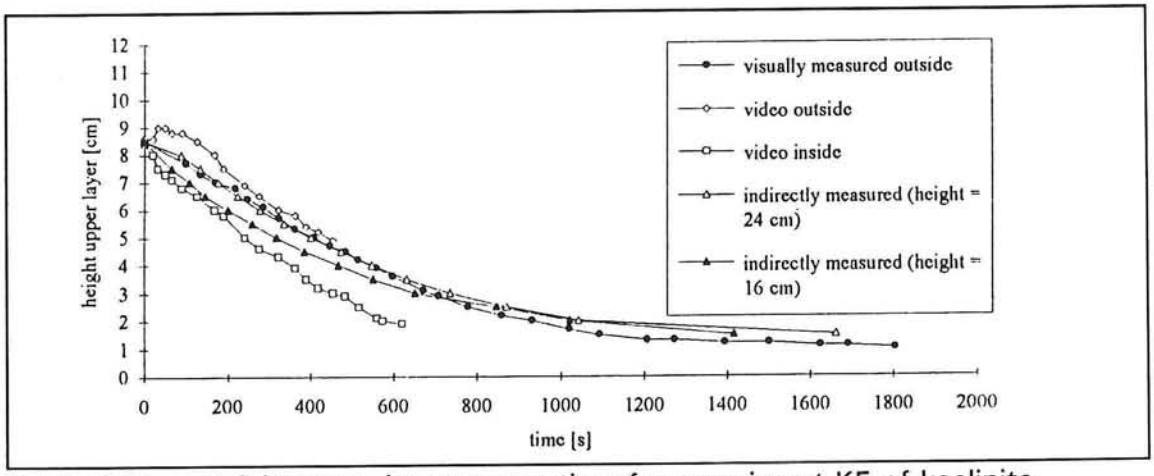


Figure C9: Height upper layer versus time for experiment K5 of kaolinite

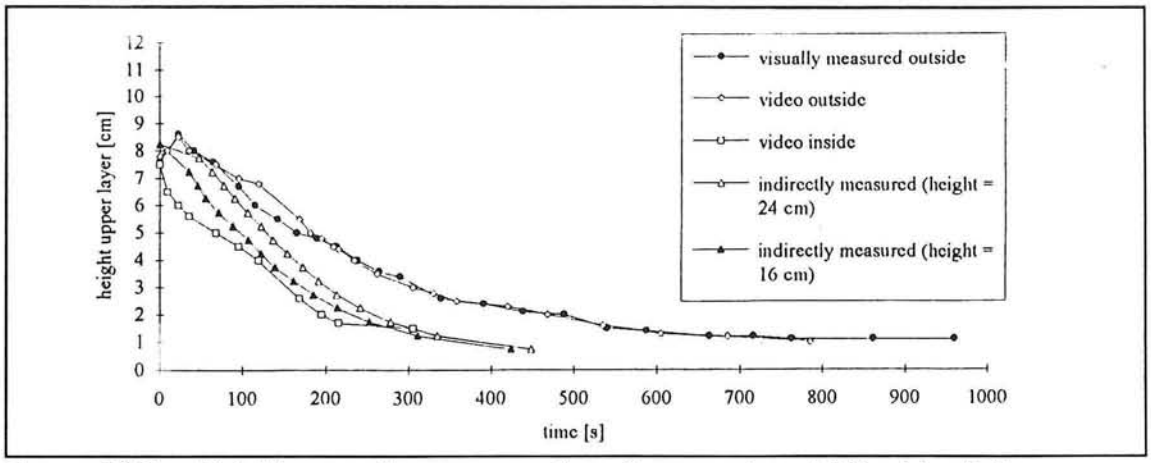


Figure C10: Height upper layer versus time for experiment K6 of kaolinite

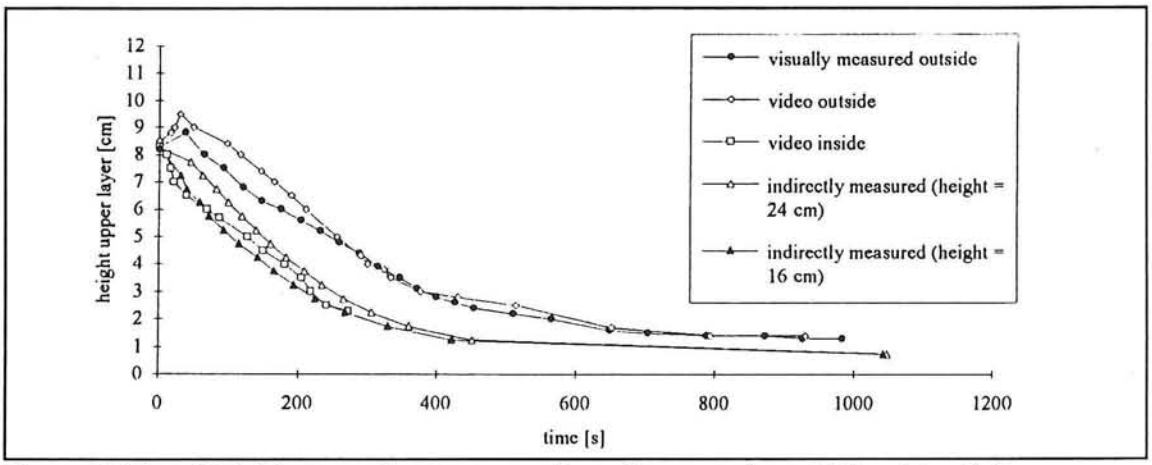


Figure C11: Height upper layer versus time for experiment K7 of kaolinite

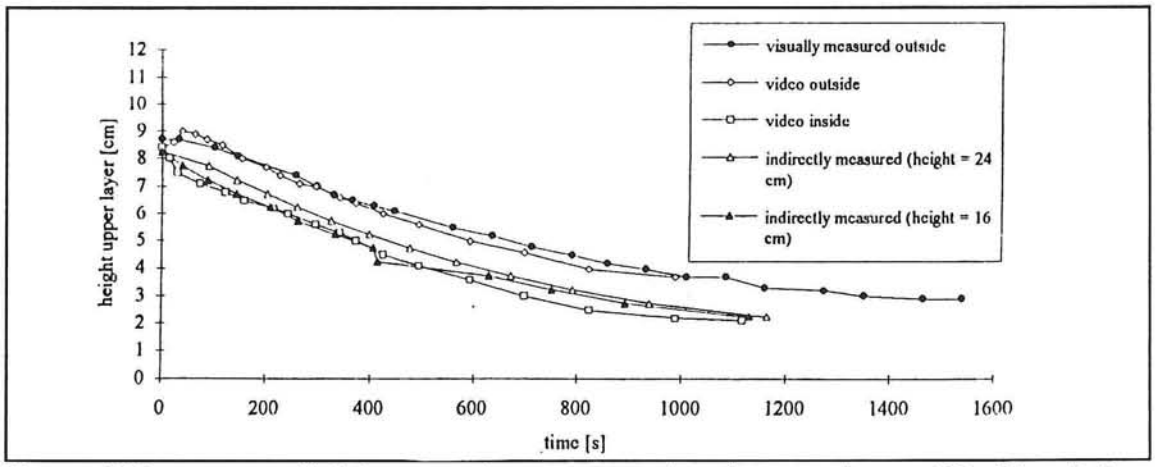


Figure C12: Height upper layer versus time for experiment K8 of kaolinite

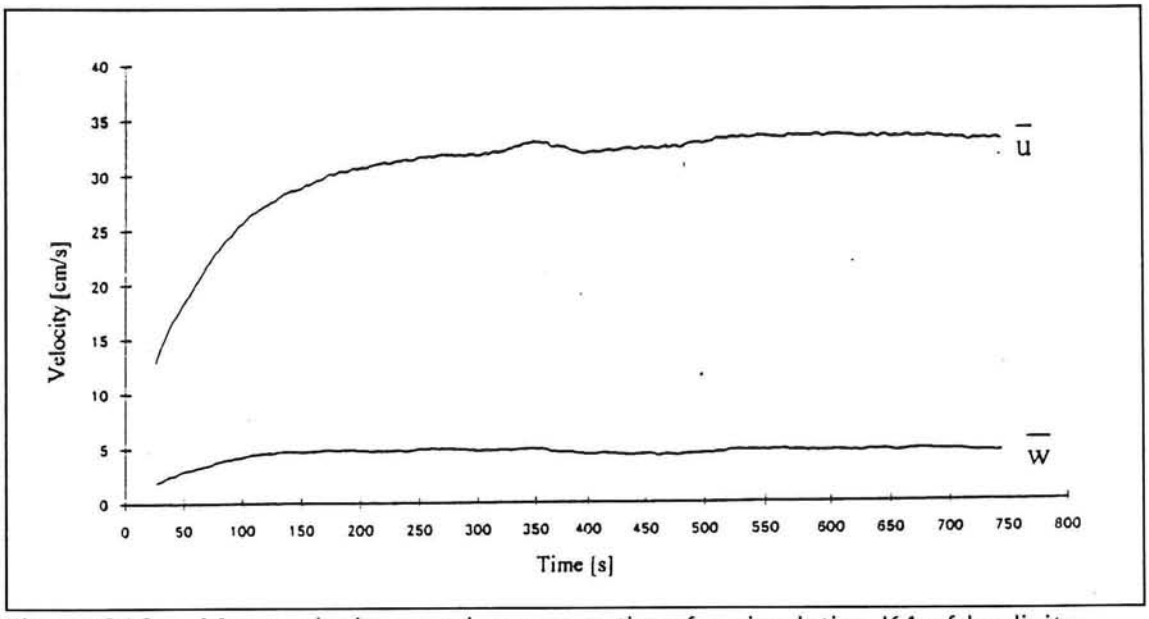


Figure C13: Mean velocity u and w versus time for simulation K4 of kaolinite

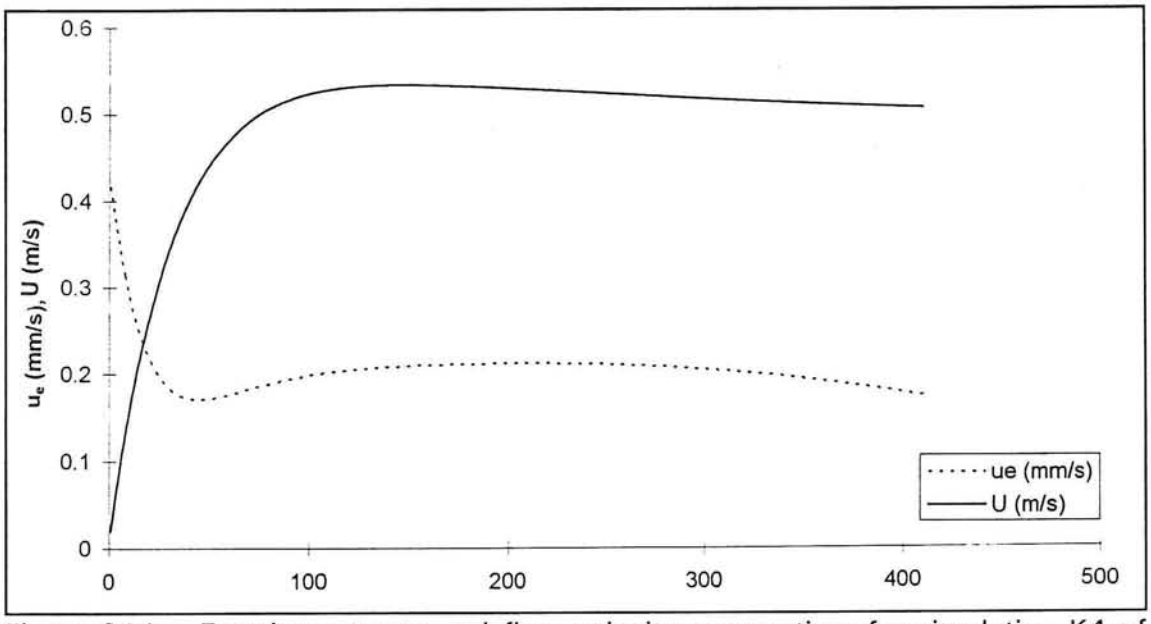


Figure C14: Entrainment rate and flow velocity versus time for simulation K4 of kaolinite

## APPENDIX D: Comparison of tidal flow simulation with experiment

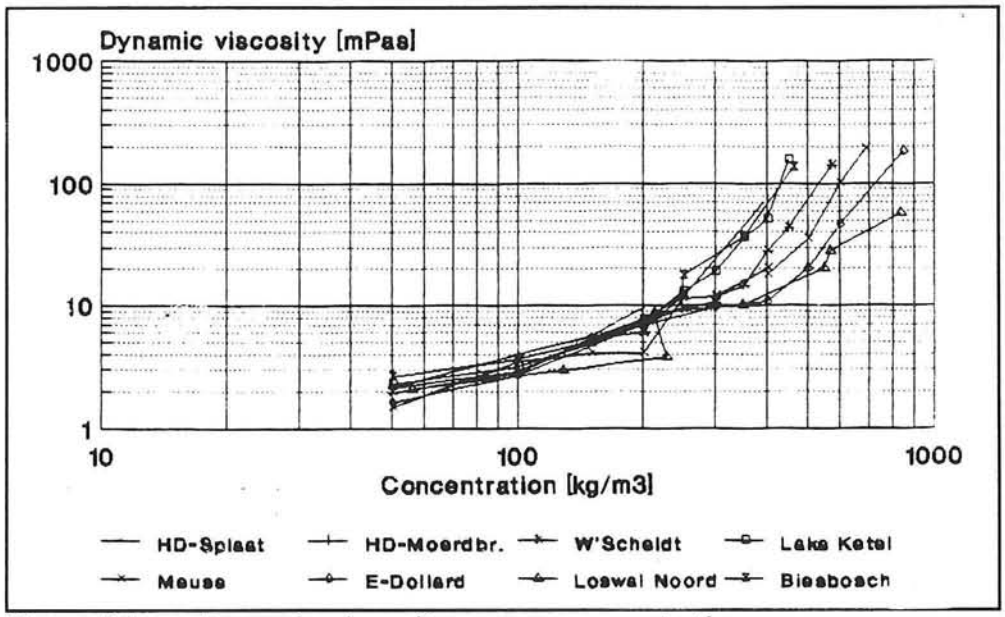


Figure D1: Dynamic viscosity versus concentration

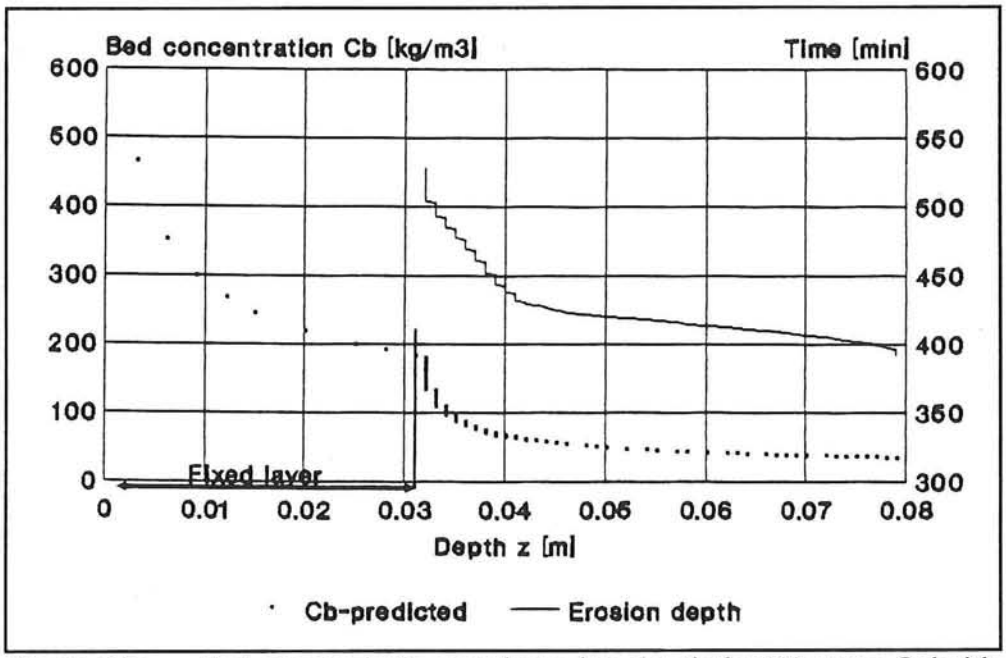


Figure D2: Bed concentration and erosion depth for Western Scheldt experiments

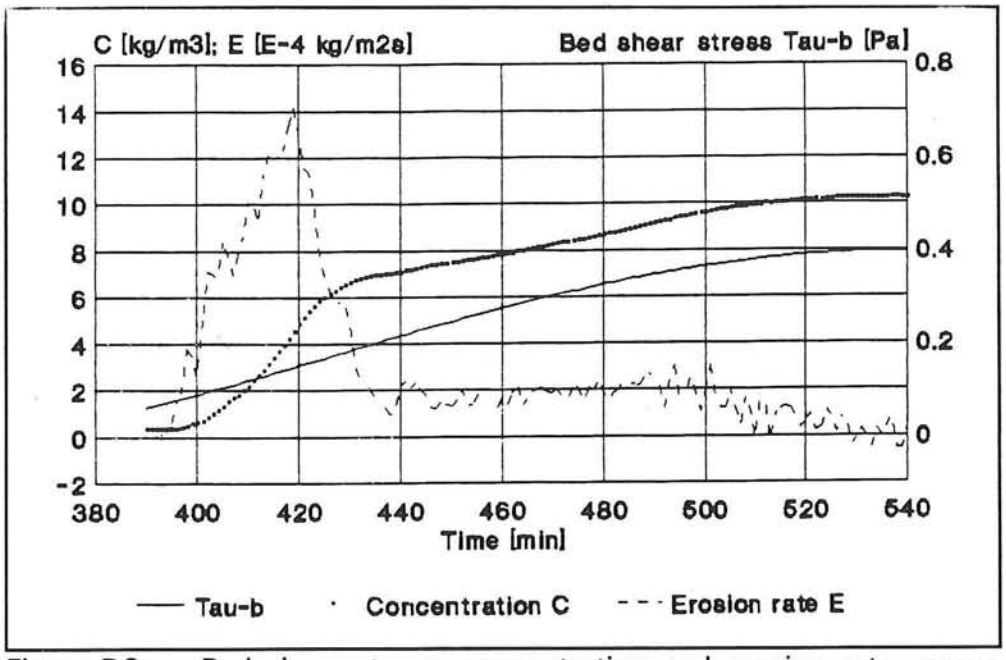


Figure D3: Bed shear stress, concentration and erosion rate versus time for Western Scheldt experiments

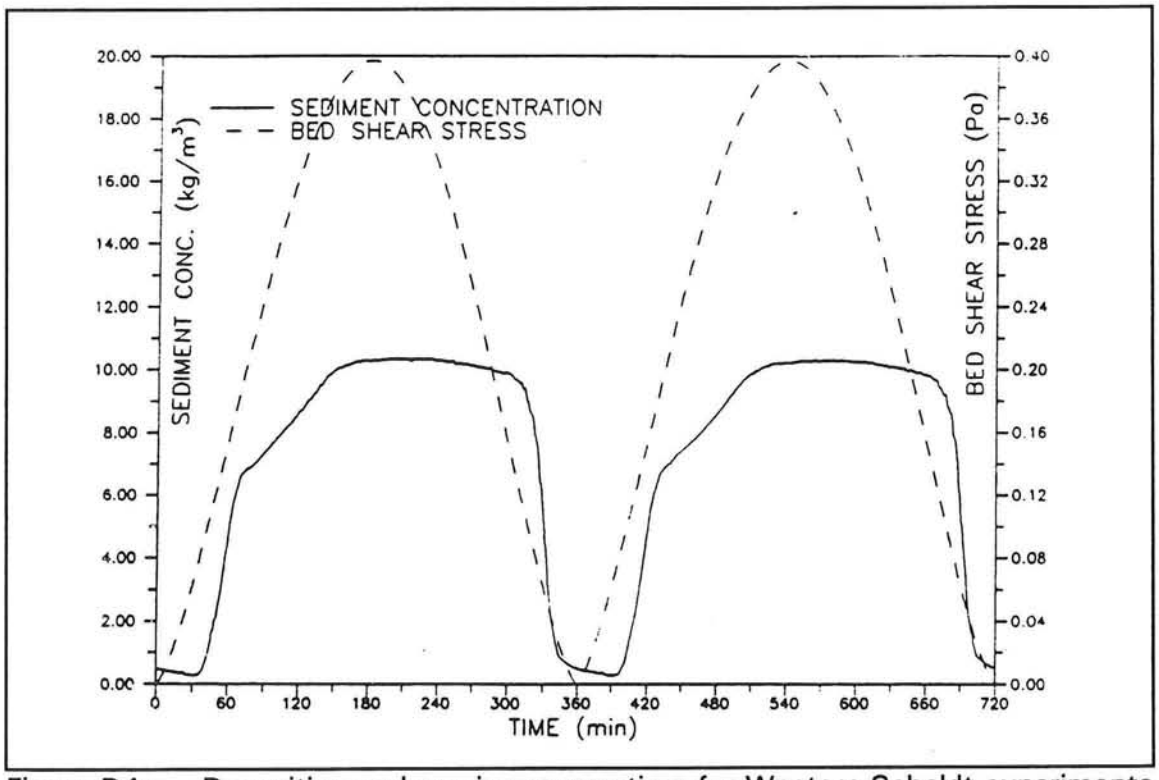


Figure D4: Deposition and erosion versus time for Western Scheldt experiments

# APPENDIX E:

## Numerical results for the Severn

## Phase I

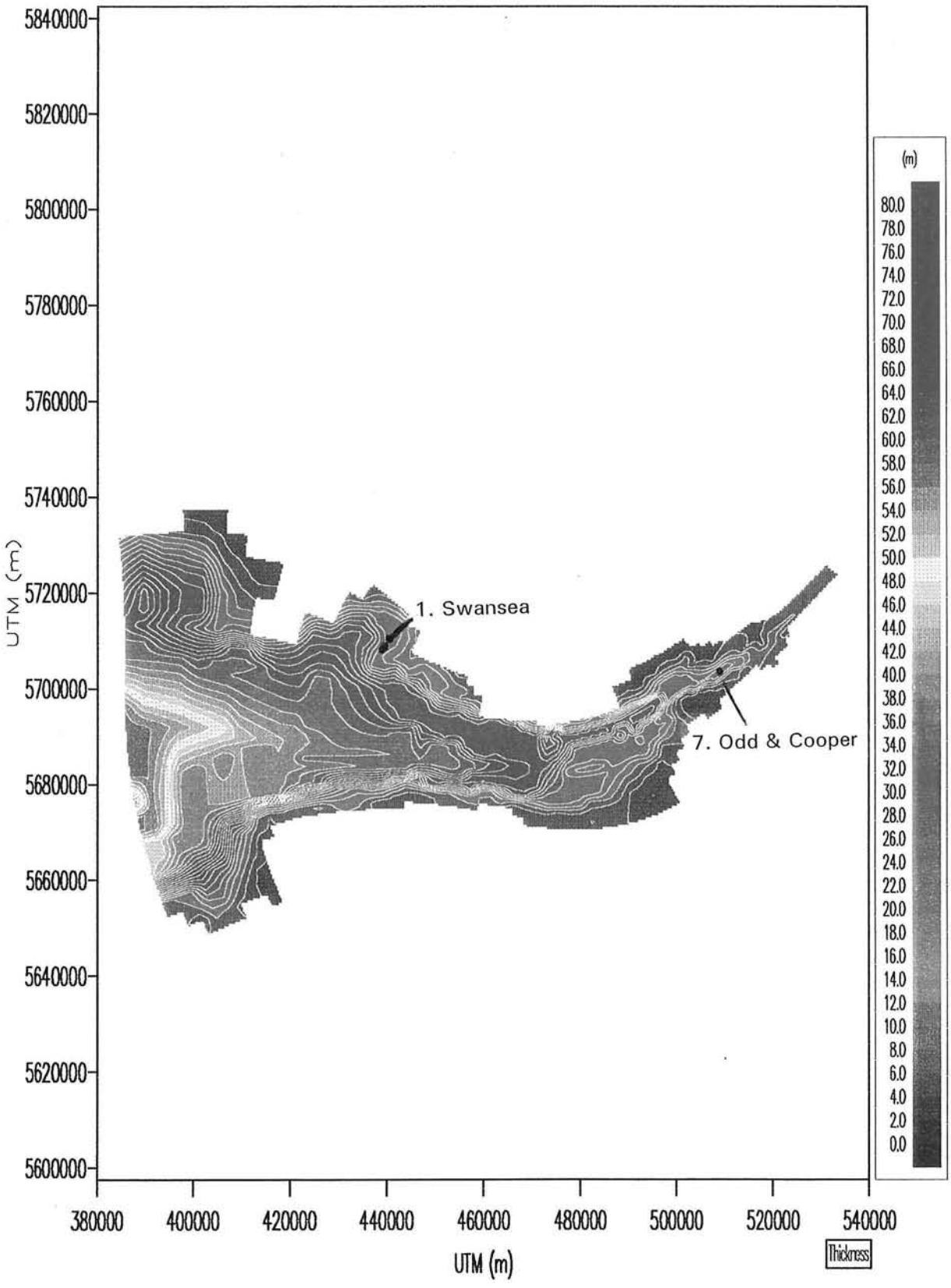


BATHYMETRY OF THE SEVERN ESTUARY

FIG. E1

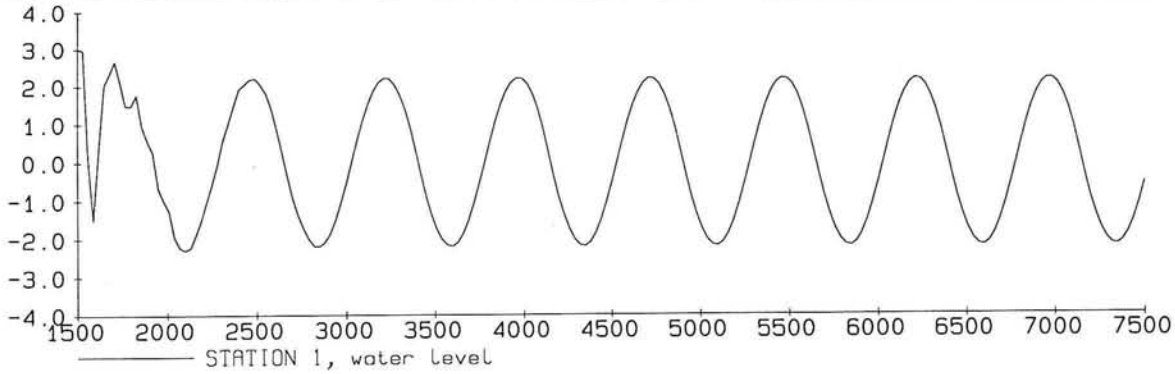


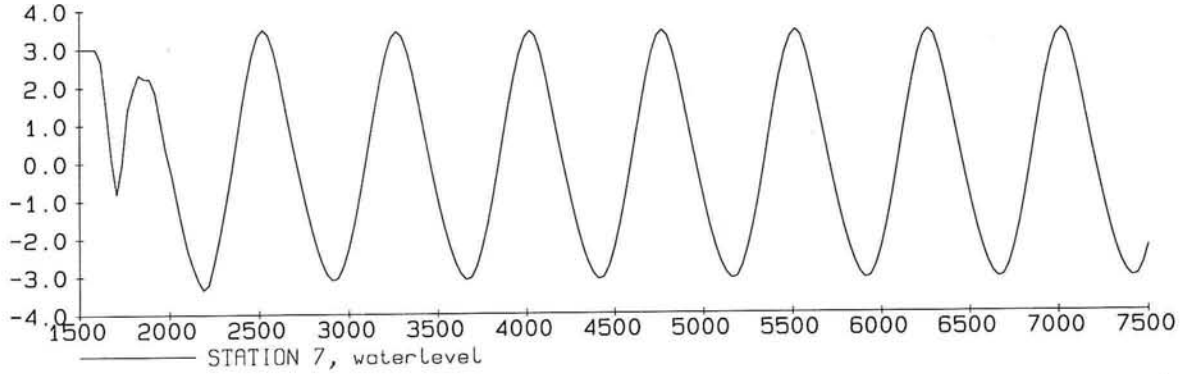


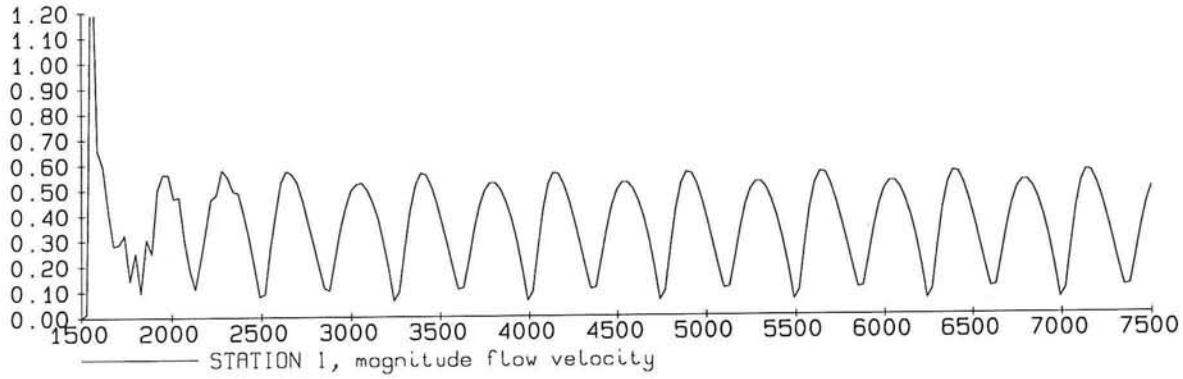


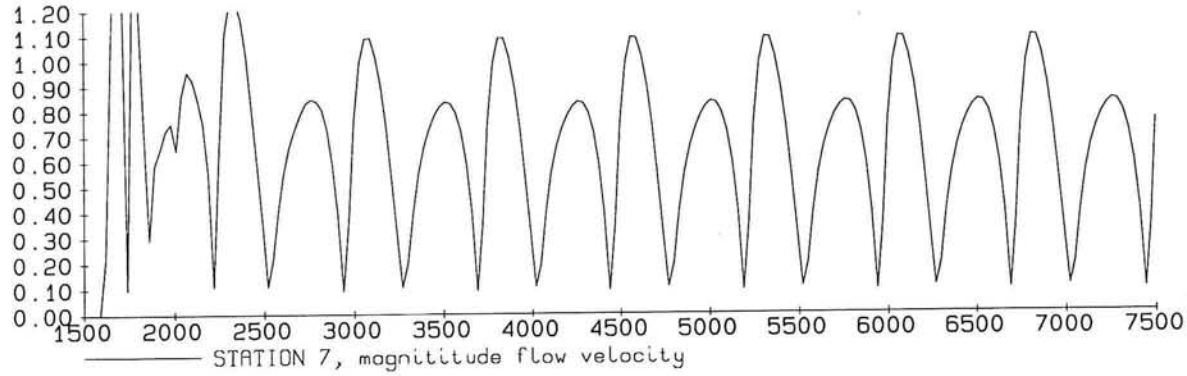


**WATER LEVELS (M) AND FLOW VELOCITIES (M/S)**
**Time in minutes**
**Neap tide**

STATIONS 1 AND 7

FIG. E2

FLOW PATTERN
At $t$ = 6000 minutes
Neap tide


FIG. E3

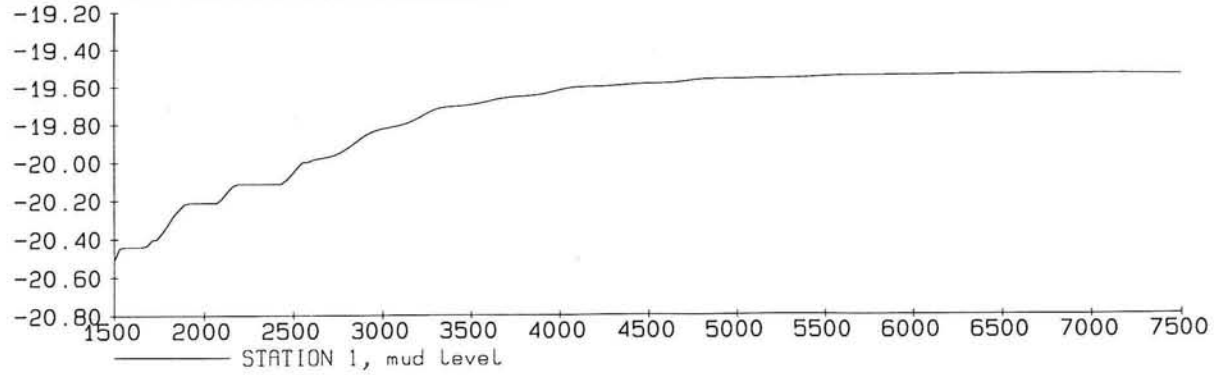


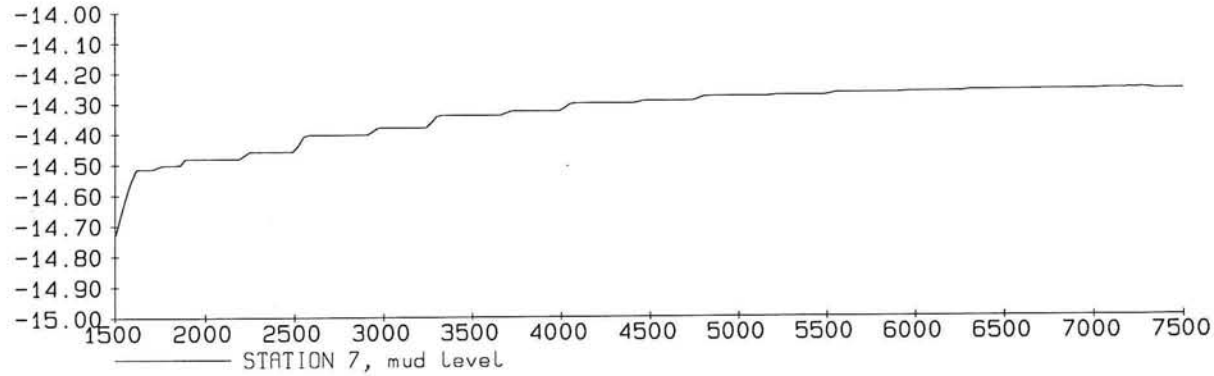


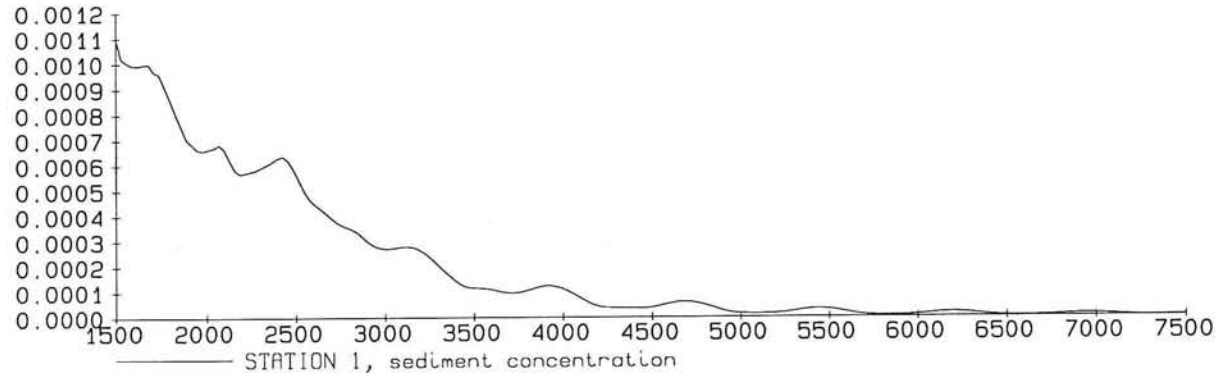


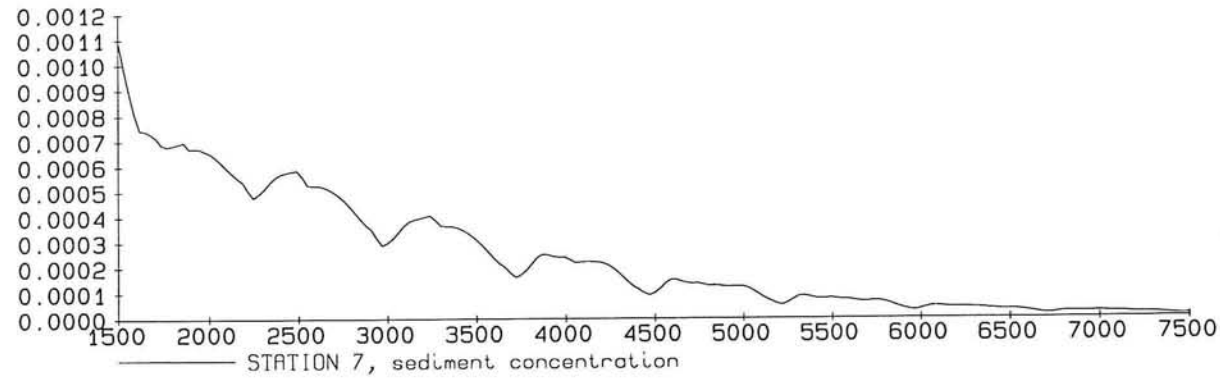


**MUD LEVELS (M) AND SEDIMENT CONCENTRATIONS (-)**
**Time in minutes**
**Neap tide**

SIMULATION 1

STATIONS 1 AND 7

FIG. E4

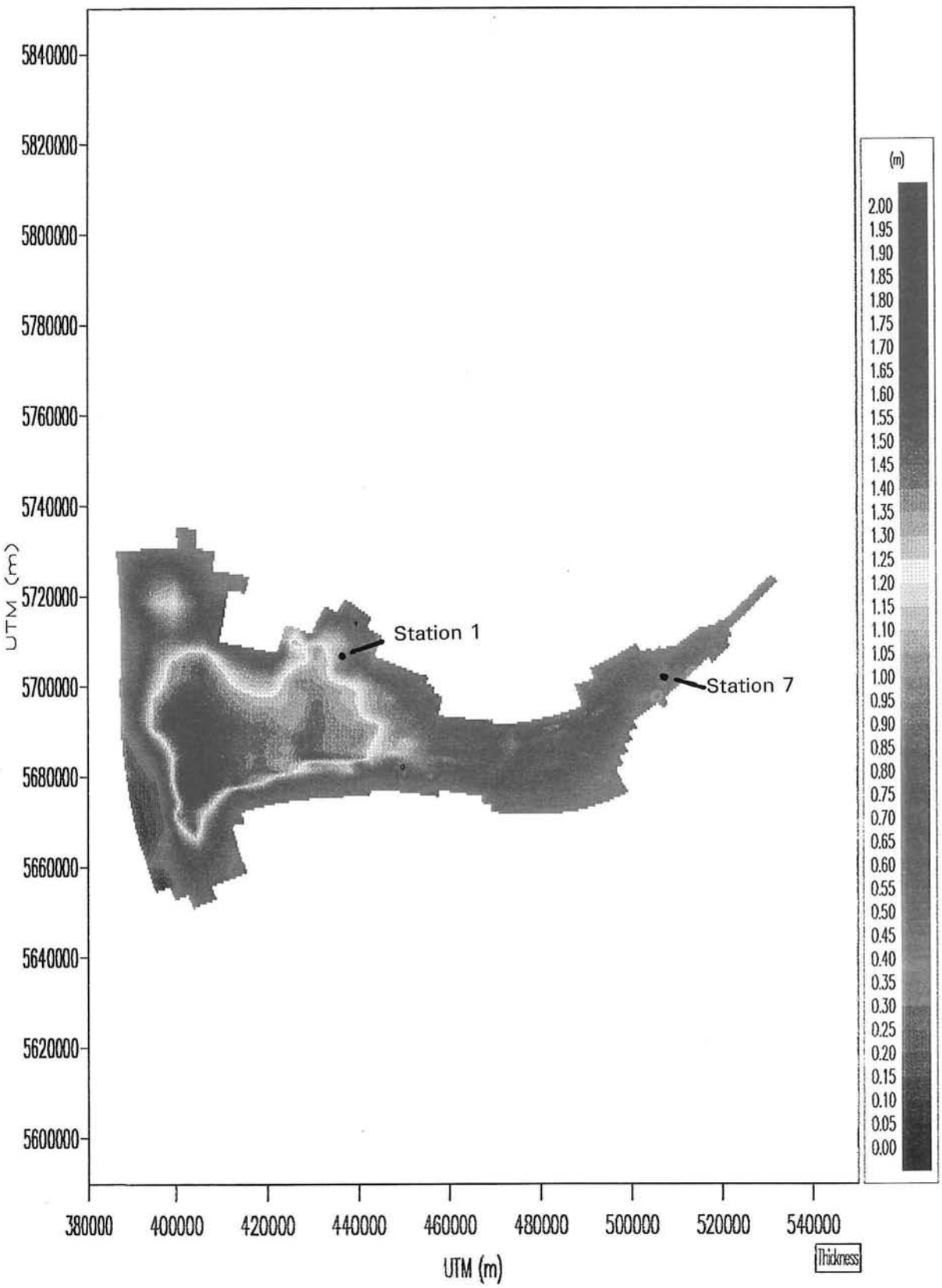


THICKNESS OF FLUID MUD LAYER
AT t = 6000 MINUTES

SIMULATION 1

FIG. E5

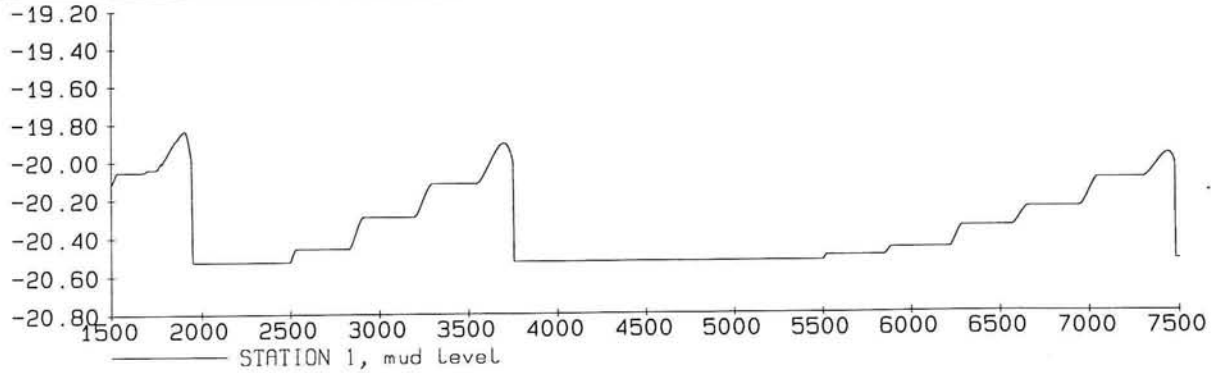


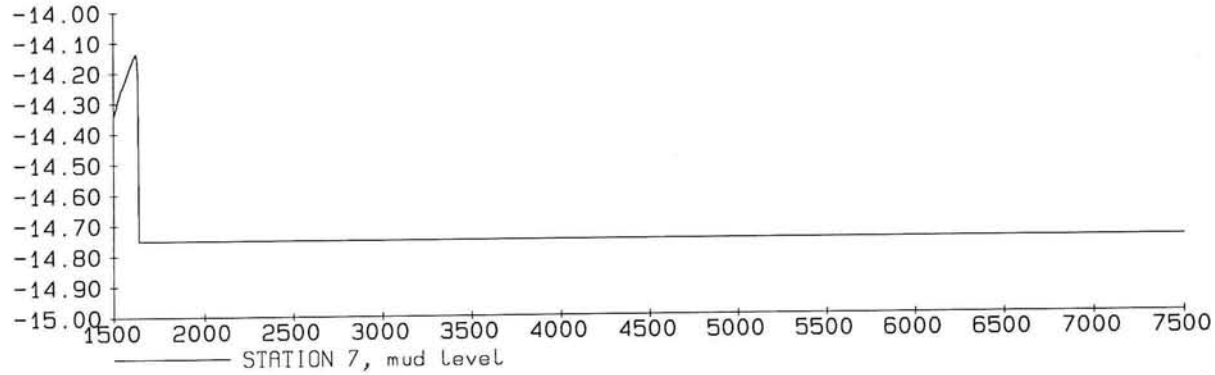


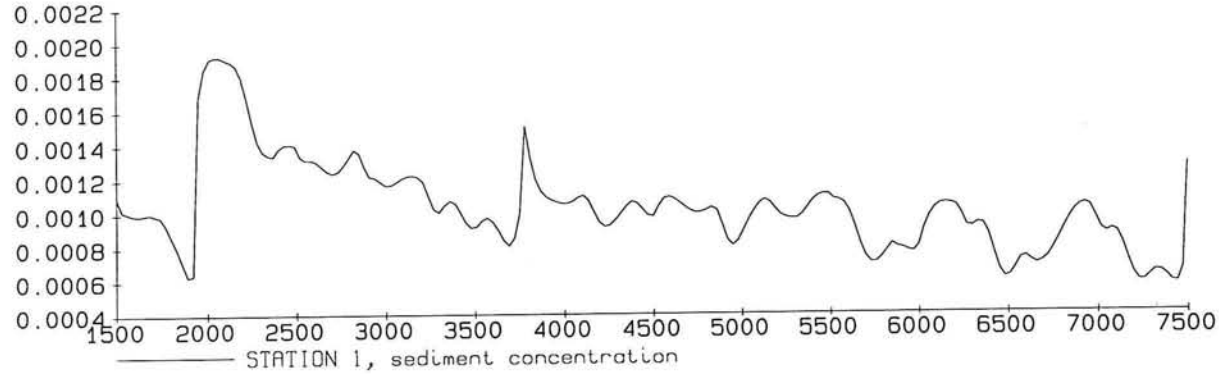


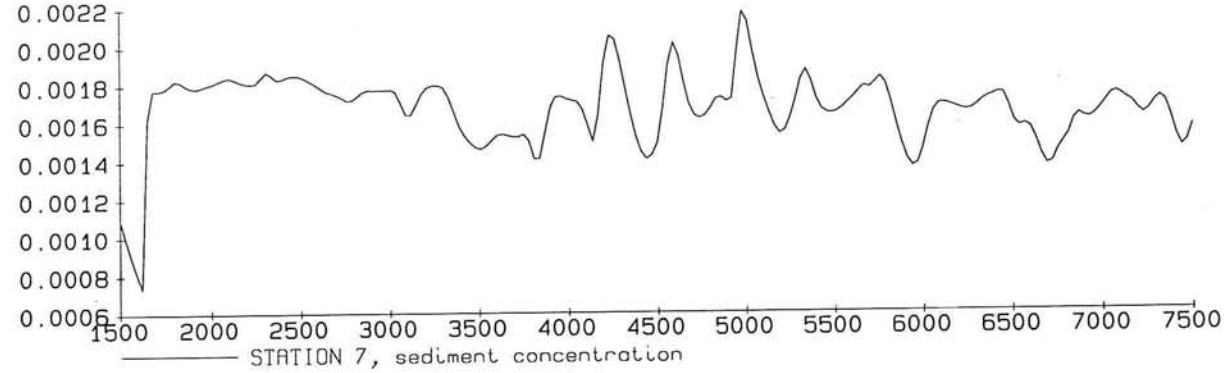


**MUD LEVELS (M) AND SEDIMENT CONCENTRATIONS (-)**
Time in minutes
Neap tide

SIMULATION 2A

STATIONS 1 AND 7

FIG. E6

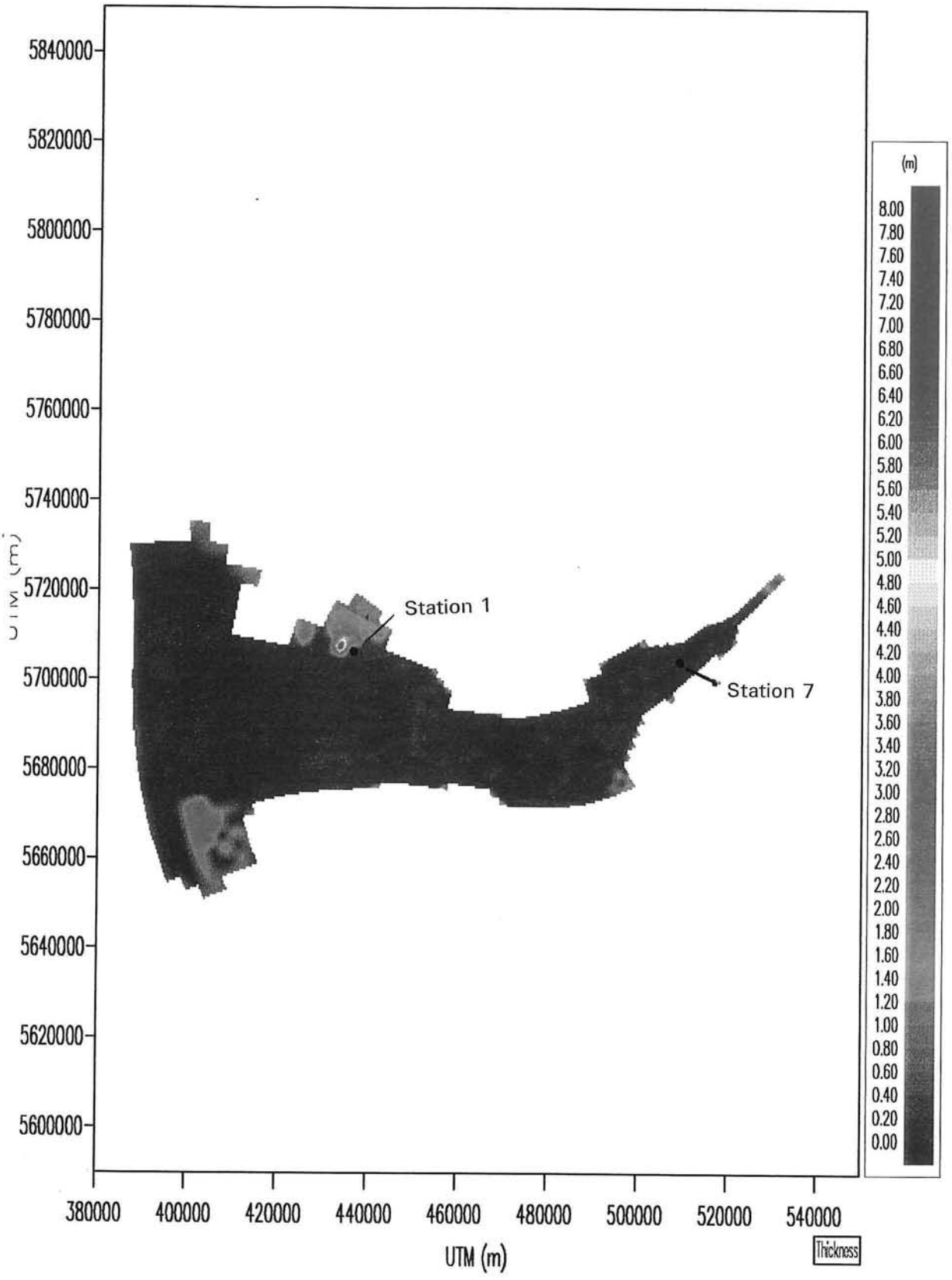


THICKNESS OF FLUID MUD LAYER
AT t = 6000 MINUTES

SIMULATION 2A

FIG. E7

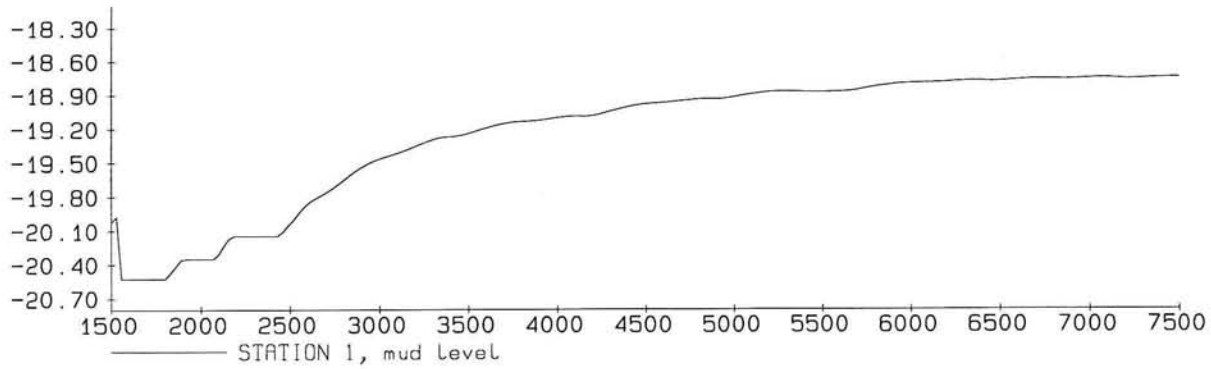


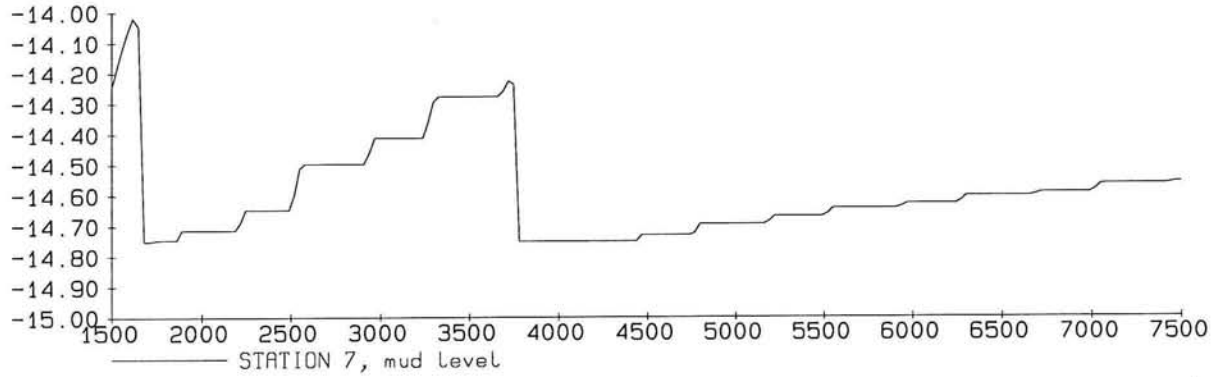


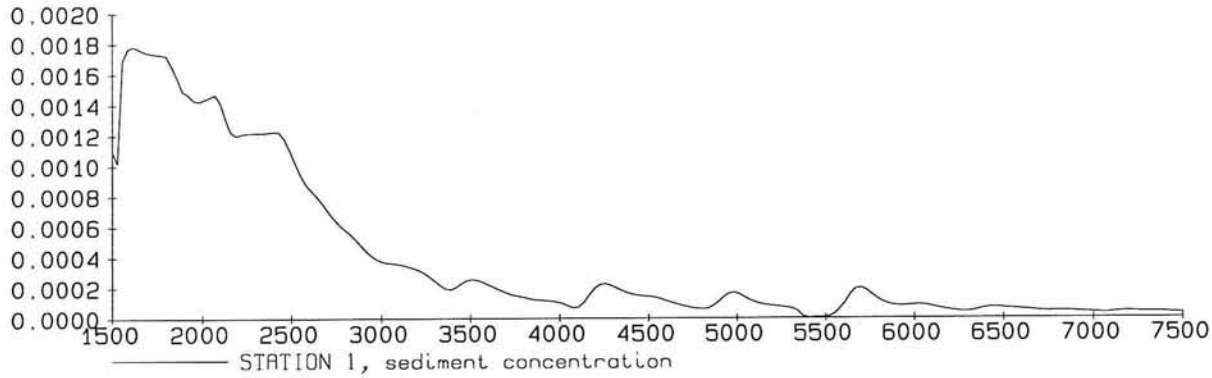


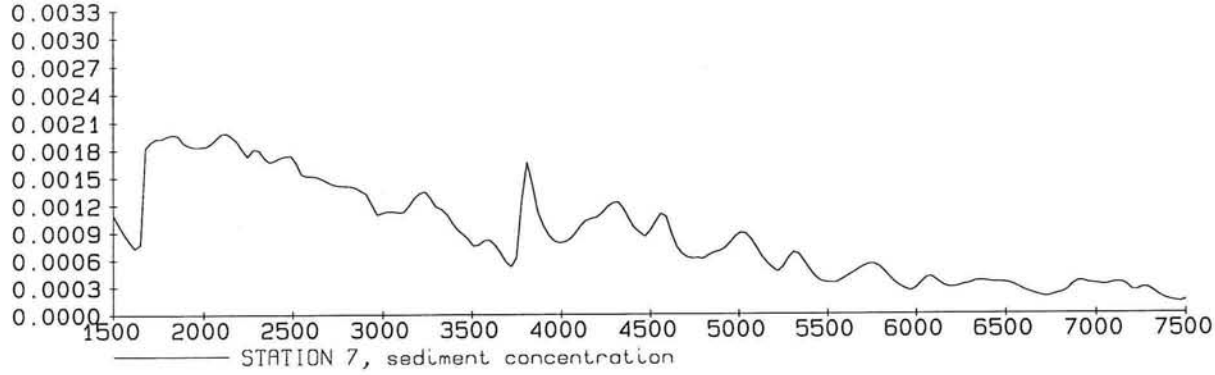


| | | |
|---|---|---|
| **MUD LEVELS (M) AND SEDIMENT CONCENTRATIONS (-)**<br>**Time in minutes**<br>**Neap tide** | | |
| | SIMULATION 2B | |
| STATIONS 1 AND 7 | | FIG. E8 |

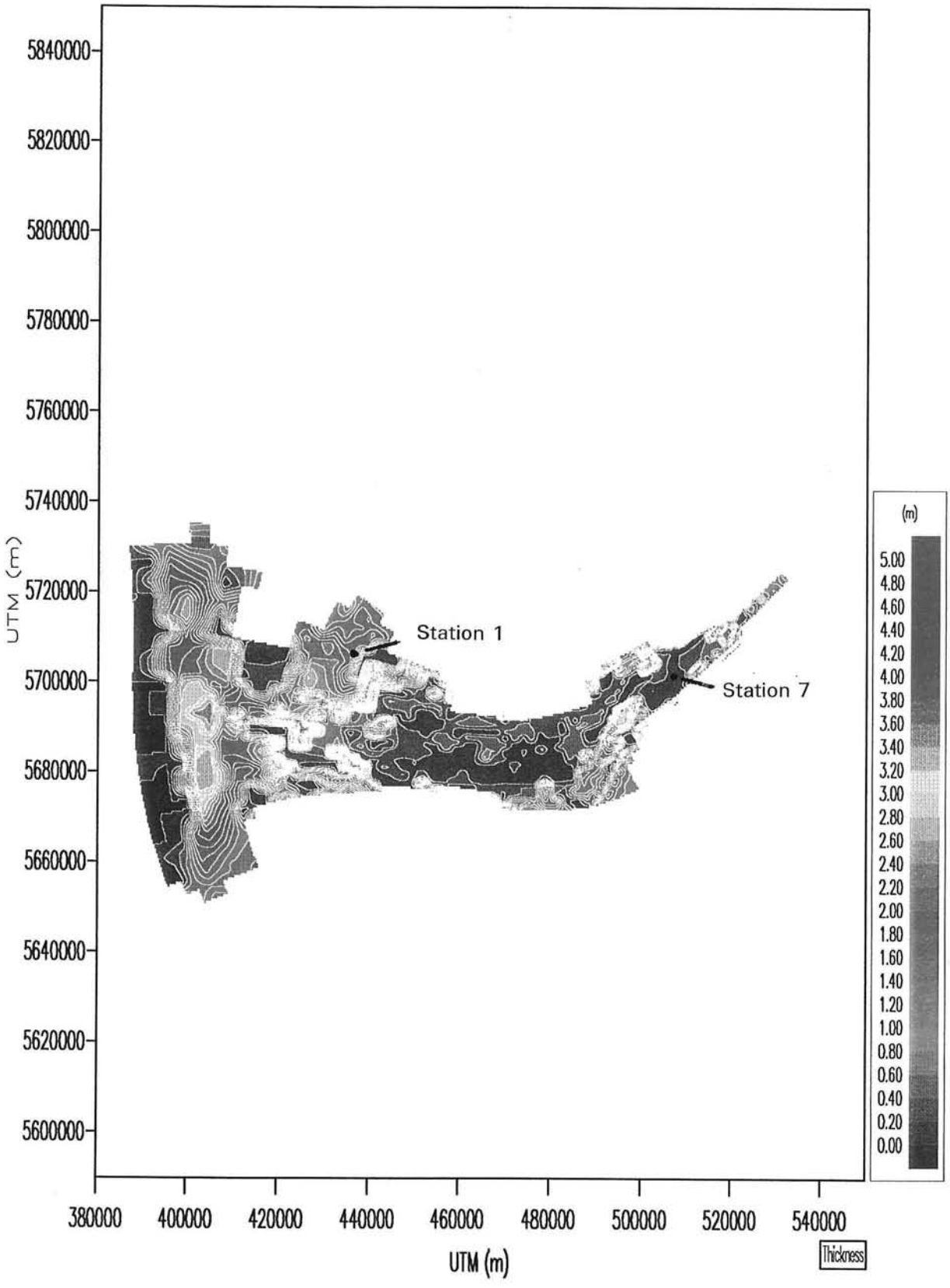


THICKNESS OF FLUID MUD LAYER
AT t = 6000 MINUTES

SIMULATION 2B

FIG. E9

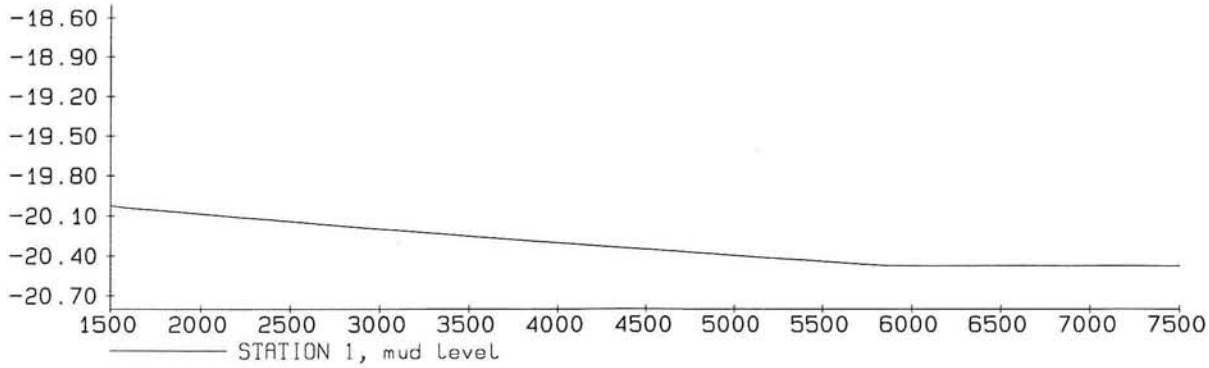


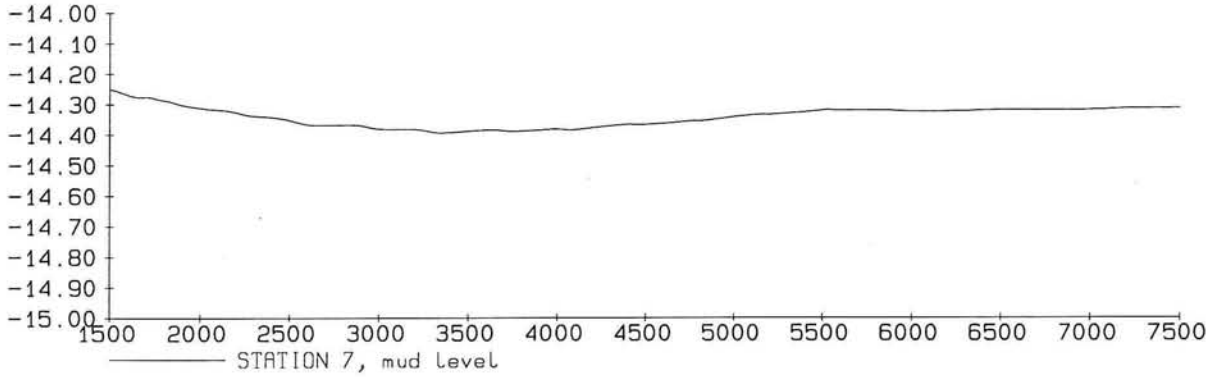


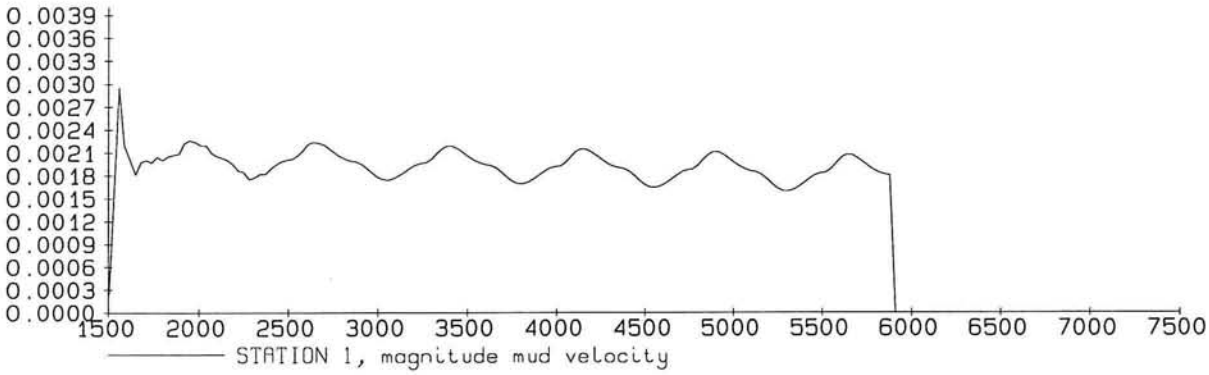


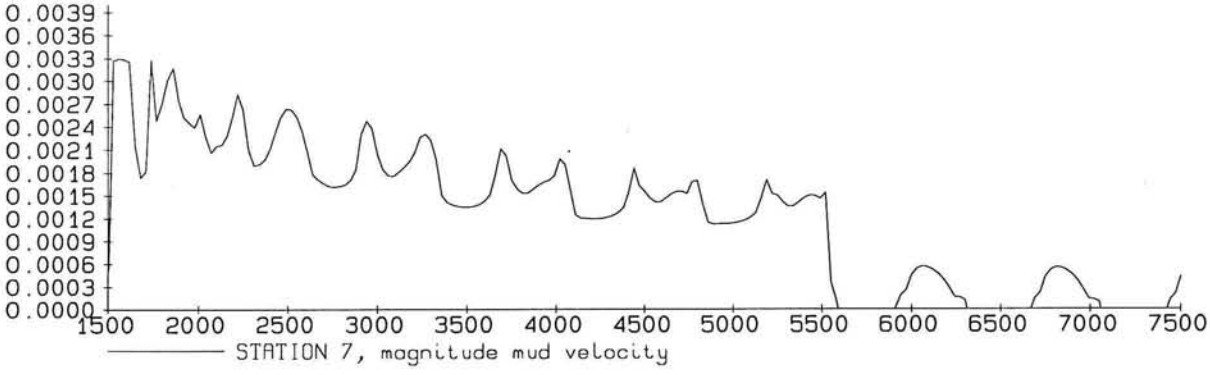


| | | |
|---|---|---|
| **MUD LEVELS (M) AND MAGNITUDE MUD VELOCITIES (M/S)**<br>**Time in minutes**<br>**Neap tide** | | |
| | SIMULATION 3 | |
| STATIONS 1 AND 7 | | FIG. E10 |

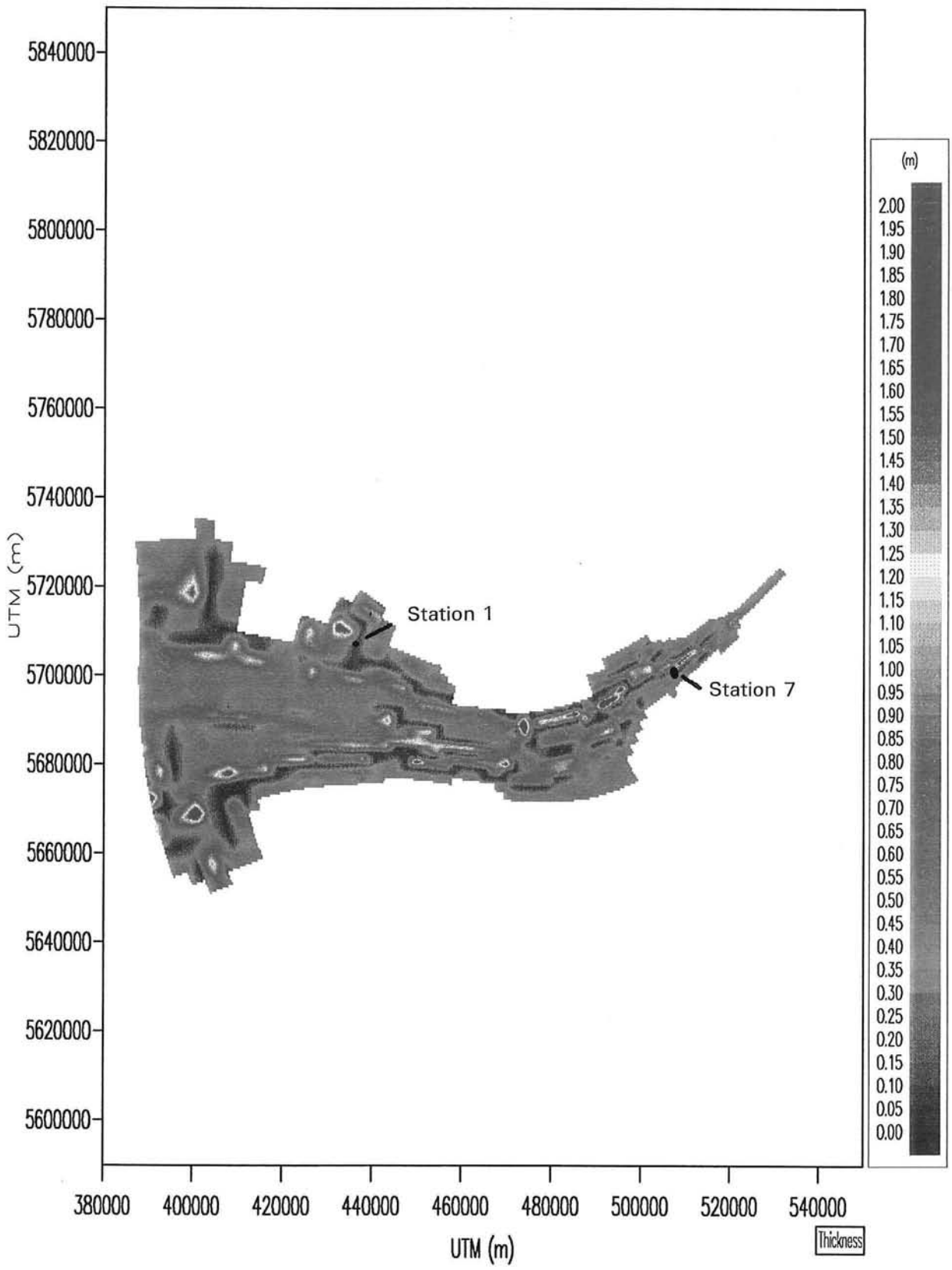


THICKNESS OF FLUID MUD LAYER
AT t = 6000 MINUTES

SIMULATION 3

FIG. E11

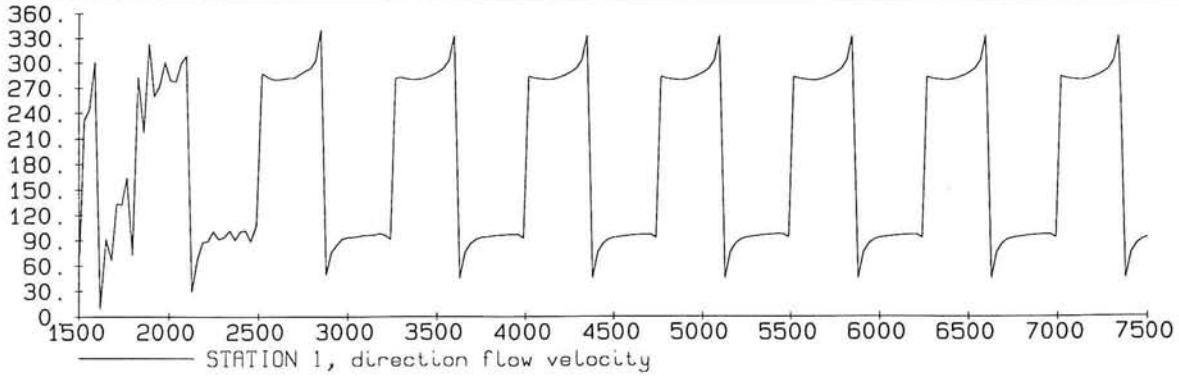


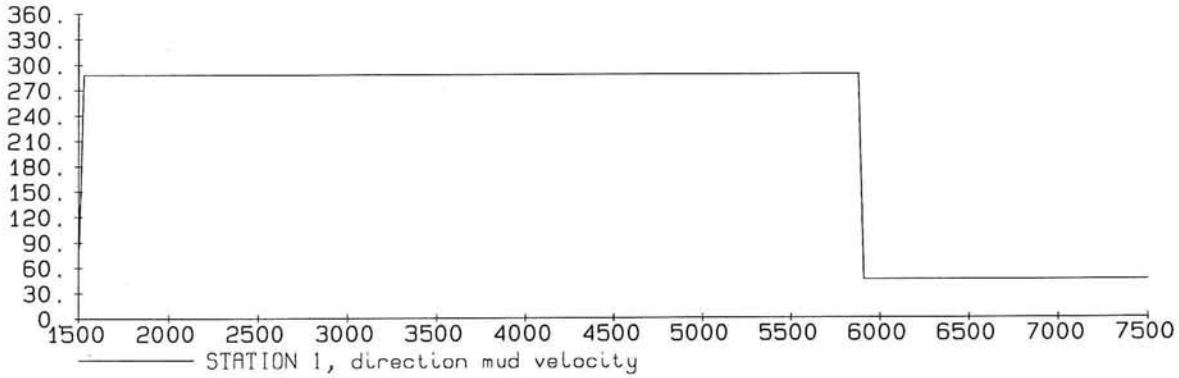


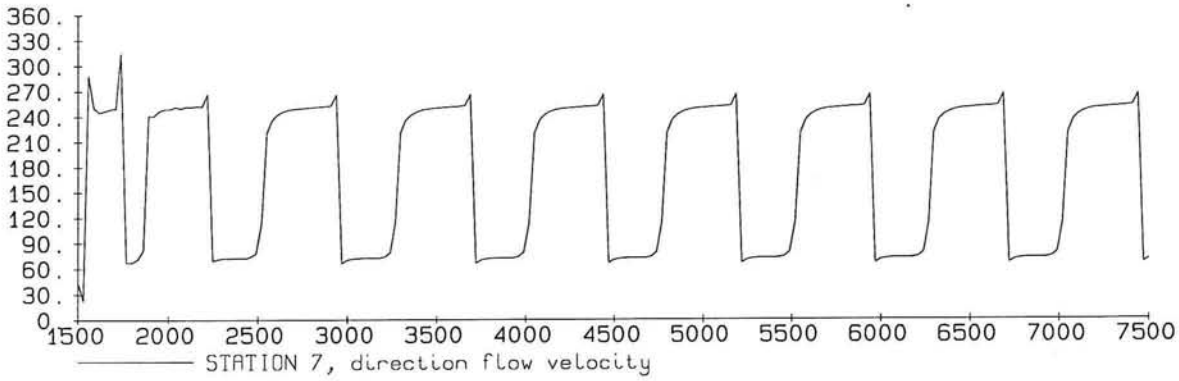


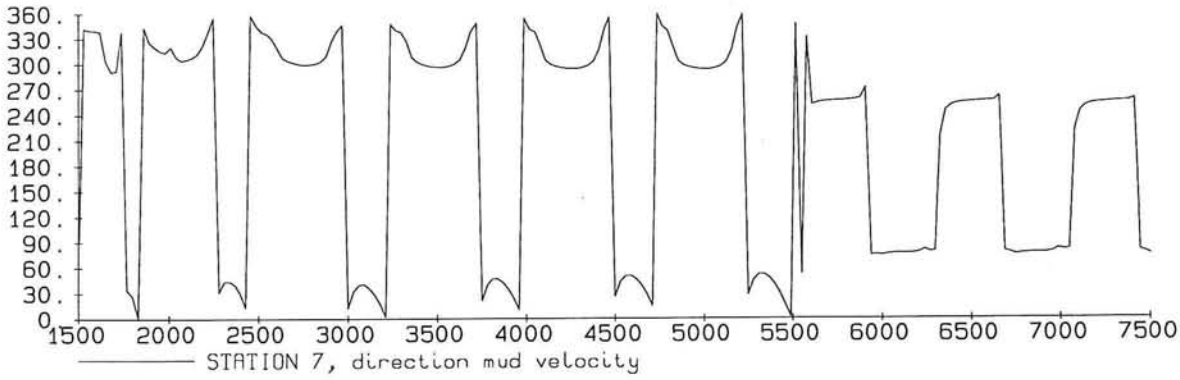


DIRECTIONS OF MUD AND FLOW LAYER (DEGREES)
Time in minutes
Neap tide

SIMULATION 3

STATIONS 1 AND 7

FIG. E12

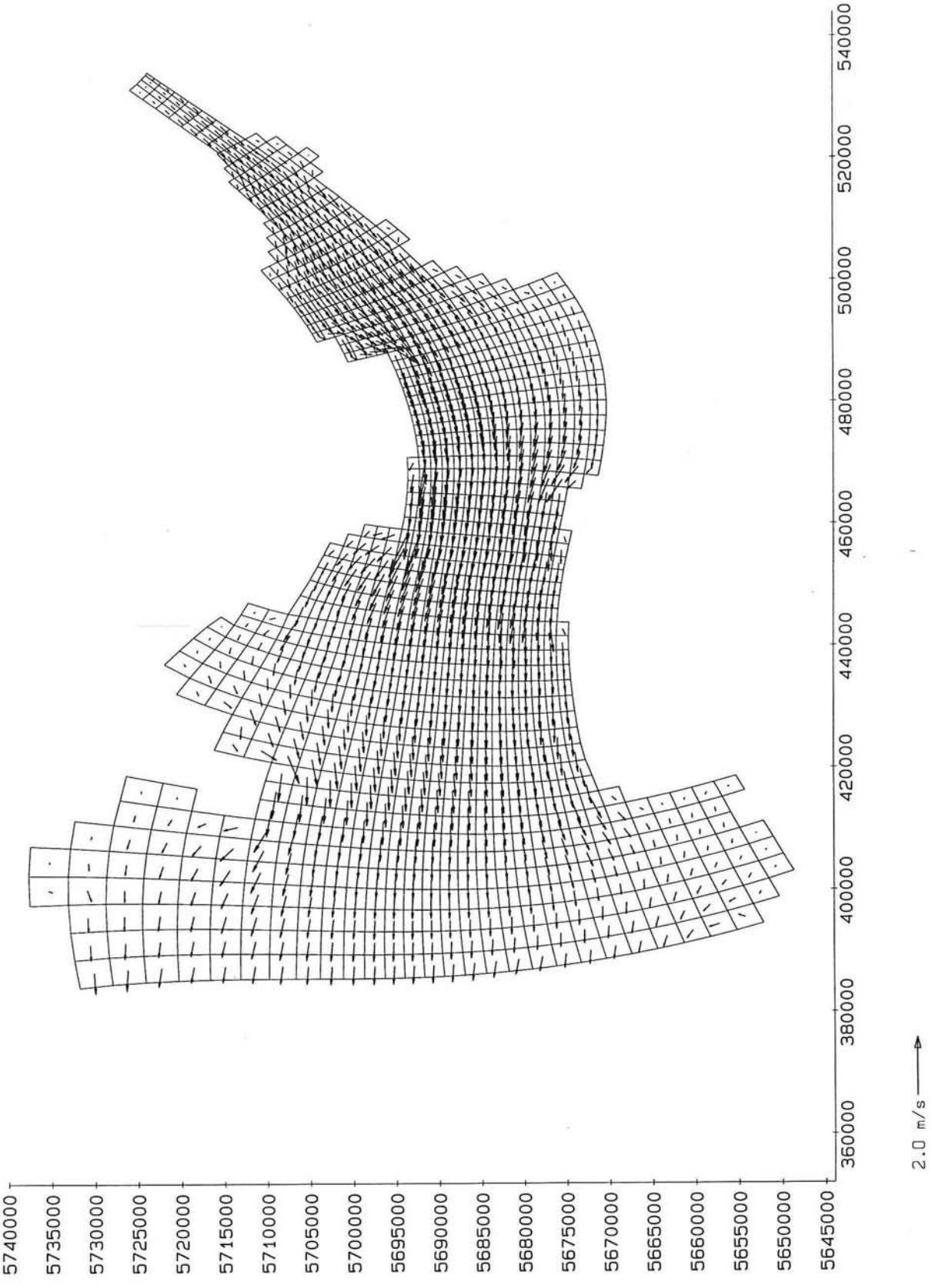


FLOW PATTERN OF SUSPENSION LAYER
At $t$ = 4125 minutes
Neap tide

SIMULATION 3

FIG. E13

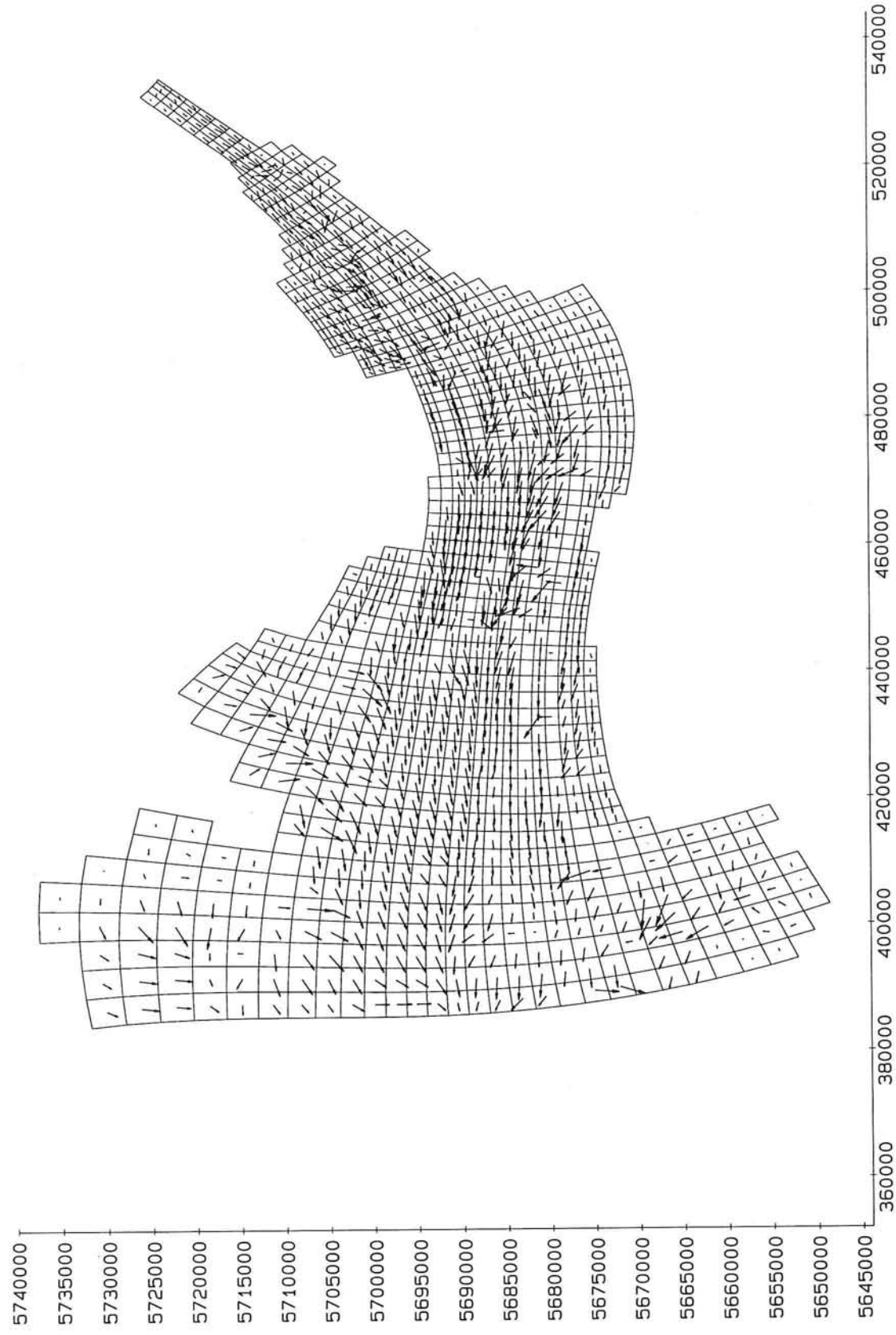


FLOW PATTERN OF FLUID MUD LAYER
At $t$ = 4125 minutes
Neap tide

SIMULATION 3

FIG. E14

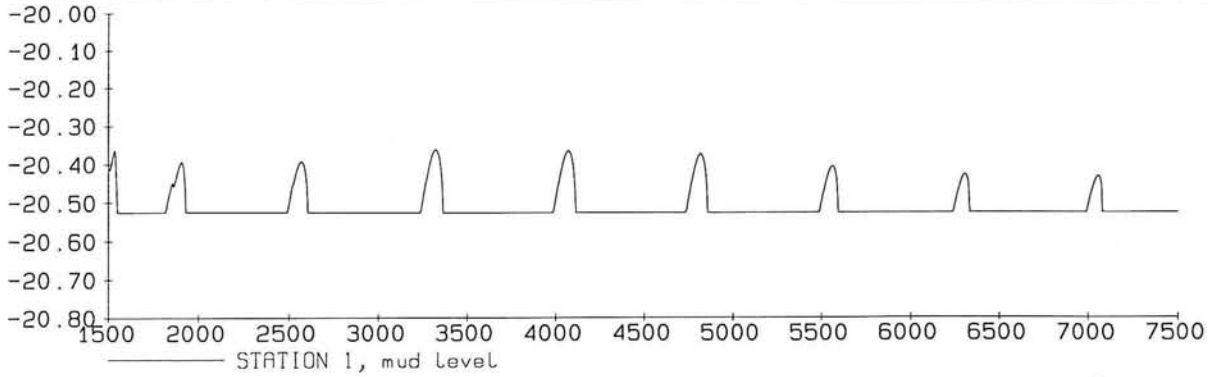


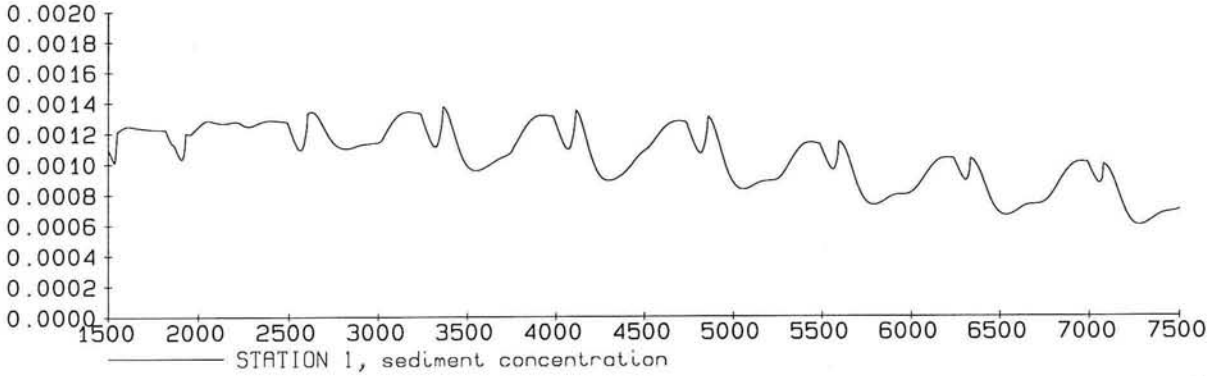


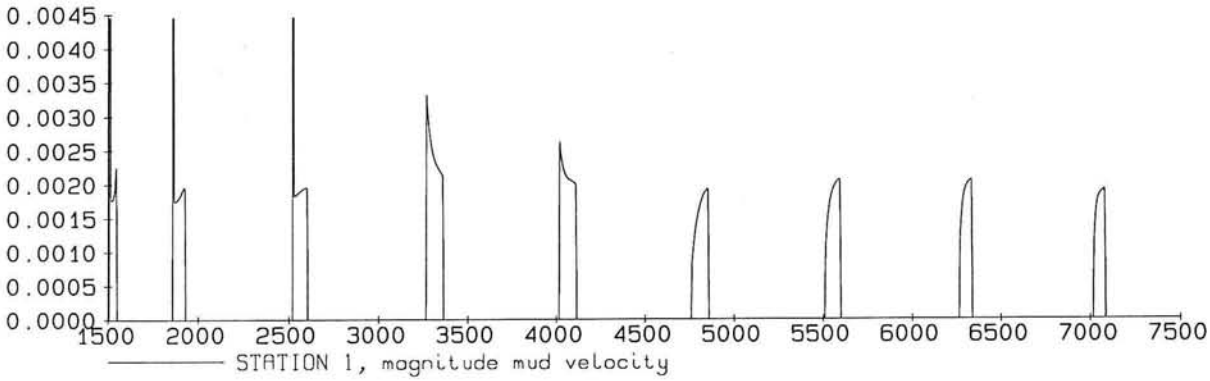


MUD LEVEL (M), SEDIMENT CONCENTRATION (-),
MAGNITUDE MUD VELOCITY (M/S)
Time in minutes, Neap tide

SIMULATION 4A

STATION 1

FIG. E15

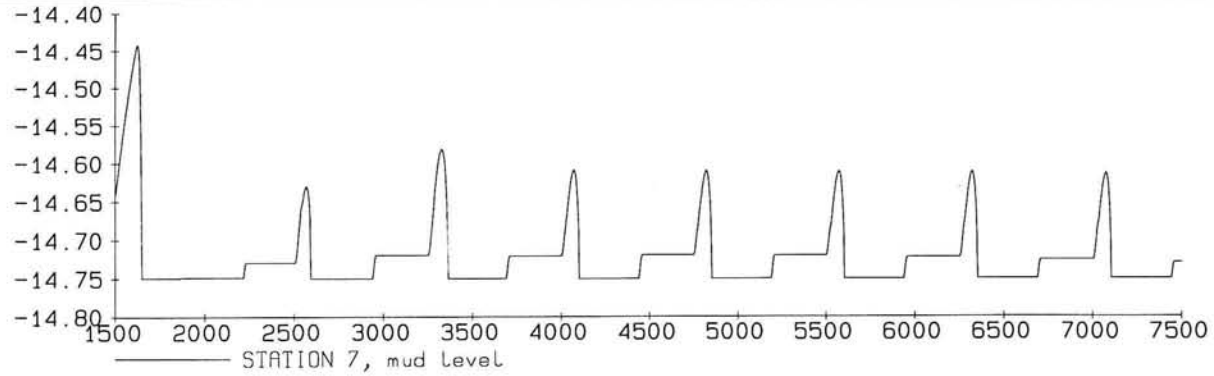


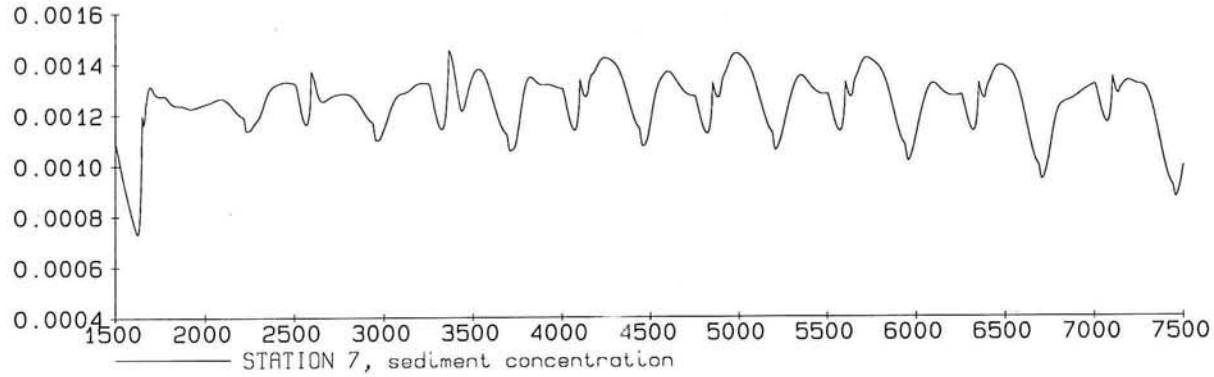


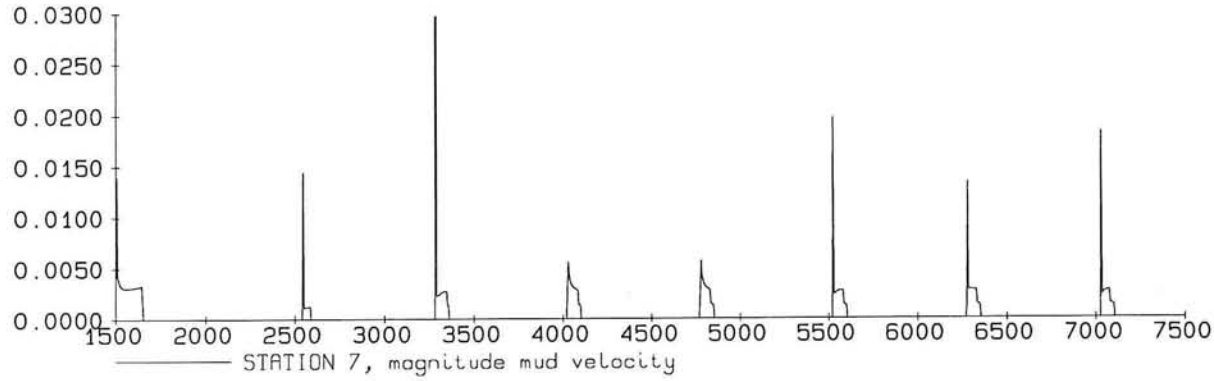


MUD LEVEL (M), SEDIMENT CONCENTRATION (-),
MAGNITUDE MUD VELOCITY (M/S)
Time in minutes, Neap tide

SIMULATION 4A

STATION 7

FIG. E16

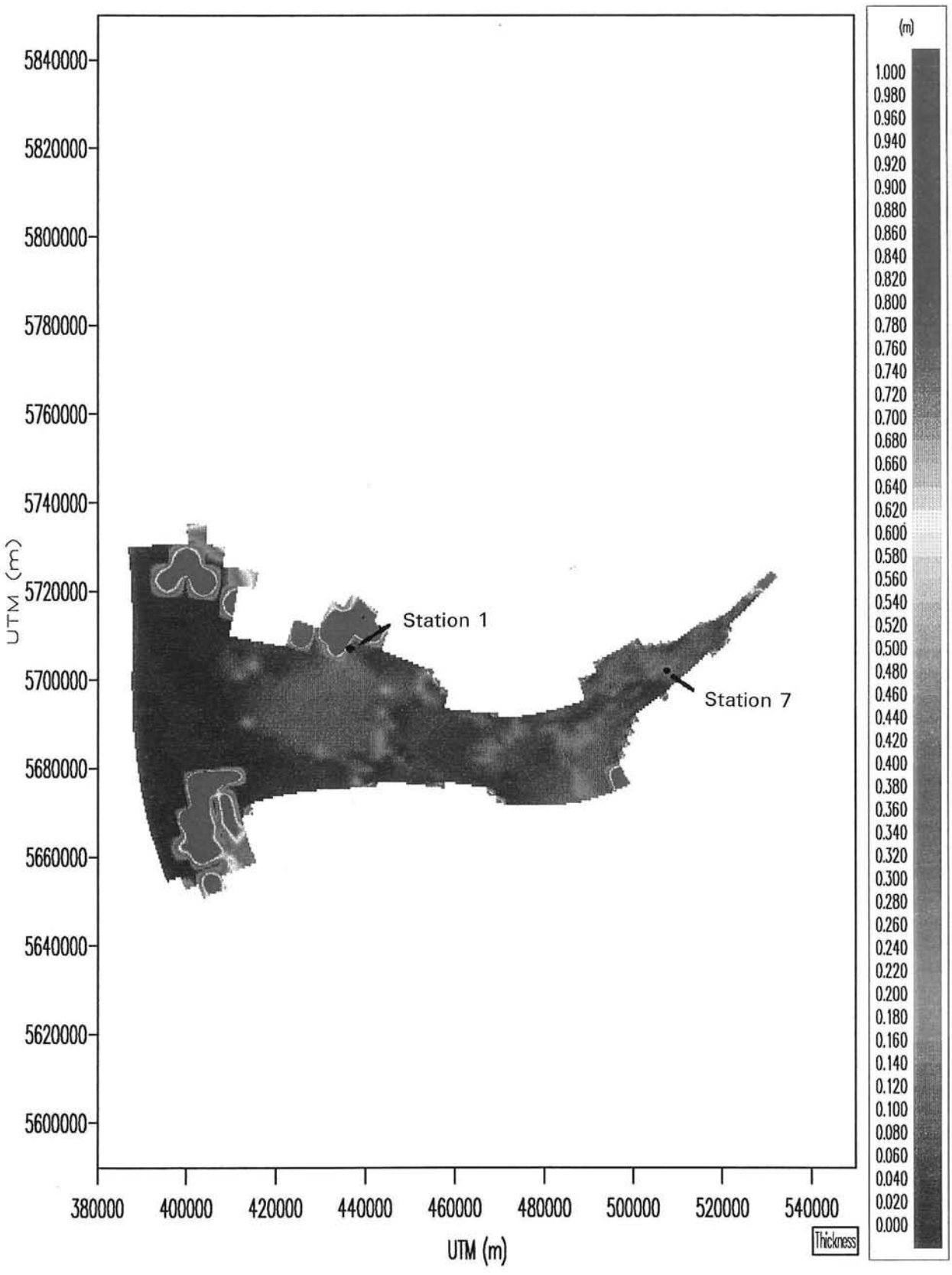


THICKNESS OF FLUID MUD LAYER
AT t = 6300 MINUTES

SIMULATION 4A

FIG. E17

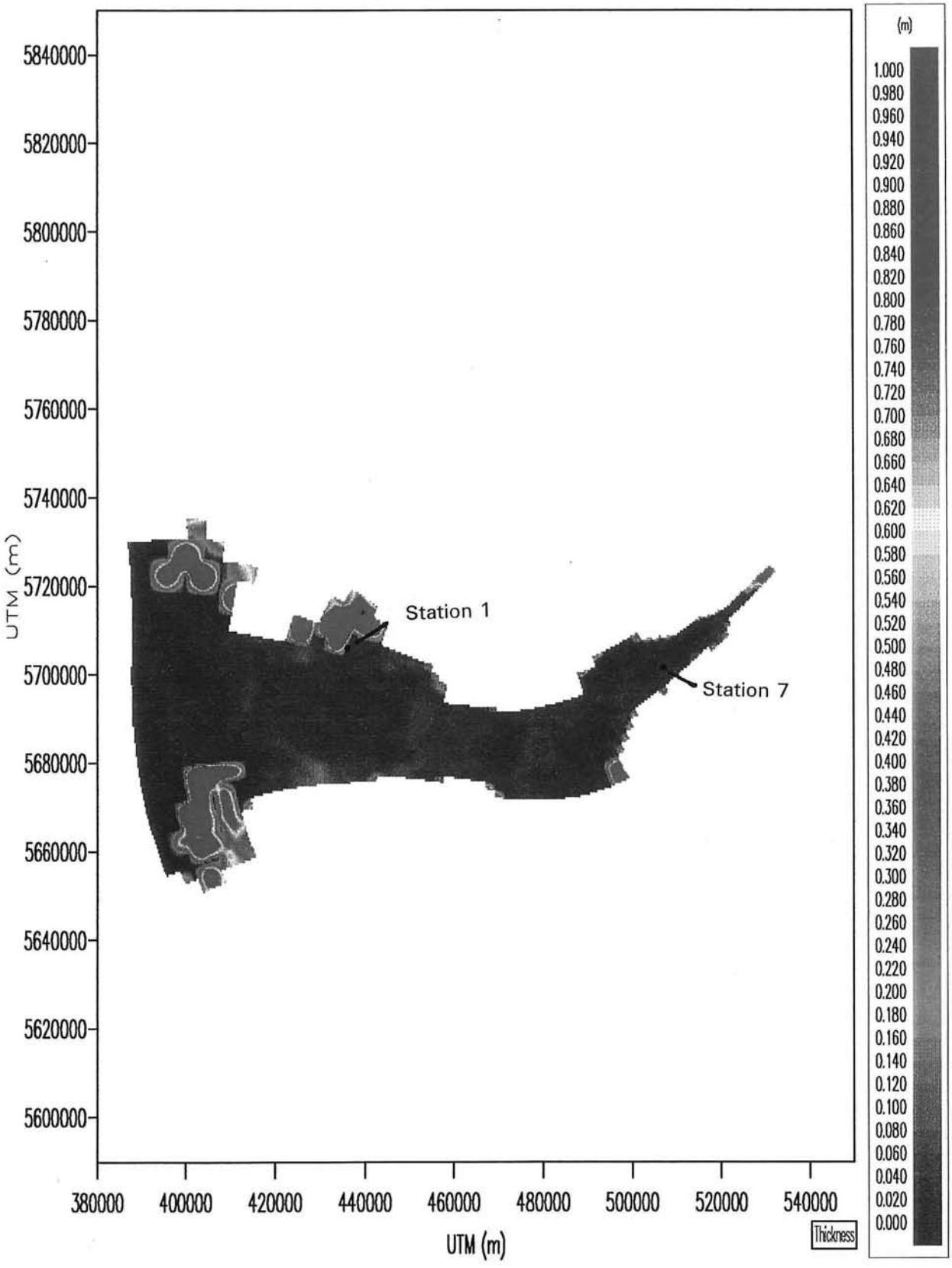


THICKNESS OF FLUID MUD LAYER
AT t = 6600 MINUTES

SIMULATION 4A

FIG. E18

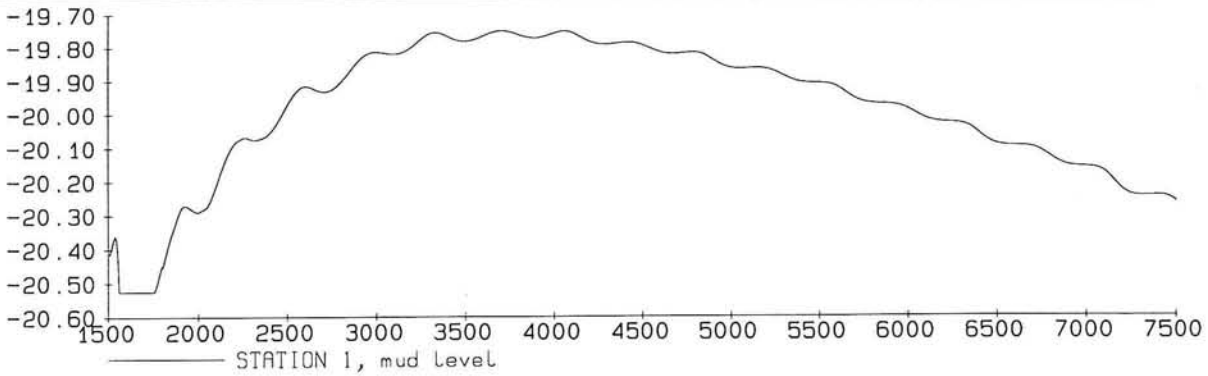


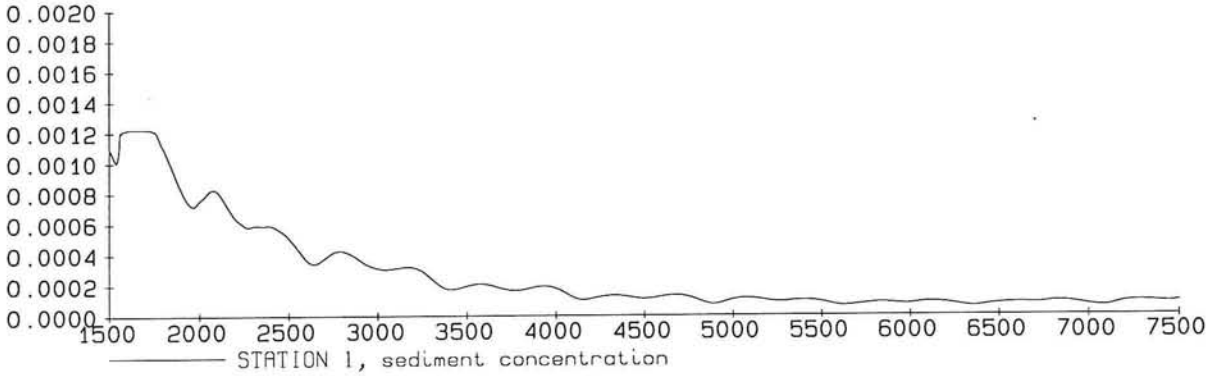


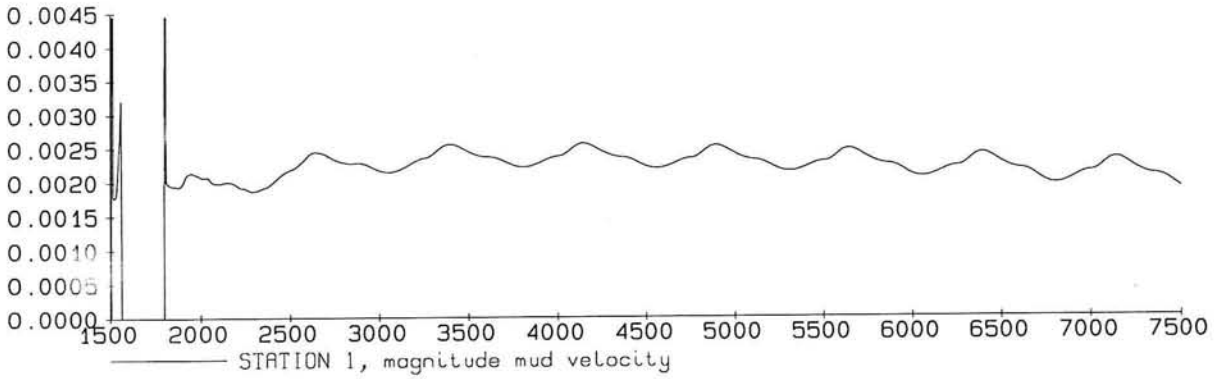


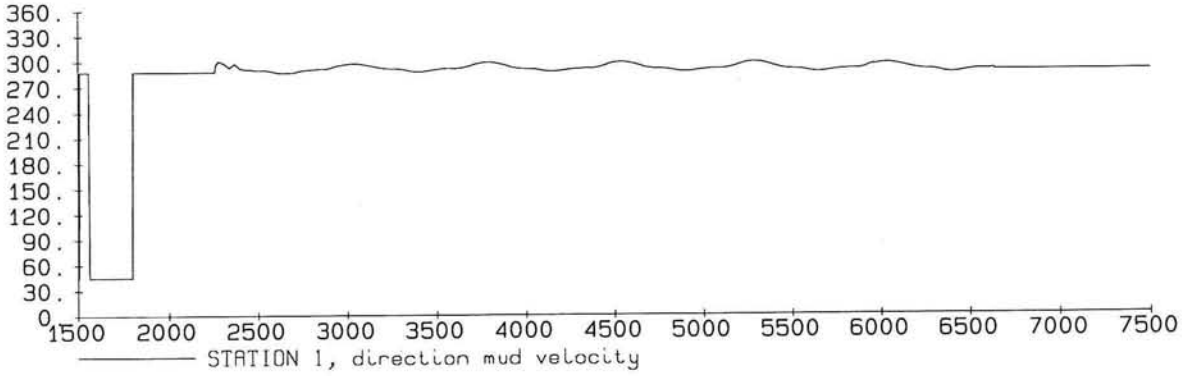


MUD LEVEL (M), SEDIMENT CONCENTRATION (-),
MAGNITUDE (M/S) AND DIRECTION (DEGREES) MUD VELOCITY
Time in minutes, Neap tide

SIMULATION 4B

STATION 1

FIG. E19

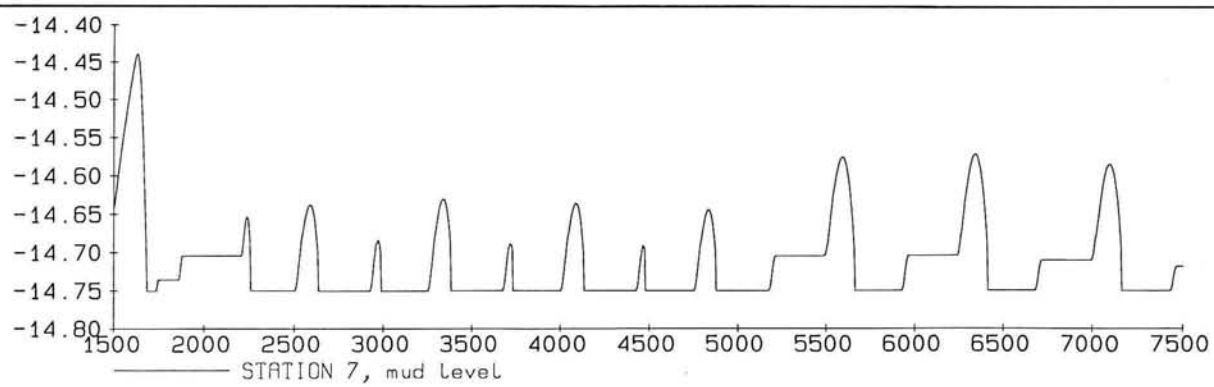


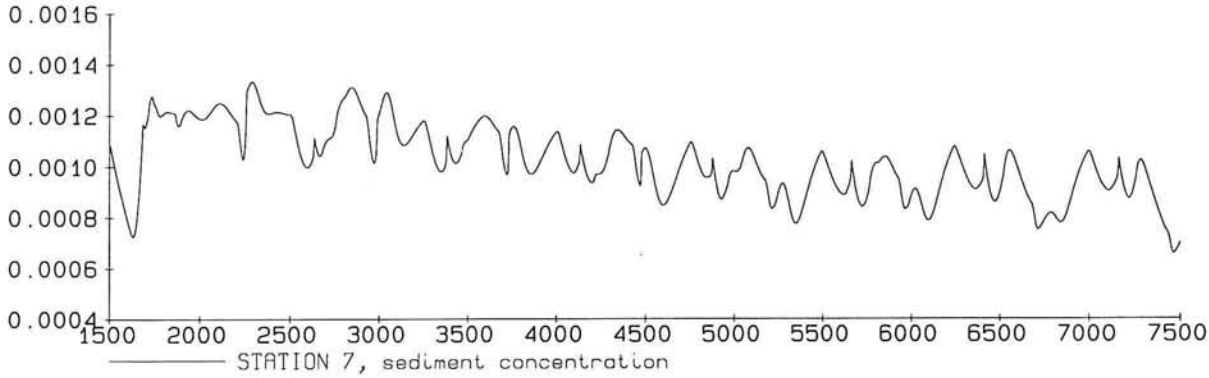


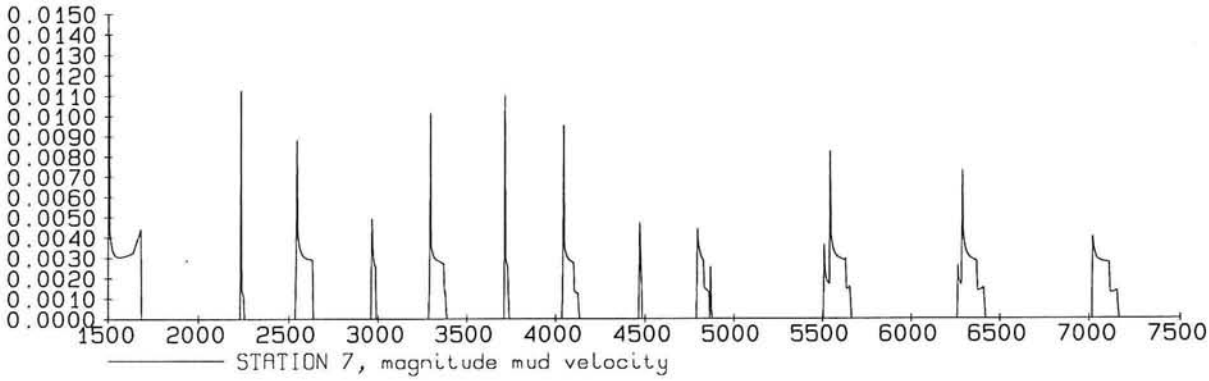


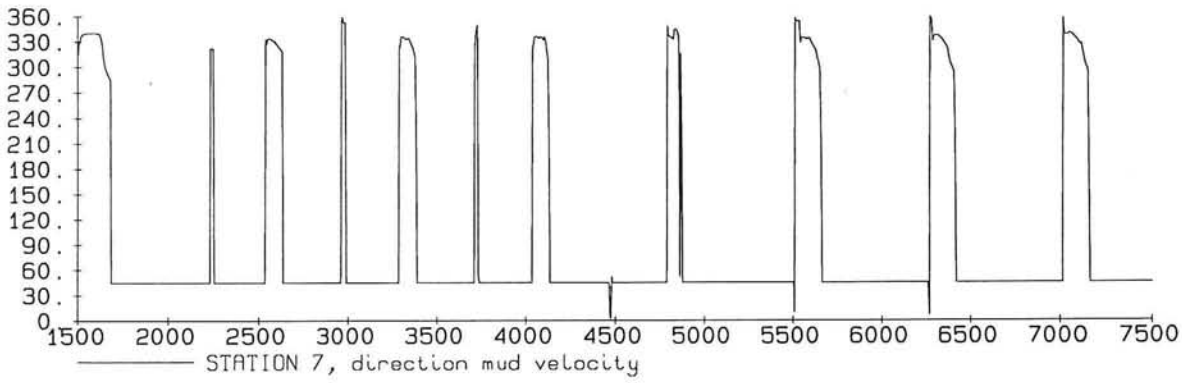


| | | |
|---|---|---|
| MUD LEVEL (M), SEDIMENT CONCENTRATION (-), MAGNITUDE (M/S) AND DIRECTION (DEGREES) MUD VELOCITY<br>Time in minutes, Neap tide | | |
| | SIMULATION 4B | |
| STATION 7 | | FIG. E20 |

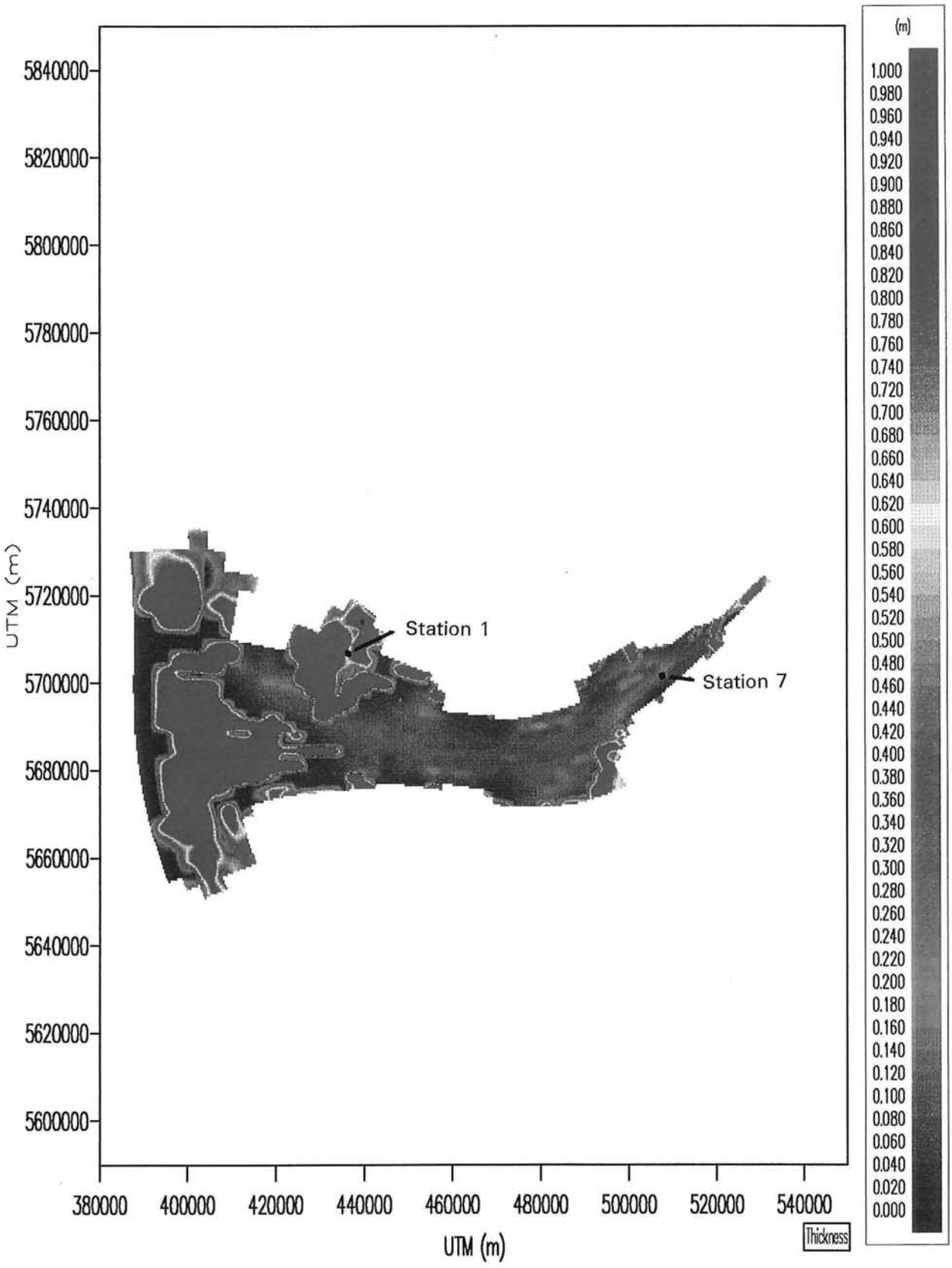


THICKNESS OF FLUID MUD LAYER
AT t = 6300 MINUTES

SIMULATION 4B

FIG. E21

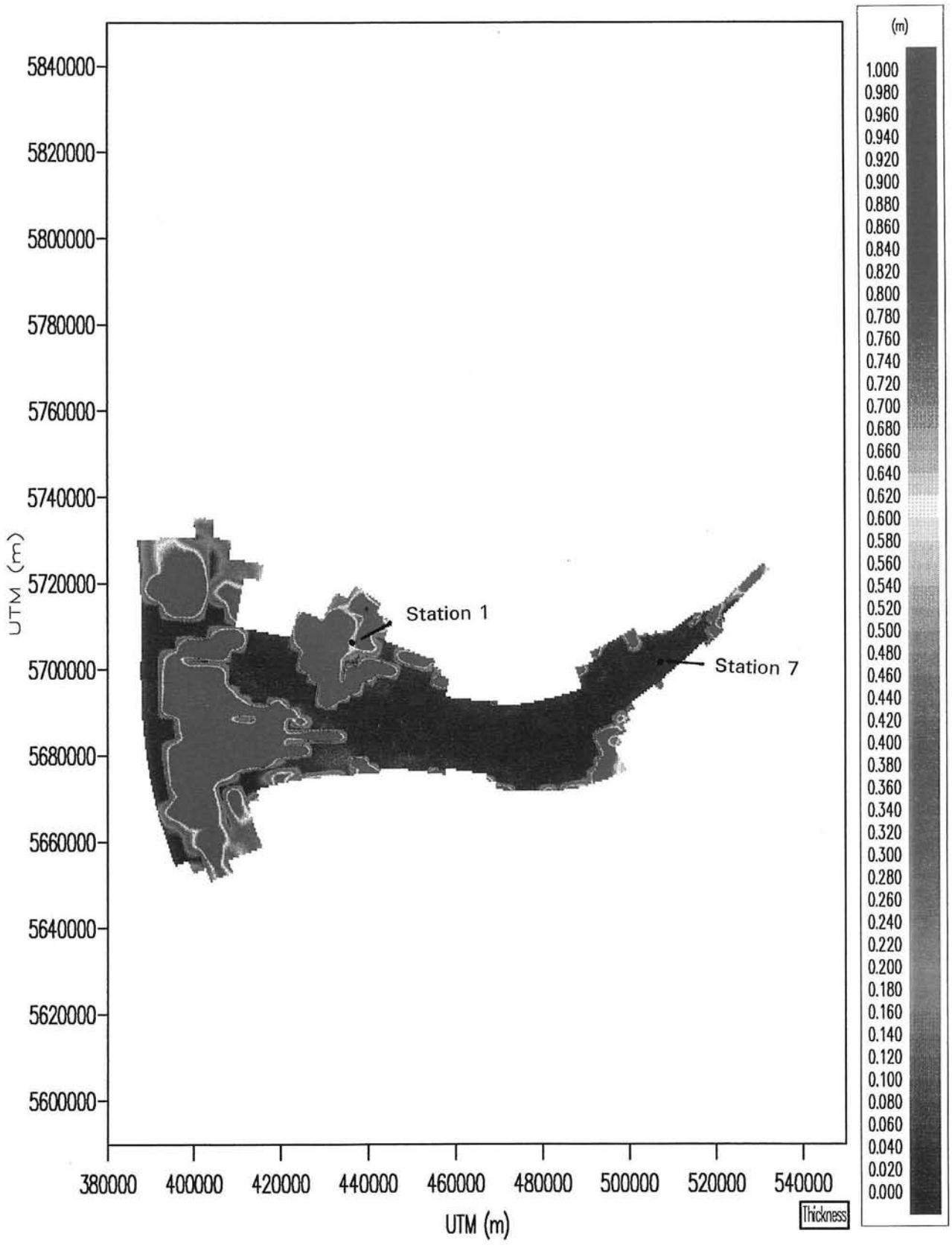


THICKNESS OF FLUID MUD LAYER
AT t = 6600 MINUTES

SIMULATION 4B

FIG. E22

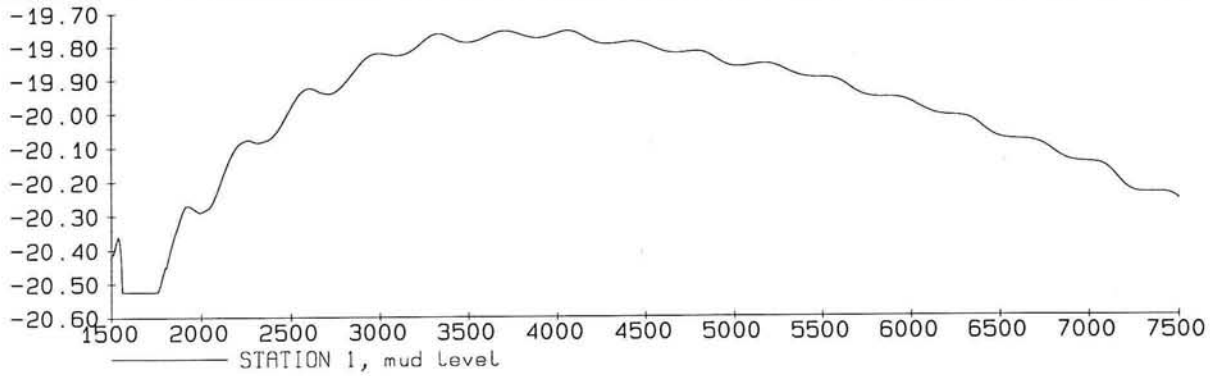


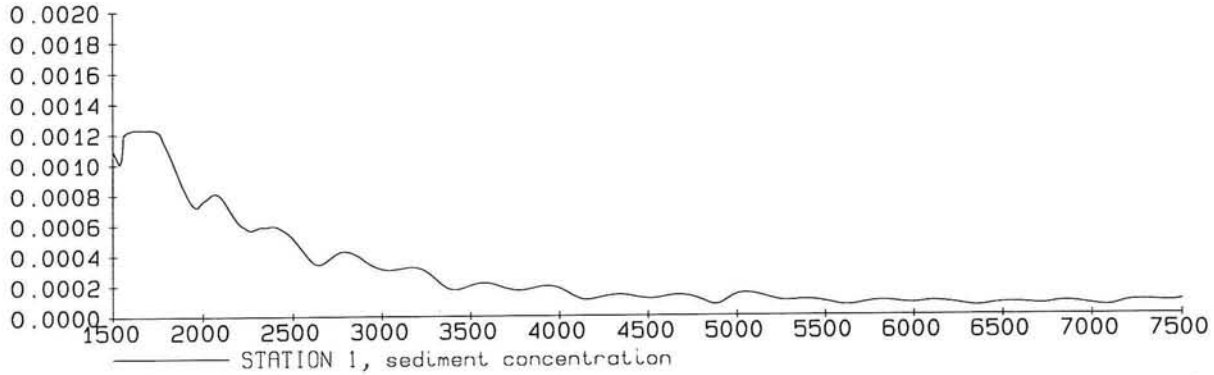


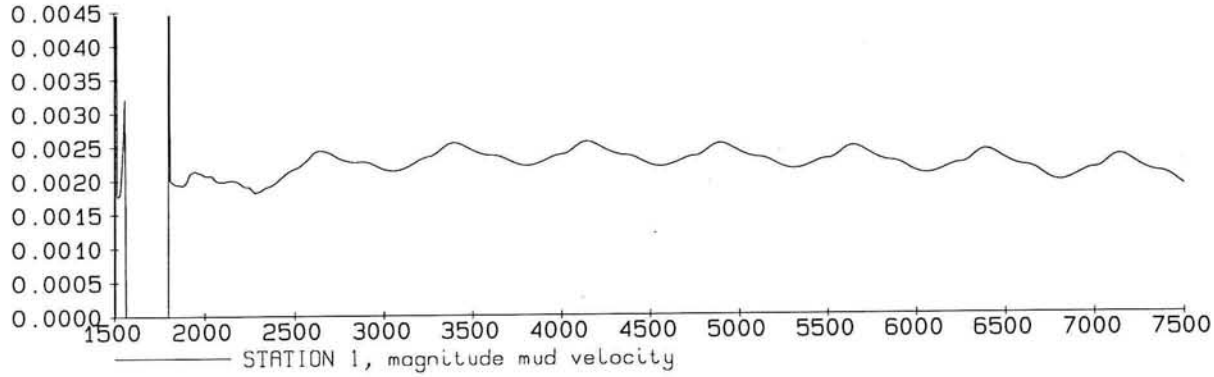


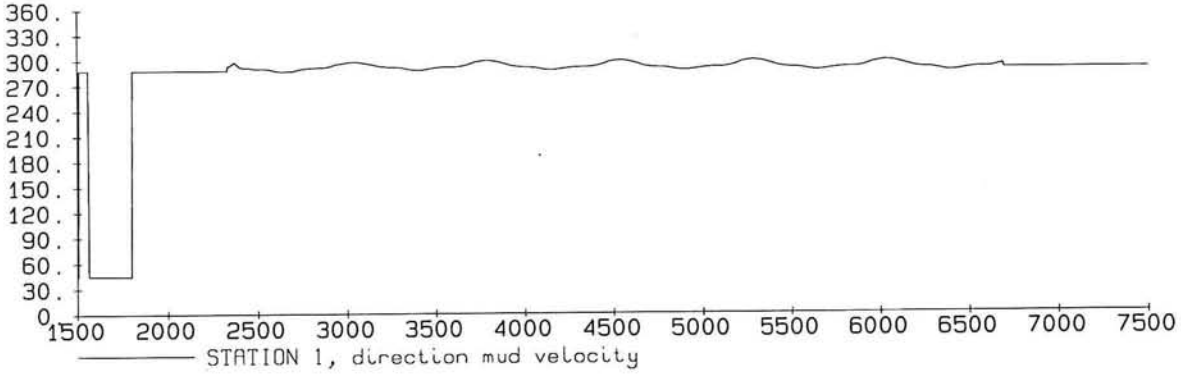


MUD LEVEL (M), SEDIMENT CONCENTRATION (-),
MAGNITUDE (M/S) AND DIRECTION (DEGREES) MUD VELOCITY
Time in minutes, Neap tide

SIMULATION 5

STATION 1

FIG. E23

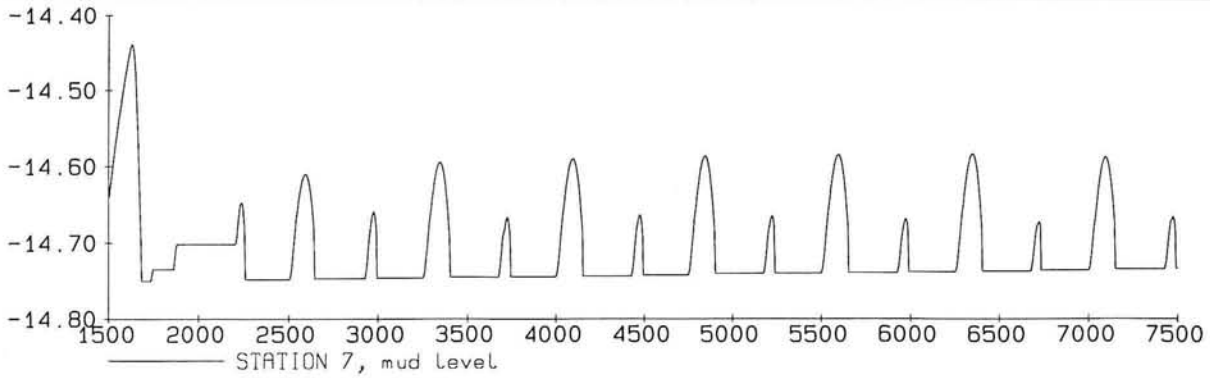


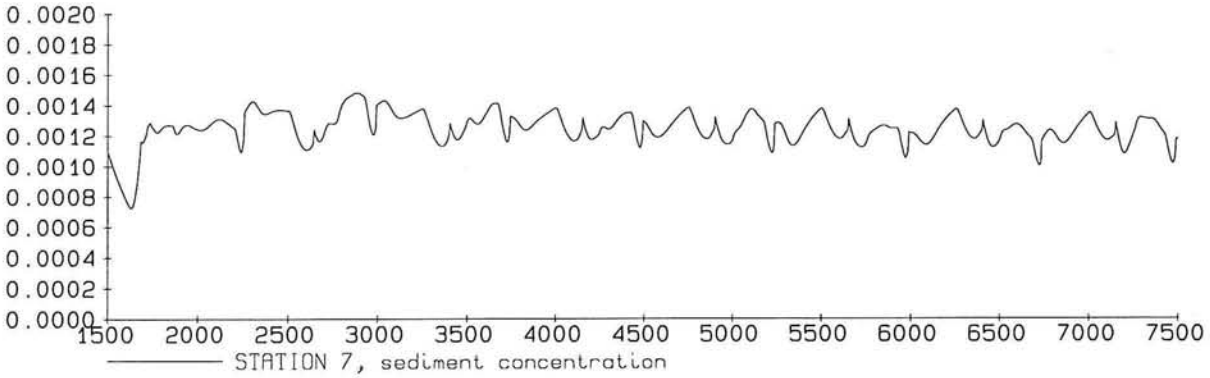


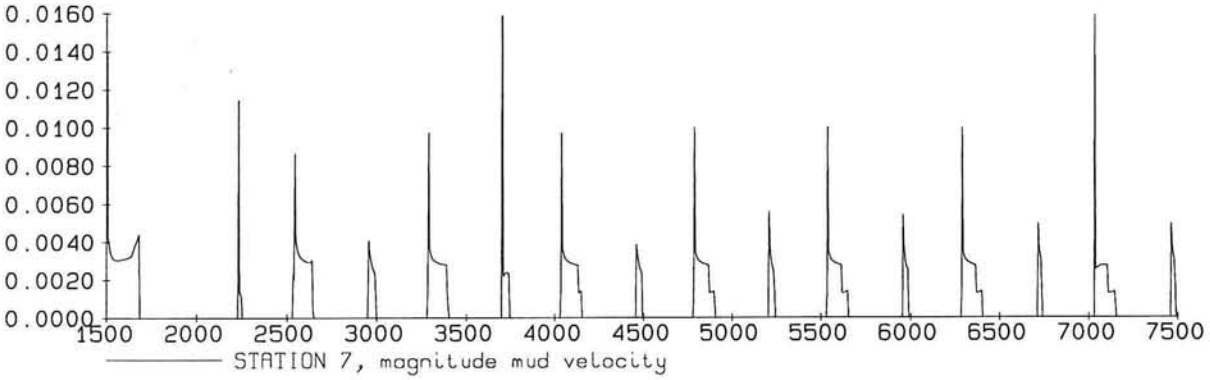


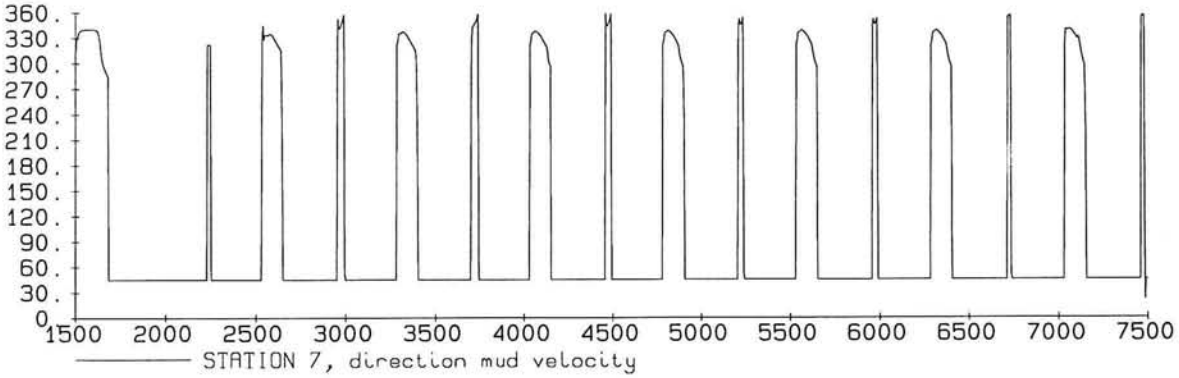


MUD LEVEL (M), SEDIMENT CONCENTRATION (-),
MAGNITUDE (M/S) AND DIRECTION (DEGREES) MUD VELOCITY
Time in minutes, Neap tide

SIMULATION 5

STATION 7

FIG. E24

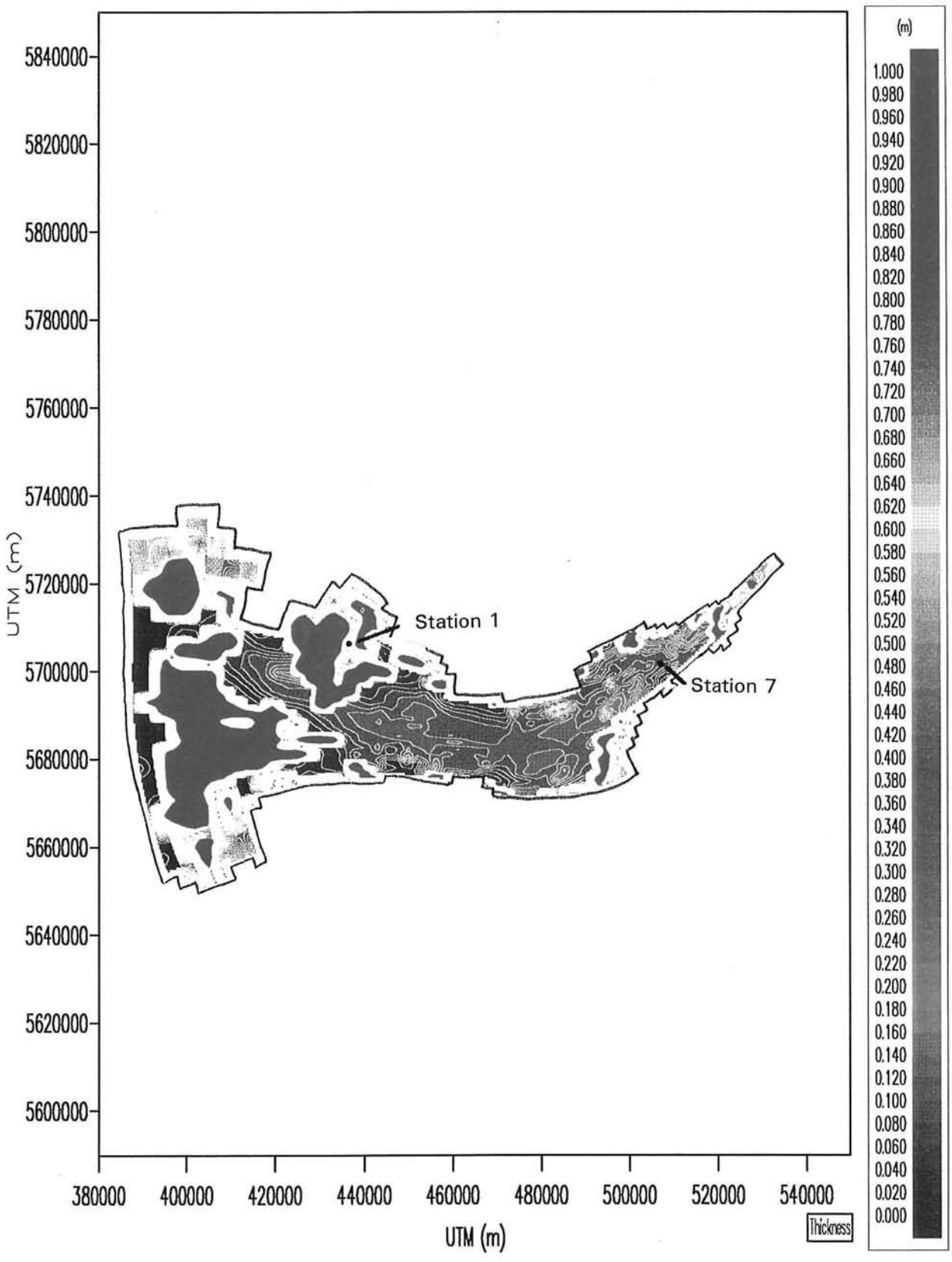


THICKNESS OF FLUID MUD LAYER
AT t = 6300 MINUTES

SIMULATION 5

FIG. E25

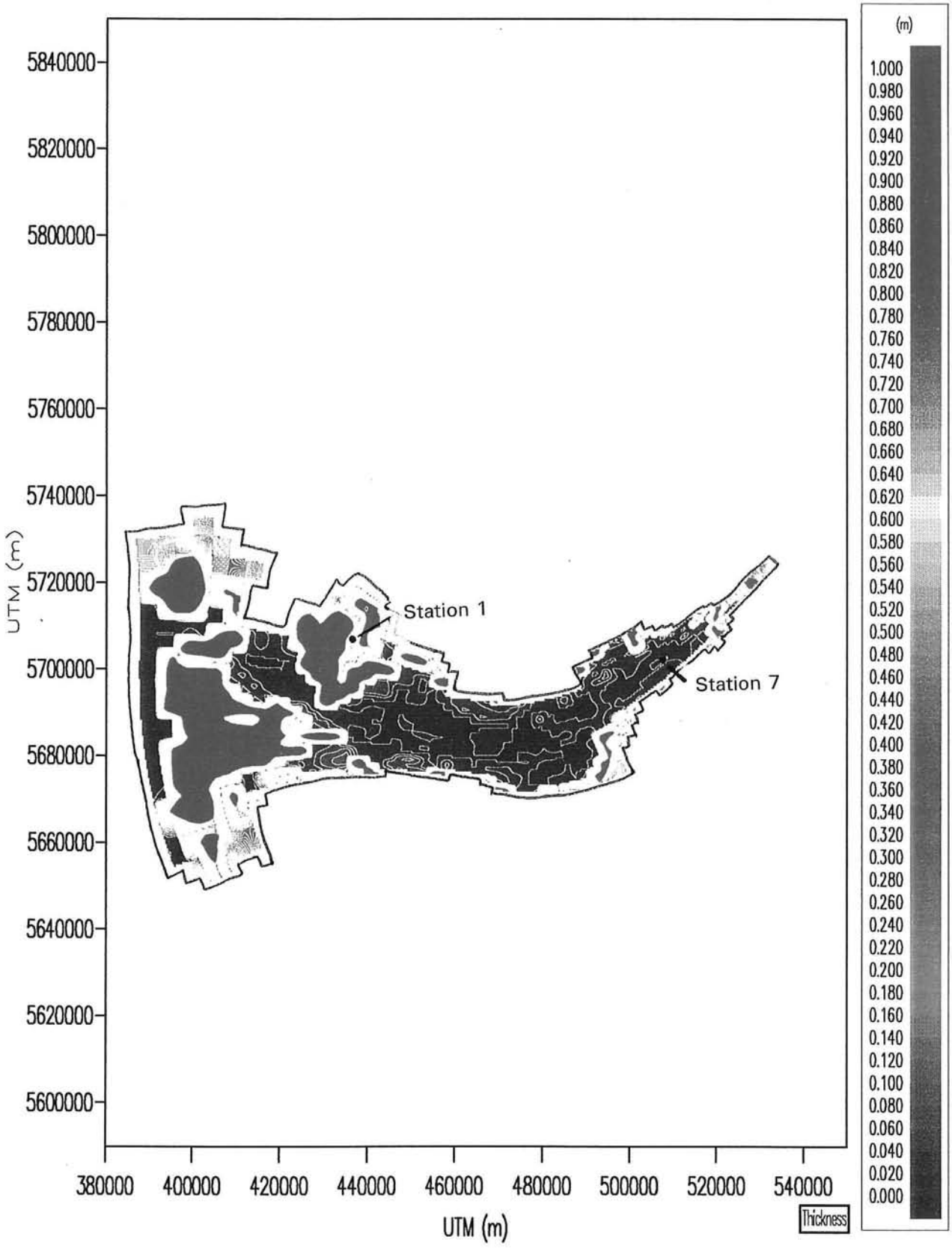


THICKNESS OF FLUID MUD LAYER
AT t = 6600 MINUTES

SIMULATION 5

FIG. E26

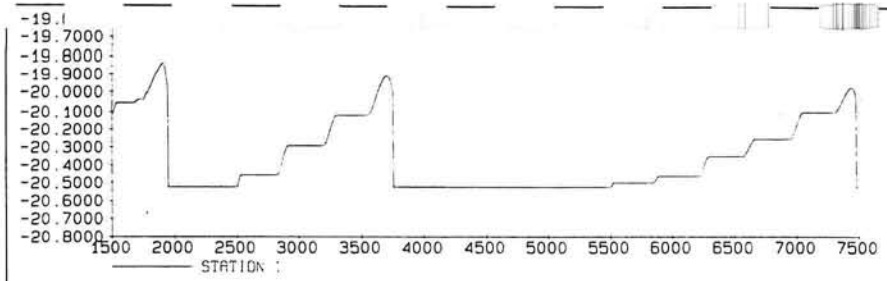


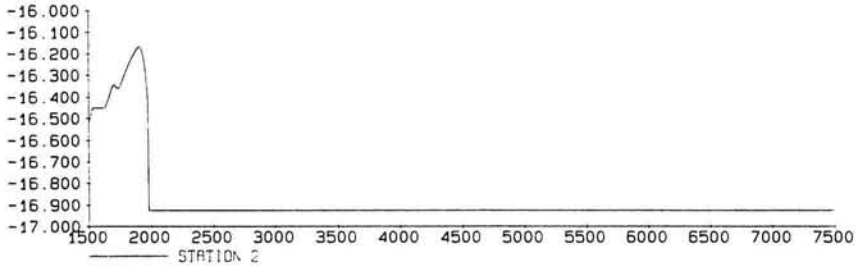


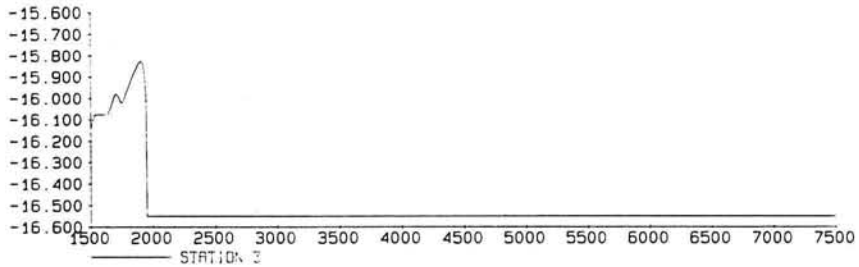


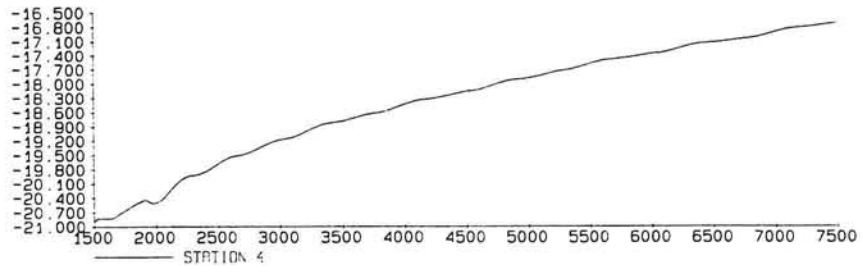


MUD LEVELS (M)
Time in minutes Neap tide

SIMULATION 2B

STATIONS IN SWANSEA BAY

FIG. E27

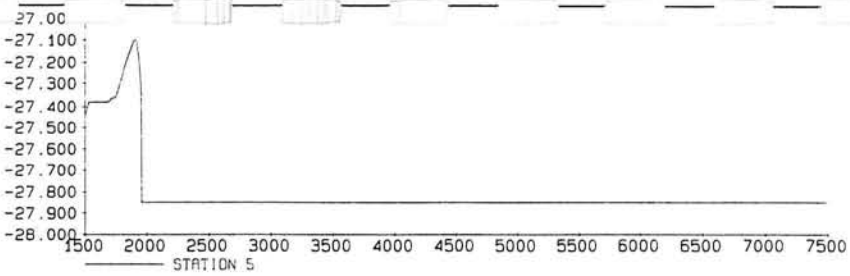


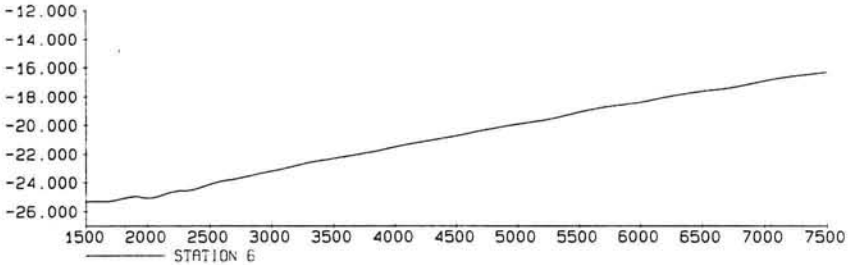


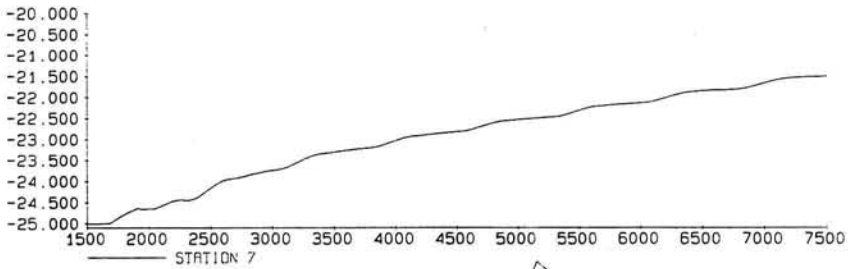


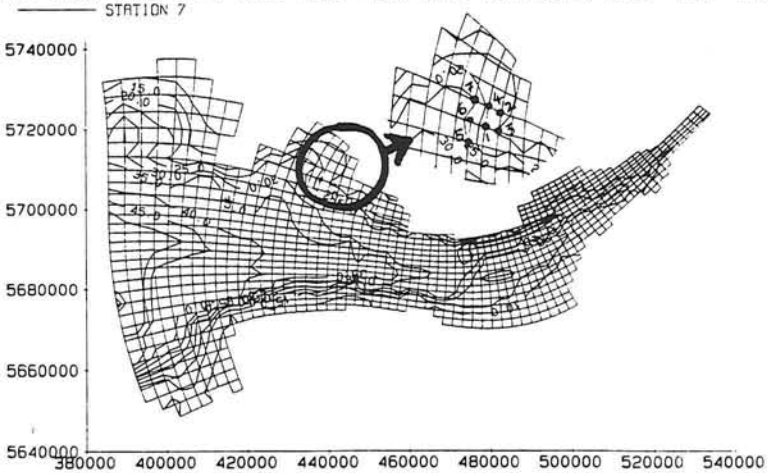


FIG. E27

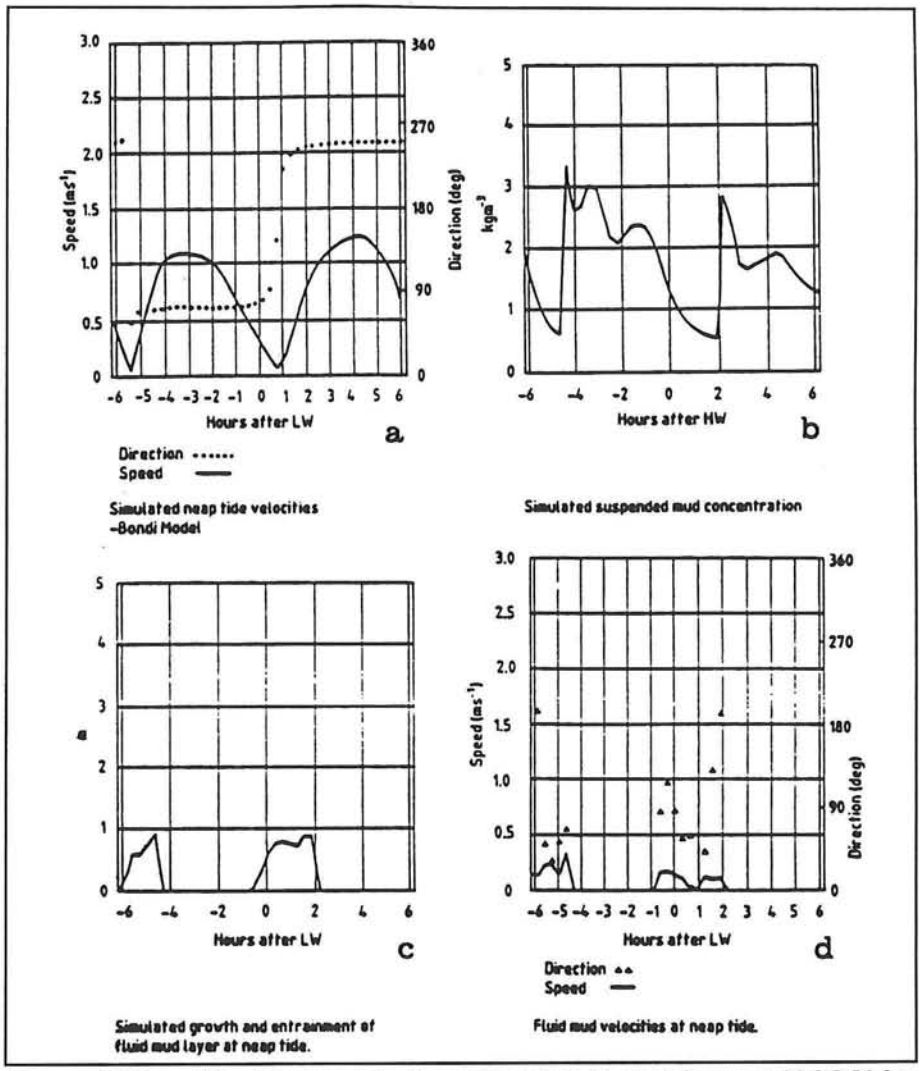


Figure E28a: Model simulated results of Odd and Cooper (1989) for station 7 at neap tide

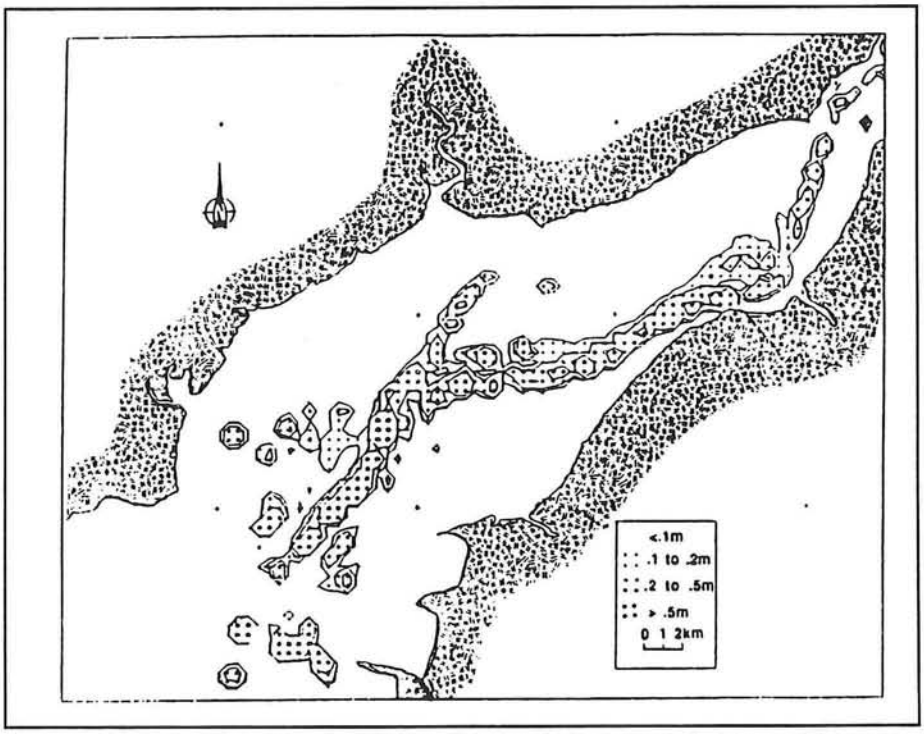


Figure E28b: Simulated distribution and depth of fluid mud layer at HW slack neap tide (Odd and Cooper, 1989)

# APPENDIX F:

## Numerical results for the Severn

## Phase II

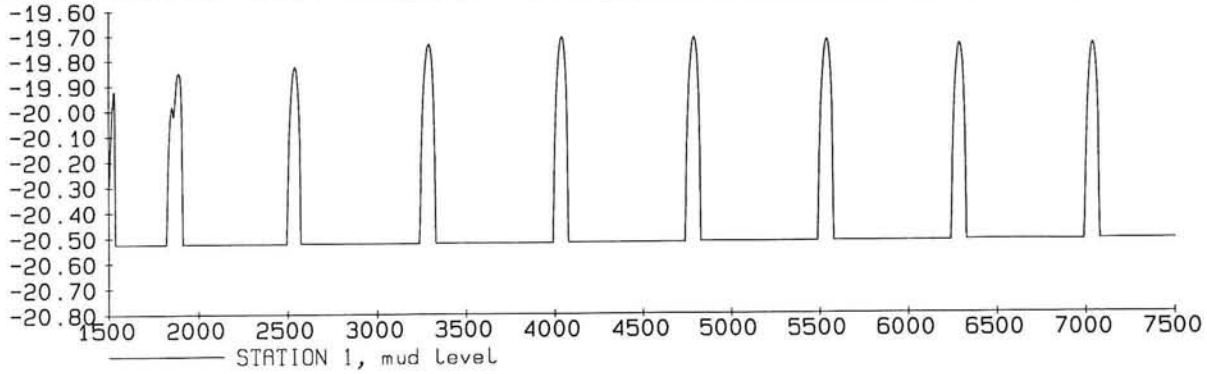


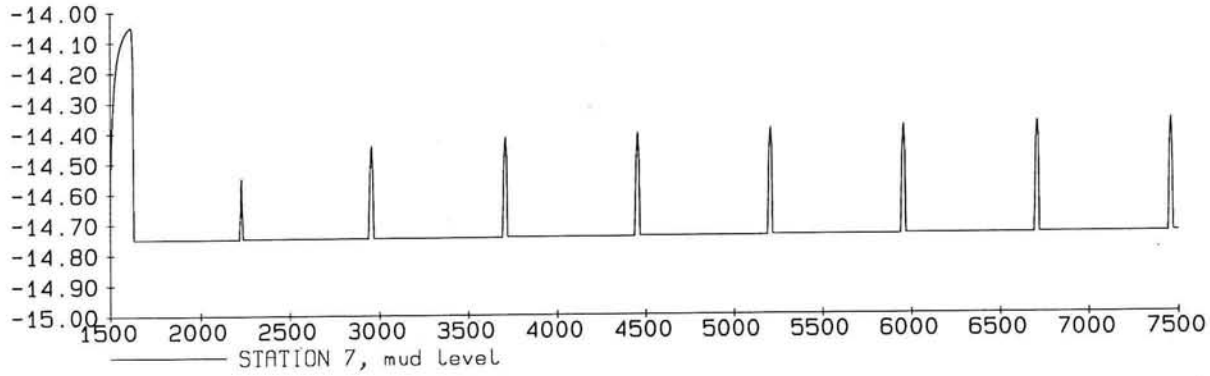


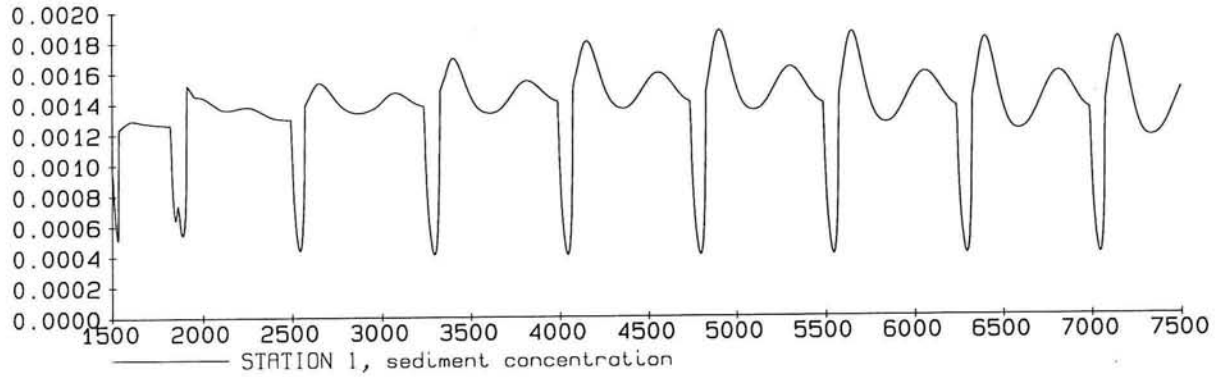


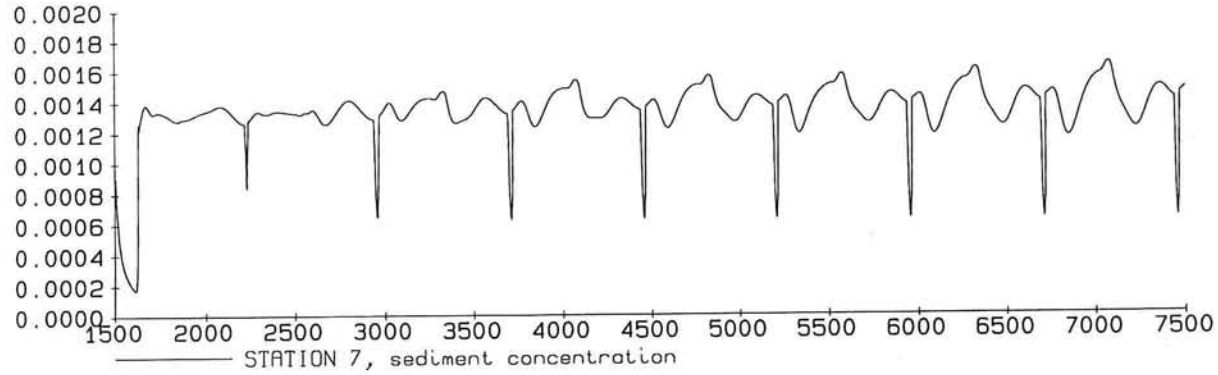


MUD LEVELS (M) AND SEDIMENT CONCENTRATIONS (-)
Time in minutes
Neap tide

SIMULATION 6

STATIONS 1 AND 7

FIG. F1

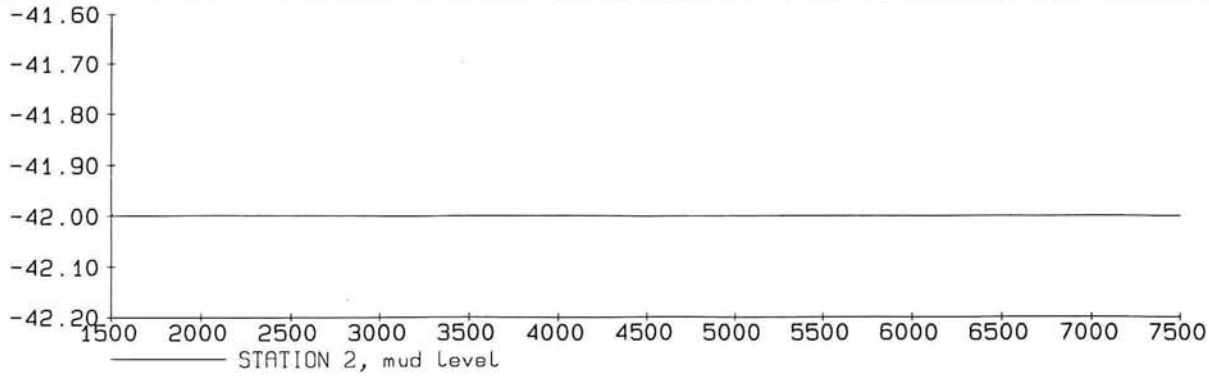


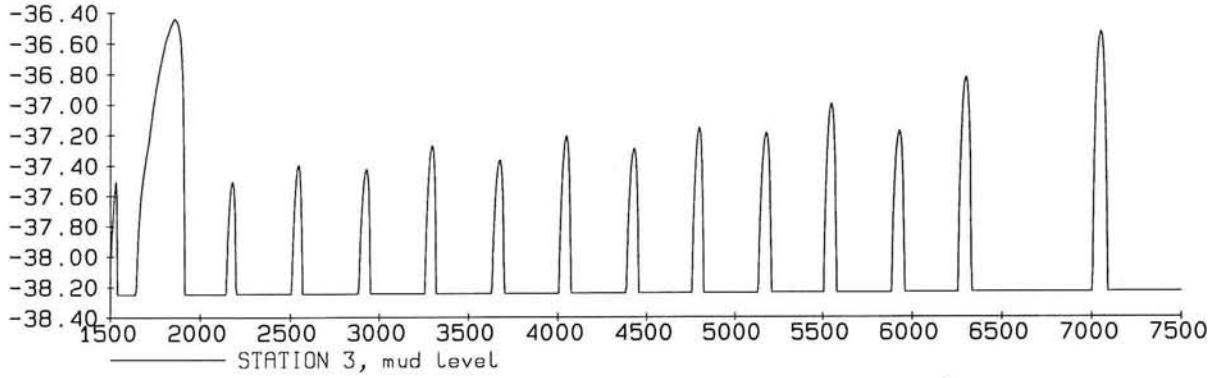


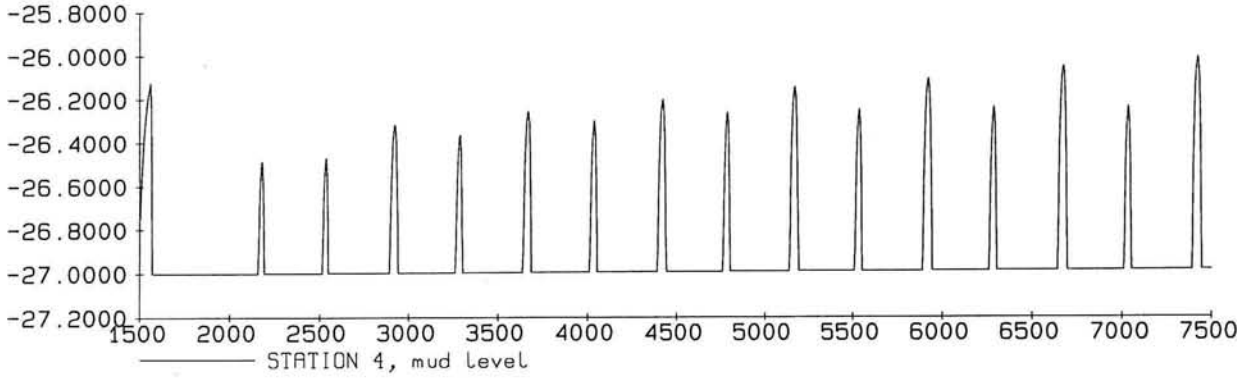


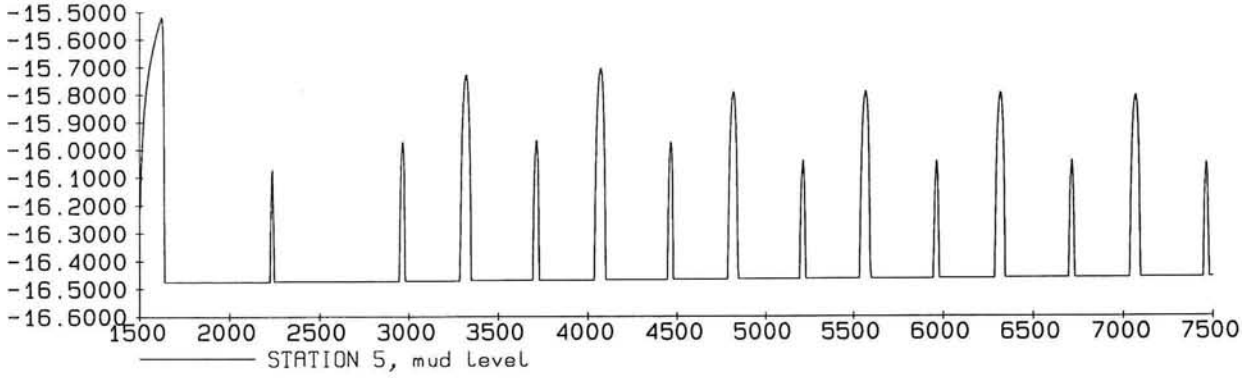


| | | |
|---|---|---|
| MUD LEVELS (M)<br>Time in minutes<br>Neap tide | | |
| | SIMULATION 6 | |
| STATIONS 2, 3, 4 and 5 | | FIG. F2 |

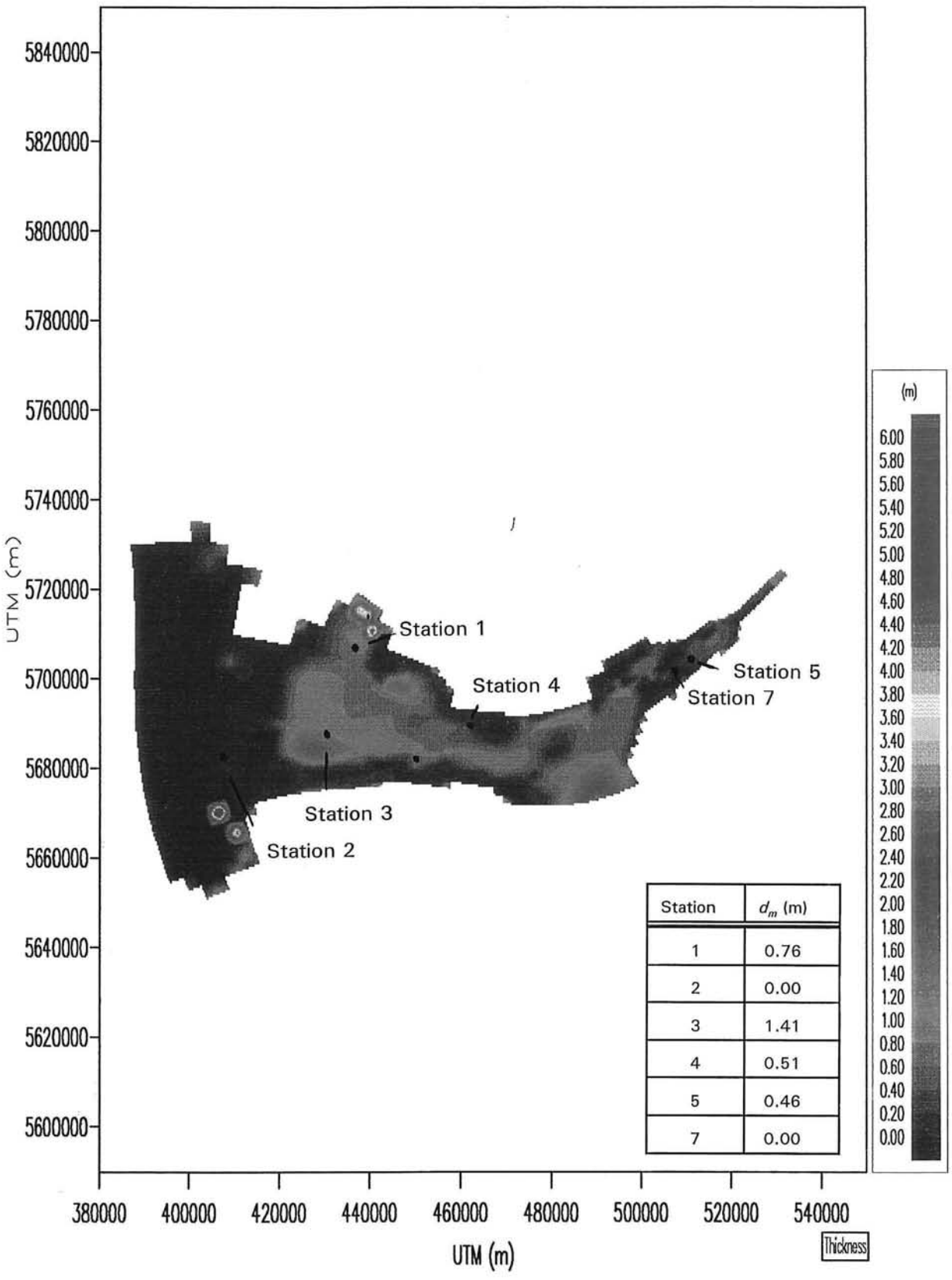


| Station | $d_m$ (m) |
|---|---|
| 1 | 0.76 |
| 2 | 0.00 |
| 3 | 1.41 |
| 4 | 0.51 |
| 5 | 0.46 |
| 7 | 0.00 |

THICKNESS OF FLUID MUD LAYER
AT t = 6300 MINUTES

SIMULATION 6

FIG. F3

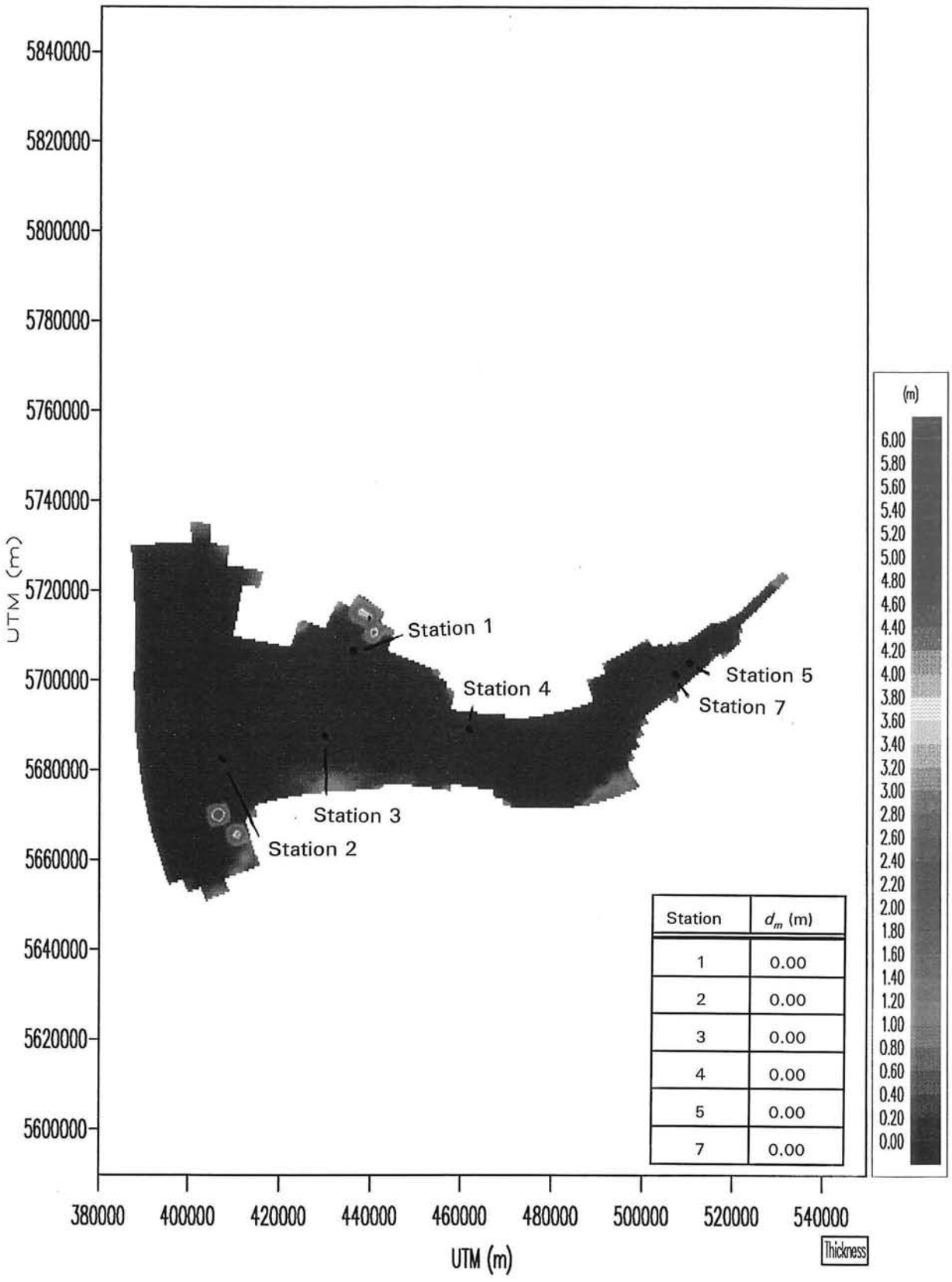


| Station | $d_m$ (m) |
|---|---|
| 1 | 0.00 |
| 2 | 0.00 |
| 3 | 0.00 |
| 4 | 0.00 |
| 5 | 0.00 |
| 7 | 0.00 |

THICKNESS OF FLUID MUD LAYER
AT t = 6600 MINUTES

SIMULATION 6

FIG. F4

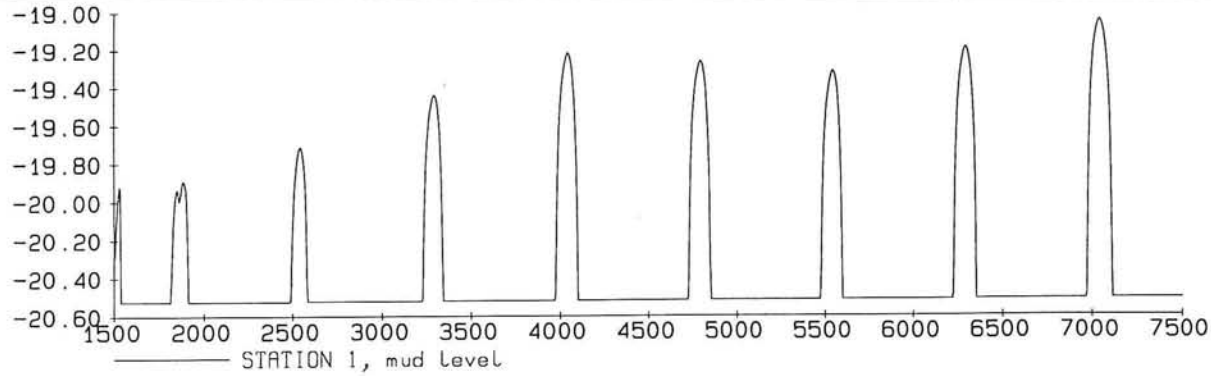


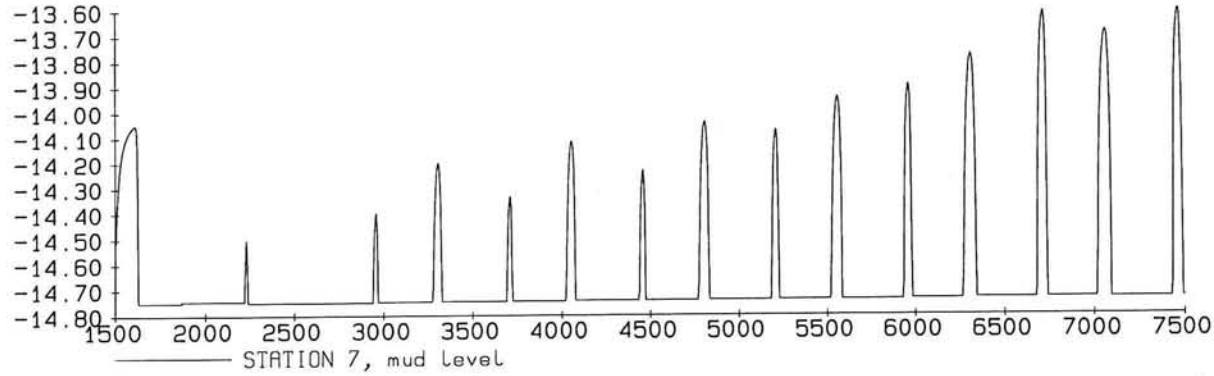


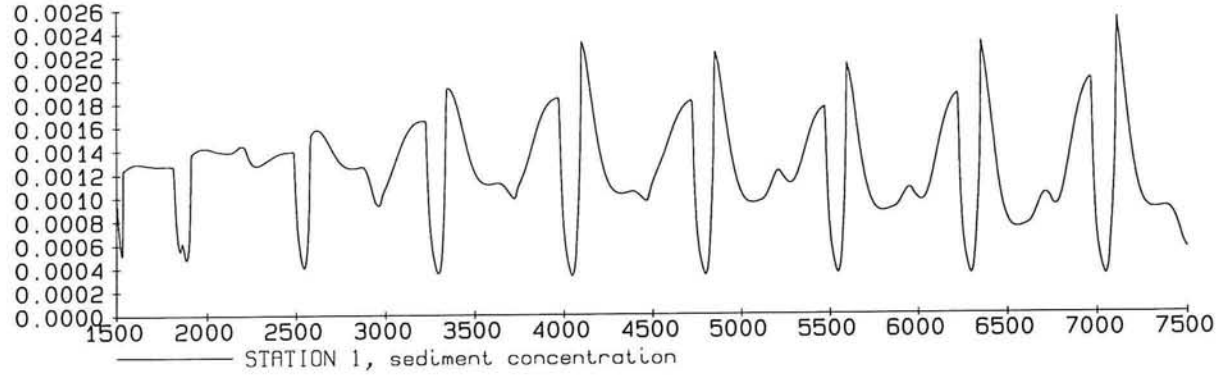


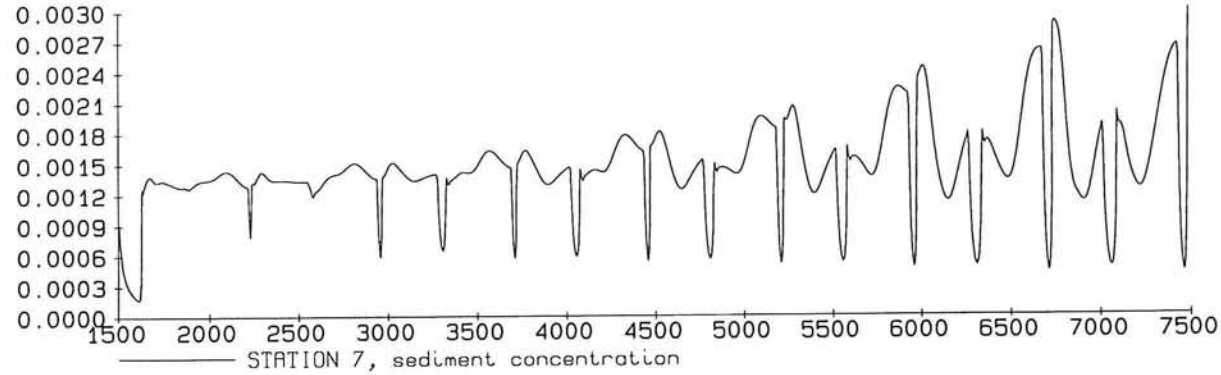


| | | |
|---|---|---|
| **MUD LEVELS (M) AND SEDIMENT CONCENTRATIONS (-)**<br>**Time in minutes**<br>**Neap tide** | | |
| | SIMULATION 7 | |
| STATIONS 1 AND 7 | | FIG. F5 |

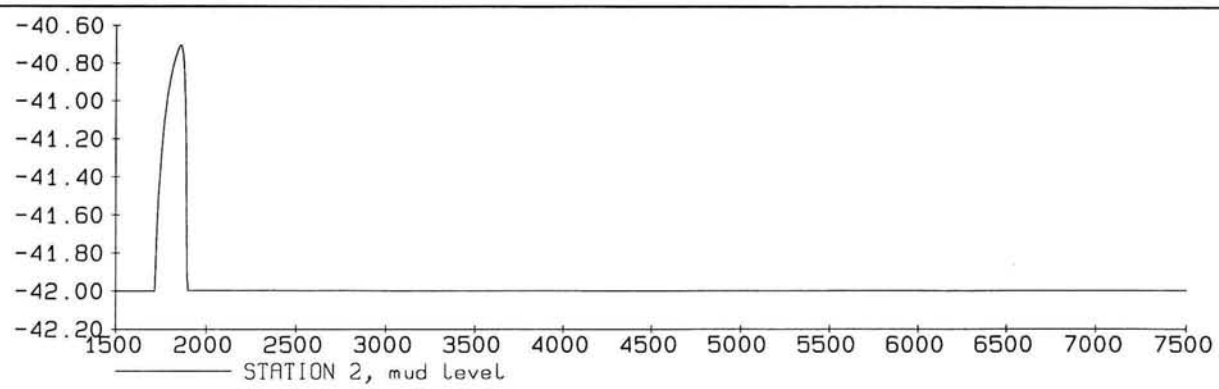


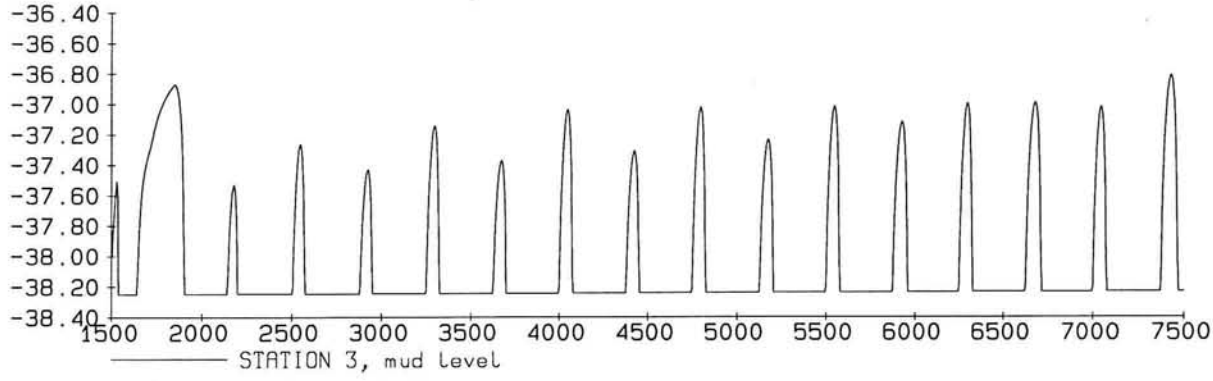


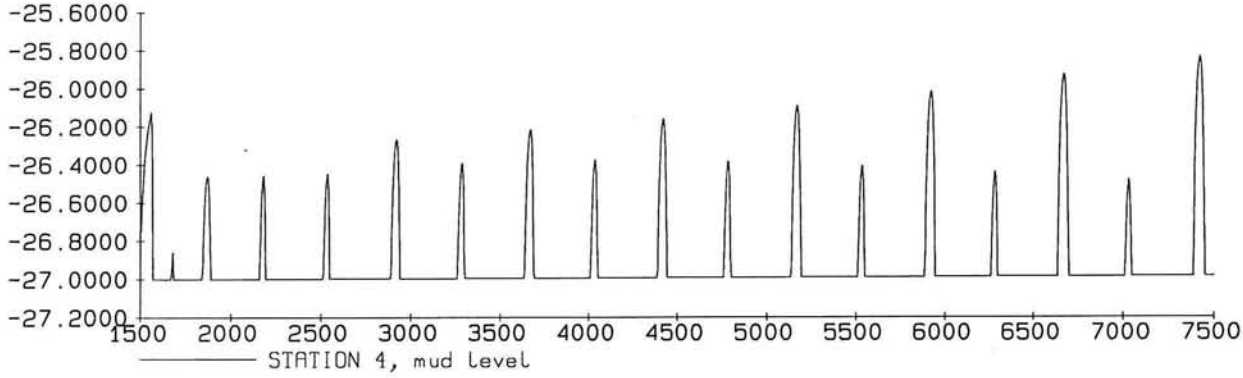


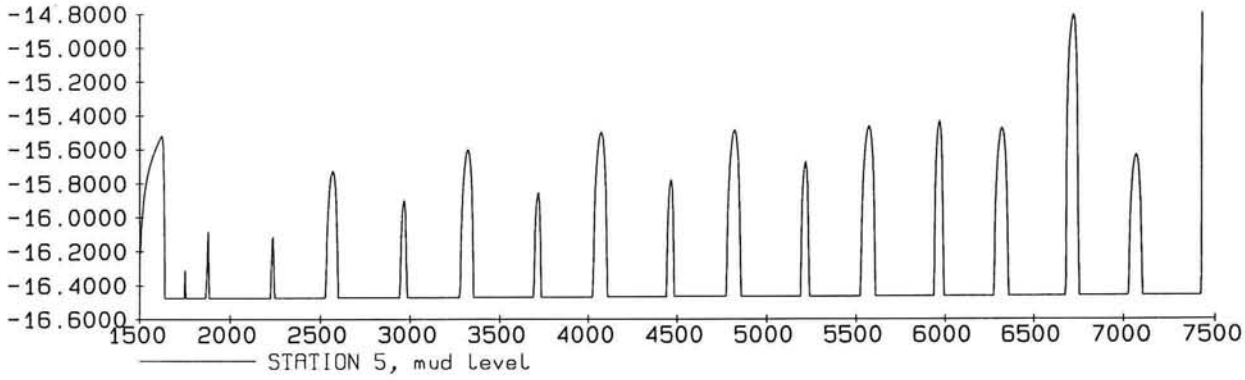


MUD LEVELS (M)
Time in minutes
Neap tide

SIMULATION 7

STATIONS 2, 3, 4 and 5

FIG. F6

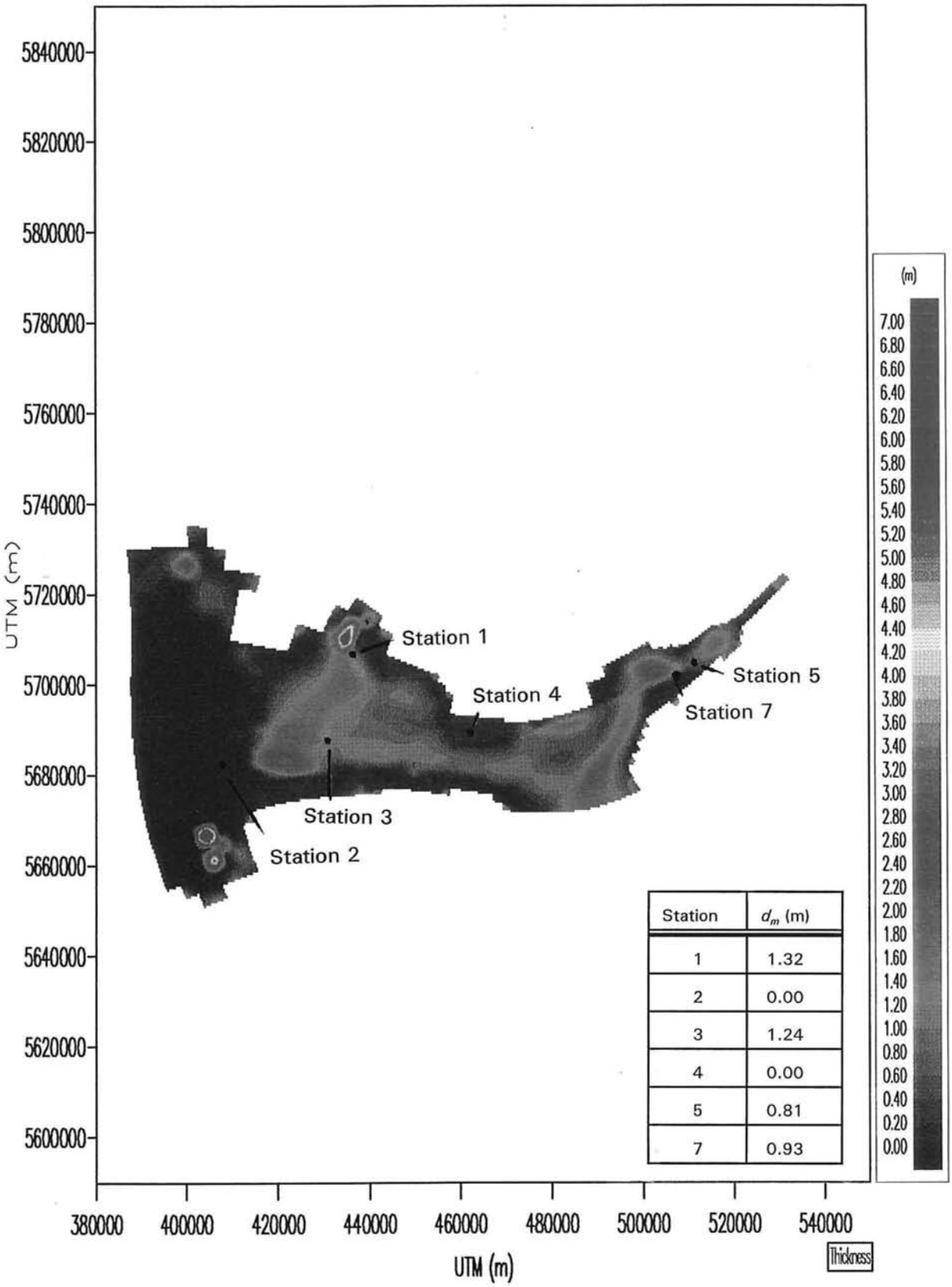


| Station | $d_m$ (m) |
|---|---|
| 1 | 1.32 |
| 2 | 0.00 |
| 3 | 1.24 |
| 4 | 0.00 |
| 5 | 0.81 |
| 7 | 0.93 |

THICKNESS OF FLUID MUD LAYER
AT t = 6300 MINUTES

SIMULATION 7

FIG. F7

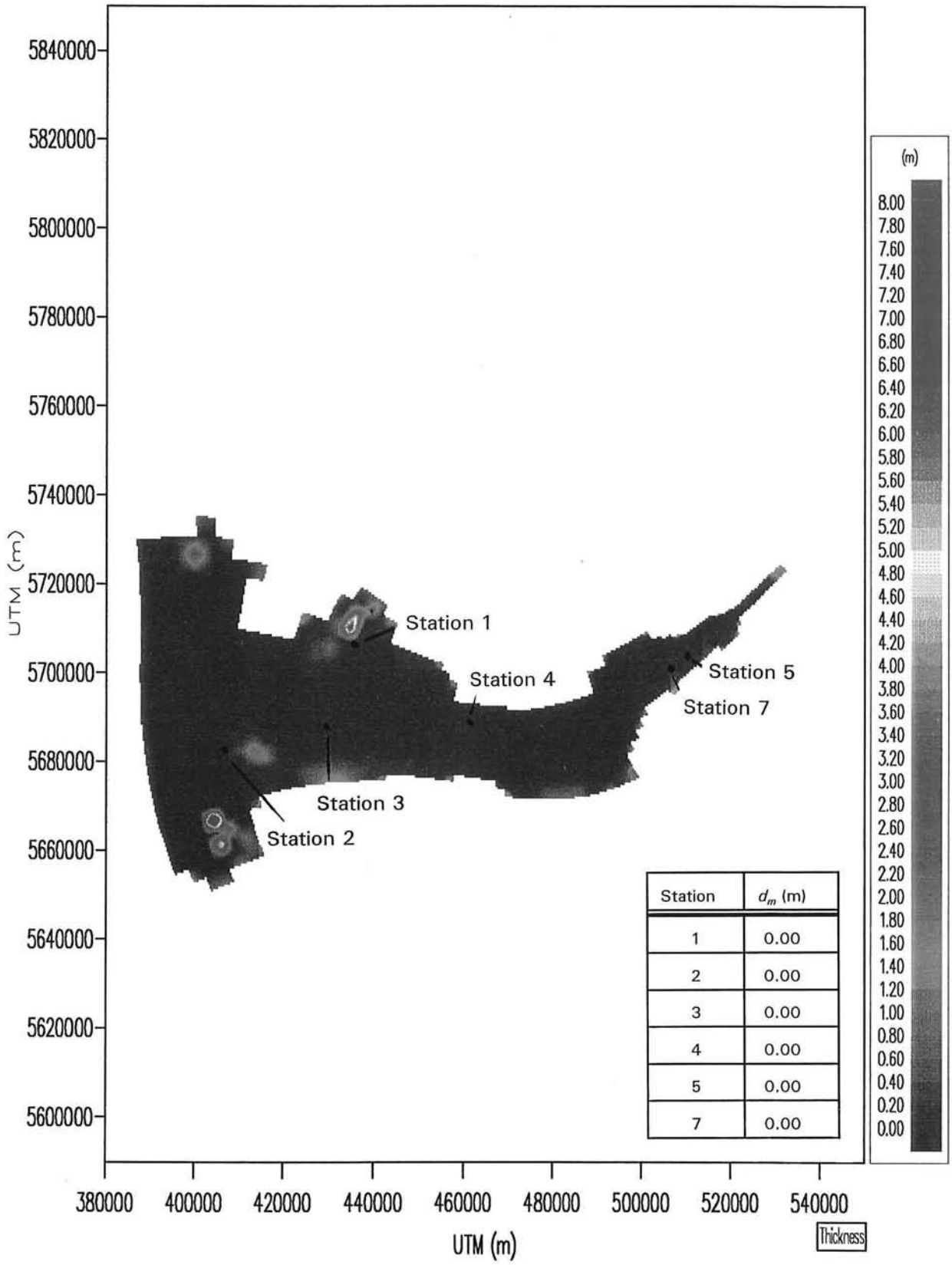


| Station | $d_m$ (m) |
|---|---|
| 1 | 0.00 |
| 2 | 0.00 |
| 3 | 0.00 |
| 4 | 0.00 |
| 5 | 0.00 |
| 7 | 0.00 |

THICKNESS OF FLUID MUD LAYER
AT t = 6600 MINUTES

SIMULATION 7

FIG. F8

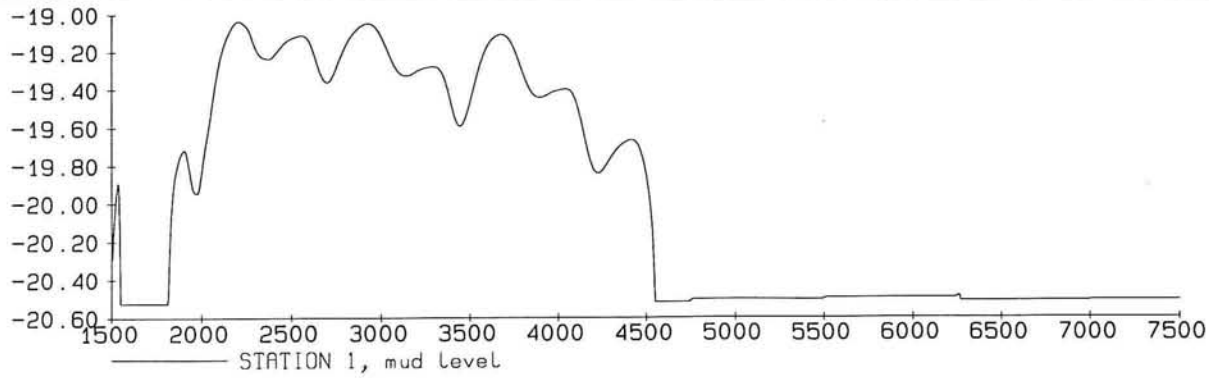


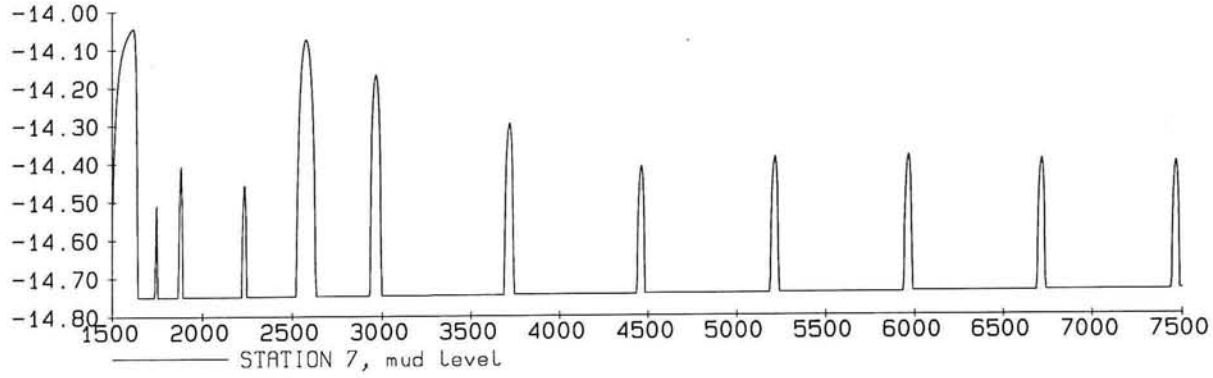


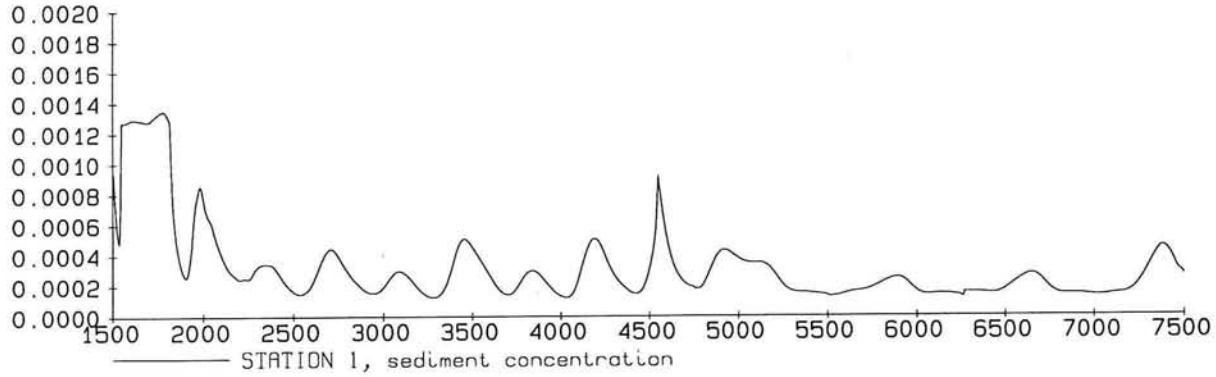


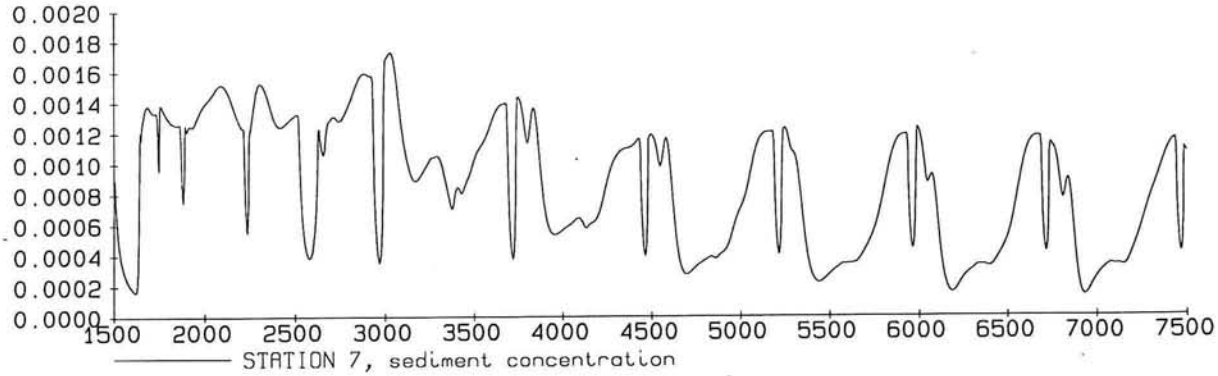


| | | |
|---|---|---|
| MUD LEVELS (M) AND SEDIMENT CONCENTRATIONS (-)<br>Time in minutes<br>Neap tide | | |
| | SIMULATION 8 | |
| STATIONS 1 AND 7 | | FIG. F9 |

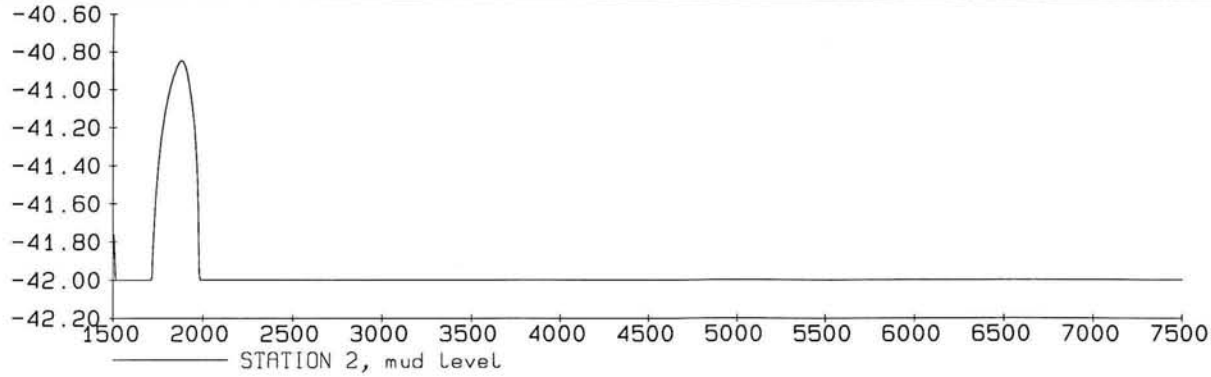


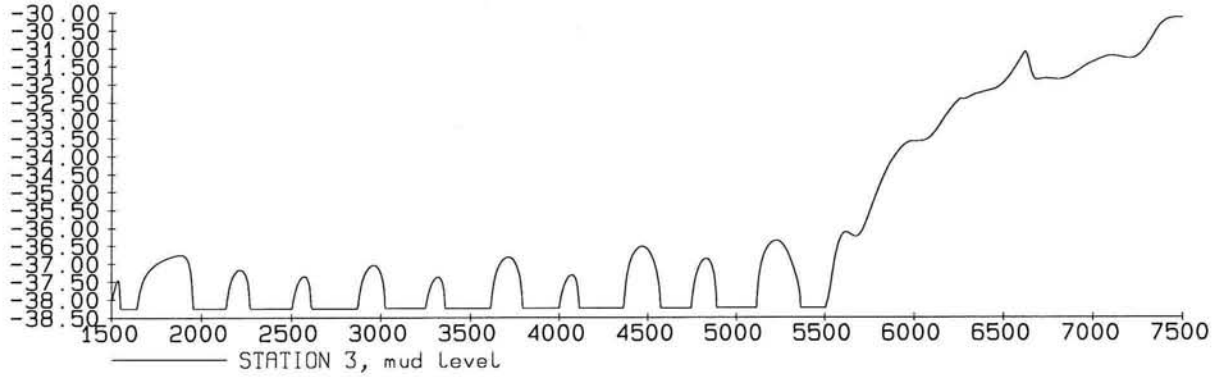


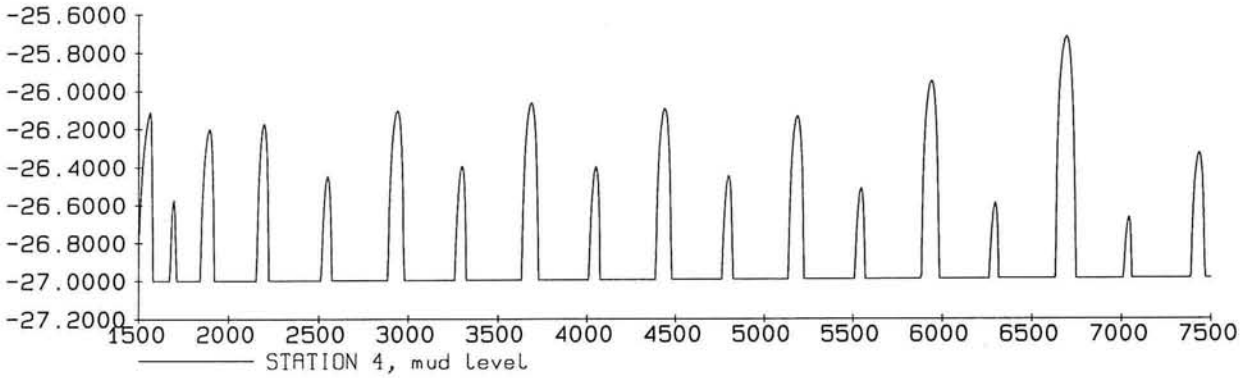


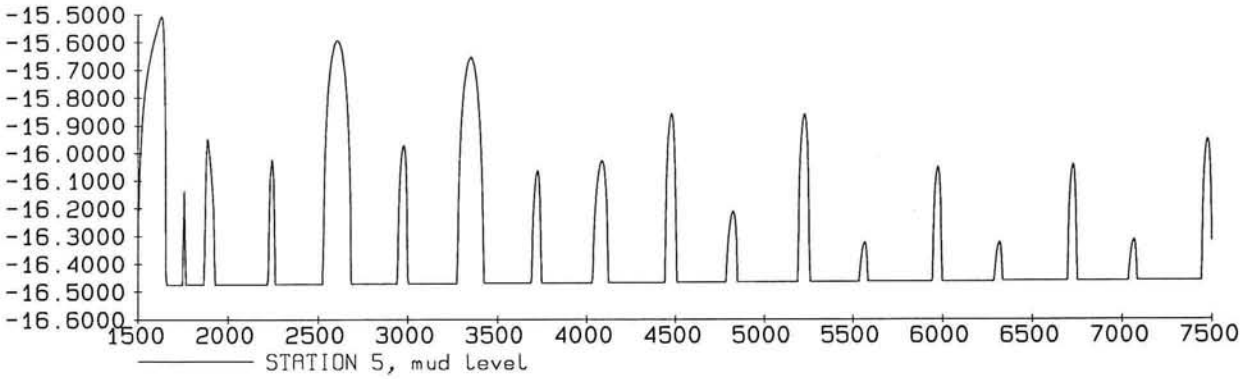


| | | |
|---|---|---|
| MUD LEVELS (M)<br>Time in minutes<br>Neap tide | | |
| | SIMULATION 8 | |
| STATIONS 2, 3, 4 and 5 | | FIG. F10 |

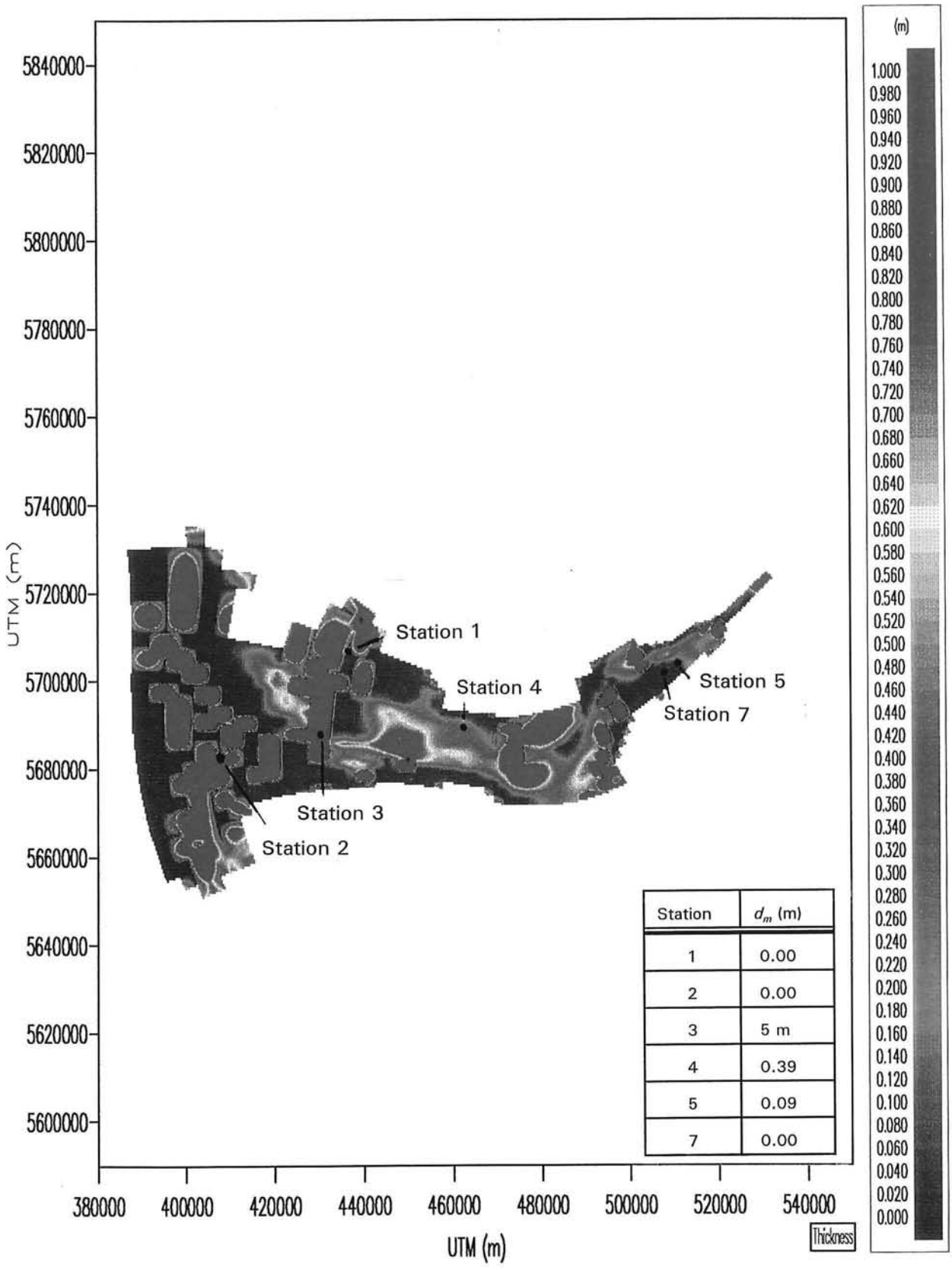


| Station | $d_m$ (m) |
|---|---|
| 1 | 0.00 |
| 2 | 0.00 |
| 3 | 5 m |
| 4 | 0.39 |
| 5 | 0.09 |
| 7 | 0.00 |

THICKNESS OF FLUID MUD LAYER
AT t = 6300 MINUTES

SIMULATION 8

FIG. F11

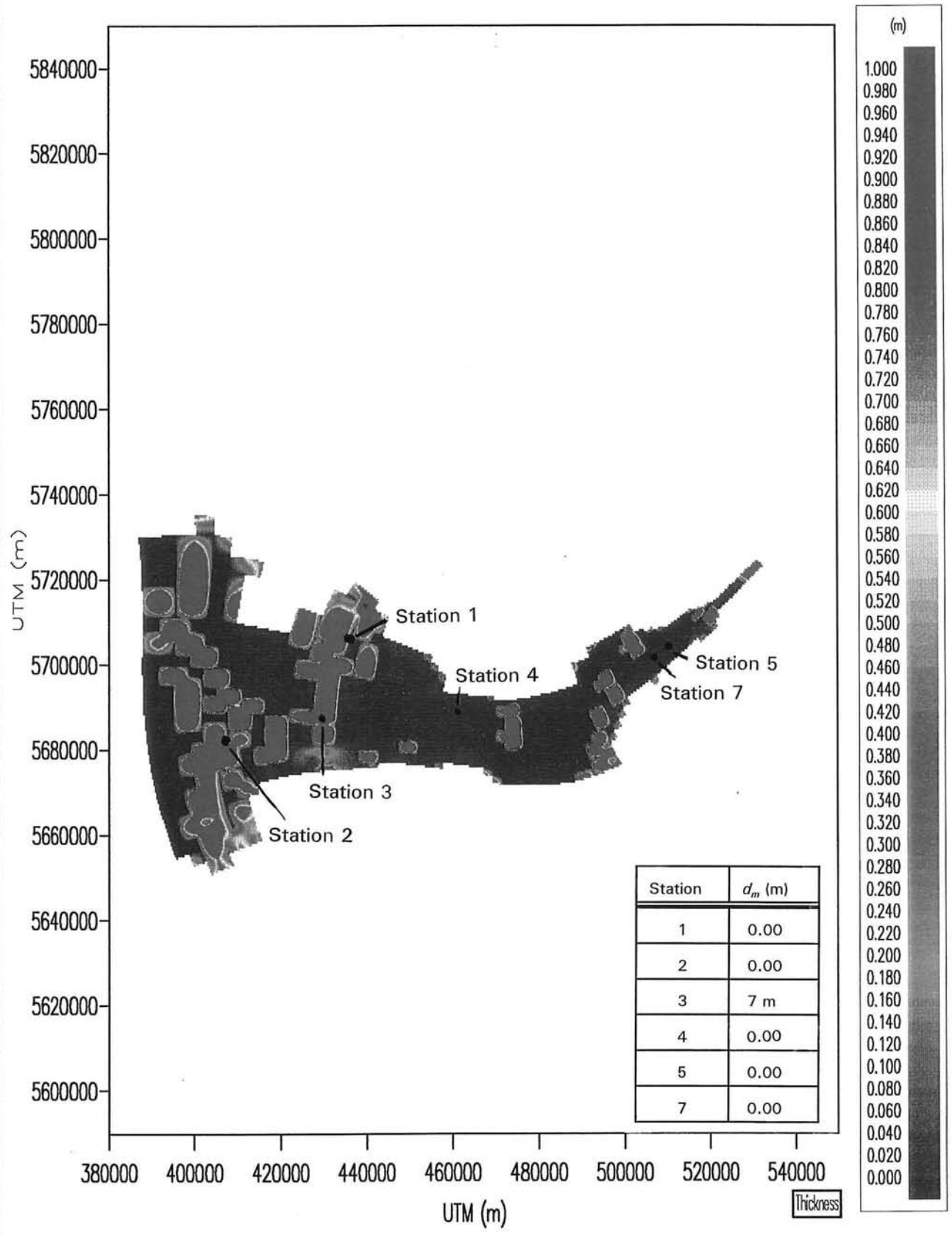


| Station | $d_m$ (m) |
|---|---|
| 1 | 0.00 |
| 2 | 0.00 |
| 3 | 7 m |
| 4 | 0.00 |
| 5 | 0.00 |
| 7 | 0.00 |

THICKNESS OF FLUID MUD LAYER
AT t = 6600 MINUTES

SIMULATION 8

FIG. F12

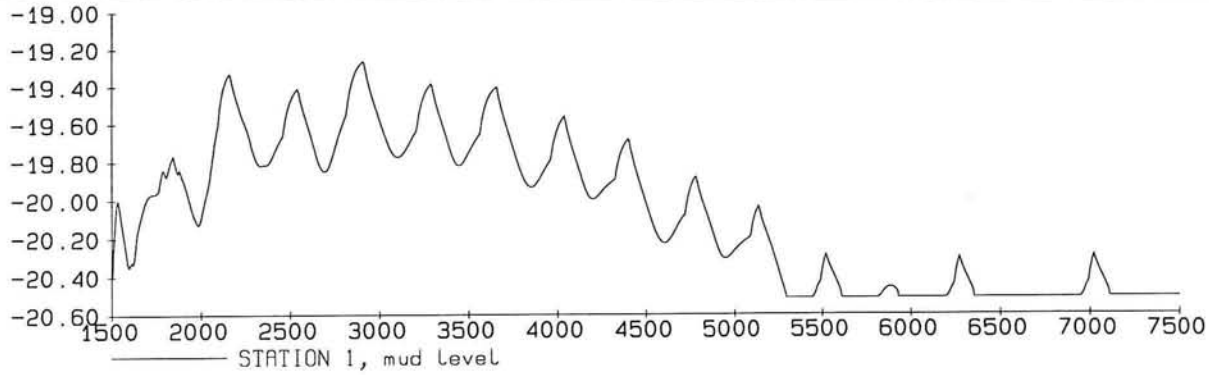


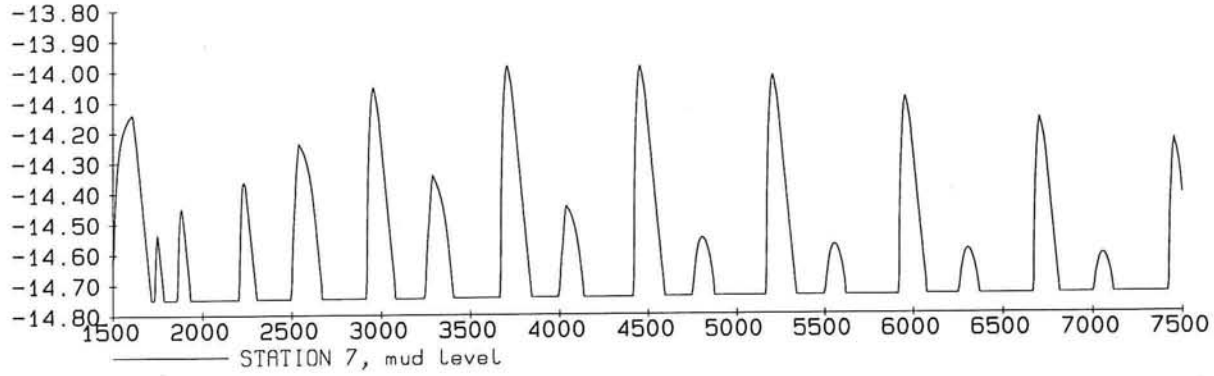


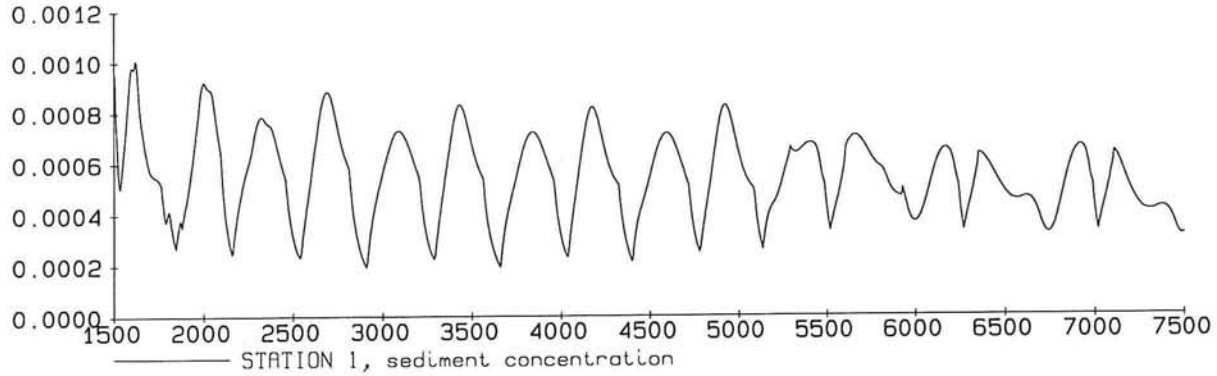


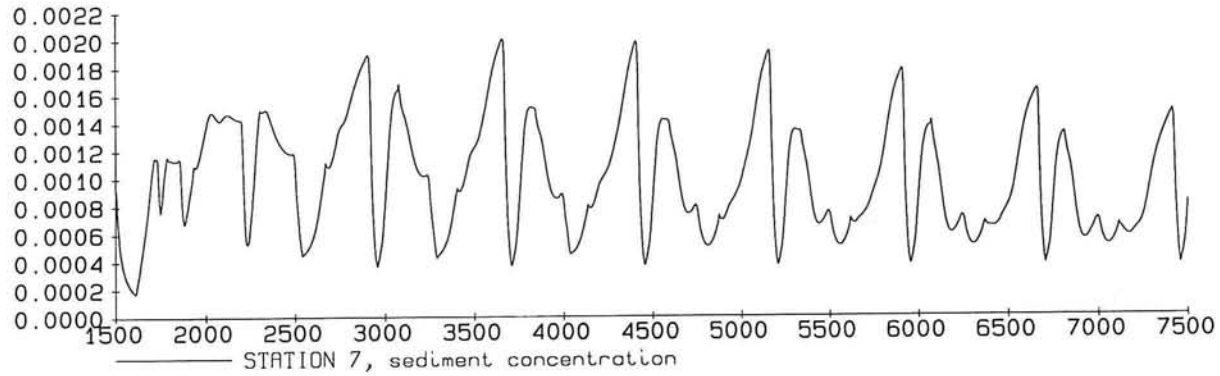


MUD LEVELS (M) AND SEDIMENT CONCENTRATIONS (-)
Time in minutes
Neap tide

SIMULATION 9

STATIONS 1 AND 7

FIG. F13

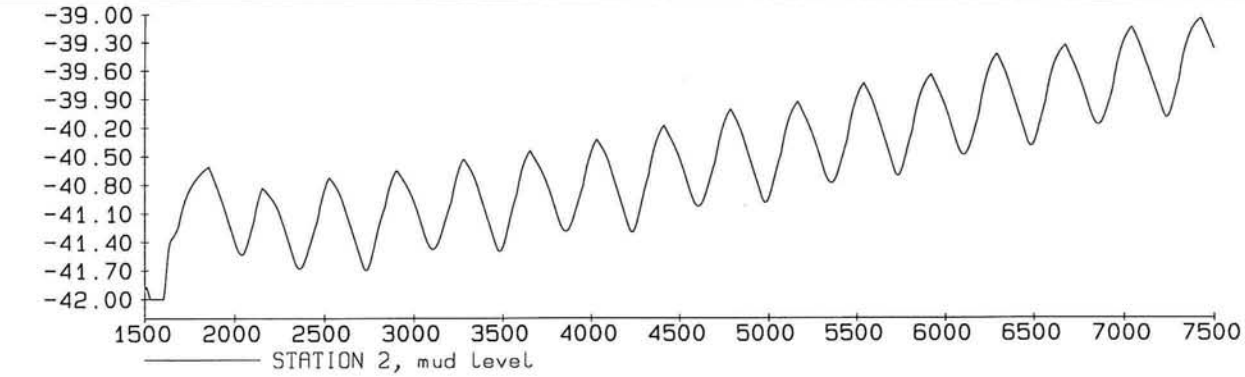


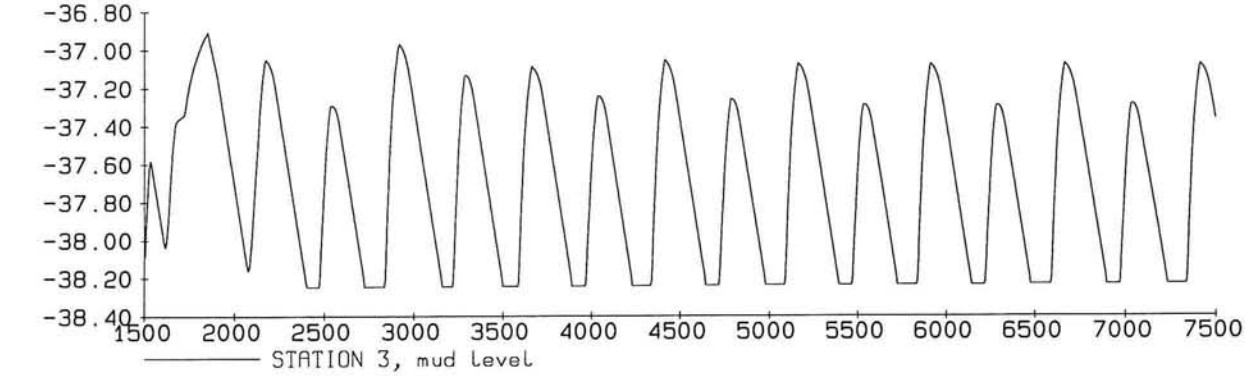


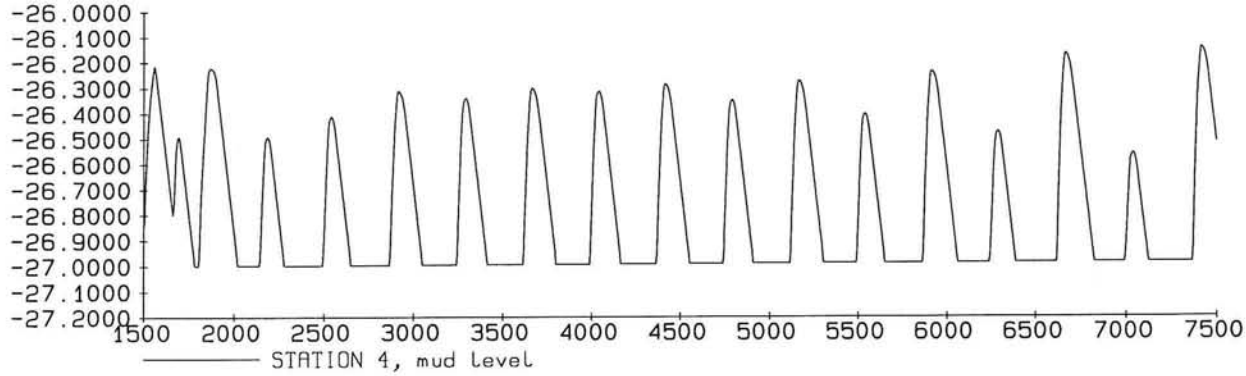


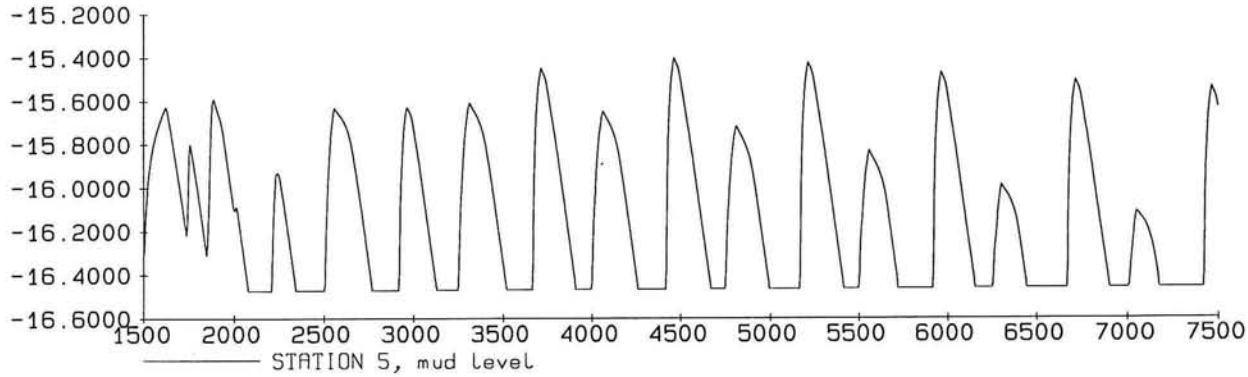


MUD LEVELS (M)
Time in minutes
Neap tide

SIMULATION 9

STATIONS 2, 3, 4 and 5

FIG. F14

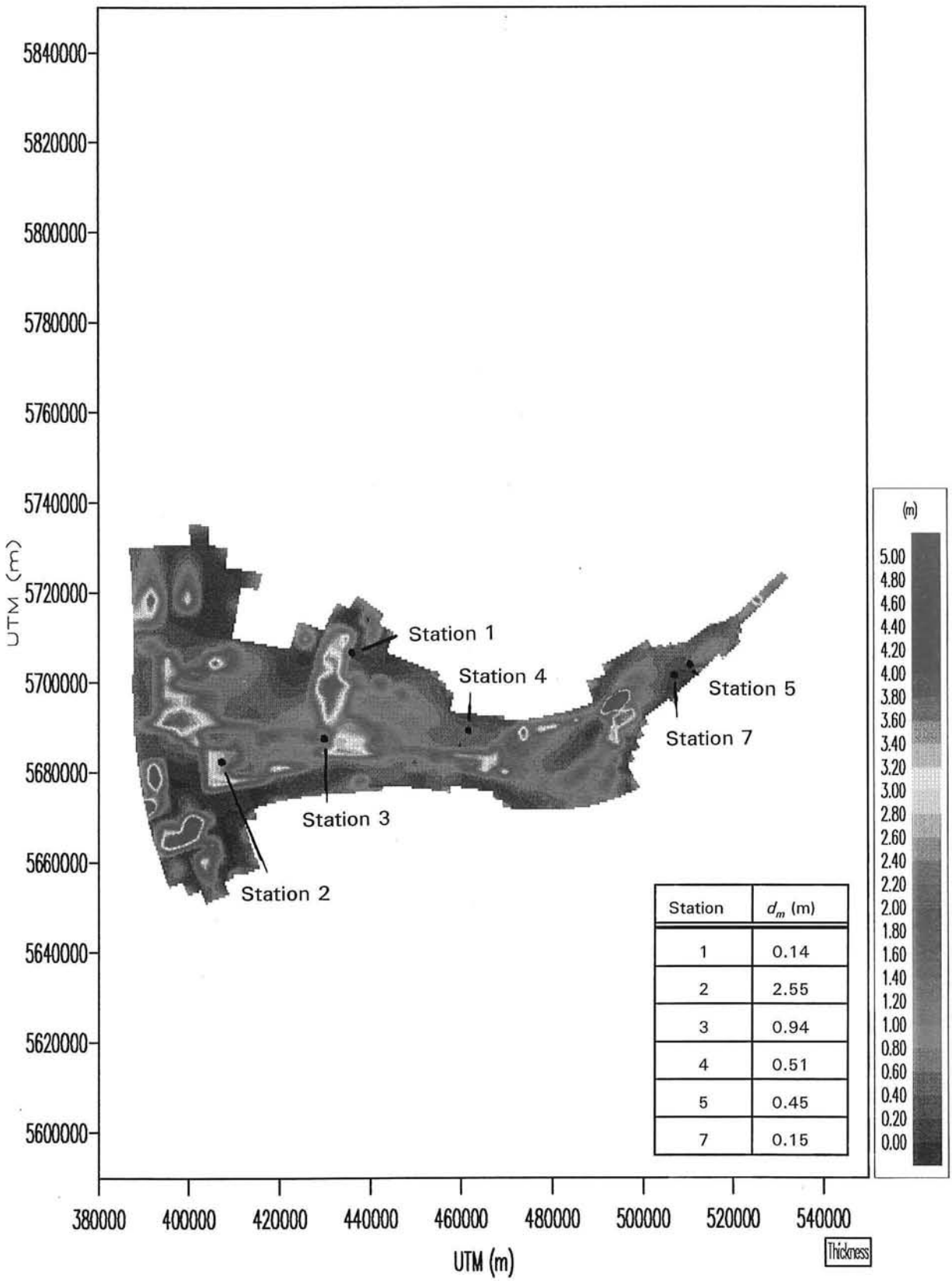


| Station | $d_m$ (m) |
|---|---|
| 1 | 0.14 |
| 2 | 2.55 |
| 3 | 0.94 |
| 4 | 0.51 |
| 5 | 0.45 |
| 7 | 0.15 |

THICKNESS OF FLUID MUD LAYER
AT t = 6300 MINUTES

SIMULATION 9

FIG. F15

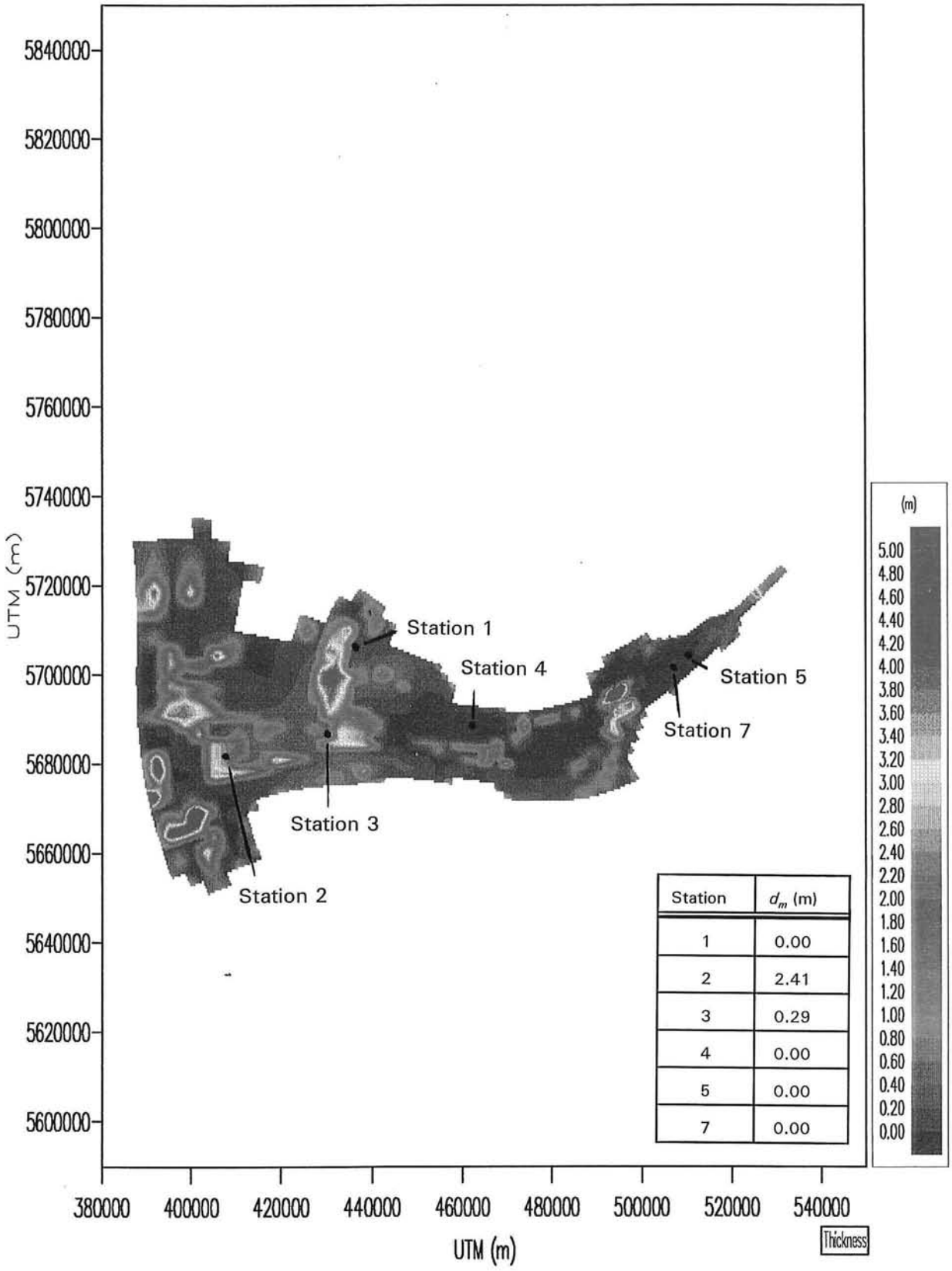


| Station | $d_m$ (m) |
|---|---|
| 1 | 0.00 |
| 2 | 2.41 |
| 3 | 0.29 |
| 4 | 0.00 |
| 5 | 0.00 |
| 7 | 0.00 |

THICKNESS OF FLUID MUD LAYER
AT t = 6600 MINUTES

SIMULATION 9

FIG. F16

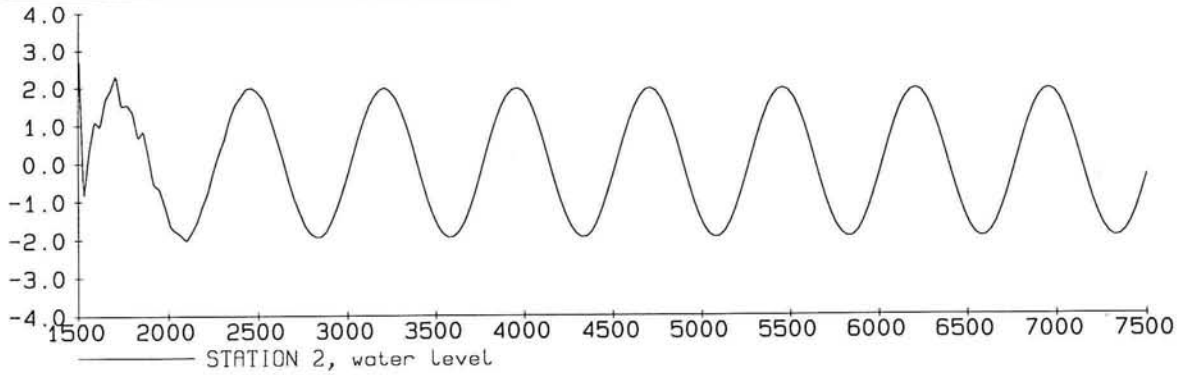


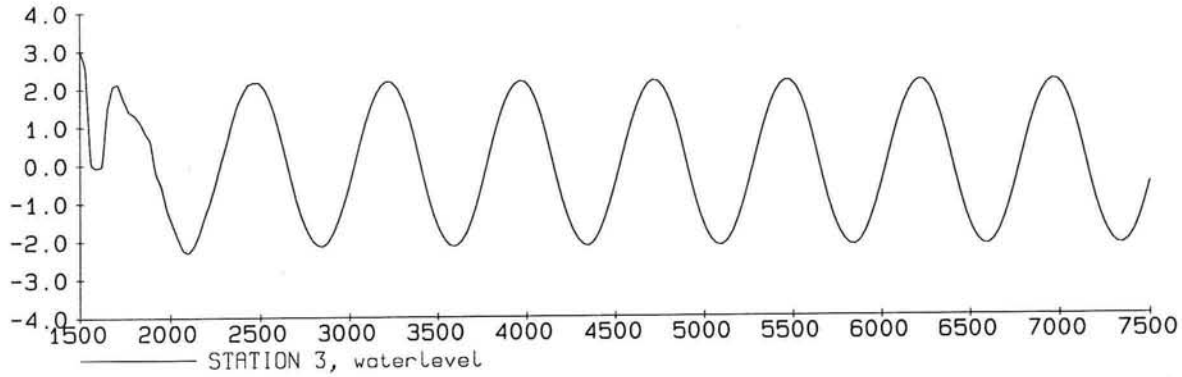


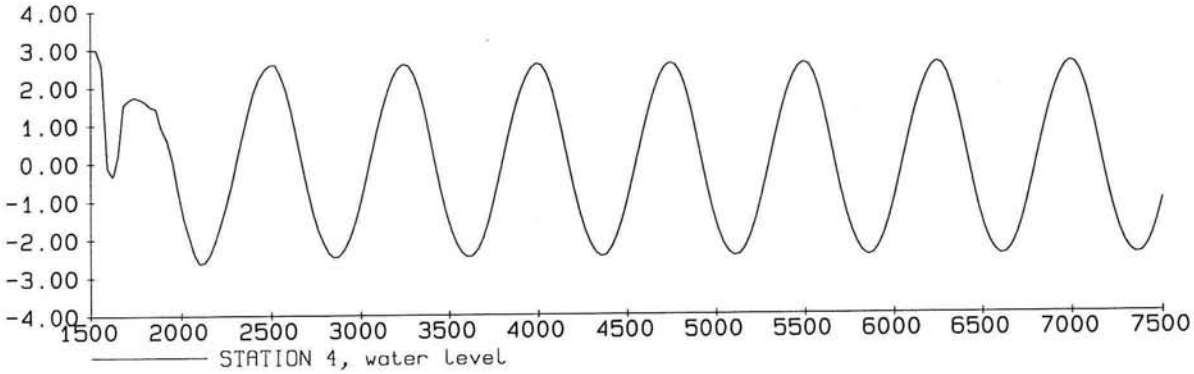


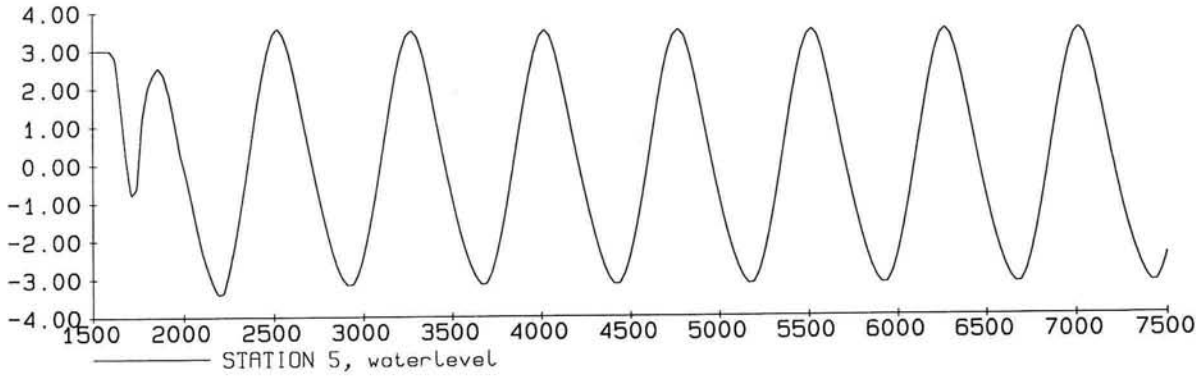


WATER LEVELS (M)
Time in minutes
Neap tide

STATIONS 2, 3, 4 AND 5

FIG. F17

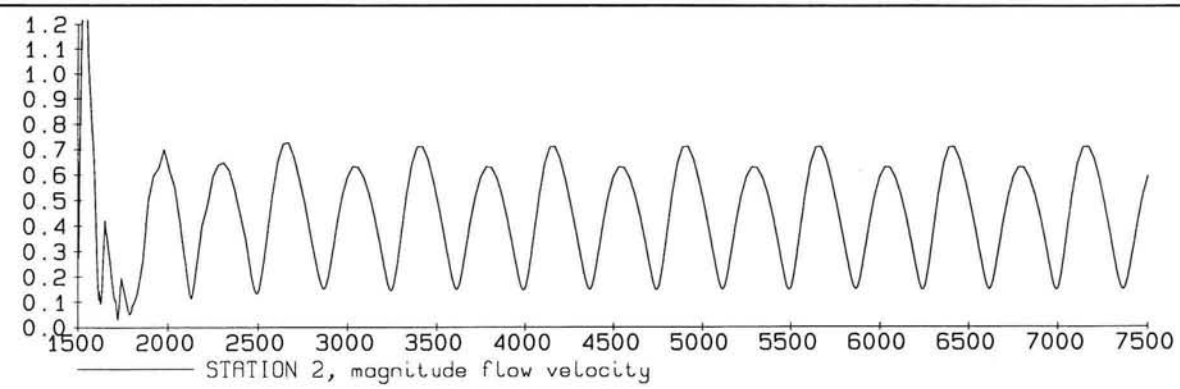


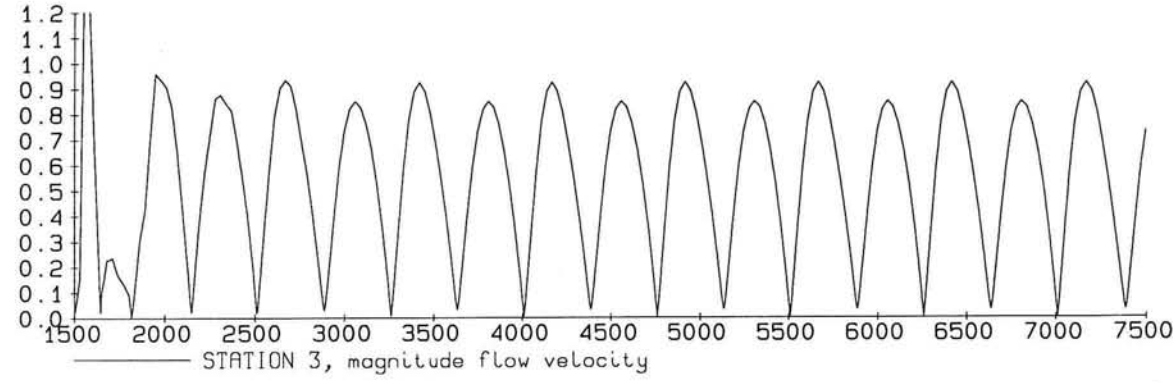


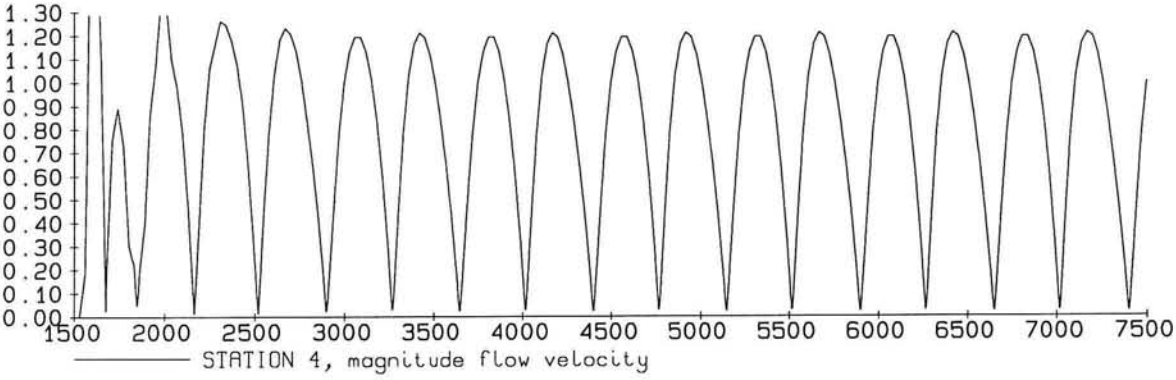


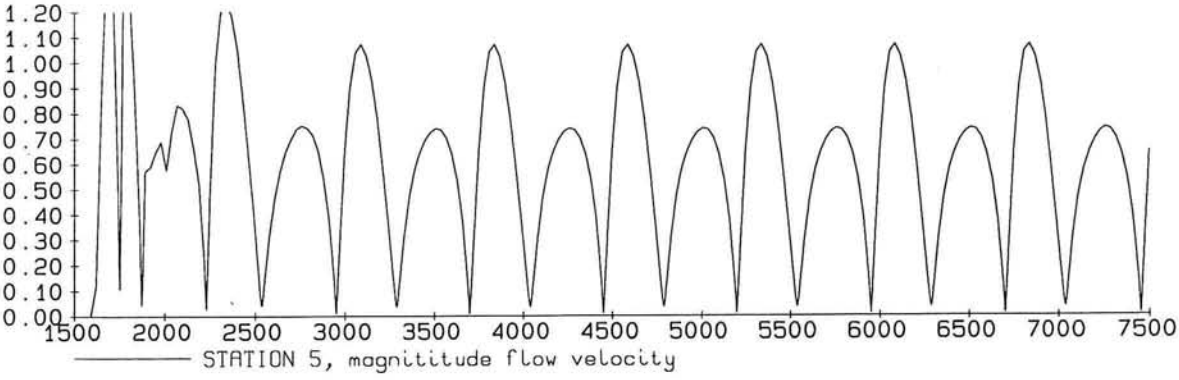


MAGNITUDE FLOW VELOCITIES (M/S)
Time in minutes
Neap tide

STATIONS 2, 3, 4 AND 5

FIG. F18

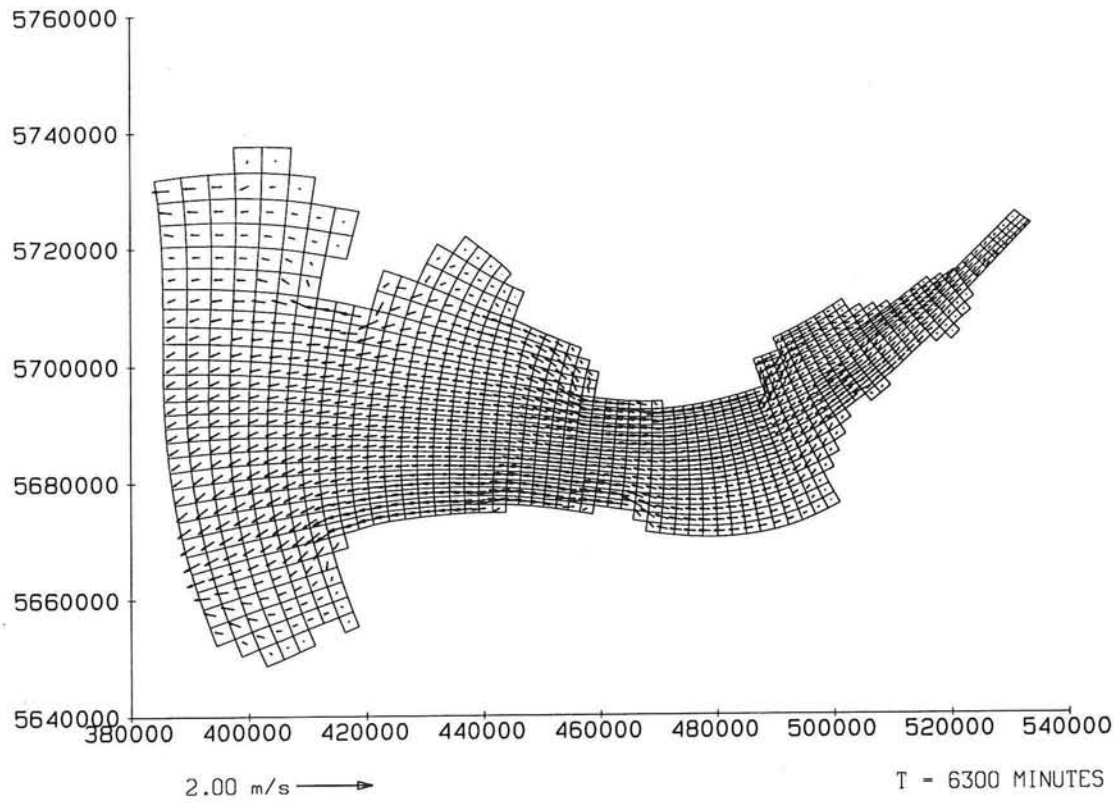


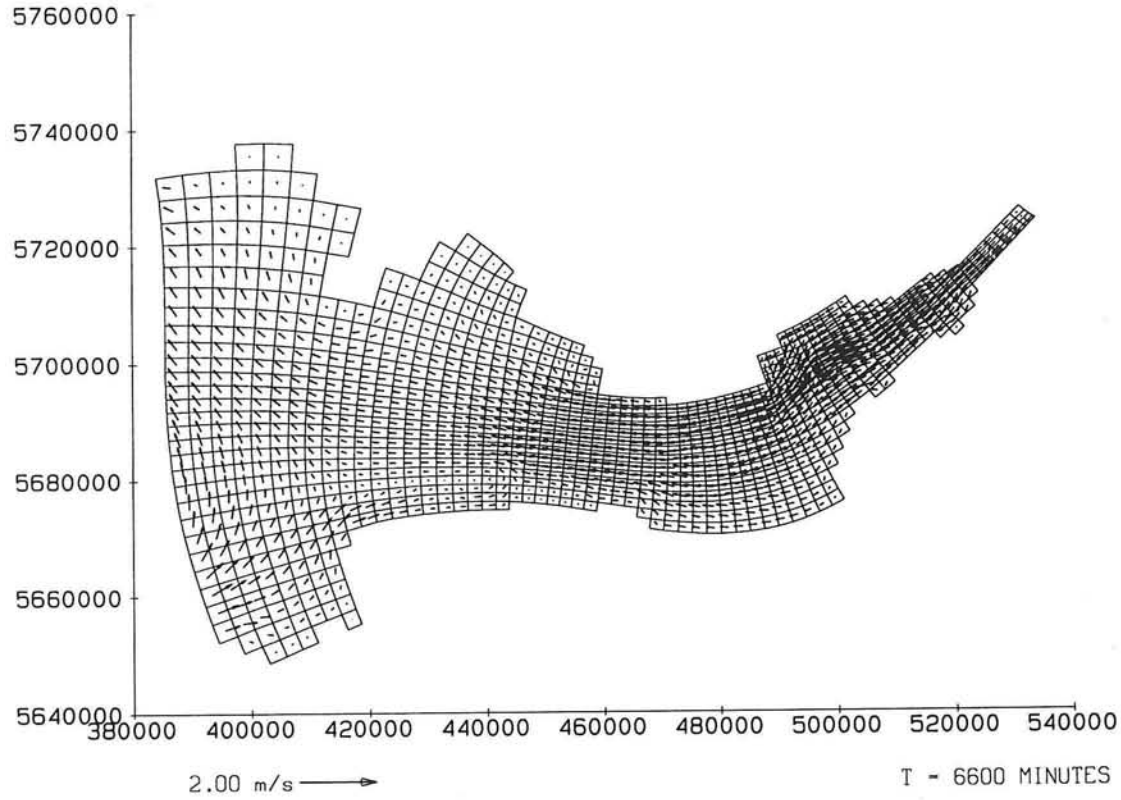


FLOW PATTERNS OF SUSPENSION LAYER
At $t$ = 6300 and $t$ = 6600 minutes
Neap tide

SIMULATION 6

FIG. F19

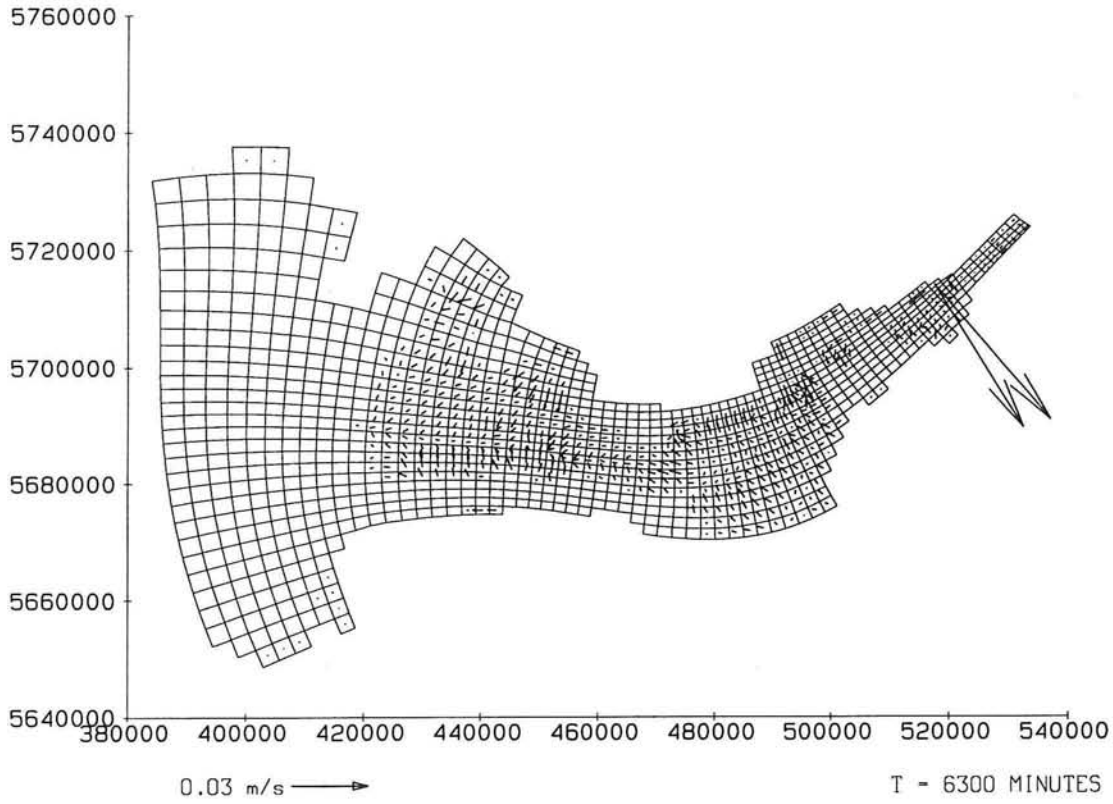


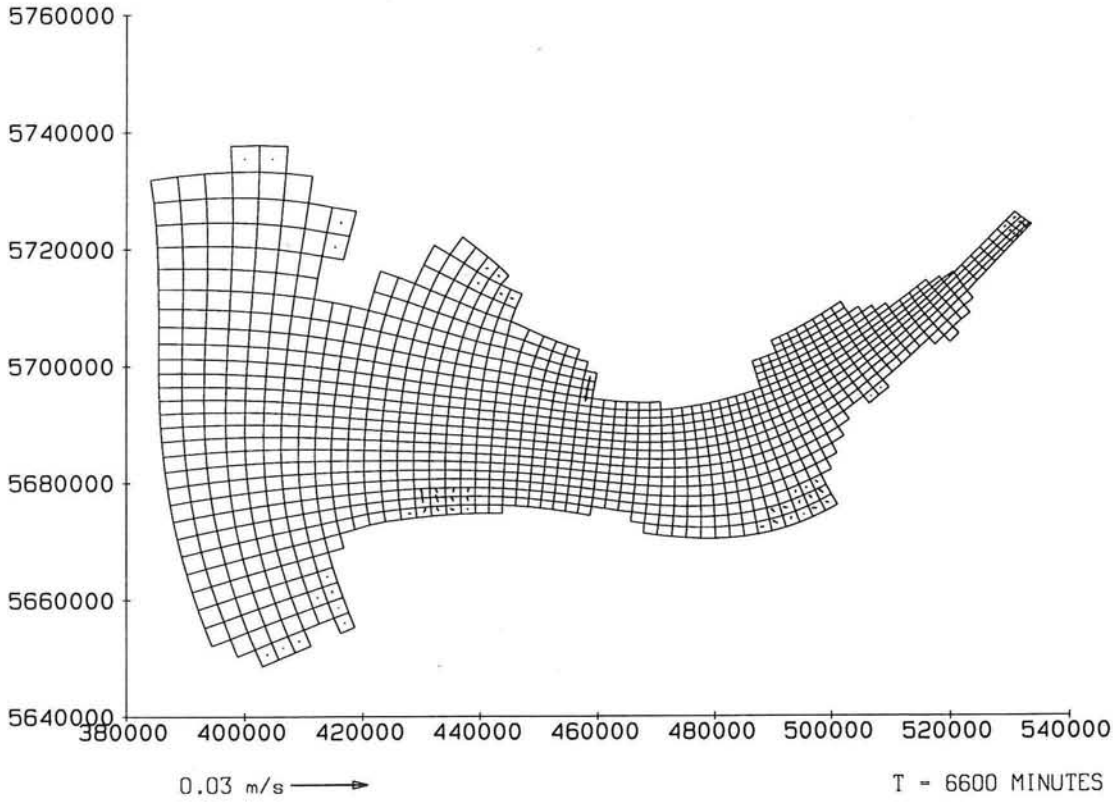


FLOW PATTERNS OF FLUID MUD LAYER
At $t$ = 6300 and $t$ = 6600 minutes
Neap tide

SIMULATION 6

FIG. F20

## LIST OF FIGURES